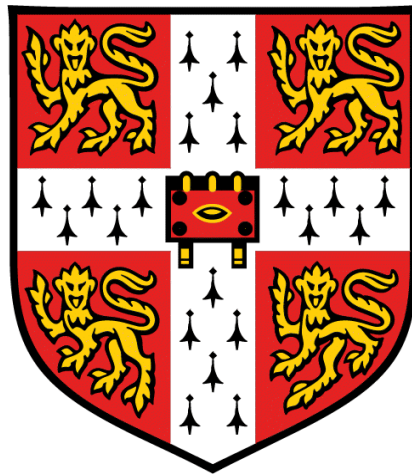


The Interaction of Obesity and Age and their effect on Adipose Tissue Metabolism in the Mouse



**A dissertation submitted for the degree of Doctor of Philosophy at the
University of Cambridge**

Ke-di Liu



King's College

Declaration

This thesis is a summary of research conducted in the Department of Biochemistry, University of Cambridge, between October 2013 and September 2017. This dissertation is the result of my own work and includes nothing which is the outcome of work done in collaboration, except where specially indicated in the text. None of the research described, in its entirety or in part, has been submitted for a degree, diploma or other qualification at any other University. This thesis does not exceed 60,000 words.

Ke-di Liu

Abstract

Numerous studies have investigated how bulk lipid metabolism is influenced in obesity and in particular how the composition of triglycerides found in the cytosol change with increased adipocyte expansion. However, in part reflecting the analytical challenge the composition of cell membranes, and in particular glycerophospholipids, an important membrane component, have been seldom investigated. Cell membrane components contribute to a variety of cellular processes including maintaining organelle functionality, providing an optimized environment for numerous proteins and providing important pools for metabolites, such as choline for one-carbon metabolism and S-adenosylmethionine for DNA methylation. Here, I have conducted a comprehensive lipidomic and transcriptomic study of white adipose tissue in mice that become obese either through genetic modification (*ob/ob* genotype), diet (high-fat diet) or a combination of the two across the life course. Specifically, I demonstrated that the changes in triglyceride metabolism that dominate the overall lipid composition of white adipose tissue were distinct from the compositional changes of glycerophospholipids. These latter lipids became more unsaturated to maintain the fluidity and normal function of the membrane in the initiation of obesity but then turned saturated after long-term administration of HFD and aging. This suggests that while triglycerides within the adipose tissue may be a relatively inert store of lipids, the compositional changes occur in cell membranes with more far-reaching functional consequences in both obesity and aging. The two-phase change of phospholipids can be correlated well with transcriptional and one-carbon metabolic changes within the adipocytes. The transcriptomic study demonstrated that the lipid metabolic pathways regulated by the peroxisome, AMPK, insulin and PPAR γ signaling were activated in the initiation of obesity but inhibited in the adipose tissue of old *ob/ob* mice along with up-regulated inflammation pathways. The brown and white adipose tissue of PPAR α -knock-out mice were also studied by lipidomic tools to get a deeper understanding of the effect of the peroxisome and PPAR system on adipose tissue and lipid metabolism during obesity. Most of the lipids were increased and became more saturated and shorter in adipose tissues of PPAR α null mice, which is in good accordance with the results of the former animal study. In conclusion, my work using different rodent models and multi-omics techniques demonstrated a protective metabolic mechanism activated in the initiation but impaired at the end of the processes of obesity and aging, which could be an explanation of the similarity of obesity and aging in terms of high incidence of the metabolic syndrome and related diseases.

Publication

Hanli Xu, Shaowei Wang, Lin-Lin Ma, Shuai Huang, Lin Liang, Qian Liu, Yang-Yang Liu, Ke-Di Liu, Ze-Min Tan, Hao Ban, Yongtao Guan, and Zuhong Lu (2017) Informative Priors on Fetal Fraction Increase Power of The Noninvasive Prenatal Screen. *Genetics in Medicine*, accepted.

Presentation

The Interaction of Diet with Epigenetic Modifications in Adipose Tissue Metabolism. Poster presented in 42nd Adipose Tissue Discussion Group (ATDG) Meeting, 14th December 2015, University of Westminster, London.

Acknowledgments

Pursuing studies as a Ph.D. student in the past four years in Cambridge has been such a wonderful, unforgettable, and sometimes overwhelming experience. I own a great debt of thanks to many people for the support they have provided.

First and foremost, I wish to express my deep gratitude to my supervisor, Prof. Jules Griffin, the best supervisor I could dream of. It was his professional guidance, unwavering support, and genuine caring and faith in me that had kept me working every time I wanted to give up during the course of this work, without whom this Ph.D. thesis would never have been written. I am also deeply grateful to Dr. Andrew Murray for providing the animals and his kind help with animal work. I'd like to give special thanks to my colleagues Xinzhu Wang, Yajing Chu, and Helena Matthews, who laid the groundwork for the obesity and aging animal study. And many thanks to Lee Roberts, Animesh Acharjee, James West, Steve Murffit, Zsuzsanna Ament, Helene Mobbs, Ben McNally and all the past and present members of the Griffin group, all of whom have offered their technical expertise and advice, gave generous amount of their time with me and have always been a pleasure to work with.

I am very grateful to all my friends met in Cambridge. Thank you for your friendship, support, and being encouraging making my time at Cambridge special. It is due to you that I have so enjoyed my time in Cambridge. I would always recall our memorable moments. Special thanks to my parents for their enduring support and encouraging me to pursue enlightenment and precious knowledge, to my sister, who passed her genuine caring over the telephone in the early days of my overseas student life. Lastly, I would like to thank Teng for her love and solid support during this long dissertation journey. I will never forget the moment I met her by the River Cam the first day I stepped into my college. Meeting and marrying her in Cambridge is the greatest gift from heaven. I dedicate this thesis to my parents and my lovely wife.

Table of Contents

Declaration	2
Abstract	3
Publication	4
Presentation	4
Acknowledgments	5
Table of Contents	6
Abbreviations	10
Chapter 1 Introduction	14
1.1 Obesity and Lipid Metabolism.....	14
1.1.1 Obesity, Energy Homeostasis, and Metabolic Syndrome	14
1.1.2 Sources of Fats and Lipid Synthesis	15
1.1.3 Lipolysis and Oxidation of Fats	18
1.1.4 Transport of Fats and Cholesterols	20
1.1.5 Diseases and Ectopic Fat Storage	21
1.2 Adipose Tissue.....	23
1.2.1 Regulation of Adipogenesis	24
1.2.2 Lipid Metabolism in Adipocytes.....	25
1.2.3 Adipose Tissue Hormones and Cytokines	27
1.2.4 Adipose Tissue and Inflammation	27
1.3 Regulation of Lipid Acyl Composition.....	29
1.3.1 Elongases and Desaturases.....	31
1.3.2 Sterol Regulatory Element-binding Proteins (SREBPs).....	36
1.4 Epigenetics and One-carbon metabolism.....	38
1.5 Mass Spectrometry in Metabolomics and Lipidomics.....	39
1.5.1 Generating Ions: Ionisation	40
1.5.2 Mass Analyser and Direct Infusion-Mass Spectrometry.....	41
1.5.3 Gas Chromatography-Mass Spectrometry	45
1.5.4 Liquid Chromatography-Mass Spectrometry.....	47
1.6 Obese mouse models.....	49
1.6.1 The <i>ob/ob</i> mouse model.....	50
1.6.2 The PPAR α null mouse model.....	51
1.7 Project Aims.....	53

Chapter 2 Materials and methods	55
2.1 Chemicals and Reagents	55
2.2 Animals and diets.....	56
2.3 Lipid Extraction	57
2.3.1 Fatty Acids (FAs) and Triacylglycerols (TGs)	57
2.3.2 Glycerophospholipids (PCs) and 1-carbon metabolites	58
2.4 GC-MS analysis for total Fatty Acids.....	59
2.5 DI-MS/MS analysis for neutral lipids.....	60
2.6 UPLC-MS analysis for phospholipids	61
2.7 Determination of 1-carbon metabolites by UHPLC-SRM-MS.....	63
2.8 Measurement of DNA Percent Methylation	65
2.9 Microarray analysis of mouse adipose tissue.....	66
2.10 Data analysis methods.....	67
Chapter 3 Lipidomics of High-fat-diet and <i>ob/ob</i> mouse models of obesity	69
3.1 Introduction.....	69
3.2 Aims and Objectives	70
3.3 Materials and Methods.....	70
3.3.1 Animals and diets.....	70
3.3.2 Lipid Extraction	71
3.3.3 GC-MS analysis for total Fatty Acids.....	71
3.3.4 DI-MS/MS analysis for neutral lipids	71
3.3.5 UPLC-MS analysis for phospholipids	71
3.3.5 Data analysis	71
3.4 Results.....	71
3.4.1 Physiological characteristics	71
3.4.2 Increase of oleic acid in adipose tissue is the key feature of both obesity and aging	73
3.4.3 Multivariate analysis of lipids in adipose tissues from different mouse models.....	78
3.4.4 Neutral lipids and phospholipids exhibit opposite changes in chain length and unsaturation in <i>ob/ob</i> mice.....	82
3.4.5 The High-fat diet (HFD) itself is the determining factor for the lipid composition in mice adipose tissue	83
3.4.6 Longer triacylglycerides (TGs) and saturated phosphatidylcholines (PCs) accumulate in adipose tissue of aged mice.....	85
3.5 Discussion.....	92
3.6 Conclusions.....	95
Chapter 4 Transcriptomics demonstrates that the peroxisome, AMPK, and PPARγ pathways are most perturbed in adipose tissue during the progression of obesity and during aging	97

4.1 Introduction.....	97
4.2 Aims and objectives.....	98
4.3 Materials and Methods.....	99
4.3.1 Animals and diets.....	99
4.3.2 Sample preparation and microarray analysis	99
4.3.3 Statistical analysis	99
4.4 Results.....	100
4.4.1 Overview and correlation of the transcriptomic changes in adipose tissue <i>ob/ob</i> genotype, HFD diet intake, and aging factors	100
4.4.2 Gene Ontology (GO) enrichment analysis reveals the different regulation of inflammatory and metabolic pathways in adipose tissue of <i>ob/ob</i> mice fed on an HFD.....	105
4.4.3 KEGG pathway enrichment analysis reveals the different regulation of inflammatory and metabolic pathways in adipose tissue of <i>ob/ob</i> fed on HFD	116
4.4.4 The expression pattern of selected genes in lipid metabolism and adipose tissue demonstrated the similarity between lipidomic and transcriptomic results	124
4.5 Discussion.....	127
4.6 Conclusion	134
Chapter 5 One-Carbon Cycle and DNA Methylation in Adipose Tissue of High-Fat-Diet and <i>ob/ob</i> mouse models.....	135
5.1 Introduction.....	135
5.2 Aims and objectives.....	136
5.3 Materials and Methods.....	136
5.3.1 Animals and diets.....	136
5.3.2 Determination of 1-carbon metabolites by UHPLC-SRM-MS.....	137
5.3.3 Measurement of DNA Percent Methylation	137
5.3.4 Multivariate statistical analysis.....	137
5.4 Results.....	138
5.4.1 1-carbon metabolism in adipose tissue of mice changes significantly with genotypes and correlates well with Phosphatidylcholine data.....	138
5.4.2 Leptin deficiency results in significant changes in DNA methylation status to influence the gene expression.....	143
5.5 Discussion.....	145
5.6 Conclusions.....	148
Chapter 6 The PPARα null mouse is characterized by saturated fatty acids in white and brown adipose tissues.....	149
6.1 Introduction.....	149
6.2 Aims and objectives.....	151
6.3 Materials and Methods.....	151

6.3.1 Animals and diets.....	151
6.3.2 Lipid Extraction	152
6.3.3 GC-MS analysis for total Fatty Acids.....	152
6.3.4 DI-MS/MS analysis for neutral lipids.....	152
6.3.5 UPLC-MS analysis for phospholipids	152
6.4 Results.....	153
6.4.1 Overview of the lipid changes in brown and white adipose tissues from PPAR α null mice	153
6.4.2 Palmitoleic acid, oleic acid, and linoleic acid decreased in inguinal adipose tissues from PPAR α null mice compared with wild-type controls.....	155
6.4.3 Short and unsaturated triacylglycerides are increased in inguinal adipose tissues from PPAR α null mice	157
6.4.4 Polar lipids were changed significantly in both brown and white adipose tissues from PPAR α null mice	159
6.5 Discussion.....	162
6.6 Conclusions.....	165
Chapter 7 Summary and Future Directions.....	166
7.1 General discussion and summaries	166
7.2 Limitations of the study	168
7.3 Future directions	170
References.....	173

Abbreviations

1-C	One-carbon
ACC	Acetyl-CoA carboxylase
ACS	Acyl-CoA synthase
ATP	Adenosine triphosphate
Agpat6	1-acylglycerol-3-phosphate O-acyltransferase 6
BAT	Brown adipose tissue
BD	Bligh and Dyer
BMI	Body mass index
Calr3	Calreticulin 3
CDP	Cytidine diphosphate
ChREBP	Carbohydrate-responsive element-binding protein
DHAP	Dihydroxyacetone phosphate
DI-MS	Direct infusion-mass spectrometry
DNL	<i>De novo</i> lipogenesis
Edem1	ER degradation-enhancing alpha-mannosidase-like 1
Elov11-7	Elongation of very long chain fatty acids protein 1-7
ER	endoplasmic reticulum
ESI	Electrospray ionisation
FAMES	Fatty acid methyl esters
Fads1/2	Fatty acid desaturase 1

FAS/Fasn	Fatty acid synthase
FAT	Fatty acid translocase
FABP	fatty acid-binding protein
FFA	Free fatty acid
GO	Gene Ontology
HFD	High-fat diet
¹ H-NMR	¹ H-Nuclear magnetic resonance
HPLC	High-performance liquid chromatography
HSL	Hormone-sensitive lipase
HTGL	Hepatic triglyceride lipase
HUFA	Highly unsaturated fatty acid
IL-6	Interleukin 6
Insig1/2	Insulin Induced Gene ½
KEGG	Kyoto Encyclopaedia of Genes and Genomes
LPL	Lipoprotein lipase
LC-MS	Liquid-chromatography mass spectrometry
LDL	Low density lipoprotein
m/z	Mass-to-charge
Mboat1/2	membrane bound O-acyltransferase domain containing ½
MC4R	Melanocortin receptor 4
MRM	Multiple reaction monitoring

MS	Mass spectrometry
MS/MS	Tandem mass spectrometry
MTP	Mitochondrial trifunctional protein
MUFA	Monounsaturated fatty acid
Myc	Myelocytomatosis gene
NIH	National Institute of health
NIST	National Institute of standards and technology
OPLS-DA	Orthogonal partial least squares discriminate analysis
O2PLS	Two-way orthogonal partial least squares
PC	Phosphatidylcholine
PCA	Principal components analysis
PE	Phosphatidylethanolamines
PLS	Partial least squares
PLS-DA	Partial least squares discriminate analysis
PPAR $\alpha/\delta/\gamma$	Peroxisome proliferator activated receptor $\alpha/\delta/\gamma$
PPREs	Peroxisome proliferator response elements
Pgc1 α/β	PPAR γ coactivator 1- α/β
PUFA	Polyunsaturated fatty acid
RCD	Regular chow diet
ROS	Reactive oxygen species
RXR	9-cis-retinoic acid receptor

SAM	S-adenosylmethionine
SCD	Stearoyl-CoA desaturase
SPE	Solid Phase Extraction
Srebf1/2	Sterol Regulatory Element Binding Transcription Factor 1/2
SREBP-1c	Sterol regulatory element-binding protein-1c
TCA	Tricarboxylic acid
TG/TAG	Triacylglycerol
THF	Tetrahydrofolate
T2DM	Type 2 diabetes mellitus
TZD	Thiazolidinediones
UCP	Uncoupling protein
UPLC	Ultrahigh pressure liquid chromatography
VIP	Variable influence on projection
VLDL	Very low density lipoproteins
WAT	White adipose tissue
WHO	World health organisation
WT	Wild-type
Xbp1	X-box binding protein 1

Chapter 1 Introduction

1.1 Obesity and Lipid Metabolism

1.1.1 Obesity, Energy Homeostasis, and Metabolic Syndrome

The prevalence of obesity has become a serious worldwide health problem, with the number of individuals classed as being obese (body mass index, BMI ≥ 30 kg/m²) doubling since 1980. In 2014, nearly 2,000,000,000 adults worldwide were estimated as being overweight and, of these, more than 500,000,000 were classed as obese according to the World Health Organisation (WHO) [1]. The fundamental cause of obesity is a positive energy balance where energy intake is greater than energy expenditure. All living organisms depend on the homeostasis of a variety of internal conditions, such as body temperature, cell number and size, acidity and alkalinity, blood glucose concentration, water and ion concentrations. Metabolic control mechanisms are required for the maintenance of energy homeostasis within an organism depending on the needs of the cell and the availability of substrates. Anabolic and catabolic pathways of basic substrates (amino acids, carbohydrates, lipids, and nucleic acids) are interconnected by intermediates which flow in cycles as both products of one reaction and substrates for subsequent reactions. For example, the Randle cycle describes the dynamic interactions between glucose and fatty acid pools [2].

After long-term intake of high-calorie foods, either high-carbohydrate or high-fat, fats accumulate in the adipose tissue (obesity) and at some point, the storage capacity of adipose tissue is exceeded and ectopic fat deposition rises followed by dysfunctions in the whole metabolism system. Obesity is a major risk factor for a number of diseases and a component in all definitions of metabolic syndrome, which is a clustering of interrelated factors that increase the risk of developing cardiovascular disease and Type 2 diabetes mellitus (T2DM) [3]. Diabetes occurs when the islets of Langerhans of the pancreas fail to produce enough insulin (type I) and/or metabolic tissues are unresponsive (resistant) to insulin (type II, T2DM). There are multiple definitions for metabolic syndrome arising from variations in the emphasis of the components of this disorder. For example, the WHO focuses on the risk factors associated with developing T2DM while the International Diabetes Foundation (IDF) emphasizes the effects of increased visceral adiposity. The principal contributing factors can be grouped in four main categories: abdominal (visceral) obesity, insulin resistance (hyperglycemia and

hyperinsulinemia), atherogenic dyslipidemia (high serum triacylglycerol (TAG) and decreased high-density lipoproteins (HDL) concentration) and endothelial dysfunctions (microalbuminuria and hypertension). Insulin resistance, T2DM, and cardiovascular diseases have been strongly associated with obesity-caused excess fat deposition and disturbed lipid metabolism.

While many factors in terms of genetics and the environment are involved in energy balance, diet, physical inactivity, and the intrauterine environment have been highlighted as major causes [4]. The extra energy intake in the diet is manifested primarily as an excess accumulation of fat of adipose tissues. At the beginning of this process, the organism remains healthy as excess energy is predominantly stored as triacylglycerides in the adipose tissue without disturbing any of the function of this tissue or other tissues across the body. During progression to ectopic fat storage, fat accumulates in the circulation system, liver, heart, and other non-adipose tissues. The accumulated fat mass and increased number of fat cells are associated with an increase in the risk for developing T2DM, cardiovascular diseases (CVD), chronic kidney disease (CKD), non-alcoholic fatty liver disease (NAFLD) [5] and several types of cancer [6], and as a result has been found to reduce life expectancy. However, the detailed pathophysiological mechanisms behind the development and maintenance of obesity and how 'benign obesity' turns into morbidity and mortality have not been fully defined. Although a few genes have been identified that fundamentally influence BMI [7, 8], the communal genetic factors of obesity are still largely unknown, and currently thought to be able to only explain a proportion of the risk of how obesity proceeds to disease.

1.1.2 Sources of Fats and Lipid Synthesis

Neutral fats, also referred to as triglycerides (TG), are a subgroup of lipids which are esters of three fatty acid (FA) chains and the alcohol glycerol. 95% of the lipids obtained from the food are TGs, with phospholipids (4.5%) and other lipids as the remainder. The major sources of FAs for TG storage are: food-derived FAs through the digestive system, *de novo* lipogenesis (DNL) in the liver and adipose tissue, and modifications (desaturation and elongation) of the existing FAs.

Feeding behavior is mainly controlled by the hypothalamus and pituitary. Appetite is a complex process resulting from the integration of numerous signals by the hypothalamus [9-12]. Neural

signals, hormonal signals such as leptin, cholecystokinin (CCK) and ghrelin, and nutrient signals such as glucose, free FAs, and amino acids are integrated by the hypothalamus. A specific sequence of neurotransmitters transported through the orexigenic or anorexigenic neurons in the hypothalamus alter food intake. The liver and gastrointestinal tract also cause meal termination by signaling through the vagus nerve to the nucleus of the solitary tract (NTS) [13-15]. Other mechanisms determining the absorption of dietary lipids through the intestine include food agitation action in stomach, solubilisation (emulsification) by bile salts, and digestion of lipids via various lipases in the gastrointestinal tract, all of which transform dietary TGs into free FAs and a mixture of mono- and diglycerides (MG and DG) [16]. The re-synthesis of TGs then occurs in the body, followed by solubilisation in lipoprotein complexes, chylomicrons in intestinal mucosal cells and very low-density lipoproteins (VLDLs) in the liver, which are released into the circulation system (blood or lymph) for delivery to the various tissues for energy production or storage [17, 18].

Lipogenic enzymes, desaturases and other enzymes indirectly involved in the *de novo* lipogenesis (DNL) can control long-term levels of particular TGs through changes in gene expression following hormonal or nutritional stimuli (substrate adaptive changes) [19-22]. Acetyl-CoA generated in the mitochondria from pyruvate dehydrogenase (PDH) and fatty acid oxidation is transported to the cytoplasm via the tricarboxylate transport system. Then acetyl-CoA is activated by the synthesis of malonyl-CoA, which is the first committed step of the fatty acid synthesis. Acetyl-CoA Carboxylase (ACC) catalyzes the synthesis of malonyl-CoA and is the major site of regulation of fatty acid synthesis [23-27]. This rate-limiting enzyme is allosterically activated by citrate and inhibited by palmitoyl-CoA and other short- and long-chain fatty acyl-CoAs. Glutamate and other dicarboxylic acids can also allosterically activate the ACC. The activation effect of insulin and the inhibition effect of α -adrenergic receptors on the ACC activity might be partly through regulating the phosphorylation of ACC [28, 29]. The synthesis of FAs from acetyl-CoA and malonyl-CoA is carried out by fatty acid synthase (FAS) [30-32]. The primary FA synthesized by FAS is palmitic acid in most tissues in mammals, which is then released from the enzyme. Palmitate may undergo separate elongation and/or unsaturation to yield other FA molecules. Insulin can stimulate both ACC and FAS synthesis while starvation inhibits the synthesis of these enzymes [30, 33, 34]. Moreover, sterol regulatory element-binding protein (SREBP1) and leptin have activating and inhibitory effects on the expression of lipogenic genes, respectively [35]. In turn, elongation and desaturation of FAs are controlled by essential enzymes such as long-chain fatty acid elongase 6 (ELOVL6)

and stearoyl-CoA desaturase-1 (SCD-1, Δ^9 desaturase), both of which are also SREBP-1c targets [36]. A change in the set point control of insulin-induced gene 1 (Insig1) / SREBP1 facilitates lipogenesis and availability of appropriate levels of fatty acid unsaturation through SCD-1 expression [37, 38].

The observed increase in fatty acid unsaturation may also be a response of ‘overloaded’ adipose tissue in obese animals, and a mechanism to cope with the large intake of fats by improving membrane receptor functionality [37, 39-41]. Specific FAs of different degrees of unsaturation can have an impact on these desaturases’ activity. For instance, saturated FFAs activate the expression of SCD-1 [42, 43]. Polyunsaturated fatty acids (PUFAs) play a key role in the regulation of three classes of desaturase, i.e. Δ^9 , Δ^6 , and Δ^5 , which are present in humans [19, 44-48]. Interestingly, monounsaturated fatty acids (MUFAs) don’t exhibit such kind of effects on the expression of either SCD-1 or other desaturases. Other transcription factors involved in the control of lipogenesis and modifications include proliferator-activated receptors (PPAR α , γ , δ), carbohydrate response element binding protein (ChREBP), and liver X receptor alpha (LXR α) [49, 50]. High insulin and carbohydrate concentrations can activate SREBP1c and ChREBP transcription factors [51] inducing lipid remodeling.

The FAs are activated to acyl-CoAs through various acyl-CoA synthetases and incorporated into TGs stored for future use. In virtually all cells except adipocytes and intestinal enterocytes, TG synthesis begins with glycerol phosphorylated by glycerol kinase to generate glycerol-3-phosphate. Two activated FAs are successively added resulting in the production of lysophosphatidic acids (LPA) and phosphatidic acid (PAs), respectively. The phosphate group of the phosphatidic acid is then replaced by a fatty acid by phosphatidic acid phosphatase (PAP1) and a TG is formed. There is no expression of glycerol kinase in adipose tissue so the building block for TG is the glycolytic intermediate, dihydroxyacetone phosphate (DHAP) which is reduced to glycerol-3-phosphate by a cytosolic glycerol-3-phosphate dehydrogenase. In the intestinal enterocytes, monoacylglycerides (MAGs) undergoes acylation with two fatty acyl-CoA yielding TGs which can then be incorporated into chylomicrons. [52, 53]

Another structurally and functionally important lipid class synthesized from phosphatidic acid is the phospholipids (PL). Phospholipids are in part synthesized by esterification of alcohol (serine, ethanolamine, choline, etc.) to the phosphate of phosphatidic acid. Another mechanism

for the synthesis of PLs is to utilize cytidine diphosphate (CDP) - activated 1, 2-diacylglycerol and an inactivated polar head group. Among these phospholipids, phosphatidylcholines (PC) are a major component of biological membranes. Length and saturation of the hydrocarbon tails of PCs are important in characterizing the cell membrane and also determines specific processes such as signal transduction. They contain primarily palmitic or stearic acid (saturated FAs) at carbon 1 and primarily oleic, linoleic or linolenic acid (unsaturated FAs) at carbon 2. A third pathway to generate PC involves the conversion of either phosphatidylserine (PS) or phosphatidylethanolamine (PE) to PC. The conversion of PE to PC requires a series of three methylation reactions using S-adenosylmethionine (SAM) as a methyl group donor, while the decarboxylation of PS leads to PE generation. The phospholipids in membranes are undergoing continuous degradation and remodeling and the FA distribution at the C-1 and C-2 positions of glycerol are continually in flux. Thus, the FA pool which originates from either dietary lipids or DNL plays a vital role not only in energy homeostasis by remodeling TGs but also in maintaining cell membrane functionality and lipid signaling. [54-56]

1.1.3 Lipolysis and Oxidation of Fats

The TG components of VLDL and chylomicrons are hydrolyzed to free FAs and glycerol in the capillaries of various tissues by lipoprotein lipase (LPL) or hepatic triglyceride lipase (HTGL) [57-60]. The glycerol is returned to the liver and kidney via the blood and can be converted to DHAP or glycerol-3-phosphate for reuse in TG synthesis. The free FAs are absorbed by most cells for oxidation to generate energy or storage in the form of TGs, with the majority of storage occurring in adipose tissue. The fatty acid receptors include fatty acid translocase (FAT/CD36), plasma membrane-associated fatty acid-binding protein (FABP_{pm}), and fatty acid transport proteins (FATPs). The expression of lipoprotein lipases are increased by insulin and decreased by fasting in adipose tissue. In response to energy demands, the FAs stored in TGs are mobilized for use by other tissues. This process uses a variety of lipases to control the direction of energy flux. The intravascular lipases are mostly LPL and HTGL, while the primary intracellular lipases are adipose triglyceride lipase (ATGL), hormone-sensitive lipase (HSL), monoglyceride lipase (MGL), and lipase A (LIPA). ATGL and HSL are involved in hydrolyzing TGs to DGs and MGs in lipid droplets (LDs), while MGL releases the final FA chain and glycerol from MG in the cytosol. LIPA is the central lipase for lysosomal lipid metabolism, in particular, cholesteryl ester metabolism. All the lipases are controlled by a complex series of interrelated signaling cascades determining the storage or release of

metabolic energy in the form of FAs. For example, epinephrine and glucagon stimulate FA release from TGs in lipid droplets, whereas insulin inhibits release and induces storage of fats through inhibiting HSL. This is a cAMP-dependent pathway in which protein kinase A (PKA) regulates the activity of ATGL and HSL. The LD-associated proteins, such as caveolin and perilipin-1, play an important role in this signaling pathway to control lipid release. FAs released from adipose tissue are bound to albumin in the blood for transport to peripheral tissues. Then the FAs released from FA-albumin complexes or lipoproteins are taken into cells via fatty acid translocase FAT/CD36, fatty acid binding protein (FABP_{pm}), or fatty acid transport proteins (FATPs). In the cytosol, the intracellular lipid-binding proteins like FABPs reversibly bind these FAs to transport them throughout the various cellular compartments, including the mitochondria, peroxisomes, endoplasmic reticulum, and nucleus. [61-64]

Oxidation of FAs occurs primarily in the mitochondria and the peroxisomes, playing a profound role in overall lipid homeostasis. Short- (4-8 carbon atoms) and medium-chain (6-12 carbon atoms) fatty acids (SCFAs and MCFAs) are oxidized exclusively in the mitochondria. Long-chain fatty acids (10-16 carbons, LCFAs) are oxidized in both the mitochondria and the peroxisomes. Very-long-chain fatty acids (17-26 carbons, VLCFAs) are preferentially oxidized in peroxisomes. The FAs are activated by the fatty acyl-CoA synthetases to form fatty acyl-CoA. The acyl-CoA molecules are transported into the mitochondria by the carnitine-acylcarnitine translocase (CAT) in the form of acyl-carnitine intermediate by the exchange actions of carnitine palmitoyltransferase 1 (CPT-1) and CPT-2. CPT-1 can be rapidly inhibited by the malonyl-CoA produced by ACC, which serves to prevent *de novo* synthesized FAs from entering the mitochondria and being oxidized. Finally, the re-generated fatty acyl-CoA molecules in the mitochondrial matrix undergo β -oxidation catalyzed by FAD-dependent acyl-CoA dehydrogenases and the mitochondrial trifunctional protein (MTP), resulting in the sequential removal of 2-carbon units in the form of acetyl-CoA. The acetyl-CoA generated in each round of β -oxidation enters the TCA cycle following conjugation with CoA for feeding the respiratory pathway with reducing potential (oxidative phosphorylation) to generate the end products CO₂ and ATP. The energy production of FA oxidation is significantly more than oxidation of carbohydrates (about 106 and 30 moles of ATP for complete oxidation of palmitate [65] and glucose [66], respectively).

The peroxisomal β -oxidation pathway [67-70] is similar to mitochondrial β -oxidation except that in the first oxidation step it is catalyzed by acyl-CoA oxidases rather than acyl-CoA

dehydrogenases. This is coupled with the reduction of O_2 to hydrogen peroxide (H_2O_2) which is degraded back to O_2 by the enzyme catalase. When catalase is not expressed highly enough for the clearance of the H_2O_2 , the increased release of reactive oxygen species (ROS) can result in damaged cell function and inflammation. For example, the damage to the pancreatic β -cell by ROS contributes to progressive insulin deficiency in obesity. There are as well other minor pathways of overall FA oxidation that may provide an effective means for the elimination of toxic levels of FAs in certain pathophysiological states, such as the microsomal ω -oxidation reactions [71-74].

1.1.4 Transport of Fats and Cholesterols

In circulation, a small proportion of free fatty acids (FFA) are bound to albumin, while most of the fats are transformed and emulsified within lipoproteins which have exterior amphiphilic proteins and lipids to be water-soluble and allow fats to move through the water inside and outside cells. Plasma lipoprotein particles include, from larger and less dense to smaller and denser (fat to protein ratio decreases): chylomicrons, very low-density lipoproteins (VLDL), intermediate-density lipoproteins (IDL), low-density lipoproteins (LDL) and high-density lipoproteins (HDL) [75-77]. These particles are synthesized in the small intestine (exogenous) or the liver (endogenous). In the exogenous pathway, dietary TGs are emulsified by bile and cleaved by pancreatic lipase into two FAs and one 2-monoacylglycerol and absorbed by enterocytes. In enterocytes, these lipids are transformed back into TGs and assembled with apolipoproteins B-48 (Apo B⁴⁸) along with cholesterols and phospholipids (PLs) to form nascent chylomicrons. The nascent chylomicrons circulate to the bloodstream through lymphatic vessels and form the mature chylomicrons after combining with Apo C -II and E which are obtained from interacting with HDL particles. The chylomicrons can activate lipoprotein lipase (LPL) to hydrolyze TGs and release glycerol and FAs into peripheral tissues, especially adipose and muscle. The hydrolyzed chylomicrons (chylomicron remnants) then circulate to the liver and interact with chylomicron remnant receptors via Apo E, followed by endocytosis by hepatocytes and hydrolysis by lysosomes. In the endogenous pathway, hepatocytes create FAs and TGs mainly via *de novo* lipogenesis (DNL). Bile is also produced in the liver from cholesterol. TGs and cholesteryl esters are assembled with Apo B-100 to form nascent VLDL particles. Like chylomicrons, nascent VLDL particles are released into the blood circulation and obtain Apo C-II and Apo E from HDL particles to form mature VLDL,

from which triglycerides would be removed by LPL and absorbed into peripheral tissues. The VLDL remnants are now called IDLs which can interact with the remnant receptors of hepatocytes and be re-absorbed by the liver. In the alternative, TGs of IDLs are removed by hepatic lipase producing LDLs (IDL remnants) which also circulate into liver and peripheral cells and are hydrolyzed by lysosomes. A residual fraction of LDLs is phagocytized by macrophages and turned into foam cells and deposit in atherosclerotic plaques (atherosclerosis) [78], which can lead to serious cardiovascular problems, including coronary heart disease (angina or heart attack) [79], carotid artery disease (stroke) [80, 81], chronic kidney disease [82] and chronic inflammatory disease [83]. All of these are common complications of obesity and diabetes [84, 85].

Animal fats are composed of mostly TGs, with lesser amounts of cholesterol and phospholipids. As mentioned above, cholesterol (or in form of cholesterol ester) is transported within lipoproteins along with TGs. Cholesterol is another important component (about 30%) of animal cell membranes, interacting with phospholipids and sphingolipids to maintain membrane integrity and alter membrane fluidity [86], and it also functions in intracellular transport and cell signaling processes [87, 88]. Just like other lipids, cholesterol is either from dietary sources or synthesized from acetyl CoA in a complex 37-step process beginning with the mevalonate pathway [89, 90]. Biosynthesis and absorption of cholesterol, which mostly occurs in the liver and the intestines, is regulated by cholesterol levels present through mechanisms that are only partly understood. SREBP is an important protein for the sense of intracellular cholesterol, which will be detailed in **Section 1.3.2**. So, it is clear that different lipids including TGs, PLs, and cholesterol are correlated and regulated through many homeostatic mechanisms. In addition, cholesterol is not only transported along with TGs within the lipoprotein, but also recycled by being excreted by the liver in a non-esterified form via bile into the digestive tract, and 95% is reabsorbed by the small intestine back into the bloodstream [91-93].

1.1.5 Diseases and Ectopic Fat Storage

Apart from cardiovascular diseases directly caused by atherosclerosis such as hypertension and coronary artery disease, the diabetic heart can also develop an abnormality in diastolic function and be at high risk of heart failure, an entity termed as diabetic cardiomyopathy [94, 95]. The structural changes in diabetic cardiomyopathy are often accompanied by fat droplet deposition.

The heart obtains FAs from the circulation in the form of albumin-FFAs, chylomicron-TAGs, and VLDL-TAGs, and the uptake rate is dependent on the FFA concentration in plasma. The FAs released from these lipoproteins can be absorbed passively by diffusion or actively by the fatty acid receptors (FAT/CD36, FABP_{pm}, and FATPs). In the cytosol, long-chain FAs are esterified to long-chain fatty acyl coenzyme A (CoA) by fatty acyl-CoA synthase (FACS). Fatty acyl CoA is mainly used in mitochondria for β -oxidation to supply energy for the heart, whereas some fatty acyl CoA is incorporated into TG by glycerolphosphate acyltransferase for storage. The TG synthesis increases when the plasma FA level is elevated in obesity. The excess TG deposition then can contribute to myocardial hypertrophy and fibrosis, and results in damage to the diastolic function of the heart. There have been many putative factors studied so far to explain the functional disorders in diabetic cardiomyopathies, such as deregulation of the renin-angiotensin system (RAS), intracellular Ca²⁺ homeostasis, increased cell death, and advanced glycosylation end-products. Another major etiological factor is metabolic derangement, especially disturbed lipid oxidation. In our previous study [95], a persistent increase in FA oxidation is observed in the heart of both type 1 (NOD mouse) and type 2 (high-fat diet (HFD)-fed *ob/ob* mouse), diabetic models. Increased oxygen consumption by FA oxidation led to a reduction in the efficiency of cardiac energy production and increased mitochondrial uncoupling through elevated levels of uncoupling protein 2/3 (UCP2/3). Production of reactive oxygen species (ROS) accumulated, accompanied by the damaged complex I of the electron transport chain. These processes finally resulted in myocardial mitochondrial dysfunction. Moreover, when FA uptake and oxidation is enhanced, the PPAR α signaling pathway is activated. This pathway increases fatty acid uptake and oxidation and up-regulates the expression and PDK4 while inhibiting GLUT-4 expression, resulting in decreased glycolysis and oxidative phosphorylation through the Randle cycle. Amino acid metabolism is also disturbed in the obese/diabetic heart. Increased circulating branched-chain amino acids (BCAAs, leucine, isoleucine, and valine) and higher protein degradation and turnover rates are observed in diabetic hearts. All of these lead to reduced respiratory capacity and a decrease in energy production for a contractile function of the heart. [96-98]

Ectopic fat storage also results in pathology in other tissues besides the cardiovascular system; for example, the most common liver disorder in developed countries, non-alcoholic fatty liver disease (NAFLD), is linked to insulin resistance and diabetes [99]. The disease begins as fat accumulation in the liver (hepatic steatosis), and sometimes it will progress to become non-

alcoholic steatohepatitis (NASH) characterized by lobular inflammation and ballooning degeneration. Up to 9% of patients with NASH will develop cirrhosis through fibrosis (thickening and scarring of connective tissue), and 40%-62% of patients with NASH-related cirrhosis will suffer complications including hepatocellular carcinoma (HCC) [100]. The liver is central to regulating storage, mobilization, and metabolism of macronutrients across the body. It is also notable that some advanced liver disease might be missed in this progression; for example, there are some cases of HCC progression in NASH without cirrhosis. In a previous study in our group, Chu and colleagues [99] identified many metabolic dysfunctions in livers of three animal models of steatosis, including increased activity of the urea cycle, fatty acid β -oxidation, total fatty acid content, total palmitoleic acid, total oleic acid, stearoyl-CoA desaturase (SCD, $\Delta 9$) activity and free fatty acids; and decreased choline metabolism, purine metabolism, omega-3 polyunsaturated fatty acids, phosphatidylcholines and short-chain acylcarnitines.

1.2 Adipose Tissue

Adipose tissue is a type of loose connective tissue principally comprised of adipocytes, but also containing macrophages, leukocytes, fibroblasts, adipocyte progenitor cells, and endothelial cells. There are two morphologically and functionally different adipose tissue forms: brown adipose tissue (BAT) and white adipose tissue (WAT). The development of these two forms involves the concerted cooperation of various transcription factors together with their coactivators and corepressors [101]. WAT comprises large lipid droplets which occupy no less than 90% of the cell in volume for the storage of fat, a thin peripheral cytoplasm, and the nucleus. The major functional role of WAT is as a reservoir of fat and insulation of the visceral organs, but it also participates in the regulation of glucose homeostasis, inflammation, angiogenesis, and hemostasis (blood coagulation). A variety of growth factors, cytokines, enzymes, and hormones are synthesized and secreted by mature adipocytes functioning as an endocrine and immune organ. On the other hand, BAT stores fats in numerous small lipid droplets which contains an abundance of mitochondria primarily tasked with oxidation of free fatty acids for non-shivering thermogenesis, especially in the neonate [102]. Molecular characteristics of BAT include expression of uncoupling protein 1 (UCP1) but no expression of leptin (UCP1⁺ and leptin⁻), while WAT shows the opposite expression pattern (UCP1⁻ and leptin⁺). Both WAT and BAT are highly vascularized and innervated [103, 104].

As the storage capacity of adipose tissue is exceeded at some point in obesity, TAGs and FFAs are released into the circulation and this leads to lipid accumulation in non-adipose tissues (ectopic fat storage) [105]. Ectopic fat is defined as the deposition of TGs within cells of non-adipose tissue that normally contain only a small amount of fats [106]. Both lipodystrophic patients and those with hypertrophic adipocytes exhibit insufficient storage capacity of adipose tissue and ectopic fat storage, resulting in insulin resistance [107, 108]. The detailed mechanism of how insulin resistance interacts with adipose tissue dysfunction has not been fully revealed, and there appears to be a number of mechanisms responsible. It is possible that the dynamic interactions of inflammatory, neural, endocrine and cell-intrinsic pathways lie beneath the etiology of insulin resistance [109].

The balance of some adipose tissue secretory proteins (adipokines) is also perturbed in obesity [110-113]. Disturbance of adipokine secretion and alteration of lipogenesis and lipolysis have been related to the occurrence and development of insulin resistance [114-117]. For example, leptin, the “satiety hormone” is secreted almost exclusively by adipocytes. Leptin regulates the amount of fats storage through directly affecting on food intake and energy expenditure, and also plays a critical role in the regulation of reproductive and immune function in humans [118] as discussed in Section 1.6.1. Increased adiposity also triggers innate immune receptors in adipose tissue and results in systemic inflammation, which combined with ectopic fat storage and disturbed adipokine production leads to dysfunction in the liver, skeletal muscle, gut, pancreas, and other organs. [119-121].

Thus, adipose tissue has an important impact on metabolic health across the whole body. There are far more underlying pathways for the pathophysiology of adipose tissue dysfunction which remain to be determined, which is of vital for us to understand the mechanism of and develop new treatment and diagnostic methods for obesity, MBS, T2DM, NAFLD, and cardiovascular diseases.

1.2.1 Regulation of Adipogenesis

The storage capacity of adipose tissue in part depends on the extent of adipocyte differentiation, expandability, and remodeling in obesity [50]. The pre-adipocyte which is the precursor of adipocyte differentiation is derived from the mesenchymal stem cells (MSCs) following receiving extracellular cues. CCAAT/enhancer binding protein alpha (C/EBP α) and

peroxisome proliferator-activated receptor gamma (PPAR γ) is the key transcription factors for the initial growth arrest of pre-adipocytes [122-124]. PPAR γ is the only factor without which the adipocyte differentiation cannot occur and no other factor has been identified that can rescue adipogenesis in the absence of PPAR γ . It is also involved in the regulation of a variety of key metabolic pathways such as lipid metabolism and glucose homeostasis. The C/EBP family of transcription factors also contain C/EBP β and C/EBP δ , which in part regulate the actions of C/EBP α and PPAR γ in mature adipocytes. The activation of C/EBP α enhances insulin sensitivity of adipose tissue. The general activation model of adipogenesis is AP-1, STAT5, KLF4, and KLF5 \rightarrow C/EBP β and C/EBP δ \rightarrow SREBP-1 and KLF15 \rightarrow PPAR γ and C/EBP α \rightarrow adipogenesis. The functions of SREBP-1 and PPAR γ will be discussed in more detail in Section 1.3. Adipogenesis can be controlled by transcription factor-mediated inhibition by members of the Krüppel-like factor family KLF2 and KLF3, GATA2 and GATA3, and members of interferon regulatory factor family IRF3 and IRF4. [122-124] Moreover, chromatin dynamics such as histone protein methylation and DNA methylation have important impacts on adipogenesis, which will be further discussed in Section 1.4.

1.2.2 Lipid Metabolism in Adipocytes

TG flux in adipose tissue is regulated by the dietary state (food intake/fasting), pancreatic and adrenal hormones, inflammatory processes and other pathophysiology processes. As discussed above, under ordinary conditions of positive energy input such as in the postprandial period, plasma TGs in VLDL and chylomicrons are released and hydrolyzed to free fatty acids (FFA) and glycerol via lipolysis catalyzed by LPL. Glycerol and FFAs are then taken up into the adipocytes by FAT/CD36, FABPpm, and FATPs. In the cytoplasm, monoacylglycerides (MAGs) and FFAs are transformed to acyl-CoA by acyl-CoA synthase (ACS). This process is then reversed in the cell resulting in TG storage in adipose tissue [114]. During negative energy input, the stored TGs are hydrolyzed by ATGL, HSL, and MGL back to FFAs (lipolysis), which are transported out of adipose tissue into the circulation, and taken up by other tissues and then go through β -oxidation to produce energy in the mitochondria [125] or peroxisome [126]. HSL is the only DG lipase identified currently but also has moderate hydrolytic activity on TG and CE, and it has the greatest activity against FAs in the sn-1/3 position. ATGL is a TG specific lipase expressed predominantly in adipose tissue. Other HSL-independent TG lipases include triacylglycerol hydrolase (TGH)/carboxylesterase 3 (predominantly expressed in the liver, also in mature adipocytes) [127, 128] and adiponectin. MGL is a specific MG lipase which has no

catalytic activity towards TG, DG or CE [129, 130]. TG uptake via FFAs and glycerol and synthesis occurs in multiple tissues, while lipolysis (release) takes place predominantly in adipose tissue. LPL and HSL are the rate-limiting enzymes in lipid uptake and lipolysis processes of adipose tissue, respectively. Moreover, there are some lipid droplet (LD) associated proteins involved in fat storage capacity of adipose tissue, such as perilipins which restrict access of TG lipases to substrates, acid-binding protein (aP2/FABP4/aFABP) that carry FFAs from the LD to the plasma membrane, caveolin-1 binding various classes of signaling molecules (e.g. PKA), lipotropin that shuttles HSL from the cytosol to the LD, and aquaporin (AQP7), a water and glycerol transport protein for glycerol export.

Many hormones are involved in the stimulation of adipose tissue TG hydrolysis via activating ATGL, HSL and other lipolysis events, including epinephrine, norepinephrine, and glucagon, but only insulin has been shown to inhibit FA release from adipose tissue. Insulin stimulates the synthesis and storage of TGs while inhibiting lipolysis in adipose tissue, acting by impeding HSL and stimulating LPL, which is vital for the regulation of fat content in adipocytes [131]. It also increases the rate of glucose uptake into adipose tissue and skeletal muscle through recruitment of GLUT 4 transporter, followed by transformation to fatty acids in adipose tissue via DNL. In obesity adipose tissue becomes refractory in terms of either the suppression effect of insulin on fat mobilization or its stimulatory effect on fat uptake and storage [132], resulting in augmented FFAs and TGs in blood. This gives rise to a positive feedback loop between circulating TGs and insulin resistance and makes the adipose tissue dysfunction worsen gradually [133, 134]. What's more, the expression of HSL is up-regulated by saturated FAs (stearate and palmitate) rather than unsaturated fatty acids (oleate and linoleate) [135], suggesting that lipolysis and release of FFA from adipose tissue would increase when saturated FAs are released from the dietary lipids or DNL. This contributes to further positive feedback regulation of insulin resistance and obesity and results in the development of lipotoxicity and MBS across the body.

Whitening (loss of mitochondria) and browning (mitochondrial biogenesis) of adipose tissue is another important way for the body to maintain energy balance in response to environmental challenges [136]. BAT was thought to be active only in the neonatal period for humans. Recently, it has been found that adults still retain some metabolically active BAT deposits which can be activated by cold and the sympathetic nervous system. The most studied regulator of the action of BAT is norepinephrine [137]. Cold exposure produces norepinephrine which

binds to β_3 -adrenergic receptors, resulting in activation of G_s type proteins. The G_s proteins stimulate phosphorylation and activation of HSL and release of FFAs via the adenylate cyclase \rightarrow cAMP \rightarrow PKA pathway. The released FFAs are used for oxidation in mitochondria or activating the uncoupling protein 1 (UCP1/thermogenin) to uncouple the proton gradient in mitochondria leading to a release of energy as heat. Norepinephrine can promote the proliferation of brown preadipocytes and the differentiation of mature brown adipocytes, and prevent brown adipocytes from undergoing apoptosis. The expression of the UCP1 gene is also under the control of the norepinephrine. It has not been fully determined how the balance between stimulatory and inhibitory actions of norepinephrine on heat generation is determined. Furthermore, like WAT, BAT also secretes certain adipokines as an endocrine/autocrine/paracrine organ, but this role is not as well established as for WAT. Identified signaling factors produced by BAT include FGF2, IGF-1, NGF, VEGF, NO, adipisin, prostaglandins, and adenosine. [138-140]

1.2.3 Adipose Tissue Hormones and Cytokines

J.M. Friedman's discovery of the "satiety factor" leptin initiated the discovery of many hormonal mechanisms that regulate food intake and energy storage, including ghrelin, orexin, and adiponectin, as well as adipokines. Adipokines are a variety of bioactive peptides secreted by adipose tissue, including leptin, agouti, angiotensin II, tumor necrosis factor-alpha ($TNF\alpha$), prostaglandins, adiponectin, plasminogen activator inhibitor-1 (PAI 1) and interleukin 6 (IL-6), and act both locally and distally through autocrine, paracrine and endocrine effects. In obesity, the production of most adipokines are associated with changes to maintain normal metabolic pathways in terms of appetite and energy balance, lipid metabolism, insulin sensitivity, immunity, blood pressure, angiogenesis, and haemostasis, all of which are linked with cardiovascular diseases when regulation is no longer controlled [116, 117]. In morbid obesity the endocrine functions of adipose tissue can be impaired, resulting in reduced adipokine production necessary for maintaining normal biological homeostasis. [110, 141-144]

1.2.4 Adipose Tissue and Inflammation

The increase in secretion of adipose tissue-derived cytokines in obesity is associated with a number of inflammatory responses. The infiltration of macrophages into adipose tissue is significantly increased during obesity and is regulated by the monocyte chemotactic protein-1 (MCP-1). The macrophages are a primary source of pro-inflammatory cytokines. [145]

The two pro-inflammatory cytokines mostly studied in adipose tissue during obesity are TNF- α and IL-6. Their increase in circulation in obesity is directly correlated with insulin resistance and T2DM. Both IL-6 and TNF- α stimulate the release of pro-inflammatory cytokines such as JUN N-terminal kinase (JNK) and nuclear factor kappa B (NF κ B). The activation of JNK increases the serine phosphorylation of the insulin receptor and insulin receptor substrate (IRS), leading to impaired insulin signaling [146, 147]. JNK and NF κ B also activate pro-inflammatory genes which result in a self-perpetuating cycle of increased inflammatory cytokine release. Moreover, TNF- α can stimulate the expression of endothelial nitric oxide synthase (eNOS) leading to an accumulation of ROS and increased oxidative stress and endoplasmic reticulum (ER) stress [148]. Oxidative stress, in turn, triggers the cell to release more NF κ B. The anti-inflammatory adipose tissue-derived hormone, adiponectin, suppresses the production of TNF- α and IL-6 but also results in suppression of adiponectin production and secretion. In addition, the increased acute phase proteins from the liver following IL-6 secretion may contribute to the promotion of sepsis.

There are 2-way paracrine interactions between adipose and lymph tissues, with the latter surrounded by pericapsular adipose tissue. Firstly, leptin secreted by the adipocytes protects T-Cells from apoptosis and enhances the switching of T-cells to a Th1 response, resulting in an increase of pro-inflammatory cytokine production and release. Leptin is involved in many signal transduction pathways in the immune and endothelial cell [149, 150]. It stimulates the expression of adhesion molecules when binding its receptor on endothelial cells. This increases the ability of neutrophils and other leukocytes to adhere to the endothelium, resulting in local inflammatory processes.

In addition, it has been reported that palmitoleate (C16:1) might act like adipokines to suppress inflammation and inhibit apoptosis of cells induced by glucose and saturated FAs [151]. Moreover, the interaction of ω -6 with ω -3 fatty acids together determines the production and subsequent action of eicosanoid precursors, which is important for the regulation of inflammation [152]. Conversely, depletion of ω -3 long-chain PUFAs are associated with hepatic insulin resistance, enhanced sterol regulatory element-binding protein 1c (SREBP-1c) and decreased peroxisome proliferator-activated receptor alpha (PPAR- α) activity, favoring lipogenesis over FA oxidation [153].

1.3 Regulation of Lipid Acyl Composition

Interestingly, it is not only the total amount of fat storage which has an impact on adipose tissue health, but also the lipid composition; in particular, the chain length and unsaturation of fatty acyl chains of specific lipids have important effects on energy balance and pathophysiology of MBS, T2DM and cardiovascular diseases [154]. There have been a number of metabolomics studies [155-160] aimed at finding potential lipid biomarkers in plasma or urine for diagnosing insulin resistance and T2DM, but evidence that either support or contradict their effectiveness is conflicting, particularly in terms of whether lipid changes are associated with fatty acid consumption direct from the diet or synthesized from glucose as a result of DNL. It is necessary to elucidate the mechanism of how these lipids are formed, control normal cell functions and their relationships with disease progression before considering them as biomarkers.

One of the major reasons for controlling *in vivo* lipid composition is to maintain proper physiochemical properties of the membrane bilayer. The average chain length of a biological membrane for eukaryotic cells from vertebrate species is strictly maintained around 18 carbon atoms, and the relative distribution between SFAs and UFAs typically follows a ratio of 2:3 [161]. The membrane pacemaker hypotheses of aging and metabolism [162] suggest that both decreasing longevity and increasing metabolic rate are correlated with increases in unsaturation of lipids within membranes. The membrane pacemaker hypothesis of aging postulates that PUFAs are more easily oxidized than saturated fatty acids or MUFAs because of the susceptibility of the *bis*-allylic hydrogens (attached on the single carbon separating two double bonds) to lipid peroxidation (the oxidative degradation of lipids whose electrons are “stolen” by free radicals [163]). This is a particular problem in mitochondrial membranes as the peroxidized lipids can induce oxidation of macromolecules, in particular, mitochondrial DNA, leading to cellular dysfunction and decline in tissue function [164-167].

Another reason for the tight regulation of membrane composition is that differences in protein activity are caused by the differences in membrane fluidity. Generally, saturated fatty acids make the membrane bilayer less fluid and inactive, which in turn has consequences for protein function and membrane transport [168], whereas unsaturated fatty acids result in a more plastic membrane and improve the function of membrane receptors and sensitivity to hormones [169, 170]. The geometry of the *cis*-double bond induces a bend in the molecule, thereby precluding rigid lipid bilayers. One process of high relevance to T2DM is glucose transport across the

membrane which may be influenced by membrane fluidity [171]. There have been studies reporting the relationship between membrane fluidity of erythrocytes and insulin sensitivity in hypertensive subjects [172], and also changes in the composition of membrane lipids associated with increased insulin sensitivity in skeletal muscles after physical training [173]. However, a study in rat brown adipose tissue [174] showed that the increase of mitochondrial activity in this tissue was related to phospholipid composition changes rather than to membrane fluidity. PUFAs result in an even greater increase in plasticity of membranes [40, 175], and have been associated with improved cardiac function following arrhythmias.

However, changes in membrane fluidity do not explain the effects of some highly unsaturated fatty acids (HUFAs, >2 double bonds), such as DHA, on protein activity as the overall membrane fluidity is only significantly increased by the first two double bonds added to a saturated acyl chain, with each subsequent double bond having less effect on membrane fluidity [166, 176]. One mechanism invoked recently is that some form of energy transfer between the flexible PUFAs and the membrane-bound proteins occur through collisions [177-181]. One piece of evidence put forward is that the lateral pressure of membrane phospholipids, which is presumed to be related to both the unsaturation of the membrane and the number of molecular collisions in the membrane, was found to be correlated with the activity of Na^+/K^+ -ATPase [180]. This presumed mechanism relied somewhat on the assumption that membranes are homogeneous environments where collisions happen in equal likelihood between proteins and any lipid molecules. However, there is increasing evidence that membranes are composed of different lipid/protein domains, including lipid rafts [182-184] mainly composed of phospholipids, sphingolipids, and cholesterol with saturated fatty acyl chains. Some proteins are resident in the lipid rafts and some move between rafts and non-raft areas of the membrane, e.g. Na^+/K^+ -ATPase, so there could be additional mechanisms for the effects of increasing the PUFA content of cell membranes on activities of enzymes such as the Na^+/K^+ -ATPase. The addition of HUFAs, especially DHA, to the membrane increases the formation and stability of lipid raft domains, which could be an alternative mechanism explaining the interactions between membrane lipid unsaturation and protein activity [183, 185, 186]. It is found that the steric incompatibility of DHA and cholesterol leads to more cholesterol incorporated into ordered lipid rafts while driving phospholipids with DHA into disordered non-raft domains. This suggests that the segregation of particular types of proteins into raft or non-raft domains might control their activity accordingly [187-189], providing an explanation for the control of Na^+/K^+ -ATPase activity by PUFA-mediated lipid domain formation. However, this idea still

needs to be tested. In addition, increases in the unsaturation of membranes could affect membrane structure and phase behavior, increasing the propensity of membranes to form hexagonal (H_{II}) phases [190-192]. The H_{II} phase propensity stimulates recruitment of certain signaling proteins into membranes and increases their activity, such as the G protein-coupled receptors and protein kinase C [191, 193-195]. The lateral surface pressure which is proportional to Na^+/K^+ -ATPase activity [180] is also related to lipid phase behavior [196]. However, the relationship between FA unsaturation and H_{II} phase propensity is not linear and oleic acid has a disproportionately large effect compared with DHA [192].

In summary, there are both supporting [167, 197, 198] and conflicting [199, 200] views to the validity of the membrane pacemaker hypotheses of metabolism and aging. The key point to address is the mechanistic gaps in our understanding, which is further complicated by the fact that the fatty acyl composition of different lipid classes in different organs/tissues/sub-cellular membranes are not the same and need to be separated out. Furthermore, it is not only the number of double bonds, but also other elements of fatty acyl composition, such as n-3/n-6 ratio and carbon length [200-202], which play important roles in relating membrane composition to metabolic rate, disease, and longevity.

1.3.1 Elongases and Desaturases

The diversity of lipids needed in cell membranes requires complex metabolic and regulatory pathways to maintain the normal structure and functions of an organism. Eukaryotic cells invest around 5% of their genes to adjust lipid synthesis and to monitor membrane lipid composition [203]. The elongation and desaturation activities of fatty acid synthase (FAS) in DNL appears to be regulated primarily at the transcriptional level, thus the relevant transcription factors, ligands, and cofactors play a vital role in the regulation of fatty acid composition. At the same time, hormones, substrate availability, circadian rhythms, and many other factors have been reported to control FA homeostasis. Then synthesized fatty acids, termed non-essential fatty acids including saturated and ω -10, ω -7 and ω -9 unsaturated FAs can be synthesized from palmitic acid (C16:0) by DNL, as shown in **Fig 1.1**, while the precursors of ω -6 and ω -3 FAs, linoleic acid ($\Delta^{9,12}$ -C18:2) and α -linolenic acid ($\Delta^{9,12,15}$ -C18:3), can only be obtained from dietary sources, and are termed essential FAs. Carbon chains are elongated and double bonds are introduced into substrate FAs through a variety of desaturases and elongases localized in

the endoplasmic reticulum (ER), as well as the peroxisomal β -oxidation pathway, to form long-chain (16C, 18C) and very-long-chain fatty acids (VLCFAs) ($\geq 20C$) of different degrees of unsaturation [204] (**Fig 1.1**). The generated FAs can be primed by an acyl-CoA synthetase and added to a phospholipid by an acyltransferase, or transferred between two phospholipids using a transacylase [205].

The elongation process in the ER is similar to the two-carbon-addition reactions performed by cytosolic FAS, but the initial and rate-controlling condensation reaction of the microsomal FA elongation is catalyzed by the elongase enzymes referred to as Elongation of very-long-chain fatty acids (ELOVLs). To date, there are seven ELOVL proteins (ELOVL1-7) identified which are highly conserved in mice, rats, and humans [206-213]. ELOVL1, ELOVL3, ELOVL6, and ELOVL7 are selective for SFAs and MUFAs while ELOVL2, ELOVL4, and ELOVL5 prefer PUFAs as substrates. The *Elovl1*, *Elovl5* and *Elovl6* genes are expressed ubiquitously, while others exhibit different tissue-specific levels of expression. Moreover, these ELOVL proteins exhibit different chain-length specificities [214, 215] and vary in activity according to tissue and physiological state.

The most common pathway from palmitic acid is ELOVL6-catalyzed elongation followed by Δ^9 -desaturation by SCDs, resulting in the production of stearic acid (C18:0) and oleic acid (Δ^9 -C18:1), respectively. Oleic acid is the precursor substrate of the ω -9 family FAs. Another pathway from palmitic acid is to be directly Δ^9 -desaturated to palmitoleic acid (Δ^9 -C16:1) which can be further elongated and/or desaturated to form other ω -7 FAs. These saturated and mono-unsaturated VLCFAs not only constitute most of the acyl chains of TGs stored in adipose tissue but also serve as essential barrier components of the plasma membrane, and some of them even act as lipokines (e.g. palmitoleic acid) and second messengers in the control of specific transcription factors and membrane proteins [216, 217].

The key elongase in the generation of stearic acid (C18:0) is the ELOVL6 enzyme which is under the control of the sterol regulatory element binding proteins (SREBPs) [218]. The deletion of the *Elovl6* gene in the mouse is related to improvement in insulin resistance without amelioration of obesity or hepatosteatosis [219] but has also been associated with partial embryonic lethality. Further elongation of SFAs and MUFAs is primarily catalyzed by the ELOVL1 and ELOVL3 enzymes. ELOVL1 is believed to catalyze the formation of SFAs

containing as many as 26-carbons [211, 213], while ELOVL 3 is involved in the synthesis of both SFAs and MUFAs with as many as 24-carbons [207, 220]. ELOVL7 [206] is also involved in the elongation of SFAs with as many as 24-carbon atoms. In addition, although ELOVL4 was thought to catalyze elongation of C28-38 PUFAs in the ω -6 and ω -3 pathways, it has also been shown to be involved in the synthesis of saturated C28 and C30 VLCFA [208].

Acyl-coenzyme A (CoA) desaturases in mammalian cells include Δ 9, Δ 6, and Δ 5-desaturases which introduce double bonds at different positions of the acyl chain counting from the carboxylic acid moiety. At the same time, these desaturases can be divided into two families referred to as stearoyl-CoA desaturases (SCDs) and fatty acid desaturases (FADS). SCDs are Δ 9-desaturases for saturated FAs, and include four isoforms (SCD-1, -2, -3 and -4) identified in the mouse to date [221-225][27, 33, 36-38]. SCD-1 is abundant in adipose tissue and liver. SCD-2 is expressed at high levels in the brain and neuronal tissues. SCD-3 is identified specifically in sebocytes in the skin and harderain and preputial glands, while SCD-4 is expressed only in the heart. In humans, only a gene highly homologous to *Scd-1* is ubiquitously expressed [226], but there is a novel form, HSCD5, expressed highly in the brain and pancreas [227]. The Δ 6 and Δ 5-desaturases have been shown to belong to the same cluster of genes [228], referred to as FADS after being cloned. Marquardt et al. suggested the names FADS1 and FADS2 for Δ 5-desaturase and Δ 6-desaturase, respectively, while there is a third putative desaturase FADS3 for which no activity has been described [229]. There are clear phylogenetic differences between SCDs and FADS families of desaturases despite sharing certain common structural features [230, 231].

All of the four SCD isoforms can be used to desaturate palmitic acid (C16:0) and stearic acid (C18:0) with a preference for stearic acid, except for SCD-3 which can only desaturate palmitic acid rather than stearic acid. The SCDs are also associated with the control of energy homeostasis and *Scd-1*^{-/-} mice appear to have reduced rates of lipid synthesis [232] and enhanced lipid oxidation [233], thermogenesis [234] and/or insulin sensitivity [235, 236] in the liver, skeletal muscle, and adipose tissue. Moreover, mice lacking SCD-1 in their skin [237] exhibit a similar hypermetabolic phenotype and are resistant to obesity. Moreover, there is a minor pathway that converts palmitic acid to ω -10 FAs (Δ^6 -C16:1) by FADS2, which to date has only been identified in sebocytes, such as in the preputial gland of *Scd-1*^{-/-} mice [238].

In the essential PUFA synthesis pathways, both linoleic acid ($\Delta^{9,12}$ -C18:2) and α -linolenic acid ($\Delta^{9,12,15}$ -C18:3) begin with sequential Δ^6 -desaturation, elongation, and Δ^5 -desaturation, leading to the synthesis of arachidonic acid ($\Delta^{5,8,11,14}$ -C20:4) and eicosapentaenoic acid (EPA, $\Delta^{5,8,11,14,17}$ -C20:5), respectively. FADS2 catalyzes the initial and rate-limiting Δ^6 -desaturation procedure [231, 239], followed by the ELOVL5-catalyzed elongation and Δ^5 -desaturation by FADS1. In an alternative route for the synthesis of arachidonic acid and EPA, the Δ^8 -desaturation activity of FADS2 may be evoked, although it is considerably lower than Δ^6 -desaturation activity so this pathway may be viewed as a minor component [240, 241]. ELOVL5 has been suggested to be involved in the elongation of 18-carbon and 20-carbon PUFAs [209]. In further elongations of arachidonic acid and EPA to 24-carbon PUFAs, both ELOVL5 and ELOVL2 [207, 210, 211] play a role. The C24:4 (ω -6) and C24:5 (ω -3) are then used as substrates for Δ^6 -desaturation by FADS2 again, followed by production of C22:5 (ω -6) and C22:6 (ω -3) through peroxisomal β -oxidation or further elongation by ELOVL2 and ELOVL4 as shown in **Fig. 1.1**.

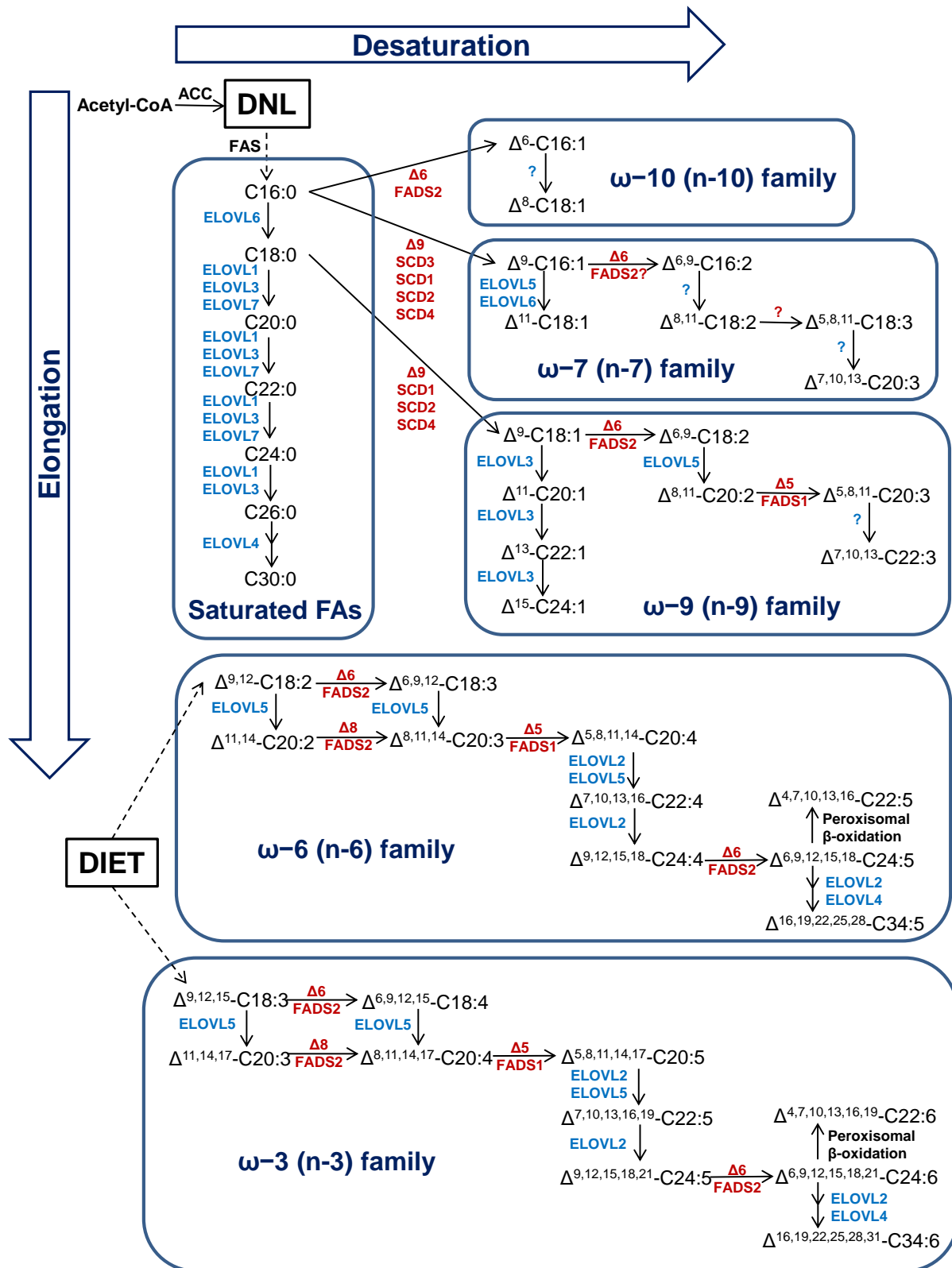


Fig. 1.1 Long chain and very long-chain fatty acid biosynthesis in mammals (modified from [204]). The saturated fatty acids (FAs) and ω-10, ω-7, and ω-9 unsaturated FAs can be synthesized from palmitic acid (C16:0) produced by *de novo* lipogenesis (DNL). The ω-6 and ω-3 unsaturated FAs can only be synthesized from precursors obtained from the diet. The elongases (ELOVLs) and desaturases (SCDs and FADSs) for steps studied to date are indicated.

1.3.2 Sterol Regulatory Element-binding Proteins (SREBPs)

The Sterol regulatory element-binding proteins (SREBPs) are membrane-bound transcription factors that bind to the sterol regulatory element (SRE) DNA sequence TCACNCCAC and regulate intracellular sterol content as well as the biosynthesis of fatty acids, triacylglycerols and phospholipids [242-244]. Humans express two distinct SREBP genes: sterol regulatory element binding transcription factor 1 (*SREBF1*) and sterol regulatory element binding transcription factor 2 (*SREBF2*). The *SREBF1* gene encodes two proteins referred to as SREBP-1a and SREBP-1c/ adipocyte differentiation-1 (ADD-1). SREBP-1a is identified primarily in the spleen and intestines and regulates both the cholesterol and fatty acid biosynthetic pathways, while SREBP-1c predominates in liver, adipose tissue, and muscle and controls SREBP-responsive genes involved in the fatty acid synthesis and differentiation of adipocytes. SREBP-1c is also a transcription factor downstream of insulin in carbohydrate and lipid metabolism. SREBP-2 predominates in the liver and controls the expression of genes in sterol biosynthesis and the LDL receptor (LDLR) gene. SREBP-1c is the predominant isoform expressed in most animal tissues and significantly elevated in livers from *ob/ob* mice [245, 246].

The expression of SREBPs is regulated in complex pathways involving different substrates, hormones, and transcription factors. SREBPs are embedded in the membrane of the endoplasmic reticulum (ER) with their C-terminal domain exposed to the cytosolic side interacting with a protein called SREBP cleavage-activating protein (SCAP). SREBP activity is controlled by the interaction of SCAP with insulin-induced protein-1 and -2 (Insig-1 and Insig-2) [247, 248]. *INSIG1* gene expression is highest in the liver while *INSIG2* is expressed ubiquitously. Both Insig-1 and Insig-2 can cause ER retention of the SREBP/SCAP complex [249]. High sterols activate expression of the SREBP-1 gene via the action of the liver X receptors (LXRs) but do not affect the SREBP-2 gene. Interestingly, the expression of Insig-1 can also be regulated by SREBPs with the SRE upstream of the transcriptional start site of the *INSIG-1* gene. Moreover, expression of Insig-1 can be regulated by PPAR δ , pregnane X receptor (PXR) and constitutive androstane receptor (CAR). The Insig-2 promoter is controlled by insulin receptor activation and nuclear receptors such as the two farnesoid X receptor (FXR) response elements. In addition, both Insig proteins activate the sterol-dependent degradation of HMG-CoA reductase (HMGR).

When SCAP no longer interacts with either of the Insights in situations like decreased PUFA intake, during the anabolic effects of insulin, or following excess SFA, the SREBP-SCAP complex migrates to the Golgi and SREBP is subjected to proteolysis sequentially by site-1 protease (S1P) and site-2 protease (S2P), generating a soluble and transcriptionally active SREBP mature protein [249]. The SREBPs has been implicated in insulin resistance [250], β cell dysfunction [251], T2DM [252], and CVD [253]. SREBP1 has been shown to occupy the promoters of 1,141 target genes involved in diverse biological pathways, particularly lipid metabolism and insulin signaling pathways [254]. Demonstrated targets include genes involved in DNL (e.g., *Acc* and *Fas*) [255-257], FA desaturation (e.g., *Scd1*) [256, 258] and elongation (e.g., *Elovl6*) [210, 218], FA re-esterification (e.g., mitochondrial glycerol-3-phosphate acyltransferase [*Gpat1*]) [259], and PL synthesis (e.g., CTP: phosphocholine cytidylyltransferase α [*Ccta*]) [260, 261].

There is a complex feedback regulatory system between PPAR γ , insulin, *Insig1*, and SREBP1. Firstly, PPAR γ agonists can induce *Insig1* expression *in vitro* and *in vivo* in WAT [262, 263] to limit the promotion of adipocyte differentiation by PPAR γ itself. Insulin can also activate SREBP1 to promote lipogenesis, while, at the same time inducing the expression of *Insig1* for restricting the production of too much active SREBP1 [262, 264-266]. This autoregulatory feedback loop has not only been suggested as a control mechanism for cholesterol synthesis in the liver [264, 267] but also reported to be involved in the pathophysiological dysregulation of WAT for *in vivo* and *in vitro* obesity models [37]. In the insulin-resistant (IR) state, this negative *Insig1*/SREBP1 regulatory feedback is suggested to be reset for the downregulation of *Insig1* and maintenance of active SREBP1 levels for maintaining lipid homeostasis. Active SREBP1 ensures enough supply of specialized FAs used for the maintenance of membrane lipid homeostasis, effectors of intracellular signaling, and lipid modification of proteins [254]. The concept that SREBP1 needs to be activated to restore the biosynthesis of phosphatidylcholine (PC) and phosphatidylethanolamine (PE) has been suggested both in *Caenorhabditis elegans* and mammalian cells [39] and *Drosophila* heart [41]. This regulatory feedback can compensate lipid perturbations in membranes and specific signaling pathways in obesity and IR, but, simultaneously, increases lipogenesis [37, 41] and may aggravate associated pathology.

1.4 Epigenetics and One-carbon metabolism

Mendelian genetics cannot completely clarify the rapid worldwide increase in the prevalence of obesity over the past years along with its underlying inherited susceptibility [268]. Epigenetics, which refers to the heritable changes in gene expression resulting from modifications to DNA or histones rather than changes in the nucleotide sequence, has attracted extensive attention in recent years as an alternative mechanism for pathologies associated with metabolic disorders [269, 270]. In particular, DNA methylation (e.g. cytosine → 5-methylcytosine) is a major epigenetic modification of the genome that regulates gene expression [271]. Although the DNA sequence is comparatively stable, epigenetic patterns can be greatly influenced by external factors, and remain dynamic all the way through the life course [272], providing an important interface between environmental factors and genetics.

Besides being influenced by hormones and adipokines, lipid metabolism can also be influenced by interactions with epigenetic mechanisms. For example, epigenetic and chromatin-modifying proteins have been found to contribute to adipogenesis and maintenance of mature adipocytes through the PPAR γ gene [273]. The fat mass and obesity associated gene (FTO) has been found to be associated with a type of demethylase [274]. Furthermore, there is evidence that high-fat diets can affect the methylation of the main anorexigenic neurohormone pro-opiomelanocortin (POMC) and leptin-related genes, having an impact on appetite [275, 276]. Methylation of the genes encoding PPAR α and the glucocorticoid receptor (GR) have been shown to be decreased when maternal protein is restricted which have a long-term impact on systemic metabolism [277], and methylation of the melanocortin-4 receptor (MC4R) is associated with exposure to long-term exposure to a high-fat diet [278].

Diet can change gene expression through epigenetic modifications as well as by the transcriptional regulation of metabolic pathways. For example, the epigenetic profile of the genome was suggested to be altered after a carbohydrate-based diet was replaced by a high-fat diet, which resulted in insulin resistance and T2DM [279, 280]. Moreover, some metabolites have been found to be used by epigenetic enzymes as necessary co-factors, such as S-adenosylmethionine (SAM) which is used as a chief methyl donor cofactor by both DNA and histone methyltransferases [281]. There are good mechanistic reasons to link changes in a high-fat diet with epigenetic modifications of DNA. SAM is mainly derived from methionine via the enzyme methionine adenosyltransferase, which is part of the choline and one-carbon (1-C)

magnetic or electrical fields and separated out depend on their mass-to-charge ratio (m/z). The m/z signals of charged molecules (or fragments) obtained by the detector are transmitted to the data processing system producing a plot of ion abundance against m/z defined as a mass spectrum, which gives information about structures and quantities of the analytes. Different configurations of the ion source and mass analyzer (or two or more mass analyzers for a tandem mass spectrometry) are actively used in research, chosen depending on their strengths and weaknesses. The use of a combination of these MS techniques allows the identification and quantification of a large number of metabolites, with a wide range of chemical properties and concentrations [292]. Due to its high sensitivity and versatility, MS is used extensively in metabolomic studies. Besides the identification of metabolites, MS easily determines the relative quantification of low-concentration and low-weight metabolites [293-295]. Moreover, absolute quantification can be achieved by MS with particular reference compounds.

1.5.1 Generating Ions: Ionisation

Many different ionisation techniques have been used to generate gas phase ions, including electron ionisation (EI), chemical ionisation (CI), electrospray ionisation (ESI), and matrix-assisted laser desorption/ionisation (MALDI), depending on the states of samples (gas/liquid/solid) and also the internal energy transferring during ionization [296]. EI, formerly known as electron impact, is the ionization technique for mass spectrometry that is only used for ionization of analytes in the gas phase. EI is very energetic that the resultant ions are mostly fragmented. The fragments generate a reproducible pattern of m/z signals, which can be matched to spectral databases for identification. However, EI requires the analyte to be a gas phase or volatile to bombard high energy electrons and is used almost exclusively combined with GC. Molecules are introduced from GC into the ion source and collided with ESI, one of the so-called “soft” ionization techniques, do not require chemical derivatization (except for enhancing or enabling ionization [297]) and minimize the fragmentation of analytes, so it can assist in the analytical interpretation of complex mixtures. In ESI, the analyte is eluted and charged by spraying it through a highly charged needle tip, followed by extensive solvent evaporation and entry into the mass separation unit. The analyte is dissolved in a polar or volatile solvent is pumped into a fine capillary with a flow rate ranging from 1 $\mu\text{l}/\text{min}$ to 1 ml/min [298]. The range of the diameter of the capillary is typically 75-150 μm [298]. A voltage (normally 2-3 kV for methanol/acetonitrile and 4 kV for water) is applied to the tip of the capillary and results in the production of an electric double layer through charge migration

from the solution species to the solution/capillary interface [299]. The electrostatic forces from the pre-organisation of charges in the electric double layer of the capillary counterbalance the surface tension to produce a Taylor cone at the needle tip [300]. When the voltage increases to some extent, the Taylor cone will be destabilized and the sample will be dispersed as a fine spray of charged droplets from the capillary with co-axial nebulizing gas (typically nitrogen) flowing around the capillary. Then evaporation of solvent increases the concentration of charge on the droplet surface. “Coulombic explosion” [301, 302] occurs when the Rayleigh limit is reached and the droplets explode resulting in the formation of a number of smaller droplets of a lesser charge. The solvent becomes less and less as the evaporation and Coulombic explosion continues, creating the spray of charged solvent free analyte ions. Two competing theories [303], known as the charge residual model and the ion evaporation model, disagree at whether the ions in the gas phase are formed prior to total droplet fissions or after successive droplet fissions. The spray of the analyte ions is then introduced into a sampling cone and an intermediate sampling vacuum followed by entering the mass analyzer, where they are analyzed for m/z . Differently charged ions will be detected under certain conditions as the charges are distributed among many sites on the analyte.

ESI has the capacity of ionizing non-volatile and high mass analytes, such as intact lipids, peptides or proteins, and allows the mass spectrometric detection of the vast majority of biological molecules among all the ionization techniques [304, 305]. ESI is especially suitable for the analysis of polar and ionic metabolites [306, 307]. ESI is by far the most frequently used ionization technique in lipidomics studies, partially due to the ease of combining the separation power of an analytical LC experiment with the interpretation power of a mass spectrometer, and the analysis of polar metabolites by LC-ESI-MS is also experiencing a rapid period of growth [293, 295]. However, ESI can suffer from some disadvantages, of which the most prominent is the strong ion suppression effect when investigating complex molecular mixtures [308, 309].

1.5.2 Mass Analyser and Direct Infusion-Mass Spectrometry

In direct infusion-MS (DI-MS), the analyte mixture is directly introduced into the mass spectrometer by ESI. A large number of lipid species can be measured in different ionization modes, so this method is also dubbed “shotgun” [310]. Anionic lipid species are easily ionized in negative mode, especially after the addition of ammonium acetate, formic acid or lithium

hydroxide, while neutral and polar lipids could be detected in positive mode [311, 312]. Ionized molecules are separated according to their mass-to-charge ratio (m/z) in a variety of mass analyzers including quadrupole, ion trap, time-of-flight (TOF), magnetic and/or electric sectors, and Fourier transform ion cyclotron resonance [313, 314]. The analyzers vary in terms of their mass accuracy, dynamic range, mass resolution, and suitability for tandem MS (MS/MS), and an extensive range of instruments are utilized in metabolomic studies.

In a quadrupole mass analyzer, ions generated at the source are accelerated and focussed by a lens, which functions as an ion guide and collisional dampening cell into the quadrupole [315-317]. A quadrupole consists of four parallel metal rods. Any opposing rods have the same applied potential, $(U+V\cos(\omega t))$ for one pair and $-(U+V\cos(\omega t))$ for the other. U and $V\cos(\omega t)$ is a direct and an alternating current voltage respectively, used to control the course of ions through the quadrupole filter. By altering $V\cos(\omega t)$ ions of a particular m/z (resonant ions) are allowed as they move along the ion flight path at the center of the four rods. Therefore, the quadrupole is widely used not only in the radio-frequency only mode as a single mass spectrometry but also functions as a mass filter accelerating the ions of interest into a collision cell in MS/MS mode. [318]

The separation and identification of analytes by m/z signals can be improved by instruments with higher resolution and mass accuracy. A high-resolution mass analyzer such as a TOF analyzer can be a powerful tool for identification works in an open profiling metabolomic study [319]. In the TOF analyzer, ions that are accelerated by an electric field are separated according to their velocities while they drift in a free-field region in flight tube. Firstly, a pulsed electric field pushes the ions into the accelerating column from where the ions enter the field-free space. Then the kinetic energy distribution of the ions is corrected by a reflectron: the ion beam is reflected towards the detector by an electrostatic field. The depth an ion penetrates the electrostatic field and the length of its flight path to the detector depend on the ion's kinetic energy. With this corrected energy distribution, ions of identical m/z would simultaneously arrive at the detector, referred to as time-of-flight focus. In the end, ions are detected by two microchannel plates with mass spectra recorded by a time-to-digital converter [319].

However, an increase in the resolution of an instrument is often correlated with relative cost. Lower resolution and mass accuracy can be compensated for by tandem MS (MS/MS) capability to a degree [320, 321]. MS/MS can isolate and select molecular ions with specific

m/z ratios in the first mass analyzer for fragmentation in a collision cell, and then separated in the second mass analyzer to obtain the fragments information to aid the identification of these analytes [322-324]. There are many methods can be used to fragment ions, producing different types of fragments and information about the structure and composition of analytes. In one process known as collision-induced dissociation (CID), the selected molecular ions are accelerated by an electrical potential and collide with neutral gas molecules within a collision cell, resulting in fragmentation of the ions [325]. The fragments are then separated and measured by their m/z value, giving more information about the original molecular ions. For example, the fragment signal in the form of a neutral loss or a characteristic signal at m/z value 74 often indicates the phospholipid headgroups in lipidomics [326].

There are different ways to combine two or more mass analyzers to perform a tandem mass spectrometry, such as triple quadrupole (QqQ), quadrupole-TOF (Q-TOF) and quadrupole linear ion trap (Q-IT) mass spectrometer. A tandem MS system of QqQ mass spectrometry (QqQ-MS) contains two quadrupole MS in series, with a radio frequency only quadrupole between them as a collision cell for CID. Multiple reaction monitoring (MRM) in QqQ-MS has shown high sensitivity, specificity, and excellent quantitation ability. Therefore, a QqQ-MS system is ideal for targeted metabolomics studies, which normally focus on the identification and quantification of specifically selected metabolites. For example, QqQ-MS has been used in the identification of drug metabolites [327]. An MRM scan mode method was used in the quantification of one-carbon metabolites of this study, in which by having three quadrupoles in series, a compound of a given mass can be selected by the first quadrupole, fragmented in the second (which acts as a collision cell), and a particular fragment then detected in the third. Three characteristics (retention time, parent ion m/z , product ion m/z) will be applied simultaneously to determine a certain compound in the TIC, which improves the sensitivity and selectivity of the quantitative method to a large extent. A diagram illustrating how to determine 5-methyltetrahydrofolate using the MRM scan mode is shown in **Fig. 1.3**. This selective LC-MS/MS method can be a highly sensitive tool for the measurement of specific metabolites. In this project, the UPLC-MRM-MS/MS method will be modified for aqueous extracts from white adipose tissue, and more fragmentation ion pairs will be chosen to measure more methyl donors.

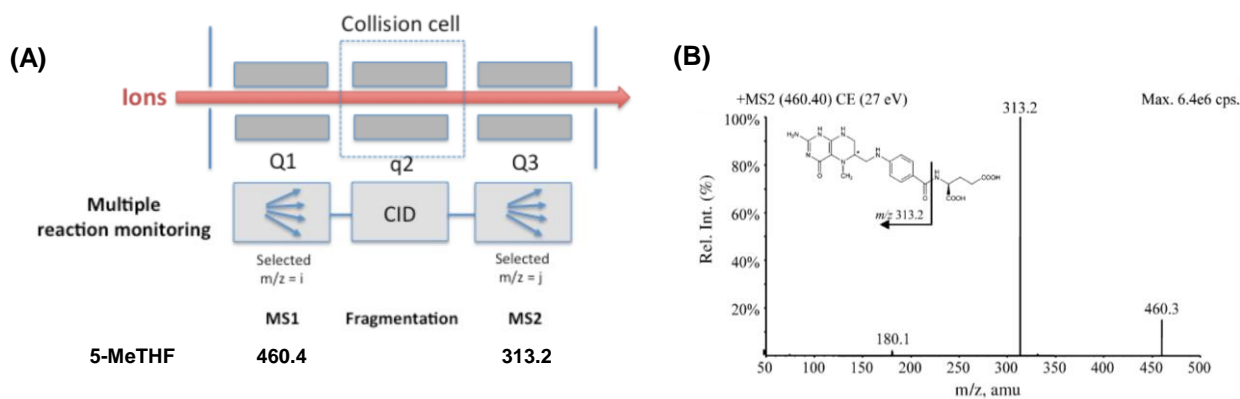


Fig. 1.3 Multiple reaction monitoring (MRM) scan mode of a triple quadrupole mass spectrometer (A), and an example to determine 5-methyltetrahydrofolate (5-MeTHF) using this mode according to its product ion spectra of $[M+H]^+$ (B) [328]

Another mass spectrometer that is often used for MS/MS is the quadrupole linear ion trap (Q-IT) mass spectrometer which consists of an ESI source, a heated capillary, and two successive rod arrays, a quadrupole and an ion trap [317, 318]. There is a lens gating entry of ions into the ion trap by pulsing from negative to positive voltages to attract and repel the ions into the aperture. This control of entry time not only maximizes signal but also diminishes the space-charge effects of an excessive quantity of ions in the trap. The ion trap is composed of three hyperbolic quadrupole rod arrays which radially restrained ions in the center by a two-dimensional radio frequency trapping field. Meanwhile, the front and rear end electrodes confine the ions axially through applying direct current potentials, and helium-filled in the ion trap (~ 1 mtorr) collide with ions and contract their trajectories to the center of the trap (kinetic cooling). When auxiliary alternating current voltages on the X-rods alter the field in the ion trap by dipole excitation, the trapped ions leave the trapping field in order of successive m/z ratio and strike a detector (such as electron multiplier and conversion diode) offering structural information [329]. Ion traps can perform MS/MS to the n th degree by confining 90% of isolated ions and fragments in the trap, and as a consequence, many mass selective operations are capable of being performed.

DI-MS is a high-throughput and easily optimized technique widely used in identification and relative quantification of lipids [330] and metabolic “fingerprinting” studies [331], but also has a number of disadvantages. Ion suppression effects can be a considerable problem when analyzing complex mixtures of metabolites [332]. Ion suppression occurs when analytes compete for the charge during the ionization process, resulting in a change in the intensity of a

particular ion [333]. This problem can be avoided, to an extent, by using chromatographic techniques to separate the analytes prior to injection into the mass spectrometer for analysis [334].

1.5.3 Gas Chromatography-Mass Spectrometry

MS becomes a particularly powerful metabolic profiling tool in identification and quantification of the metabolomes in combination with prior separation, usually by chromatography [335], therefore providing higher sensitivity in terms of the size of metabolome detected. Chromatography utilizes a column which varies in length, diameter and chemical property (stationary phases) to provide separation of different chemicals [336-338]. A mixture of metabolites is separated out depending on their different chemical properties as they travel through the column. The metabolites eluted at different time are then subject to mass spectrometry (MS) analysis for both identification and the further separation of co-eluting peaks.

Gas-chromatography (GC) was first projected in 1941 by Martin and Synge [339], suggesting that the mobile phase in a liquid-liquid chromatography system could be substituted with a vapor. After significant developments in technology, it has eventually become possible to couple the chromatography to mass spectrometry. The GC-MS technique finally came into shape when Gohlke and McLafferty [340] combined a gas chromatography to a TOF mass spectrometer During the 1950s. GC-MS has since become an important technique in a wide range of fields, especially in lipid biochemistry, lipidomics and metabolomics due to its high chromatographic resolution. GC consists of a carrier gas mobile phase and column coated with a solid stationary phase. It is usually a separation method more robust than liquid chromatography (LC). It can separate and analyze volatile (i.e. with a low m/z) and thermally stable gaseous or aqueous phase metabolites following derivatization prior to analysis.

Since GC-MS requires the analytes to be volatile and thermally stable, derivatization can be used to introduce volatility to complicate metabolites or remove the polar functional group, so it is required for identification of much low volatility and unstable metabolites. In general, the most useful derivatives are trimethylsilyl ethers (TMS) for hydroxyl groups, methyl esters for carboxyl groups, and alkyl oximes for carbonyl groups. A 2-step protocol using methoxyamine hydrochloride followed by N-methyl-N-(trimethylsilyl)-trifluoroacetamide (MSTFA) is

commonly used in the aqueous metabolomic analysis to increase the volatility of the metabolites such as monosaccharides [341, 342]. The derivatization most commonly used for fatty acids is hydrolysis of complex lipids and methylation of the released free fatty acids to form fatty acid methyl esters (FAMES) to increase the volatility and mask the polar carboxyl group [343]. Some research used boron trifluoride and methanol for acidic esterification of the fatty acids.

The GC system consists of the GC column as the stationary phase and the carrier gas functioning as the mobile phase [344, 345]. The sample is injected, vaporized and pushed by the carrier gas through the heated GC column. The velocity that different compounds move through the column depends on their partition between the mobile and stationary phases. The separation is dependent on analyte chemistry, column dimensions, stationary phase type, carrier gas flow rate, and the temperature of the column [346, 347]. A programmed temperature gradient can be adjusted and applied to control the velocity for better separation. The stationary phase also has a significant impact on the identification of analytes. Different columns could be used to separate fatty acid methyl esters based on molecular weight, unsaturation, or cis/trans isomers. Provisional identifications can also be made using commercially available standards, but this kind of tentative identifications had better be further verified by spectrometric techniques. [346, 348]

After separation in the column, compounds are eluted through a heated transfer line to the ion source, which commonly uses EI as the ionization technique [349, 350]. In EI an energetic beam of electrons generated from a filament impact the analyte to produce a radical cation that loses an electron. The Ionised analytes undergo further fragmentations removing the excess internal energy gained from ionization. The ions and fragments enter a mass analyzer, typically quadrupole mass analyzers to generate a mass spectrum, amplified by the detector and sent to a computer to convert the signal into a visual display. Since the fragmentation in EI is extremely reproducible with the same ionization energy (typically 70 eV), standardization of fragmentation libraries could be compared with the fragments to provide structural information for analyte identification. One of the most famous commercially available databases is the National Institute of Standards and Technology (NIST)/ Environmental Protection Agency (EPA)/ National Institutes of Health (NIH) mass spectral library. [351]

GC-MS overall is a robust analytical approach with high sensitivity and good resolution. However, the additional derivatization step must be used for many samples to make them thermally stable and volatile, but this process may introduce variability, contamination and recovery losses into the samples and can mask metabolite structural information [352, 353]. What is more important, the range of analytes that can be analyzed is limited by its m/z range, preventing applying to larger metabolite species. The large and polar metabolites cannot be analyzed by GC because they are neither volatile nor able to be made volatile by derivatization. These difficulties can be overcome by a combination of GC-MS with other analytical techniques such as DI-MS and LC-MS so that the metabolome coverage can be increased to a large extent.

1.5.4 Liquid Chromatography-Mass Spectrometry

The atmospheric pressure interface between a liquid chromatography (LC) and a mass spectrometer (MS) became possible after development of the Atmospheric Pressure Ionisation (API) ionisation interface, including ESI and Atmospheric Pressure Chemical Ionisation (APCI), and nano-spray technique in the 1980s from original work of John Fenn's group [354]. LC-MS has a number of advantages and has become a popular technique for metabolomic analysis [355]. In contrast to GC-MS, LC-MS can not only apply to measure volatile samples. It is a high throughput method that is suitable for a good dynamic range of species (including intact lipids, peptides, and other macromolecules) and has the potential for analyte identification from the spectral data. Even with a low-resolution chromatography, the mass spectrometer can operate in both negative and positive ion mode to broaden the screening coverage of analytes. LC-MS can also be very sensitive with good resolution and mass accuracy.

DI-MS often suffers from a matrix effect named "ion suppression" [332], which means co-eluting compounds including prominent phospholipids, especially when using positive ionization, can compete for a charge during ionization and decrease the ionization of certain analytes of interest. The ionization efficiencies individual analytes are based on their chemical characteristics, so that the observed count for a specific ion depends on not only itself but also other analytes and contaminants co-eluted and co-ionised [333]. What makes the problem more complicated is that the interfering compounds may not be seen in the mass spectrum and both low and high concentration analytes are affected [356]. The use of an internal, either offline or

online, liquid chromatography (LC) separation [357], especially the high-resolution high-performance liquid chromatography (HPLC) and ultra-performance liquid chromatography (UPLC), prior to MS analysis can significantly reduce the detrimental ionization properties, so UPLC-MS can be more accurate with good resolution [355]. HPLC is a widely used technique for separating lipid classes by normal phase chromatography and often coupled to detectors including ultra-violet detection [358] and evaporative light scattering detection [359, 360]. However, ESI-MS detector is much better than these detectors in terms of selectivity and choice of mobile phase [357], although identification of metabolite species is still a considerable challenge and some analyses can be low-throughput because of relatively long chromatography runs.

Although most thermally labile, polar or high molecular mass compounds can be directly analyzed by LC-MS, there may be some problems in ionization of some labile compounds and those without enough innate polarity. Ammonium adducts can be produced by adding ammonium acetate or formic acid to the mobile phase to aid the ionization of metabolites before injecting them into the HPLC or UPLC columns [361]. The column has a narrow tube packed with chemically modified silica which interacts with the analytes in the mobile phase (the solvent) to separate chemical classes of the analyte. The column chemistries include normal phase, ion exchange, partition, displacement, size exclusion and reversed phase chromatography (RPC). This study used some type of RPC columns which have a non-polar stationary phase and rely on the principles of hydrophobic and electrostatic forces [362, 363]. An aqueous and moderately polar mobile phase is commonly selected for an RPC column.

Retention of analyte molecules by the stationary phase relies on the solvophobic theory and the contact surface area around the non-polar segment of the molecules with the stationary phase within the aqueous eluent [362, 364]. The binding of analytes to the RPC stationary phase can be decreased and analytes eluted from the column by reducing the polarity and surface tension of the mobile phase. The larger non-polar molecules are eluted after polar molecules in RPC [365]. Higher resolutions and faster separations can be achieved by using a sub-2 μm particle size column and elevated column temperature [366]. Both flow rates and pressure increase with smaller column packing particles, while effective pressure is reduced by increasing the temperature. The separated analyte molecules are then introduced into a mass spectrometer via an ESI or APCI.

In contrast to GC-MS, libraries for sample identification for LC-MS data are limited, because ESI-MS spectra and fragmentation patterns are affected by many factors including the instrument type, ion source, and mobile phases [353]. However, there are a lot of resources available providing pertinent reference material, structural information and MS/MS patterns of lipids, such as the LIPID MAPS (<http://www.lipidmaps.org/>) [367], Cyber Lipid Center (<http://www.cyberlipid.org/>), and LipidBank (<http://lipidbank.jp/>).

1.6 Obese mouse models

Animal models are widely used as a strategy to study how obesity and metabolic syndrome results in different diseases. They offer more logistic advantages over human tissue studies, such as ease of drug interventions and selective genetic manipulation and better tissue and organ availability alongside disease developmental progress [368]. The metabolic syndrome can be induced in several well-established obese mouse strains with high-fat feeding or other diets. These models are generally classified into three categories: (1) genetic models, such as *ob/ob* mice, *db/db* mice, PPAR α knockout mice, SREBP-1c transgenic mice, and acyl-coenzyme A oxidase (AOX) null mice; (2) nutritional models, such as mice fed on high-fat diet (HFD), choline-deficient (CD) diet, fructose, cholesterol and cholate diet; (3) combinational models of genetic and nutritional models. Actually, in humans, obesity is also commonly caused by excessive food intake along with a lack of physical activity [369, 370] and genetic susceptibility [371]. The lipid composition of the white adipose tissue of diet-induced obesity depends on the food consumed. High carbohydrate diet leads to excessive DNL in the liver and adipose tissue and the newly synthesized lipids (such as C16:0 and C18:1) will dominate. HFD results in reduced DNL and the WAT is filled with TAGs composed of the FAs directly from the diet. The expression of genes associated with DNL is activated by a high carbohydrate diet, inhibited by HFD [268, 372]. To date, membrane lipids have not fully been examined and will be the focus of this study. The composition of WAT of genetic-induced obese humans is decided by the pathways the gene is in control of. For example, PPAR δ activation results in more oxidative catabolism of FAs and TCA cycle intermediates, while the PPAR γ activation was distinguished by the sequestration of lipids into WAT [373, 374]. The WAT of *ob/ob* mouse is dominated by DNL-lipids resulting from mutations in the gene responsible for the production of leptin, which will be discussed in details below.

Rodents are by far the most commonly used pre-clinical model of human obesity. While the literature supports the notion that many similarities exist between rodents and humans, notable differences emerge related to fat deposition and the function of adipose tissue. In humans, adipose tissue is found in specific locations (adipose depots), such as around internal organs (visceral fat, including mesenteric, epididymal and perirenal adipose tissues), beneath the skin (subcutaneous fat), intermuscular (muscular system), in bone marrow (yellow bone marrow), around the heart (epicardial adipose tissue), and in the breast tissue [375, 376]. Adipose depots in different parts have different physical and biochemical profiles [377-379]. The visceral fat in the abdomen is mostly semi-fluid while the subcutaneous and intramuscular fat is not consistently spaced. The visceral fat is more linked to obesity-related diseases than the subcutaneous fat does. Mice have in total of eight major adipose depots [380]. The largest is the paired gonadal depots which are attached to the testes and epididymis in males and the ovaries and uterus in females and enclose the inguinal group of lymph nodes [381]. The gonadal depots comprise about 30% of the dissectible fat [381]. The other two adipose depots in the abdominal cavity are the paired retroperitoneal depots surrounding the kidney. These adipose depots extend into the pelvis when they reach a particular size. The omental depot which originates near the spleen and stomach and can extend into the ventral abdomen and the mesenteric depot which forms a glue-like web supporting the intestines include many lymphoid tissues [382]. The two superficial depots are the paired inguinal depots (anterior to the upper segment of the hind limbs) and the subscapular depots (under the skin between the dorsal crests of the scapulae) which are paired medial mixtures of BAT adjacent to regions of WAT and also often covered by a "frosting" of WAT [383]. Besides these eight major depots, there are also some minor depots in mice such as the paired popliteal depots (between the major muscles behind the knees, each containing one large lymph node) [384] and the pericardial (surrounds the heart) [385, 386].

1.6.1 The *ob/ob* mouse model

One of the commonly used and well-characterized models of obesity is the *ob/ob* mouse, a strain with mutations in the leptin gene. Mutant mice are indistinguishable from the littermates at birth, but they become heavier rapidly within 2 weeks and gain weight throughout their lives, reaching about three times the weight of their unaffected littermates [387].

Leptin is a hormone yielded in adipocytes, which regulates adipose mass through controlling food intake [388], which provides a link between nutritional state and several important physiological progressions [389-391]. Mice with mutations in leptin (*ob/ob*) or the receptors (*db/db*) exhibited noticeable obesity phenotypes [392, 393], e.g. increased appetite, hyperglycemia, and hyperinsulinemia [394-396]. Interestingly, *ob/ob* mice gained extra fat and weight even after restricted to a diet which was adequate for the maintenance of lean mice. However, these mice significantly reduced their food intake and body mass and raised the energy expenditure back after the administration of leptin [397-399].

Microarray comparisons showed that gene expression of adipose tissue of *ob/ob* mice are significantly different from wild-type mice [400], which indicated that leptin deficiency (or obesity) not only influence the phenotype of adipose tissue but also have an effect on the expression of genes associated with lipid biosynthesis and/or immune systems [389, 401]. In *ob/ob* adipose tissue, expression of SREBP-1c and its target genes are reduced than in wild-type, but the opposite happens in the liver [402]. Alteration of SREBP-1c also has an global effect on other genes necessary for fatty acid synthesis, including SCD-1 [403], ACC [404], FAS [405], elongase [406], $\Delta 5$ and $\Delta 6$ desaturase [407]. Insulin motivates SREBP-1c gene transcription [408, 409], synthesis and secretion of which could also be inhibited by leptin. Leptin deficiency leads to increase of insulin content and expression of SREBP-1c [410, 411], which results in increased FAs and TAGs biosynthesis, and also the occurrence of diseases like diabetes and fatty liver [412].

1.6.2 The PPAR α null mouse model

Peroxisome proliferator-activated receptors (PPARs) are nuclear receptors controlling the expression of genes associated with organogenesis, cell differentiation, proliferation, inflammation, carbohydrate, and lipid metabolism and energy homeostasis [373, 374, 413, 414]. The PPAR family of nuclear receptors is composed of three members: PPAR α , PPAR β/δ (commonly referred to as PPAR δ), and PPAR γ . The different functional properties of the PPAR subtypes result from subtle differences in binding site preference, tissue distribution and their ability to bind different co-repressors and coactivators [415]. PPAR α reportedly activates the proliferation of peroxisomes [416], while the activation of PPAR δ and PPAR γ cannot lead to peroxisome proliferation.

PPARs form permissive heterodimers with the retinoid X receptors (RXRs) which bind to PPAR-responsive elements (PPREs) in target DNA through the DNA-binding domain (DBD) [417]. The function of PPARs is dependent on the precise shape of their ligand-binding domain (LBD) modification [418]. Upon ligand binding, to PPARs the complex of the PPAR/RXR heterodimer with co-repressors is exchanged for the formation of the co-activator complex which leads to transcriptional activation of target genes [419, 420]. The LBD of the PPARs is large and can accommodate a variety of lipids including endogenous FAs, derivatives of linoleic acid, eicosanoids, and oxidized and nitrated FAs, linking lipidomics with transcriptomics. However, the concentration required for these FAs to bind to PPARs is higher than would be encountered *in vivo*, and as such, it is still yet to be conclusively determined whether any of the various lipid ligands represent the ‘true’ physiological ligand. One of the primary co-activators of the PPARs is peroxisome proliferator-activated receptor- γ coactivator-1 α (PGC-1 α) [421]. The primary function of PGC-1 α is to stimulate mitochondrial biogenesis and oxidative metabolism and as such is most abundant in tissues that have a high demand for energy production, such as brown adipose tissue (BAT), skeletal muscle, heart, brain, and kidney. The endogenous ligands PPAR α include certain members of the metabolites of arachidonic acid such as leukotriene B₄ and 15-Hydroxyicosatetraenoic acid family. Activation of PPAR α in 3T3-L1 preadipocytes increase expression of enzymes of the β -oxidation pathway when co-expressed with PGC-1 [422]. The widely prescribed lipid-lowering drugs of the fibrate (phenoxyisobutyrate) class reportedly increase FA oxidation [423] and decrease VLDL particles and circulating TAGs [424] through activation of PPAR α . Fibrates also increase HDL cholesterol in a similar way through the activated expression of lipoprotein lipase and apolipoprotein A-V, and increased macrophage cholesterol efflux helps to alleviate inflammation and atherosclerotic plaque formation in the vasculature, reducing the risk of cardiovascular disease [425]. Other factors that influence the expression and activity of PPAR α include stress, insulin, leptin, growth hormone, hepatocyte nuclear factor 4 (HNF4), and COUP-TFII.

PPAR α is important for the lipid homeostasis through the activation of peroxisomal and mitochondrial β -oxidation, microsomal ω -hydroxylation/oxidation, lipogenesis, ketogenesis, lipid binding and transport/lipoproteins, and cholesterol metabolism, and has anti-inflammatory and anti-atherogenic effects. Mice lacking the PPAR α gene, which is susceptible to adipocyte hypertrophy, hypercholesterolemia but normal triglycerides, are used as models

of spontaneous late-onset obesity with stable caloric intake and a marked sexual dimorphism [426]. Females have higher serum triglycerides and gain more fat than males, while the males show a delayed occurrence of obesity and original centrilobular-restricted steatosis. Hepatic peroxisomal proliferation is inhibited along with decreased expression of some hepatic target genes in these transgenic mice [426]. Interestingly, genes associated with the peroxisome were changed significantly in the obese and old wild-type mice [427]. , Li et al. [428] demonstrated that the expression of PPAR γ increased significantly in PPAR α null mice along with a profound perturbation induced by these changes in terms of metabolism in adipose tissues. Fat cells from the liver of the PPAR α null mice expressed substantial levels of PPAR γ transcripts when compared with lean cells.

PPAR α is highly expressed in tissues that oxidize fatty acids at a rapid rate, such as liver, BAT, heart, intestines, muscle, and kidney [429], where it promotes FA β -oxidation and transport, and decreases glycolysis [216, 429, 430]. Uptake of FAs into the liver can be increased by activation of PPAR α , followed by the activation of peroxisomal β -oxidation and mitochondrial β -oxidation. Thus, PPAR α is thought to have a profound effect on systemic metabolism and in particular the handling of lipids across the organism. On the other hand, it appears that PPAR α plays a limited role in adipogenesis due to the low levels of expression, as the obese PPAR α null mice appear to have normal WAT. The metabolomics study conducted by Atherton et al. [431] demonstrated a decrease in the hepatic concentration of glucose and glycogen of PPAR α null mice which increased in an age-dependent manner. This suggested the important role PPAR α plays in gluconeogenesis and its interaction with the aging process. It also demonstrated that white adipose tissue changes with the low expression of PPAR α in this particular tissue. This was hypothesized to be a consequence of overall changes in systemic metabolism altering the lipids that are stored in white adipose tissue.

1.7 Project Aims

This thesis aims to investigate how the metabolic composition (lipidome and metabolome) of adipose tissue is influenced by both diet and genetic-induced models of obesity, and in particular how the composition of phospholipids, the major component of sub-cellular membranes, vary. In addition, the 1-C metabolism pool of methylation donors was investigated

and in turn, the methylation of key genes in white adipose tissue (WAT) was measured to understand the link between the metabolome and altered gene expression and the pathways behind these alterations. To achieve this, I conducted:

(1) In Chapter 3, a lipidomic study of aging examining the metabolome of white adipose tissue from wild-type and *ob/ob* mice on a regular chow diet (RCD) or high-fat diet (HFD) to better define how diet influences the lipidome. It was hypothesized that a high-fat diet, a genotype associated with leptin deficiency, and aging, all-cause characteristic variations in lipid profiles but would exhibit differences mirroring the pathways of different lipid metabolism and signaling. Especially, the composition of membrane lipids (PCs, lysoPCs, PEs and PSs) would be changed by diet/genotype/age in a different way compared with the neutral lipids (FAs, DGs and TGs).

(2) In Chapter 4, a microarray study was performed on adipose tissues from 2- and 10-month animals, to examine the gene expression of essential enzymes involved in lipid metabolism in adipose tissue. It was hypothesized that there be a correlation between the transcriptomic patterns of obesity and aging, especially in inflammatory, metabolic and transcriptional pathways.

(3) In Chapter 5, an LC-MS quantitative method was established to profile methyl donors in adipose tissue to understand how high-fat diet and leptin deficiency influences the turnover of 1-C methyl donors. It was hypothesized that changes in phospholipids may correlate with 1-C metabolism, as choline was involved in not only lipid metabolism but also 1-C cycle as shown in **Section 1.4**. In addition, four genes associated with obesity and diabetes were chosen from the literature to determine their methylation status for validation of the suggested mechanism of a PC/1-C/epigenetics regulation system.

(4) In Chapter 6, the lipid changes in BAT, visceral (epididymal) WAT, and subcutaneous (inguinal) WAT of PPAR α null mice were profiled and compared with wild-type controls to understand how the lipidome changes under the regulation of important transcriptional factors. It was hypothesized that PPAR α null mice might have more “bad fat” (saturated and shorter lipids) in store as some of the key transcription factors in PPAR α related pathways might not be activated, such as SREBP-1c and PPAR γ .

Chapter 2 Materials and methods

2.1 Chemicals and Reagents

The FAME standard mix (Supelco 37 Component FAME Mix, certified reference material, TraceCERT®, in dichloromethane (varied conc.), ampule of 1 mL) was purchased from Sigma Aldrich (Gillingham, Dorset, UK) with analytes detailed in **Table 2.1**. All other chemicals used in the experiment (mentioned in sections 2.3 – 2.9) were of analytical grade.

Analyte	Concentration
Methyl butyrate	400 µg/mL
Methyl hexanoate	400 µg/mL
Methyl octanoate	400 µg/mL
Methyl decanoate	400 µg/mL
Methyl undecanoate	200 µg/mL
Methyl laurate	400 µg/mL
Methyl tridecanoate	200 µg/mL
Methyl myristate	400 µg/mL
Methyl myristoleate	200 µg/mL
Methyl pentadecanoate	200 µg/mL
Methyl cis-10-pentadecenoate	200 µg/mL
Methyl palmitate	600 µg/mL
Methyl palmitoleate	200 µg/mL
Methyl heptadecanoate	200 µg/mL
the cis-10-Heptadecanoic acid methyl ester	200 µg/mL
Methyl stearate	400 µg/mL
trans-9-Elaidic acid methyl ester	200 µg/mL
the cis-9-Oleic acid methyl ester	400 µg/mL
Methyl linolelaidate	200 µg/mL
Methyl linoleate	200 µg/mL
Methyl arachidate	400 µg/mL
Methyl γ-linolenate	200 µg/mL
Methyl cis-11-eicosenoate ≤	200 µg/mL
Methyl linolenate	200 µg/mL
Methyl heneicosanoate	200 µg/mL
cis-11,14-Eicosadienoic acid methyl ester	200 µg/mL
Methyl behenate	400 µg/mL
cis-8,11,14-Eicosatrienoic acid methyl ester	200 µg/mL
Methyl erucate	200 µg/mL
cis-11,14,17-Eicosatrienoic acid methyl ester	200 µg/mL
cis-5,8,11,14-Eicosatetraenoic acid methyl ester	200 µg/mL
Methyl tricosanoate	200 µg/mL
cis-13,16-Docosadienoic acid methyl ester	200 µg/mL

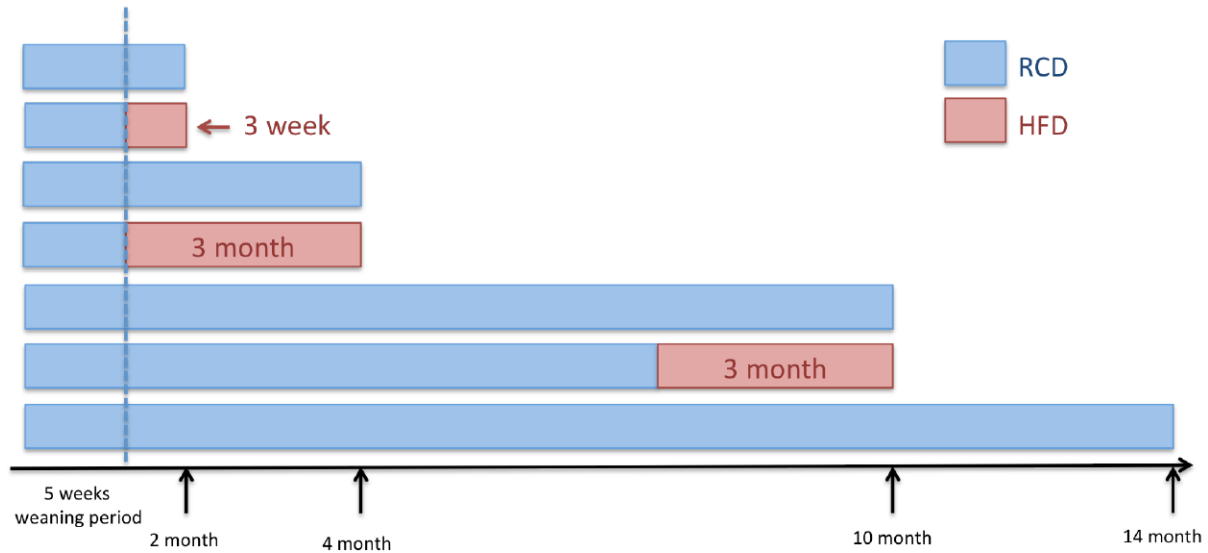
Methyl lignocerate	400 µg/mL
cis-5,8,11,14,17-Eicosapentaenoic acid methyl ester	200 µg/mL
Methyl nervonate	200 µg/mL
cis-4,7,10,13,16,19-Docosahexaenoic acid methyl ester	200 µg/mL

Table 2.1 The analytes present in the FAME standard mix (Supelco 37 Component FAME Mix, certified reference material, TraceCERT®, in dichloromethane (varied conc.), ampule of 1 mL) used in GC-MS experiments.

2.2 Animals and diets

Five-week-old male *ob/ob* mice and their wild-type (C57B1/6J, WT) controls were purchased from a commercial breeder (Harlan UK). This study focussed on tissues from male offspring, as female offspring are more sensitive to pubertal parameters, such as cycling, estrus and vaginal opening, which were all reported [432] to be changed by leptin, and may add uncertainty to our metabolism study. Therefore, I controlled for sex differences but did not address them in the present study. Mice were housed in a temperature-controlled (24 °C) and humidity-controlled (55%) facility, with a 12h:12h (06:00-18:00, 18:00-06:00) light-dark cycle and access to water *ad libitum*. Mice (n=10/age group/genotype) fed a regular chow diet (RCD, caloric content: 11.5% fat, 26.9% protein, 61.6% carbohydrate) (RM1, special diet services UK) were sacrificed at the age of 2-, 4-, 10- and 14-months. A separate group of mice was switched to a custom-produced high-fat diet (HFD, caloric content: 55% fat, 29% protein, 16% carbohydrate; fatty acid composition: 27% saturated fatty acid, 48% monounsaturated fatty acid, and 25% polyunsaturated fatty acid) (diet code: 829197; special diet services, UK) at different stages for various lengths of time and were sacrificed at the age of 2-months (3-week high-fat feeding) 4-months (12-week high-fat feeding) and 10 months (12-week high-fat feeding). This HFD diet has been previously described [433]. The study also examined the effects of obesity and aging on epigenetic profiles, therefore the time points were spread over a long period. 4-months was chosen because mice were switched to the HFD only after the weaning period (5 weeks) and the initial HFD was shorter for the 2-month old group (only 3 weeks). 14-months was initially chosen to maximize the influence of aging, but many 14-month-old mice died during the HFD feeding. At each time point, animals (after overnight fasting) were killed by CO₂ asphyxiation, and white adipose tissue (from paired gonadal depots within the abdominal cavity attached to the epididymis and testes) was rapidly dissected, snap frozen in liquid nitrogen and stored at -80°C until further analysis. Three *ob/ob* and three

control mice at post-mortem were measured by dual-energy X-ray absorptiometry (DEXA, PIXImus, Lunar, Madison, WI) to determine body lean and fat mass ([94] conducted by Dr. Xinzhu Wang, University of Cambridge.). All animal procedures were approved by the UK Home Office and the University of Cambridge and carried out under the supervision of a project or personal license holder.



No.	Genotype	Age (months)	Diet	No.	Genotype	Age (months)	Diet
wt 01-10	WT	2	RCD	ob 01-10	<i>ob/ob</i>	2	RCD
wt 11-20	WT	4	RCD	ob 11-20	<i>ob/ob</i>	4	RCD
wt 21-30	WT	10	RCD	ob 21-30	<i>ob/ob</i>	10	RCD
wt 31-40	WT	14	RCD	ob 31-40	<i>ob/ob</i>	14	RCD
wt 41-50	WT	2	HFD	ob 41-50	<i>ob/ob</i>	2	HFD
wt 51-60	WT	4	HFD	ob 51-60	<i>ob/ob</i>	4	HFD
wt 61-70	WT	10	HFD	ob 61-70	<i>ob/ob</i>	10	HFD

Table 2.2 Schematic of the study design of the *ob/ob* and wild-type (C57B1/6J, WT) mice of different ages fed with high-fat (HFD) or regular chow diet (RCD).

2.3 Lipid Extraction

2.3.1 Fatty Acids (FAs) and Triacylglycerols (TGs)

Tissues were extracted using a chloroform-methanol Folch method [434]. ~20 mg frozen tissues were pulverized in chloroform-methanol (400 μ l; 2:1 v/v) using a TissueLyser (Qiagen), then the mixture was sonicated for 10 minutes. Water (80 μ l) was added and samples were then centrifuged (13,200 rpm, 10 min). The resulting aqueous and organic layers were collected in

separate glass tubes. The remaining liquid and pellet were separated two further times following the same procedure of chloroform-methanol (2:1) addition, sonication, water addition, and centrifugation to create a 'triple extraction' procedure. The two phases were separated, and the aqueous and organic layers from each step of the extraction were collected in new glass tubes and combined respectively. Organic extracts were dried overnight in a fume hood, and aqueous extracts were evaporated to dryness using an evacuated centrifuge (Eppendorf, Hamburg, Germany). Extracts were stored at -20°C until analysis.

2.3.2 Glycerophospholipids (PCs) and 1-carbon metabolites

Intact lipids were extracted by a modified Bligh and Dyer (BD) method [435] from adipose tissue to separate aqueous-soluble metabolites from lipids. Approximately ~50 mg frozen tissue was pulverized in methanol-chloroform (300 µl, 2:1 v/v) using a TissueLyser (Qiagen, West Sussex, UK). Then the mixture was sonicated for 10 min. Chloroform-water (1:1) was added (100 µl of each component) and samples were then centrifuged (16,600 refs, 20 min). The resulting aqueous and organic layers were collected in separate tubes. The remaining liquid and tissue pellet were extracted again following the same procedure of methanol-chloroform (2:1) addition, sonication, chloroform-water (1:1) addition, and centrifugation. The two phases were separated, and the aqueous and organic layers from each step of the extraction were combined respectively in tubes to create a 'double extract'. Organic extracts were dried overnight in a fume hood under a stream of nitrogen gas, and aqueous extracts were evaporated to dryness using an evacuated centrifuge (Eppendorf, Hamburg, Germany). Extracts were stored at -20°C until use.

Different solid phase extraction (SPE) methods were tested as a preliminary experiment to further separate different fractions of lipids from organic extracts obtained using the method above and improve their detection. The optimized pre-treatment method finally chosen is: The CHROMABOND® NH₂ (3 ml, 500 mg) column was washed by using 10 ml methanol and then conditioned using 10 ml hexane before the sample application. The dried organic extract was reconstituted in 1 ml n-hexane and slowly aspirated through the column. The fraction of cholesteryl esters was firstly eluted with 1 ml hexane. Then all TAGs were eluted from the column using 2 ml hexane-ethyl acetate (85:15, v/v). Finally, the column was continuously eluted using 1 ml chloroform-methanol (2:1, v/v) and 2 ml methanol to obtain the fractions of

monoacylglycerides and phospholipids. Each fraction was dried under the flow of nitrogen in a fume hood. Dried extracts were stored at -20°C until injection.

2.4 GC-MS analysis for total Fatty Acids

Organic-phase metabolites were derivatized by acid-catalyzed esterification [140]. Chloroform-methanol (1:1 v/v; 400 µl) and BF₃–methanol (10%; 125 µl) (Sigma-Aldrich, Dorset, UK) were added to the dried organic phase and incubated at 80 °C for 90 min. Once cool, water (500 µl; milliQ) and hexane (1000 µl) were added and samples were vortex-mixed for 1 min. The aqueous layer was discarded and the remaining organic layer was evaporated to dryness in a fume hood, then reconstituted in hexane (1000 µl) for GC-MS analysis. GC-MS analyses were made using a Trace GC Ultra coupled to a DSQ single-quadrupole mass spectrometer (ThermoScientific). The derivatized organic samples were injected with a split ratio of 50:1 onto a 30 m x 0.25 mm 70 % cyanopropyl polyphenylene-siloxane 0.25 µm TR-FAME stationary phase column (ThermoScientific). The injector temperature was set to 230 °C and helium carrier gas was at a flow rate of 1.2 ml/min. The initial column temperature was 60 °C for 2 min, increased by 15 °C/min to 150 °C and then increased at a rate of 4 °C /min to 230 °C (transfer line =240 °C; ion source=250 °C; electron ionization =70 eV). The detector was turned on after 240 s, and full-scan spectra were collected using three scans/s over a range of 50 to 650 m/z.

GC-MS chromatograms were processed using Xcalibur (version 2.1; Thermo Scientific). Data were extracted by the Quan Browser in the Xcalibur and the peaks were integrated and normalized so that the total sum of peaks in a chromatogram was set to 10000. Overlapping peaks were separated using traces of single ions. Peak assignment was based on mass fragmentation patterns matched to the National Institute of Standards and Technology (NIST) database of mass spectra (NIST Standard Reference Database 1A. www.nist.gov/srd/). Identification of metabolites from organic phase GC-MS analysis was supported by comparison with a FAME standard mix (Supelco 37 Component FAME Mix; Sigma Aldrich, Gillingham, Dorset, UK) as detailed in **Table 2.1**, which was injected after every 10 samples. For example, a lot of structural information was generated for saturated fatty acids including a characteristic McLafferty rearrangement ion at m/z 74, a molecular ion and many other

fragment ions. PUFAs typically has little or no molecular ion abundance but multiple sites of radical cation formation [326].

2.5 DI-MS/MS analysis for neutral lipids

The dried organic phase in part 2.2.1 was reconstituted in methanol/chloroform (1:1,300 μ l), then an internal standard mix (400 μ l, diluted in 1:1 methanol/chloroform; contained 5 μ M 1,2-di-O-octadecyl-sn-glycerol-3-phosphocholine, 10 μ M 1,2-di-O-phytanyl-sn-glycerol-3-phosphoethanolamine, 5 μ M N-heptadecanoyl-D-erythro-sphingosylphosphorylcholine, 5 μ M C8-ceramide, 50 μ M undecanoic acid, 5 μ M trilaurin and 10 μ M β -sitosterol acetate) was added and the solution was sonicated for 10 min. 40 μ l of the solution was transferred to the appropriate well on a glass coated 240 μ l low well plate (Plate+™, Esslab, Hadleigh, UK) with 160 μ l of MS-mix (7.5 mM NH₄AC IPA: MeOH (2:1)), after which the plate was sealed for analysis.

Samples were infused into a Thermo Exactive benchtop Orbitrap (Hemel Hempstead UK), using an Advion Triversa Nanomate (Ithaca US). The Nanomate infusion mandrel was used to pierce the seal of each well before analysis, after which with a fresh tip, 5 μ l of sample was aspirated followed by an air gap (1.5 μ l). The tip was pressed against a fresh nozzle and the sample was dispensed using a 0.2 psi nitrogen pressure. Ionization was achieved by a 1.2 kV voltage. The Exactive started acquiring data 20 s after the aspiration of the sample began. Then the analysis was stopped and the tip was discarded before a new sample was analyzed. Throughout the analysis, the sample plate was kept at 15°C. The Exactive acquired data from 185 to 2000 m/z, with a resolution of 100,000, with automatic gain control sat at 3,000,000 – initially in positive mode (1.2 kV, 0–1.2 minutes), then in negative mode (-1.5 kV, 1.2–2.3 minutes). The maximum filling time of the trap was set at 10.00 ms in positive mode and set at 250 ms in negative mode.

A selected subset of samples was infused into a Thermo LTQ Velos Orbitrap Elite (Hemel Hempstead UK), using an Advion Triversa Nanomate (Ithaca US) for lipid identification. The LTQ-Orbitrap Velos was controlled either manually or set-up using the data-dependent precursor selection. Generally, the selected masses were isolated with a 1.5 m/z width in the linear ion trap and then fragmented using either the linear ion trap with 35% relative collision energy or in the higher-energy Collision-induced Dissociation (HCD) collision cell, with a

range of collision energies from 5% to 75% relative collision energy. All spectra were recorded in the Orbitrap set at 100,000 resolution.

DI-MS chromatograms were processed using Xcalibur (version 2.1; Thermo Scientific). The mass data were averaged from the chromatogram for the period of sample injection and the “exact masses” were exported; the data points summed between M and M+1, to give variables which corresponded to individual peaks, normalized to the total spectral area across all TG types and integrated. The average carbon number per chain and average unsaturation were computed after identification of the TGs by matching the “exact masses” and MS/MS data to those in the LIPID MAPS (<http://www.lipidmaps.org/>) [367]. ESI generates abundant $[M+NH_4]^+$ molecular ions for TGs when ammonium ions are present in the solvent system. The side chains were identified by three “diglyceride type ions” in MS/MS spectra ($[M+H-R_1CH_2COOH-NH_3]^+$, $[M+H-R_2CH_2COOH-NH_3]^+$ and $[M+H-R_3CH_2COOH-NH_3]^+$ correspond to loss of one esterified fatty acyl group at the *sn*-1, *sn*-2, or *sn*-3 position of glycerol as the free carboxylic acid with ammonia). These diglyceride ions can be further decomposed by CID to create “monoglyceride” ions ($[R_2CH_2CO]^+$ or $[R_3CH_2CO+74]^+$) and the neutral loss (difference in mass between the diglyceride ion” and the “monoglyceride ion”) reveals the third FA group.

2.6 UPLC-MS analysis for phospholipids

Chromatography was performed on an ACQUITY UPLC System (Waters Corporation, Elstree, Hertfordshire, UK) equipped with an Acquity UPLC 1.8 μ m HSS T3 column (2.1 \times 100 mm; Waters Corporation) coupled to a Waters Q-ToF Xevo mass spectrometer (Waters MS Technologies, Ltd., Manchester, UK). The column temperature was kept at 55°C.

For the analysis of TAGs, the desolvation gas temperature was 3 kV and the cone voltage was 50 V. The binary solvents were 10 mM ammonium acetate, 0.1% formic acid (Solvent A) and analytical grade acetonitrile/isopropanol (1:9) with 10 mM ammonium acetate, 0.1% formic acid (Solvent B). The temperature of the sample organizer was set at 4°C. Mass spectrometric data were collected in centroid mode over the mass range of *m/z* 50-1200 with a scan duration of 0.2 s. As lock mass, a solution of 2ng/ μ l (50:50 acetonitrile: water) leucine enkephaline (*m/z* 556.2771) was infused into the instrument at 3 μ l/min. Dried organic phase samples were reconstituted in methanol-chloroform (1:1,100 μ l), then diluted 20-fold further prior to

injection onto the column. The gradient started from 60% A/40%B, reached 100% B in 10 min, returned to the initial conditions in 0.1 min and remained there for the following 2 min; the eluent flow rate was 0.400ml/min.

The phospholipids extracts (fractions D) described in section 2.3.2 were reconstituted in 200 μ l initial mobile phase (isopropanol/acetonitrile/water, 2:1:1) prior to injection of 3 μ l onto the column, respectively. A lyso-phosphocholine C17:0 internal standards (in initial mobile phase) was spiked into each sample to give a final concentration of 20 μ M. The binary solvent system used was HPLC-grade acetonitrile: water 60:40, 10 mM ammonium formate (solvent A) and HPLC-grade acetonitrile: isopropanol 10:90, 10 mM ammonium formate (solvent B). The gradient used was: 0 min, 40% B, 2 min, 43% B, 2.1 min, 50% B, 12 min 54% B, 12.1 min, 70% B, 18 min, 99% B. The eluent flow rate was 0.400 ml/min. The temperature of the sample organizer was set at 4°C. The electrospray source was operated in positive ion mode with the source temperature set at 120°C and a cone gas flow of 50 L/h. The desolvation gas temperature was 550°C and the nebulizer gas flow rate was set at 900 L/h. The capillary voltage was 2 kV and the cone voltage was 30 V. Mass spectrometry data was collected in centroid mode over the mass range of m/z 200–1200 with a scan duration of 0.2 s. As lockmass, a solution of 2 ng/ μ l leucine enkephaline (m/z 556.2771) in 50:50 acetonitrile: water was infused into the instrument at 3 μ l/min.

Tandem mass spectrometry was performed as an additional function for data collection to allow fragmentation data to be collected. The MS/MS method was operated with a collision energy ramp starting at 20 eV and finishing at 40 eV. The data dependent acquisition method was performed on a pooled sample, in which the most abundant 5 peaks from a survey scan were selected, and the corresponding ions were subjected to MS/MS analysis.

UPLC-MS data were processed using the Micromass Markerlynx Applications Manager (Waters Corporation). Peaks were detected, deconvoluted, noise-reduced and integrated, and then matched, and retention time aligned across the samples. The ion-intensities for each peak were detected and normalized to the total response across all phospholipid types. Individual peaks were normalized to the total integrated area of the sample. Lipid species were identified using exact mass, tandem mass spectrometry data, and data-dependent acquisition (DDA) data. ESI generates both $[M+H]^+$ and $[M-H]^-$ ions for PLs, but the polar head group typically drives a preference for formation of either positive ion (PC) or

negative ion (PS, PI, PA, and PG). PE yields both positive and negative molecular ions by either the ionization method. The fragment ions observed in positive mode are mostly from the neutral losses of the phospho-headgroups or formation of the headgroups ions. For example, the $[M-NH_3CH_2CH_2HPO_4]^+$ ($[M-140]^+$) ions were observed in MS/MS spectra of PEs due to the neutral losses, while phosphocholine ions with m/z 184 were observed for PCs in positive ion mode.

2.7 Determination of 1-carbon metabolites by UHPLC-SRM-MS

The aqueous component of the extract described in section 2.3.2 was thoroughly dried under nitrogen and reconstituted in 25 μ l aqueous 100 mM dithiothreitol (Sigma Aldrich, Haverhill, Suffolk, UK) containing the following internal standards at a concentration of 50 μ M: [$U^{13}C$, $U^{15}N$] *L*-glutamic acid and *L*-proline (Cambridge Isotope Laboratories, Tewkesbury, MA, UK); *L*-leucine- d_{10} , *L*-phenyl- d_5 -alanine and *DL*-homocysteine-3, 3, 4, 4- d_4 (CDN Isotopes, Pointe-Claire, QC, Canada); *L*-valine- d_8 (Sigma Aldrich). This mixture was thoroughly vortexed and sonicated for 15 mins. at room temperature after which a further 100 μ l 10 mM ammonium acetate (Sigma Aldrich) was added and the resulting solution transferred into 300 μ l liquid chromatography vials (Chromacol, Welwyn Garden City, Herts., UK) and capped with PTFE screw caps with silicone septa (Agilent Ltd., Stockport, Cheshire, UK). One-carbon cycle metabolites were analyzed via a targeted assay using a Thermo Quantiva triple quadrupole mass spectrometer coupled to an Ultimate 3000 UHPLC liquid chromatography system (Thermo Fisher, Hemel Hempstead, Herts., UK). A C18PFP column (150 \times 2.1mm, 3 μ m; Advanced Chromatography Technologies, Aberdeen, UK) was used to separate the compounds. Mobile phase A consisted of aqueous 0.1% formic acid, and mobile phase B consisted of 0.1 % formic acid in acetonitrile. The following gradient was used to separate the compounds: 100% A was held for 1.5 mins, followed by a linear increase of B from 0% to 100% over 3 mins with a further re-equilibration for 1.5 mins to give a total run time of 6 mins. The flow rate was 400 μ l/min and the injection volume was 2.5 μ l. The mass spectrometer was operated in positive ion mode with the following parameters: a spray voltage of 3.5 kV, sheath gas 50 arb. units auxiliary gas 15 arb., sweep gas 2 arb., ion transfer tube temperature 350 $^\circ$ C and a vaporizer temperature of 400 $^\circ$ C. Compound dependent parameters are listed in **Table 2.3** and were established by infusion of a 100 nM standard of the relevant compound prepared in a solution of 4:1 acetonitrile: water with 0.1% formic acid at a flow rate of 15 μ l/min using the automatic

optimisation protocol available through the Xcalibur software (ThermoScientific, Hemel Hempstead, UK).

Compound	Precursor (m/z)	Product (m/z)	Collision Energy (V)	RF Lens (V)
Glycine	76.07	48.20	6	30
Serine	106.08	60.20	10	39
Cytosine	112.10	95.11	18	84
Betaine	118.15	58.23	26	67
Cysteine	122.03	59.14	24	34
Valine-d ₈	126.20	80.20	10	41
Methylcytosine	126.13	109.16	19	78
Homocysteine	136.18	90.12	10	52
Homocysteine-d ₅	141.20	95.12	10	52
Leucine-d ₁₀	142.23	96.24	8	35
Methionine	150.05	61.16	23	36
Glutamic acid ¹³ C ₅ ¹⁵ N ₁	154.13	89.09	15	47
Phenylalanine-d ₅	171.12	125.15	13	41
S-Adenosyl Homocysteine	385.15	136.13	20	73
S-Adenosyl Methionine	399.44	250.15	16	79

Table 2.3 SRMs and detection parameters for 1-carbon metabolism pathway intermediates and relevant internal standards.

UHPLC -MS chromatograms were processed using Xcalibur (version 2.1; Thermo Scientific). The mass data were averaged from the chromatogram for the period of sample injection; the data points summed between M and M+1, to give variables which corresponded to individual peaks. The ion-intensities for peaks of Cysteine and Homocysteine were normalized to the area of the internal standard Homocysteine-d₅. Ion-intensities for all the other one-carbon metabolites were normalized to the area of the internal standard Glutamate acid ¹³C₅¹⁵N₁.

2.8 Measurement of DNA Percent Methylation

DNA was extracted using the QIAamp DNA Mini Kit (Cat. no. 51304) except with some modifications: ~50 mg frozen adipose tissue was pulverized in 180 µl Buffer ATL using a TissueLyser (Qiagen, West Sussex, UK) with 5 mm stainless steel beads for 20 s at 30 Hz. The sample was centrifuged briefly to ensure that all the tissue debris was at the bottom of the tube. 20 µl proteinase K was then added to the tube which was incubated for 56°C for 1 h in a shaker incubator. Briefly, the 2 ml microtube was centrifuged to remove drops from inside the lid before 200 µl Buffer AL was added to the sample, then the solution was mixed again by pulse-vortexing for 15 s, and incubated at 70°C for 10 min. The 2 ml microtube was briefly centrifuged to remove drops from inside the lid. Then the Tissue Protocol in the QIAamp DNA Mini Kit (Cat. no. 51304) and QIAamp DNA Blood Mini Kit Handbooks was conducted from step 4.

The concentration of DNA was measured by absorbance at 260 nm using a Thermo Scientific NanoDrop 2000c UV-Vis spectrophotometer and then diluted to 4 ng/µl using water. *OneStep* qMethyl™ Kit (Catalog No. D5310) was used to determine the methylation status of four genes (Lhfpl2, Rgs3, ACSL1, and AKT2). *OneStep* qMethyl™ Kit was performed on a StepOnePlus™ (Cat. No. 4376600, ThermoFisher, Hemel Hempstead, UK) using a Real-Time PCR System. The kit contains Human Methylated DNA & Non-methylated DNA Standards with an MGMT primer set for validating the effectiveness of the *OneStep* qMethyl™ system.

Information about these five genes:

(1) *Acs11*: acyl-CoA synthetase long-chain family member 1 [*Mus musculus* (house mouse)]

NCBI Gene ID: 14081

NCBI Reference Sequence: NC_000074.6

Base pair size: 65015 bp

Forward: 5' - TGC GGC CGC GAC TCC TTA AATA- 3'

Reverse: 5' -AGG GAA ACG AGG CCG TGG AG - 3'

(2) *Akt2*: thymoma viral proto-oncogene 2 [*Mus musculus* (house mouse)]

NCBI Gene ID: 11652

NCBI Reference Sequence: NC_000073.6

Base pair size: 47897 bp

Forward: 5' - CGT TGC TGC CGC CAG TTC ATA AAT- 3'

Reverse: 5' - GAG CCT CCA GGT CCG TGG TC- 3'

(3) Lhfp12: lipoma HMGIC fusion partner-like 2 [*Mus musculus* (house mouse)]

NCBI Gene ID: 218454

NCBI Reference Sequence: NC_000079.6

Base pair size: 137757 bp

Forward: 5' - ACC GGA CTG AGC GAC CCT C- 3'

Reverse: 5' - GGC AGG TGA CAA TGA CAT GAC ACA TAT T- 3'

(4) Rgs3: the regulator of G-protein signaling 3 [*Mus musculus* (house mouse)]

NCBI Gene ID: 50780

NCBI Reference Sequence: NC_000070.6

Base pair size: 143185 bp

Forward: 5' - AGC CAA GTC AGG TGG AAA TCT- 3'

Reverse: 5' - CTC CAT GGC GTC CCT GTT- 3'

(5) MGMT: O-6-methylguanine-DNA methyltransferase [*Homo sapiens* (human)]

NCBI Gene ID: 4255

NCBI Reference Sequence: NC_000010.11

Base pair size: 303800 bp

Forward: 5' - GGT GTG AAA ACT TTG AAG GA - 3'

Reverse: 5' - CAC TAT TCA AAT TCC AAC CC - 3'

2.9 Microarray analysis of mouse adipose tissue

RNA was extracted using the RNeasy lipid tissue kit (Qiagen GmbH, Hilden, Germany). Approximately 100mg of tissue was used per sample for RNA isolation and procedures were carried out according to the manufacturer's instructions. Extracted RNA was quantified by ribogreen and its purity assessed by evaluating absorbance ratios using a Fluostar microplate reader (BMG Labtech). The level of degradation of each sample was assessed using a bioanalyzer (Agilent, UK). Illumina Bead Station 500 (Illumina Inc., San Diego, CA, USA) was used to perform transcriptomics. Approximately 25,600 transcripts were interrogated using the MouseRef-8 v2.0 Expression Bead Chip, which was chosen for mouse whole-genome expression profiling. The Bead Chip content was derived from the National Center for Biotechnology Information Reference Sequence (NCBI RefSeq) database (Build 36, Release 22), supplemented with probes derived from the Mouse Exonic Evidence Based

Oligonucleotide (MEEBO) set, as well as exemplary protein-coding sequences described in the RIKEN FANTOM2 database.

2.10 Data analysis methods

Multivariate statistical analysis was performed within SIMCA 14 (Umetrics, Umea, Sweden). The supervised pattern recognition tool partial least squares discriminate analysis (PLS-DA) was used. PLS-DA is a regression extension of the unsupervised pattern recognition tool principal components analysis (PCA) and finds the maximum covariance between predefined classes [436, 437]. The dataset is commonly visualized using scatter plots, which summarise the observations by revealing clusters and outliers in the data along the new latent dimensions in the data. Loading plots for these models display the variables (metabolites in this thesis) responsible for the clustering of the observations. The contribution of each variable to the clustering was ranked using the coefficient plot. The robustness of the multivariate model generated was assessed by R^2 and Q^2 . R^2 shows the percentage of variation explained in the model, whereas Q^2 indicates the predictive power of the model, which is considered to be significant when $Q^2 > 40\%$.

The PLS-DA method was also used to link different factors like genotype, age, and diet with the profiles of total FAs, TGs, PCs, 1-C metabolites, transcriptomics, and DNA methylation data sets. A separate model was built treating genotype, age, and diet as a factor (response variable) and lipidomics, 1-C metabolites and transcriptomics data set as a factor (predictor variables). For each of the data types (for example total FAs, TGs) we selected variables based on variable importance in projection (VIP) scores that estimate the importance of each variable in the projection used in a PLS model and is often used for variable selection. A variable with a VIP Score close to or greater than 1 can be considered important in the given model. The selection of variables was done for genotype, diet, and age and further Venn diagram representation was performed to find out which variables were unique to a factor and which overlap between the genotype, age and diet factors. Further to correlate between two data sets (e.g. FAs vs. TGs; FAs vs. 1 Carbon metabolites data etc), two-way orthogonal PLS (O2PLS) was used. O2PLS is a generalization of PLS and in contrast to PLS and OPLS, it is bidirectional (i.e. $X \leftrightarrow Y$) [438].

Gene Set Enrichment Analysis (GSEA) is a computational analysis that determines whether a priori selected set of genes shows statistically significant, concordant differences between two biological states. GSEA was performed using this website <http://amp.pharm.mssm.edu/Enrichr/>.

Chapter 3 Lipidomics of High-fat-diet and *ob/ob* mouse models of obesity

3.1 Introduction

Animal models are widely used as a strategy to study the mechanisms of metabolic syndrome and how obesity results in different diseases. The metabolic syndrome can be induced in several well-established obese mouse strains with high-fat feeding in part caused by ectopic fat deposition in animals where the storage of fat is close to its maximum. One of the commonly used and well-characterized models of obesity is the *ob/ob* mouse, a strain of mouse with a mutation in the gene for the production of leptin [439-441].

Leptin is a hormone produced in adipocytes, which regulates adipose mass through controlling food intake [388], and provides a link between nutritional state and several important physiological progressions [389-391]. Mice with mutations in the gene leptin (*ob/ob*) or its receptors (*db/db*) exhibit noticeable obesity phenotypes [392, 393], increased appetite, hyperglycemia, and hyperinsulinemia [394-396]. Moreover, *ob/ob* mice significantly reduce their food intake and body mass and raise energy expenditure back to control levels after the administration of leptin [397-399]. Interestingly, *ob/ob* mice gain extra fat and body mass even after being restricted to a diet which is an adequate amount for the maintenance of lean mice, indicating that obesity arises because of mechanisms in addition to increased appetite.

Microarray comparisons have demonstrated that gene expression of adipose tissue of *ob/ob* mice are dramatically different from wild-type mice [400], which indicates that leptin deficiency not only influences the phenotype of adipose tissue but also has an effect on the expression of genes associated with lipid biosynthesis and/or immune system [389, 401]. In *ob/ob* adipose tissue, expression of SREBP-1c and its target genes are reduced compared with wild-type animals, but the opposite situation is found in the liver. These alterations in the expression of SREBP-1c also have global effects on other genes necessary for fatty acid synthesis, including SCD-1 [403], ACC [404], FAS [405], elongase [406], $\Delta 5$ and $\Delta 6$ desaturase [407]. Insulin induces SREBP-1c gene transcription [408, 409], synthesis and secretion while this process is in part inhibited by leptin. In this manner, leptin deficiency leads to an increase in insulin content and expression of SREBP-1c [410, 411], which results in

increased FAs and TAGs biosynthesis, and also increased the occurrence of diseases such as diabetes and fatty liver disease [412].

Previous lipidomic studies only focused on FAs and TGs in adipose tissue. The neutral lipid act as an energy reservoir in adipose tissue so it should be most affected by the composition of diet and the DNL process in the liver and adipose tissue, while the cell membrane and some membrane-bounded cellular components such as the peroxisome and the mitochondria play a key role in regulating the energy homeostasis. The compositional differences may reflect in the compositions of the lipid building blocks.

3.2 Aims and Objectives

In this Chapter I aim to:

- i. Profile the lipid changes associated with diet-induced obesity.
- ii. Profile the lipid changes associated with genetic-induced obesity resulting from a failure to produce leptin in the *ob/ob* mouse.
- iii. Compare and contrast the two mouse models

3.3 Materials and Methods

3.3.1 Animals and diets

All animals and samples described in **Chapter 2 (section 2.2)** were used for the lipidomic study in this Chapter. The WAT from paired gonadal depots within the abdominal cavity attached to the epididymis and testes in male mice was examined in this study not only because of the abundance and availability of the WAT, but due to the signaling functions of the WAT (e.g. through producing leptin and adipokines) relative to the BAT which seems to mainly respond to signals and generates body heat [174, 235, 442]. Further, the visceral adipose tissue is linked to insulin resistance [443], type 2 diabetes [444], inflammatory diseases [445], and other obesity-related diseases[446].

3.3.2 Lipid Extraction

Lipid extraction from mouse adipose tissue was performed according to **Chapter 2 (section 2.3)**.

3.3.3 GC-MS analysis for total Fatty Acids

GC-MS analysis for total fatty acids from mouse adipose tissue was performed according to **Chapter 2 (section 2.4)**.

3.3.4 DI-MS/MS analysis for neutral lipids

DI-MS/MS analysis for neutral lipids from mouse adipose tissue was performed according to **Chapter 2 (section 2.5)**.

3.3.5 UPLC-MS analysis for phospholipids

UPLC-MS analysis for phospholipids from mouse adipose tissue was performed according to **Chapter 2 (section 2.6)**.

3.3.5 Data analysis

Data analysis were performed according to **Chapter 2 (section 2.10)**.

3.4 Results

3.4.1 Physiological characteristics

Physiological characteristics of the mice used in the present study were measured previously [94, 95] conducted by Dr. Xinzhu Wang, University of Cambridge. Body weight was increased by both *ob/ob* genotype and high-fat diet in all age groups, while the genotype was dominant (**Fig 3.1**, >70% of the total variation by two-way ANOVA). Body fat composition of the 10-month (10M) old group was determined by DEXA (**Fig 3.2**). The lean weights remained stable in mice of any genotype fed on any diet, while fat mass significantly increased in *ob/ob* mice

fed on an RCD, and wild-type mice fed on HFD compared with the wild-type mice fed on an RCD. Interestingly, HFD did not induce further fat weight gain in *ob/ob* mice (10M-OB-HFD = 48 ± 3.1 g, 10M-OB-RCD = 43.5 ± 2.6 g). Hyperglycemia and hyperinsulinemia were observed in all *ob/ob* mice compared with age-matched WT controls as shown in **Table 3.1**. **Further**, glucose tolerance was impaired in 10M-OB-RCD mice (**Fig 3.3A**). The *ob/ob* mice fed on an HFD exhibited high levels of glycosylated hemoglobin (HbA_{1c}) as shown in **Fig 3.3B**, indicating the long-term effect of a high blood glucose level.

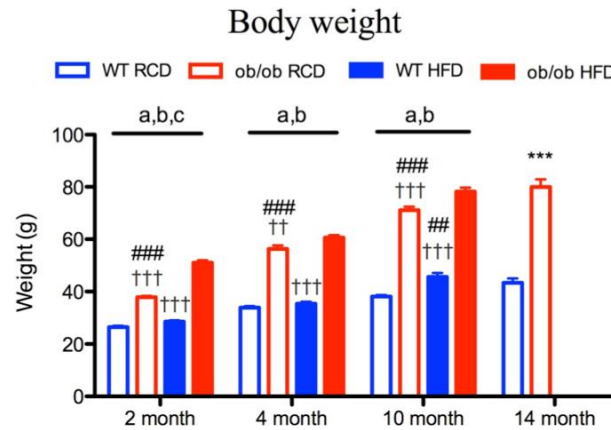


Fig 3.1 Body weight of *ob/ob* and wild-type (WT) mice on either a regular chow diet (RCD) or a high-fat diet (HFD) (n=6-10/group). All data are mean ± SEM. Statistical significance with two-way ANOVA is indicated by a: genotype-dependent, b: diet-dependent, and c: interaction between genotype and diet. # P<0.05, ## P<0.01, ### P<0.001 compared with WT animals on RCD. †P<0.05, ††P<0.01, †††P<0.001, compared with *ob/ob* mice on HFD using *Bonferroni's* post-hoc analysis. * P<0.05, ***P<0.001, compared with WT animals on the same diet using Student's t-test. This figure was redrawn from a previous study [94].

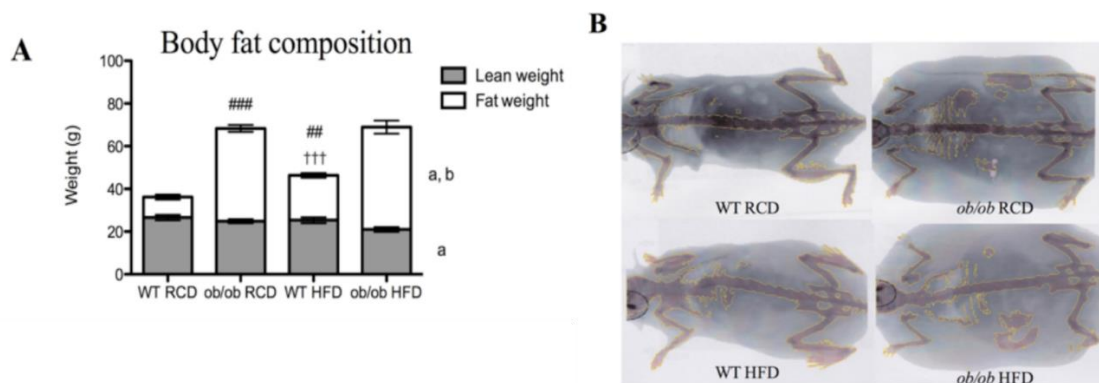


Fig 3.2 Body fat composition determined by dual-energy x-ray absorptiometry (DEXA) (n=3-4/group). **A**: body fat composition of 10-month old animals fed on a regular chow diet (RCD) or a high-fat diet (HFD). All data are mean ± SEM. Statistical significance with two-way ANOVA is indicated by a: genotype-dependent, b: diet-dependent, and c: interaction between genotype and diet. # P<0.05, ## P<0.01, ### P<0.001 compared with WT animals on RCD. †P<0.05, ††P<0.01, †††P<0.001, compared with *ob/ob* mice on HFD using *Bonferroni's* post-hoc analysis. * P<0.05, ***P<0.001, compared with WT animals on the same diet using Student's t-test. **B**: representative scanning images of DEXA of 10-month old animals fed on either RCD or HFD. [94]

Insulin(ng/L)

		2 month	4 month	10 month	14 month
RCD	<i>ob/ob</i>	6.98 ± 1.63*	28.59 ± 4.49**	44.47 ± 3.49***	43.29 ± 6.71**
	WT	0.98 ± 0.13	1.04 ± 0.25	1.2 ± 0.35	1.6 ± 0.75
HFD	<i>ob/ob</i>	19.6 ± 4.66*	13.24 ± 2.82*	33.17 ± 9.87*	
	WT	0.55 ± 0.15	0.7 ± 0.17	2.15 ± 0.57	

Glucose(mmol/L)

		2 month	4 month	10 month	14 month
RCD	<i>ob/ob</i>	8.36 ± 1.49**	6.78 ± 1.07*	6.16 ± 0.57***	4.95 ± 0.67
	WT	3 ± 0.33	3.29 ± 0.3	3.12 ± 0.28	3.48 ± 0.17
HFD	<i>ob/ob</i>	6.82 ± 0.44***	5.35 ± 0.38*	3.89 ± 0.25	
	WT	4.23 ± 0.32	4.09 ± 0.29	2.76 ± 0.65	

Table 3.1 Plasma insulin and glucose levels in *ob/ob* and wild-type mice. All data are mean ± SEM. * P<0.05, **P<0.01, ***P<0.001 compared with WT animals on RCD or HFD using t-test. The data was tabulated from a previous study [94, 95].

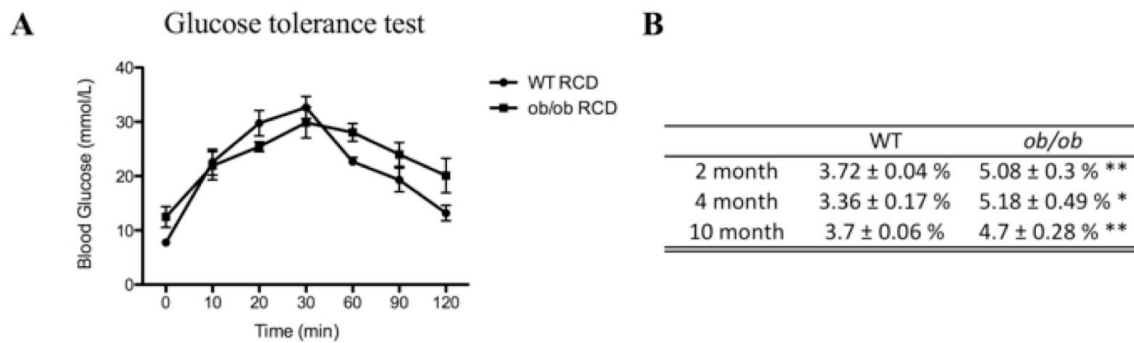


Fig 3.3A: Glucose tolerance test performed on 10-month old mice fed on a regular chow diet (RCD) after overnight fasting (n=5/group). **B:** HbA_{1c} levels of *ob/ob* and WT controls on a high-fat diet (HFD) (n=5/group). [94]

3.4.2 Increase of oleic acid in adipose tissue is the key feature of both obesity and aging

Total FA compositions of the two diets (RCD and HFD) were analyzed by GC-MS (**Fig 3.4**). The percentage of each FA species (relative to the sum of all the FAs) were semi-quantified and calculated as shown in **Fig 3.5** RCD diet contains much less fat (11.5%) than HFD (55%), and is dominated by C18:2 ω 6 (51.59%) which accounts for more than a half of total fatty acids detected. The content of C16:0 (16.35%) and C18:3 ω 3 are also of a higher percentage compared with HFD diet. The HFD diet comprises a relatively diversified distribution of fatty acids: C18:2 ω 6 and C16:0 drop to 34.91% and 12.80% of the total, respectively, while other FAs, especially C18:1 ω 9 (29.38%), account for higher percentages in the HFD diet. I then compared the total FA composition in adipose tissues of all the mice with the two diets.

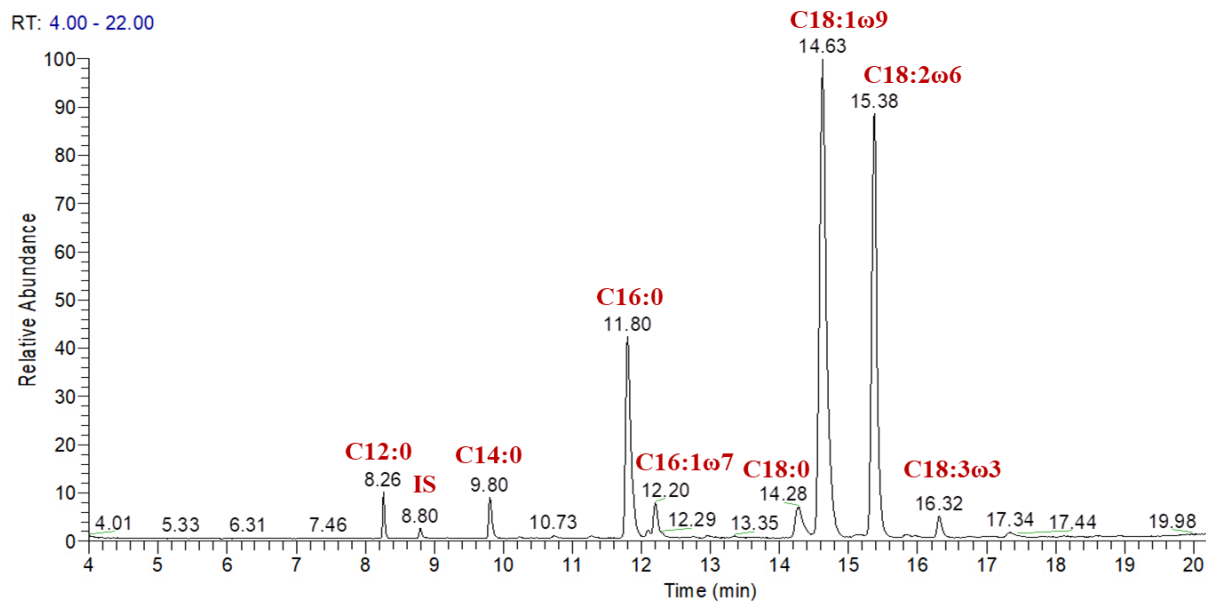


Fig 3.4 A representative GC-MS total ion chromatogram (TIC) from the analysis of methyl esterification-derivatized organic extracts of the adipose tissue (retention time 4.00–20.00 minutes). IS, internal standard (D25-tridecanoic acid). Total fatty acids are identified from extract retention times, referring to a FAME standard mix and comparison of corresponding mass spectrum within the NIST Mass Spectral Library.

Overall diet composition		14:0	16:0	16:1ω7	18:0	18:1ω9	18:2ω6	18:3n3	Others
RCD composition		0.67%	16.35%	0.63%	3.41%	19.50%	51.59%	5.05%	2.80%
HFD composition		3.81%	12.80%	0.25%	5.81%	29.38%	34.91%	3.67%	9.37%

Diet	Genotype	Age	14:0	16:0	16:1ω7	18:0	18:1ω9	18:2ω6	18:3n3	Others
RCD	WT	2 month	1.64%±0.03%	26.30%±1.07%	4.59%±0.40%	2.98%±0.38%	31.91%±0.71%	29.72%±1.74%	0.88%±0.51%	1.98%±1.06%
		4 month	1.05%±0.03%	25.92%±0.46%	5.34%±0.40%	4.00%±1.49%	31.70%±0.70%	27.46%±1.00%	1.50%±0.23%	3.04%±0.52%
		10 month	1.04%±0.17%	23.10%±0.47%	4.23%±0.38%	2.85%±0.16%	37.95%±1.03%	27.11%±0.67%	0.93%±0.32%	2.80%±0.70%
		14 month	0.98%±0.05%	23.02%±1.40%	5.17%±0.84%	2.26%±0.63%	38.05%±0.52%	26.96%±0.45%	0.94%±0.32%	2.61%±0.95%
	OB	2 month	1.63%±0.04%	29.43%±0.45%	7.13%±0.02%	3.49%±0.11%	38.22%±0.26%	16.27%±0.52%	1.39%±0.10%	2.44%±0.07%
		4 month	1.22%±0.10%	27.30%±0.43%	6.72%±0.08%	2.50%±0.14%	43.64%±0.66%	15.02%±0.58%	0.91%±0.11%	2.70%±0.58%
		10 month	0.64%±0.10%	19.98%±0.58%	4.41%±0.14%	1.77%±0.14%	53.23%±0.62%	16.65%±0.48%	0.69%±0.07%	2.63%±0.55%
		14 month	1.04%±0.11%	20.74%±0.72%	4.98%±0.26%	2.75%±0.30%	49.03%±0.60%	18.24%±0.99%	0.56%±0.16%	2.66%±0.33%
HFD	WT	2 month	1.95%±0.07%	15.81%±0.72%	2.24%±0.22%	2.91%±0.13%	40.62%±0.64%	32.91%±0.90%	1.98%±0.16%	1.58%±0.48%
		4 month	1.84%±0.03%	14.47%±0.73%	1.63%±0.34%	3.19%±0.10%	42.79%±0.80%	30.90%±0.63%	1.86%±0.11%	3.33%±0.31%
		10 month	1.52%±0.26%	14.28%±1.14%	1.69%±0.54%	3.42%±0.52%	42.65%±2.64%	31.10%±1.30%	1.44%±0.36%	3.90%±0.79%
		2 month	1.85%±0.15%	21.71%±1.08%	2.94%±0.27%	3.69%±0.52%	42.38%±1.06%	23.53%±1.34%	1.22%±0.21%	2.67%±0.71%
	OB	4 month	1.23%±0.06%	18.92%±0.88%	2.10%±0.08%	3.53%±0.18%	51.12%±1.30%	20.42%±2.15%	0.42%±0.17%	2.28%±0.20%
		10 month	1.33%±0.06%	21.58%±1.28%	3.01%±0.54%	3.41%±0.17%	55.80%±2.21%	11.32%±1.17%	0.14%±0.07%	3.41%±0.45%

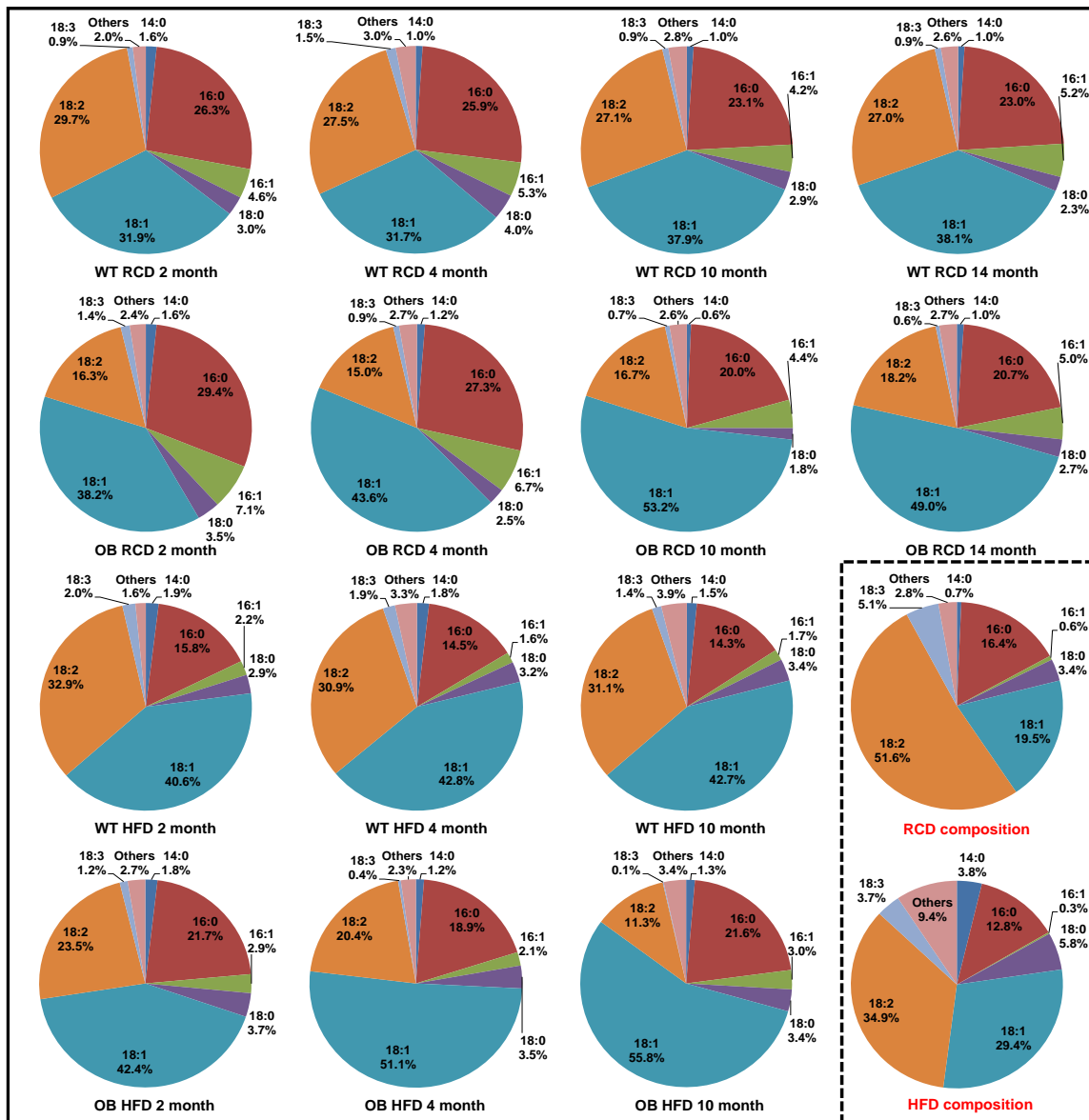


Fig 3.5 Total fatty acid (FA) composition in adipose tissues from *ob/ob* (OB) mice and wild-type (WT) controls aged between 2 and 14 months fed by regular chow diet (RCD) and high-fat diet (HFD), and total FA composition in the two diets. The color depth indicates the relative content of the FA comparing different animal groups (Red means more; blue means less).

It is obvious in **Fig 3.5** that the adipose tissues of RCD-fed wild-type (WT-RCD) mice have markedly different total FA compositions compared with the RCD diet itself. The content of C18:2 ω 6 was decreased from 51.59% in the RCD diet to 15.02%-29.72% in adipose tissues of WT-RCD mice ($P < 0.0001$ using two-way ANOVA). C18:3 ω 3 was also decreased from 5.05% to 0.56%-1.50% but not significantly ($P > 0.05$) according to the results of two-way ANOVA. On the contrary, the percentages of C16:0 (from 16.35% to 19.98%-29.43%), C16:1 ω 7 (from 0.63% to 4.41%-7.13%) and C18:1 ω 9 (from 19.50% to 31.70%-53.23%) were increased in WT-RCD mice compared with the RCD diet. The adjusted P-values by Dunnett's multiple comparisons test in two-way ANOVA were summarized as below ($P < 0.05$ were in red). These

changes suggest that DNL, desaturation by SCDs, and elongation by ELOVL6 play an important role in the FA composition of WT-RCD adipose tissues.

	14:0	16:0	16:1 ω 7	18:0	18:1 ω 9	18:2 ω 6	18:3 ω 3	Others
RCD vs. WT-RCD-2 month	0.9974	<0.0001	0.2657	0.9997	<0.0001	<0.0001	0.2176	0.9994
RCD vs. WT-RCD-4 month	0.9997	<0.0001	0.0932	0.9996	<0.0001	<0.0001	0.3238	0.9999
RCD vs. WT-RCD-10 month	0.9997	0.0076	0.3659	0.9996	<0.0001	<0.0001	0.2288	>0.9999
RCD vs. WT-RCD-14 month	0.9998	0.0086	0.1502	0.9943	<0.0001	<0.0001	0.2317	0.9999
RCD vs. OB-RCD-2 month	0.9971	<0.0001	0.0057	>0.9999	<0.0001	<0.0001	0.2809	0.9997
RCD vs. OB-RCD-4 month	0.9996	<0.0001	0.0115	0.9974	<0.0001	<0.0001	0.1713	>0.9999
RCD vs. OB-RCD-10 month	>0.9999	0.2879	0.2491	0.947	<0.0001	<0.0001	0.1324	0.9999
RCD vs. OB-RCD-14 month	0.9997	0.149	0.1551	0.9995	<0.0001	<0.0001	0.1328	>0.9999

Total FA composition of the RCD-fed *ob/ob* mice (OB-RCD) clearly exhibit further increases in C18:1 ω 9 (from 31.70%-38.05% to 38.22%-53.23%, P<0.0001 in every age group) and a considerable decrease in C18:2 ω 6 (from 26.96%-29.72% to 15.02%-18.24%, P<0.0001 in every age group) compared with the WT-RCD group. The adjusted P-values by Dunnett's multiple comparisons test in two-way ANOVA were summarized as below (P<0.05 were in red). Thus, the efficiency of *de novo* synthesis of fatty acids was increased in *ob/ob* mice, presumably because of their raised appetite and hence increased consumption of carbohydrates from the RCD diet, and further modification related enzymes, such as the Δ 6 desaturase FADS2, is not enough for the newly synthesized FAs. The newly synthesized 16-carbon FAs (C16:0 and C16:1 ω 7) were more in younger (2 and 4 months) OB-RCD mice compared with older (10 and 14 months) OB-RCD animals, as C18:1 ω 9 dominated the total fatty acid profile of the older animals (over a half).

	14:0	16:0	16:1 ω 7	18:0	18:1 ω 9	18:2 ω 6	18:3 ω 3	Others
WT-RCD-2 month vs. OB-RCD-2 month	>0.9999	0.0773	0.2745	0.9998	<0.0001	<0.0001	0.9998	0.9999
WT-RCD-4 month vs. OB-RCD-4 month	>0.9999	0.7573	0.7565	0.6718	<0.0001	<0.0001	0.9976	>0.9999
WT-RCD-10 month vs. OB-RCD-10 month	>0.9999	0.0814	>0.9999	0.9745	<0.0001	<0.0001	>0.9999	>0.9999
WT-RCD-14 month vs. OB-RCD-14 month	>0.9999	0.5309	>0.9999	>0.9999	<0.0001	<0.0001	>0.9999	>0.9999

However, in the profile of WT-HFD mice, C16:0 (from 23.02%-26.30% to 14.28%-15.81%) and C16:1 ω 7 (from 4.23%-5.34% to 1.63%-2.24%) significantly decreased, whereas C18:1 ω 9 (from 31.70%-38.05% to 40.62%-42.79%) and C18:2 ω 6 (from 26.96%-29.72% to 30.90%-32.91%) increased in all age groups compared with the corresponding WT-RCD mice at any ages. The adjusted P-values by Dunnett's multiple comparisons test in two-way ANOVA were summarized as below (P<0.05 were in red). This phenomenon has been pretty obvious in the 2-month old mice which were switched to HFD only after weaning period (5 weeks) with shorter HFD feeding (3 weeks) compared with other groups (3 months). These changes largely follow the fatty acid profiles of the HFD itself, showing the adipose tissue is dominated by diet.

However, adipose tissue from WT-HFD mice still has significantly more C16:0 and C18:1 ω 9 and slightly less C18:2 ω 6 and C18:3 ω 3 compared with the HFD diet, indicating a certain level of *de novo* lipogenesis.

	14:0	16:0	16:1 ω 7	18:0	18:1 ω 9	18:2 ω 6	18:3 ω 3	Others
WT-RCD-2 month vs. WT-HFD-2 month	0.9998	<0.0001	0.3024	>0.9999	<0.0001	0.0572	0.9242	0.9992
WT-RCD-4 month vs. WT-HFD-4 month	0.8924	<0.0001	<0.0001	0.8831	<0.0001	<0.0001	0.9966	0.9986
WT-RCD-10 month vs. WT-HFD-10 month	0.9957	<0.0001	0.0887	0.9910	<0.0001	0.0006	0.9948	0.8609

In OB-HFD mice, the FA composition is a mixture of HFD dietary FAs and *de novo* synthesized FAs. The HFD still exhibited a great effect to increase specific FAs like C18:1 ω 9, C18:2 ω 6 and C14:0 when compared to OB-RCD mice, while the inability to produce leptin also triggered more *de novo* synthesis of FAs and increased the content of C16:0 and C18:1 ω 9 compared with the WT-HFD mice. The adjusted P-values by Dunnett's multiple comparisons test in two-way ANOVA were summarized as below (P<0.05 were in red).

	14:00	16:00	16:1 ω 7	18:00	18:1 ω 9	18:2 ω 6	18:3 ω 3	Others
OB-RCD-2 month vs. OB-HFD-2 month	>0.9999	<0.0001	0.0005	>0.9999	0.0006	<0.0001	>0.9999	>0.9999
OB-RCD-4 month vs. OB-HFD-4 month	>0.9999	<0.0001	<0.0001	0.9783	<0.0001	<0.0001	0.9999	>0.9999
OB-RCD-10 month vs. OB-HFD-10 month	0.9985	0.7740	0.8756	0.7417	0.1607	<0.0001	0.9997	0.9964
WT-HFD-2 month vs. OB-HFD-2 month	>0.9999	0.0012	>0.9999	0.9998	0.9452	<0.0001	0.9998	0.9976
WT-HFD-4 month vs. OB-HFD-4 month	0.9996	0.0005	>0.9999	>0.9999	<0.0001	<0.0001	0.8943	0.9823
WT-HFD-10 month vs. OB-HFD-10 month	>0.9999	<0.0001	0.9581	>0.9999	<0.0001	<0.0001	0.9620	>0.9999

In addition, aging is also associated with more C18:1 ω 9 in adipose tissue of most of the four groups of animals, while C16:0, C18:2 ω 6 and C18:3 ω 3 decline in adipose tissue in older mice, which means more DNL and FA elongation by ELOVL6 and desaturation by SCDs occurring as the mice ages, which is remarkably similar to the FA alteration pattern induced by leptin deficiency. Moreover, the FA composition in *ob/ob* mice is more unstable to the aging factor than that in wild-type animals. These suggest there might be some connection between obesity and aging in metabolism. The adjusted P-values by Dunnett's multiple comparisons test comparing in two-way ANOVA 2-month old mice and 10-month old mice were summarized as below (P<0.05 were in red).

	14:00	16:00	16:1 ω 7	18:00	18:1 ω 9	18:2 ω 6	18:3 ω 3	Others
WT-RCD-2 month vs. WT-RCD-10 month	>0.9999	0.3780	>0.9999	>0.9999	0.0014	0.6445	>0.9999	0.9993
OB-RCD-2 month vs. OB-RCD-10 month	0.9645	<0.0001	0.0740	0.5950	<0.0001	>0.9999	0.9953	>0.9999
WT-HFD-2 month vs. WT-HFD-10 month	>0.9999	0.9683	>0.9999	>0.9999	0.8673	0.9245	>0.9999	0.7703
OB-HFD-2 month vs. OB-HFD-10 month	0.9994	>0.9999	>0.9999	>0.9999	<0.0001	<0.0001	0.9423	0.9931

The influences on major FAs in adipose tissue are summarized as below:

	16:0	16:1 ω 7	18:1 ω 9	18:2 ω 6	18:3 ω 3
<i>Ob/ob</i>	↑	↑	↑	↓	↓
HFD	↓	↓	↑	↑	↑
Aging	↓	↓	↑	↓	↓

3.4.3 Multivariate analysis of lipids in adipose tissues from different mouse models

Next, neutral lipids (TGs, DGs, and sterols) from all the adipose tissue samples were determined by DI-MS. Because neutral lipids dominate the adipose tissue and few polar lipids can be identified from the DI-MS profile, an SPE-UPLC-MS method was developed to separate and detect membrane lipids (lysoPCs, PCs, PEs, PSs) from adipose tissues. Following the Bligh and Dyer (BD) method [435, 447] for tissue extraction of both polar and neutral lipids, different SPE methods were tested as a preliminary experiment to further separate different fractions of lipids and improve their detection. The optimized pre-treatment method as described in section 2.6 gives four fractions which separated phospholipids well according to the total ion chromatography (TIC) (**Fig 3.6**). The fraction D was used for studying membrane lipids (lysoPCs, PCs, PEs, PSs) from adipose tissues.

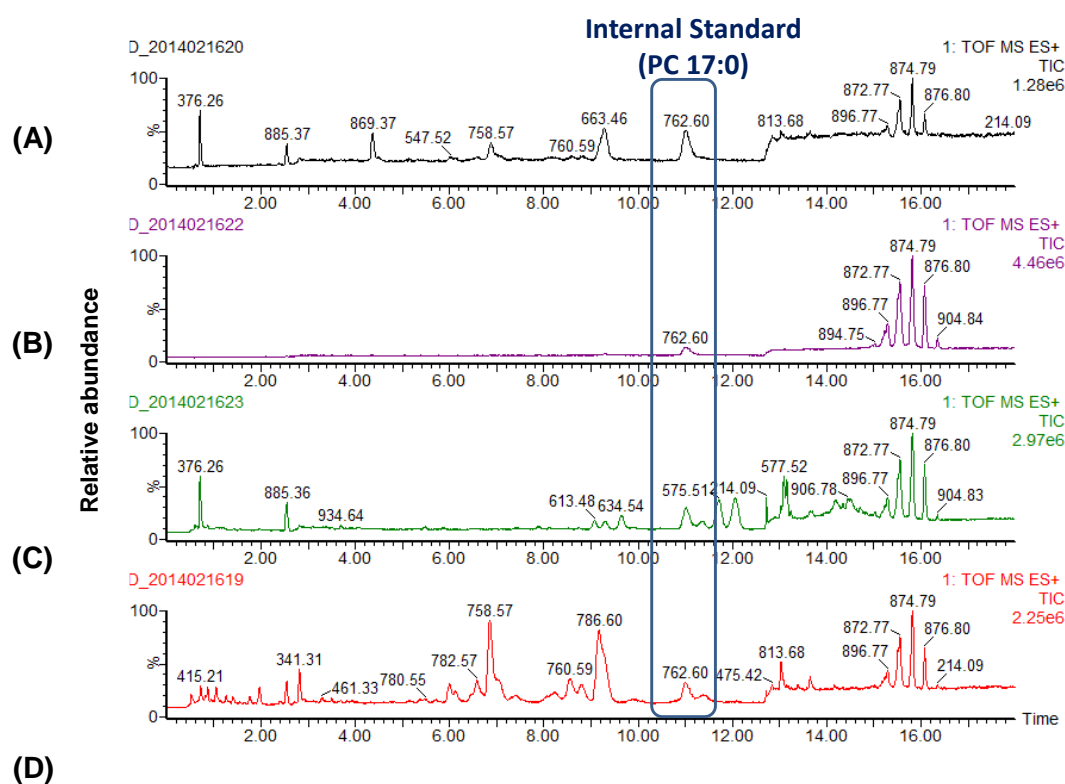


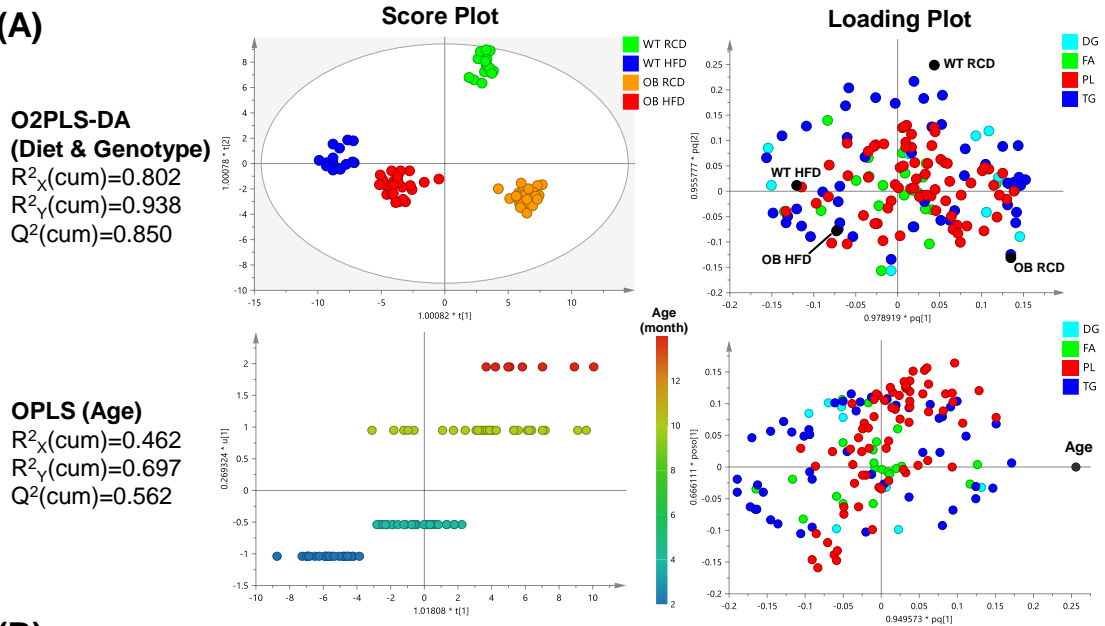
Fig. 3.6 Total ion chromatographs (TICs) of fractions by the optimized solid phase extraction (SPE) method. (A) the fraction of cholesteryl esters; (B) the fraction of triacylglycerides; (C) the fraction of monoacylglycerides; (D) the fraction of phospholipids. Internal standard: lyso-phosphocholine C17:0.

In total, I systematically measured 157 species in 7 major lipid classes—FA, DG, TG, lysoPC, PC, PE, and PS. These metabolites in adipose tissue of the *ob/ob* and wild-type mice fed on the RCD and HFD diets were readily differentiated by two-way orthogonal partial least squares (O2PLS-DA, **Fig 3.7A** first row, $Q^2=0.850$). It is apparent in the O2PLS-DA scores plot both the WT-HFD and OB-RCD groups can be separated well from the WT-RCD group along directions of the first component (horizontal) and the second component (vertical), respectively. The OB-HFD group is closer to the WT-HFD group than to the OB-RCD ones, indicating that the genotype does not influence the metabolic profile as much as HFD does, reflecting that the composition of the HFD had a more profound effect on the composition of adipose tissue than obesity per se. This analysis shows that in the upper right loading plot TG species have the widest distribution along both the first and second components, but phospholipids were only distributed along the first component (horizontal). This suggests that TGs were altered by both genotype and diet, whereas PC composition was influenced more by diet than by genotype (and hence contributing to only one component). Applying OPLS, the model for correlating lipids with aging was not as strong as the models for genotype and diet (**Fig 3.7A** second row, $Q^2=0.562$). However, it is apparent from the loading plot that the TGs explain aging effects better than other lipid species, as TGs have the widest distribution along the first OPLS component (horizontal). Furthermore, more OPLS-DA and OPLS models were established in segments according to the three factors (diet, genotype, and aging) using each class of these metabolites (FA, DG, TG, PC, lysoPC, PE, PS). The table in **Fig 3.7B** shows how well the lipid data fitted the models. All the neutral lipids (FA, DG, and TG) were fitted well in OPLS-DA models that differentiate different diets and genotypes (all $Q^2>0.48$), while for the phospholipids only PCs could be used to build a good model to differentiate OB/WT mouse genotype. LysoPCs, PEs or PSs can be used to build a moderately significant ($Q^2 >0.4$) OPLS-DA model for diet comparison. As for age, only the PLS model of TGs has a relatively high Q^2 (0.602), while PCs produce models with acceptable Q^2 values (0.409). Interrogation of the corresponding loadings plots and the variable influence on projection (VIP) for these OPLS (-DA) models identified individual metabolites responsible for the separation across the two diets, two genotypes and ages examined. The validity of these models built by OPLS or OPLS-DA were checked by a cross-validation function using a permutation approach within the SIMCA P⁺ software. The ANOVA of the cross-validated residuals (CV-ANOVA) was applied to ensure that these models were not over-fitted. As shown in **Table 3.2**, all the models used for further investigation pass validation. For every successive component built for a model, the cross-validation was calculated until the generation of new components doesn't improve the model's

predictive power. Models with Q^2 values greater than 0.4 are considered significantly predictive. **Fig 3.7C** illustrates metabolites changed most significantly with diet, genotype, and age from acceptable multivariate models in **Fig 3.7B**. Moreover, percentages of lipids with the same total FA carbons or total FA unsaturation are added up respectively for the seven lipid classes in **Fig 3.8** (the corresponding significance statistics is in **Table 3.3**) and **Fig 3.9** (the corresponding significance statistics is in **Table 3.4**), to provide weighted average information about how individual lipid classes are influenced by elongation and desaturation according to genotype, diet and age factors.

Quantity	SS	DF	MS	F	p	SD
Genotype						
FA						
Total corr.	91	91	1			1
Regression	44.1973	2	22.0987	42.0229	1.41E-13	4.70092
Residual	46.8027	89	0.525873			0.725171
DG						
Total corr.	91	91	1			1
Regression	51.1833	6	8.53055	18.2109	1.76E-13	2.92071
Residual	39.8167	85	0.468432			0.684421
TG						
Total corr.	91	91	1			1
Regression	79.6603	10	7.96603	56.9019	1.99E-32	2.82242
Residual	11.3397	81	0.139996			0.37416
PC						
Total corr.	91	91	1			1
Regression	52.8279	8	6.60349	14.3584	6.21E-13	2.56972
Residual	38.1721	83	0.459905			0.678163
Diet						
FA						
Total corr.	91	91	1			1
Regression	61.8452	4	15.4613	46.1377	9.59E-21	3.93209
Residual	29.1547	87	0.335112			0.578889
DG						
Total corr.	91	91	1			1
Regression	70.3386	6	11.7231	48.2284	2.53E-25	3.4239
Residual	20.6614	85	0.243075			0.493026
TG						
Total corr.	91	91	1			1
Regression	80.2061	4	20.0515	161.617	0	4.47789
Residual	10.7939	87	0.124068			0.352233
PC						
Total corr.	91	91	1			1
Regression	72.5976	8	9.07469	40.9294	1.10E-25	3.01242
Residual	18.4024	83	0.221716			0.470867
Age						
TG						
Total corr.	91	91	1			1
Regression	54.7458	8	6.84322	15.6668	8.10E-14	2.61596
Residual	36.2542	83	0.436798			0.660907
PC						
Total corr.	91	91	1			1
Regression	37.1973	8	4.64966	7.17291	3.50E-07	2.15631
Residual	53.8027	83	0.648225			0.805125

Table 3.2 Results from CV-ANOVA of the OPLS/OPLS-DA models for lipid species changed most significantly by genotype/diet/age

(A)**(B)**

	Genotype (OPLS-DA)			Diet (OPLS-DA)			Age (OPLS)		
	$R^2_X(\text{cum})$	$R^2_Y(\text{cum})$	$Q^2(\text{cum})$	$R^2_X(\text{cum})$	$R^2_Y(\text{cum})$	$Q^2(\text{cum})$	$R^2_X(\text{cum})$	$R^2_Y(\text{cum})$	$Q^2(\text{cum})$
All	0.617	0.946	0.872	0.299	0.931	0.894	0.462	0.697	0.562
FA	0.181	0.555	0.486	0.297	0.765	0.680	0.164	0.419	0.371
DG	0.844	0.585	0.562	0.573	0.892	0.881	0.865	0.421	0.368
TG	0.872	0.905	0.875	0.672	0.892	0.862	0.843	0.665	0.602
PC	0.720	0.686	0.581	0.731	0.852	0.798	0.728	0.612	0.409
lysoPC	0.463	0.434	0.392	0.615	0.658	0.592	0.679	0.476	0.370
PE	0.324	0.419	0.331	0.740	0.683	0.595	0.489	0.484	0.384
PS	0.394	0.278	0.192	0.821	0.602	0.447	0.327	0.123	0.056

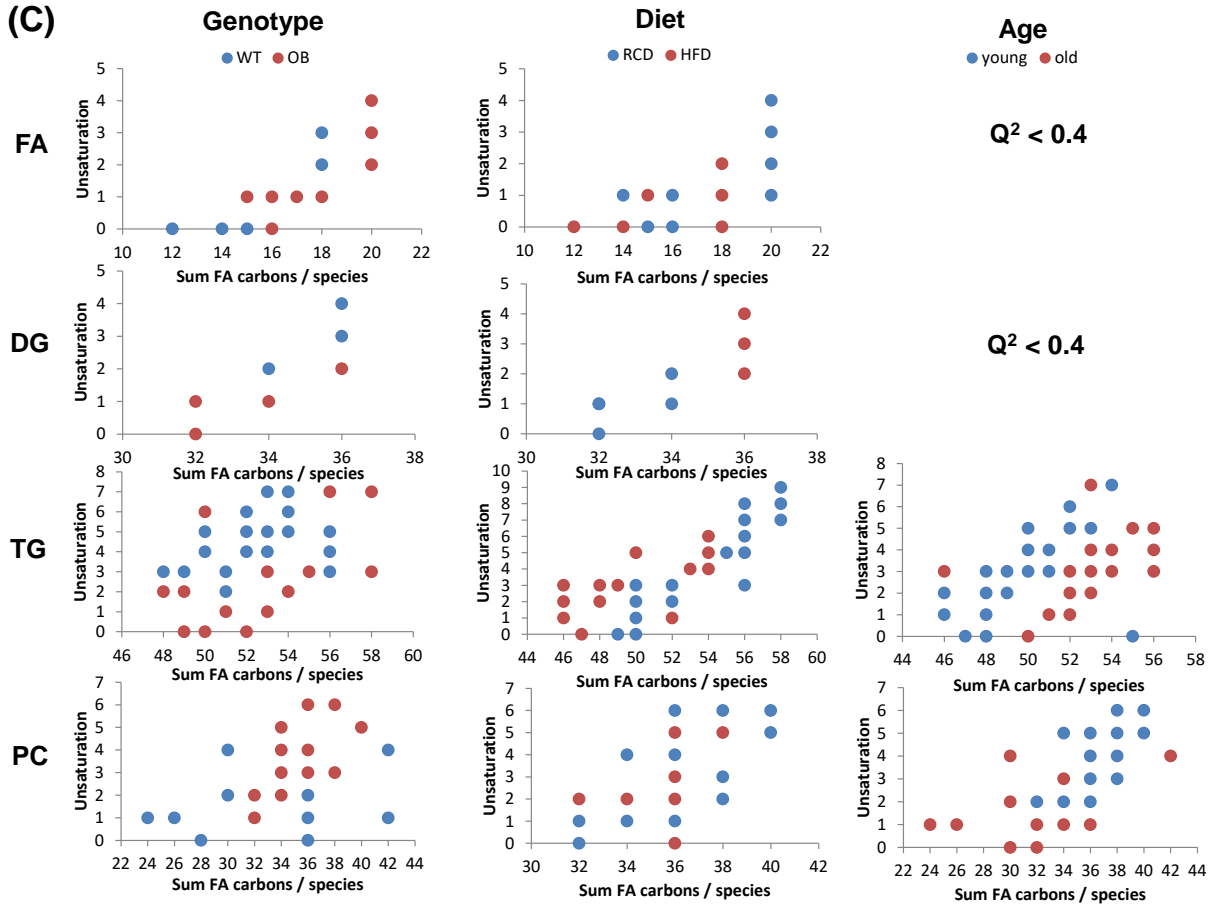
(C)

Fig 3.7 (A) Multivariate analysis of adipose tissues from different mouse models (OB/WT, RCD/HFD, 2/4/10/14-month) using all classes of lipids (30-40 samples in each group); **(B)** OPLS-DA and OPLS model for each class of lipids detected in adipose tissue, and the specific lipids which changed the most according to these models. **(C)** Lipid species changed most significantly by genotype/diet/age according to the models in (B)

3.4.4 Neutral lipids and phospholipids exhibit opposite changes in chain length and unsaturation in *ob/ob* mice

As shown in the first row of **Fig 3.8**, the total content of 16-carbon FAs increased in all younger *ob/ob* groups (2 months and 4-month animals) fed on either RCD or HFD. This could be due to the increase in total C16:0 (palmitate) and C16:1 ω 7 (palmitoleate) which was reported in **Fig 3.5**. On the other hand, the total content of 18-carbon FAs slightly decreased, in part because of the decrease of C18:2 ω 6 offsetting the increase of C18:1 ω 9 in *ob/ob* mice. Thus, the average per chain length carbon number decreased from 17.49 (WT) to 17.40 (*ob/ob*) (**Fig 3.10**, the corresponding significance statistics is in **Table 3.5**). Side chain length also decreased in DGs and TGs, due to rise in 32/34-carbon DGs and 50/52-carbon TGs, and a decrease in 36-carbon DGs and 54-carbon TGs in most groups (**Fig 3.8**, second and third rows). The average per chain carbon number decreased from 17.49 and 17.42 to 17.44 and 17.39 for DGs and TGs, respectively (**Fig 3.10A**). Interestingly, total content of 16-carbon FAs were moderately decreased while total content of 18-carbon FAs increased a bit in adipose tissue of older *ob/ob* mice fed on RCD diet (10 months and 14 months), as C18:1 ω 9 synthesized from DNL induced by aging dominated the total fatty acid profile of older animals (over a half).

The changes in unsaturation of all neutral lipids are much more significant than changes in chain length across the individual animal models. The major peak that dominated the FA profiles was monosaturated FAs in all *ob/ob* profiles (**Fig 3.9**, first row) because of the dominance of C18:1 ω 9 (**Fig 3.5**). In the left column of **Fig 3.7C**, it is also obvious that all the monosaturated FAs are more in the *ob/ob* adipose tissue. All other FAs decreased to some degree compared with monosaturated FAs, although the saturated FAs didn't decrease as much as polyunsaturated FAs presumably because of increased *de novo* FA synthesis provided a supply of C16:0. Overall this meant the average per chain degree of unsaturation (DU) of FA, DG and TG declined markedly from wild-type (1.07, 1.19 and 1.12) to *ob/ob* mice (0.92, 1.07 and 1.03) (**Fig 3.10B**).

Interestingly, phospholipids, especially PCs exhibited a completely opposite trend in *ob/ob* mice. PCs were slightly longer and more unsaturated in *ob/ob* mice (WT, 17.53, 0.99 vs. OB, 17.63, 1.12), in particular in older animals (10 months, 14 months) fed on RCD diet and younger animals (2 months) fed on HFD diet (**Fig 3.10**). It is apparent that the most significant change in the fifth row of **Fig 3.8** is that all the DU>2 PCs increased, forming an even distribution in the OB-RCD unsaturation profiles. The left column of **Fig 3.9** also demonstrates that in spite of the flood of newly synthesized C16:0 and C18:1 from DNL, more highly unsaturated FAs (DU>2) are selectively incorporated into PCs, in contrast with the increased neutral lipids (FAs, DGs and TGs) with DU<2. There are more fluctuations in the DU of PCs in adipose tissue of wild-type animals compared with *ob/ob* mice, presumably because activated DNL by leptin deficiency in *ob/ob* mice led to more control on the lipid composition. LysoPCs and PEs also become more unsaturated in *ob/ob* (lysoPC 0.73, PE 0.77) compared to WT mice (lysoPC 0.71, PE 0.72) in older animals fed on the RCD diet and younger animals fed on the HFD diet (**Fig 3.10B**). Interestingly, the DU of phospholipids was decreased in adipose tissue of mice fed on HFD at 10 months. The mechanism to maintain unsaturation of membrane lipid may be impaired in old mice fed on HFD. Furthermore, longer FAs (>18 carbons) were incorporated into the PEs and PSs (**Fig 3.8**, the sixth and seventh rows), compared with other lipids (FA, DG, TG, lysoPC, PC). The PEs containing 38 carbons are the dominant species in every PE chain length profile, and the PS profiles have three major components (36-carbon, 38-carbon, 40-carbon). For neither phospholipid class was the average per chain carbon number less than 18.

3.4.5 The High-fat diet (HFD) itself is the determining factor for the lipid composition in mice adipose tissue

When examining FA chain length differences (**Fig 3.8**, the first row), it is consistent with **Fig 3.5** that more 18-carbon FAs and fewer 16-carbon FAs were detected in adipose tissue from HFD-fed mice reflecting the FA-content of the diet. This resulted in an elongation for all other lipid classes following feeding of HFD. The increases and decreases in side chain length of DGs and TGs largely reflects the variations of 16-carbon and 18-carbon FAs (**Fig 3.8**, the second and third rows), e.g. 54-carbon TGs (mostly comprised of three 18-carbon FA chains) increased in HFD-fed mice, while 50-carbon TGs (mostly composed of two 16-carbon FAs and one 18-carbon FA) and 52-carbon TGs (one 16-carbon and two 18-carbon FA chains) decreased when changing the diet from RCD to HFD. The changes of 32, 34, 36-carbon DGs

in HFD-fed mice adipose tissues are similar to the 50, 52, 54-carbon TGs, respectively. The average per chain carbon number in every lipid class increased after HFD feeding (FA, 17.51, DG, 17.59, TG, 17.44) compared with the RCD diet (FA 17.37, DG 17.37, TG 17.38) (**Fig 3.10A**).

Considering the degree of unsaturation (DU), changes were not as large as those in FA chain length of these lipids. As described above, C16:0 and C16:1 decreased, while C18:1, C18:2 and C18:3 increased across the neutral lipids. The decline in C16:0 resulted in decreases of total saturated FA species (**Fig 3.9**), whereas decreased C16:1 and increased C18:1 contributed to a slight increase in the total monounsaturated FAs content. The small increase in C18:2 also produced a small rise of lipids whose DU is 2. These changes in unsaturation of FAs were also detected in the profiles of DGs and TGs, with increased highly unsaturated TGs (DU>3) and DGs (DU>2), and decreased TGs (DU<3) and DGs (DU<2). The average per chain DU of FA, DG and TG increased from 0.95, 1.06 and 1.05 to 1.01, 1.22 and 1.12, respectively in HFD-fed mice compared with RCD-fed ones (**Fig 3.10B**).

In phospholipids, the chain length changes of lysoPC and PC with diet were similar to those of FAs and DGs. While 16-carbon lysoPCs and 32/34-carbon PCs decreased, 18-carbon lysoPCs and 36-carbon PCs increased notably in the adipose tissue of HFD-fed mice compared with the RCD feeding (**Fig 3.8**, the fourth and fifth rows). Computed average per chain length carbon number of the four phospholipid classes also demonstrate that they have become longer in HFD-fed mice (lysoPC, 17.80, PC, 17.65, PE, 18.68, PS, 18.27) in comparison to those in RCD-fed mice (lysoPC, 17.64, PC, 17.51, PE, 18.63, PS, 18.13) (**Fig 3.10A**). Moreover, all the membrane lipids exhibit similar trends to neutral lipids to become more desaturated when comparing HFD-fed mice with RCD-fed mice (**Fig 3.9**, the 4th-7th rows). The average per chain DU increased from (0.70, 1.03, 0.72 and 0.51) to (0.74, 1.08, 0.78 and 0.57) for lysoPC, PC, PE and PS, respectively (**Fig 3.10B**).

Considering the identified lipids which are most changed by HFD in **Fig 3.7C** (medium column), it is striking that although there are more 18-carbon FAs in HFD-fed mice (red blots), all the 20-carbon FAs were increased in RCD-fed mice (blue blots). This reflects the fact that adipose tissue from the RCD-fed mice has a more diversified distribution of lipids in part due to *in vivo* DNL and modifications. In HFD-fed mice, most of the FAs stored in adipose tissue directly relate to diet with few modifications. Accordingly, a large number of long, highly

unsaturated TGs were in higher concentration in adipose tissue from RCD-fed mice, even though the average chain length and average DU of TGs were greater in HFD-fed mice (18-carbon FAs and 54-carbon TGs account for a greater proportion in adipose tissue lipid composition). More long, highly unsaturated PCs were detected in RCD-fed mice adipose tissues but the trend is not as apparent as in the pool of TGs. This suggests some selective partition of most dietary FAs incorporated into TGs, so that membrane lipids are more determined by DNL and *in vivo* modifications and less directly by the fat content of the diet.

3.4.6 Longer triacylglycerides (TGs) and saturated phosphatidylcholines (PCs) accumulate in adipose tissue of aged mice

As discussed previously in **Fig 3.5**, C18:1 increased while C16:0 decreased sharply with age. These total FA changes are mostly reflected in longer-chain containing TGs in aged mice as shown in **Fig 3.7C**. There are more 54-carbon TGs and less 50-carbon TGs in older mice (the third row of **Fig 3.8**). The average per chain carbon numbers of TG in adipose tissue is 17.33, 17.42, and 17.47 for 2-month, 4-month, and 10-month mice respectively (**Fig 3.10A**). DGs also exhibit a similar trend, containing longer fatty acids (average per chain carbon number: 17.41<17.47<17.52 for 2, 4, 10-month respectively, **Fig 3.10A**).

Interestingly, PCs again demonstrated a totally different trend compared with neutral lipids. In the bottom right plot of **Fig 3.7B**, there are more saturated and monounsaturated PCs in older mice compared with the equivalent younger animals. The averaged DU of PCs in adipose tissue is 1.12, 1.09, and 1.08 for 2-month, 4-month, and 10-month mice, respectively (**Fig 3.10B**). Saturated and DU=1 PCs increased with age while DU=2 PCs decreased with age in WT-RCD, OB-RCD, and OB-HFD profiles (the fifth row of **Fig 3.9**). In the WT-HFD group, the DU=2 PCs increased in aged mice. One possible explanation is that HFD influences more greatly the PC composition of adipose tissue in aged mice. Other phospholipids show a similar trend, becoming more saturated (average per chain DU: PE 0.78>0.77>0.76 and PS 0.58>0.50>0.49 for 2, 4, 10-month respectively, **Fig 3.10B**).

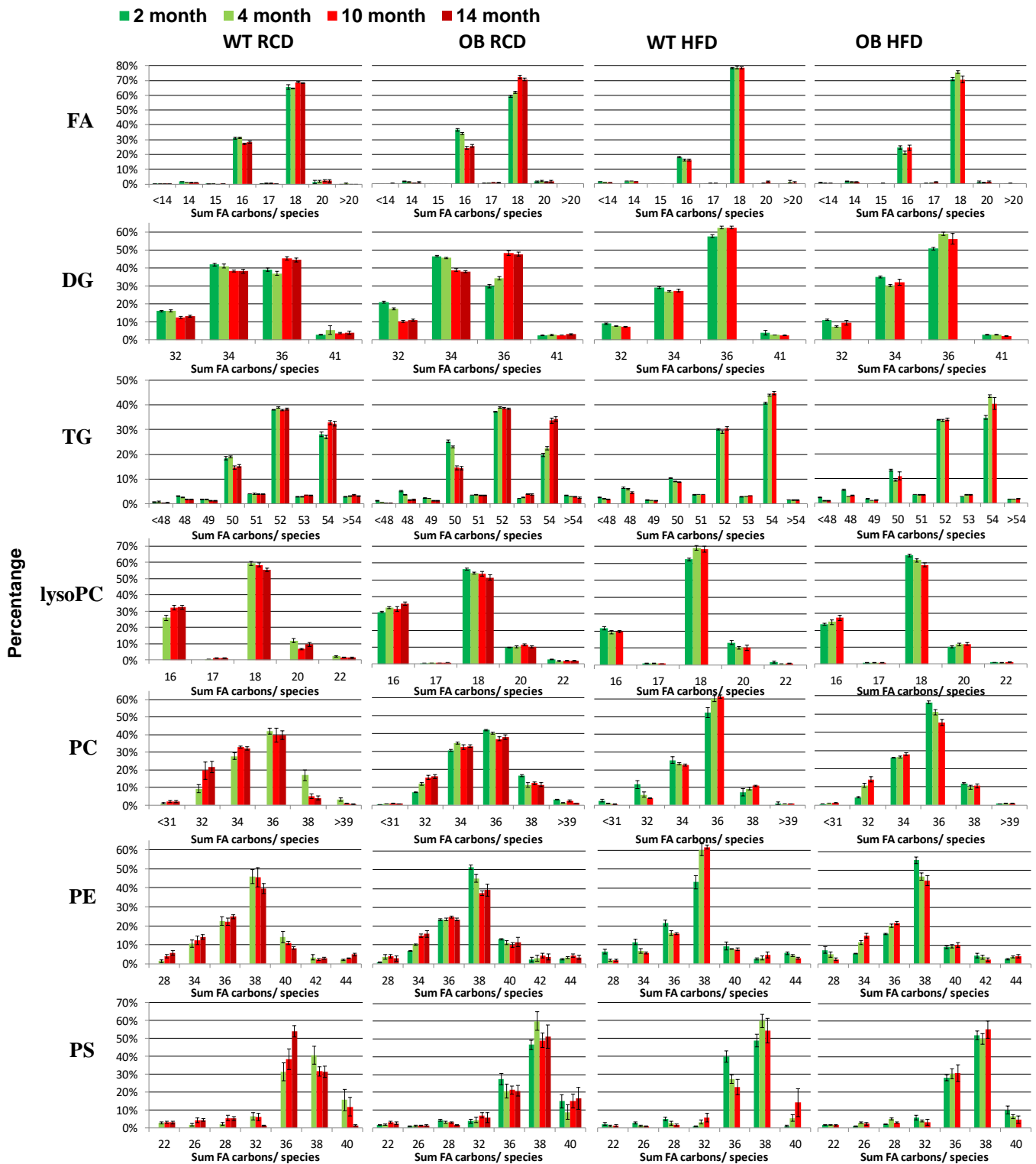


Fig 3.8 Side chain length varies in adipose tissues from *ob/ob* (OB) mice and wild-type (WT) controls aged between 2 and 14 months fed on a regular chow diet (RCD) or a high-fat diet (HFD). The values are the percentage relative to the sum of all the lipids of the same category (e.g. the sum of all the FAs/DGs/TGs...)

(A)		Mean Difference (%)	16C-FA	18C-FA	50C-TG	52C-TG	54C-TG	32C-PC	34C-PC	36C-PC	38C-PC
Genotype	WT-RCD-4 month vs. OB-RCD-4 month	-2.7640	2.6010	-4.0620	0.0185	4.4910	-2.6340	-6.7920	1.7410	5.8280	
	WT-RCD-10 month vs. OB-RCD-10 month	2.9280	-3.4950	0.0425	-0.7343	-0.7149	4.1320	0.5932	2.8750	-7.3040	
	WT-HFD-4 month vs. OB-HFD-4 month	-4.9220	3.2520	-0.1759	-4.4540	0.4872	-5.0680	-3.1080	9.3040	-0.6535	
	WT-HFD-10 month vs. OB-HFD-10 month	-8.6240	7.9510	-2.2540	-3.4930	4.2640	-10.2600	-5.1570	16.1900	0.2295	
Diet	WT-RCD-4 month vs. WT-HFD-4 month	15.1600	-14.0700	9.8790	9.8000	-16.8900	3.5120	4.4390	-18.4100	7.8310	
	WT-RCD-10 month vs. WT-HFD-10 month	11.3600	-9.7770	5.8420	7.4110	-11.8500	15.7800	10.1700	-21.7900	-5.9000	
	OB-RCD-4 month vs. OB-HFD-4 month	13.0000	-13.4200	13.7600	5.3270	-20.8900	1.0790	8.1230	-10.8500	1.3490	
	OB-RCD-10 month vs. OB-HFD-10 month	-0.1916	1.6680	3.5450	4.6530	-6.8700	1.3830	4.4190	-8.4790	1.6340	
Aging	WT-RCD-4 month vs. WT-RCD-10 month	3.9270	-4.1750	4.3120	1.0240	-5.9190	-10.2600	-5.1860	2.1440	12.1200	
	WT-HFD-4 month vs. WT-HFD-10 month	0.1280	0.1176	0.2747	-1.3650	-0.8776	2.0070	0.5445	-1.2370	-1.6110	
	OB-RCD-4 month vs. OB-RCD-10 month	9.6180	-10.2700	8.4160	0.2707	-11.1200	-3.4910	2.1990	3.2770	-1.0130	
	OB-HFD-4 month vs. OB-HFD-10 month	-3.5740	4.8170	-1.8040	-0.4033	2.8990	-3.1860	-1.5050	5.6480	-0.7281	
(B)		Adjusted P-value	16C-FA	18C-FA	50C-TG	52C-TG	54C-TG	32C-PC	34C-PC	36C-PC	38C-PC
Genotype	WT-RCD-4 month vs. OB-RCD-4 month	0.8183	0.8607	0.3265	>0.9999	0.2053	0.8525	0.0073	0.9828	0.0398	
	WT-RCD-10 month vs. OB-RCD-10 month	0.9140	0.8074	>0.9999	0.9999	>0.9999	0.3782	>0.9999	0.8062	0.0037	
	WT-HFD-4 month vs. OB-HFD-4 month	0.1457	0.6603	>0.9999	0.1852	>0.9999	0.0968	0.6757	<0.0001	>0.9999	
	WT-HFD-10 month vs. OB-HFD-10 month	0.0007	0.0026	0.9549	0.6758	0.4183	<0.0001	0.1825	<0.0001	>0.9999	
Diet	WT-RCD-4 month vs. WT-HFD-4 month	<0.0001	<0.0001	<0.0001	<0.0001	<0.0001	0.4866	0.1887	<0.0001	0.0003	
	WT-RCD-10 month vs. WT-HFD-10 month	0.0003	0.0033	0.0801	0.0070	<0.0001	<0.0001	<0.0001	<0.0001	0.1036	
	OB-RCD-4 month vs. OB-HFD-4 month	<0.0001	<0.0001	<0.0001	0.0660	<0.0001	0.9993	0.0007	<0.0001	0.9968	
	OB-RCD-10 month vs. OB-HFD-10 month	>0.9999	0.9812	0.4740	0.1433	0.0027	0.9948	0.2230	<0.0001	0.9857	
Aging	WT-RCD-4 month vs. WT-RCD-10 month	0.7330	0.6667	0.2204	0.9991	0.0187	<0.0001	0.1031	0.9457	<0.0001	
	WT-HFD-4 month vs. WT-HFD-10 month	>0.9999	>0.9999	>0.9999	0.9977	0.9999	0.9762	>0.9999	0.9988	0.9935	
	OB-RCD-4 month vs. OB-RCD-10 month	<0.0001	<0.0001	0.0001	>0.9999	<0.0001	0.6038	0.9454	0.6789	0.9995	
	OB-HFD-4 month vs. OB-HFD-10 month	0.4627	0.1143	0.9707	>0.9999	0.7219	0.6469	0.9913	0.0396	>0.9999	

Table 3.3 The mean differences (A) and adjusted P-values (B) when comparing side chain length in the adipose tissues from *ob/ob* (OB) mice and wild-type (WT) controls aged between 4 and 10 months fed on a regular chow diet (RCD) or a high-fat diet (HFD) using the Dunnett's multiple comparisons test in two-way ANOVA ($P < 0.05$ were in red). The values are the percentage relative to the sum of all the lipids of the same category (e.g. the sum of all the FAs/DGs/TGs...)

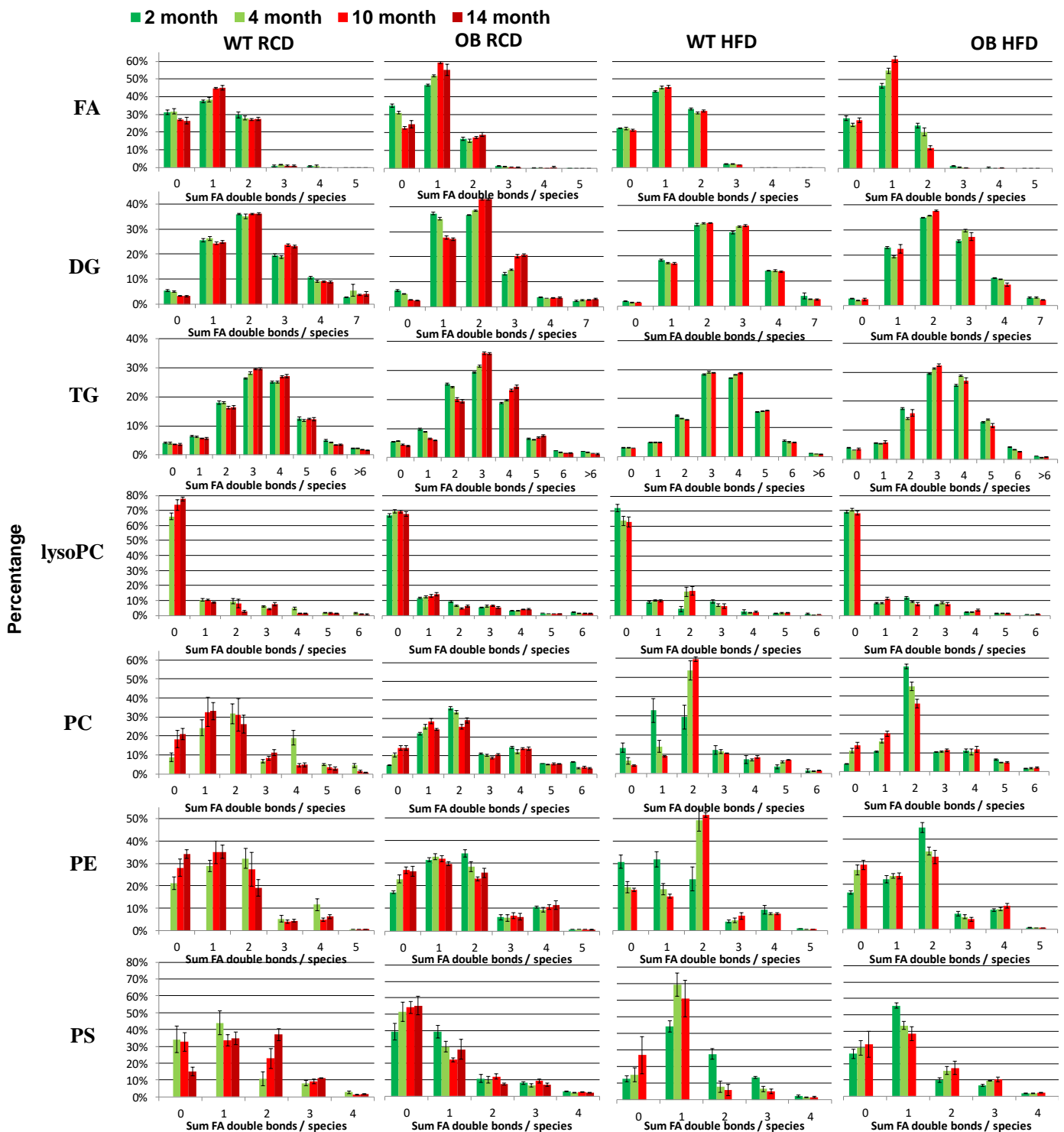


Fig 3.9 Side chain unsaturation varies in adipose tissues from *ob/ob* (OB) mice and wild-type (WT) controls aged between 2 and 14 months fed on a regular chow diet (RCD) or a high-fat diet (HFD). The values are the percentage relative to the sum of all the lipids of the same category (e.g. the sum of all the FAs/DGs/TGs...)

(A)	Mean Difference (%)	0U-FA	1U-FA	2U-FA	2U-TG	3U-TG	4U-TG	5U-TG	0U-PC	1U-PC	2U-PC	3U-PC	4U-PC
	Genotype	WT-RCD-4 month vs. OB-RCD-4 month	0.4584	-13.5900	12.3000	-6.4030	-3.3780	5.3960	5.7000	-1.5930	-1.1130	-1.8690	-3.5320
WT-RCD-10 month vs. OB-RCD-10 month		4.5030	-14.5300	9.8970	-3.7650	-6.3520	3.7850	5.5500	4.1740	4.1150	5.6450	-0.4061	-9.1570
WT-HFD-4 month vs. OB-HFD-4 month		-2.3520	-9.5830	10.4700	-0.9616	-2.1010	-0.5938	1.9900	-4.5870	-2.0690	8.7070	0.7126	-3.3370
WT-HFD-10 month vs. OB-HFD-10 month		-5.7470	-15.6700	20.3100	-3.3590	-3.4190	1.7070	4.1820	-9.7790	-11.2100	23.6800	-0.8240	-3.3790
Diet	WT-RCD-4 month vs. WT-HFD-4 month	9.5880	-6.8820	-3.0270	4.9120	-1.0220	-2.9790	-3.7980	2.2500	10.2300	-22.0900	-4.6670	12.0100
	WT-RCD-10 month vs. WT-HFD-10 month	5.9990	-0.7747	-4.7160	3.6460	0.6786	-1.8080	-3.3950	14.1700	23.6500	-28.3900	-2.1460	-3.8640
	OB-RCD-4 month vs. OB-HFD-4 month	6.7770	-2.8720	-4.8540	10.3500	0.2548	-8.9690	-7.5090	-0.7442	9.2720	-11.5100	-0.4218	1.7180
	OB-RCD-10 month vs. OB-HFD-10 month	-4.2520	-1.9120	5.7010	4.0510	3.6110	-3.8860	-4.7620	0.2190	8.3250	-10.3500	-2.5640	1.9150
Aging	WT-RCD-4 month vs. WT-RCD-10 month	4.5290	-6.5680	0.7618	1.7090	-1.5040	-1.8730	-0.5707	-9.5010	-8.2740	0.4545	-1.6030	14.5000
	WT-HFD-4 month vs. WT-HFD-10 month	0.9401	-0.4612	-0.9265	0.4425	0.1961	-0.7021	-0.1671	2.4220	5.1470	-5.8460	0.9173	-1.3760
	OB-RCD-4 month vs. OB-RCD-10 month	8.5740	-7.5090	-1.6410	4.3480	-4.4780	-3.4840	-0.7209	-3.7340	-3.0450	7.9680	1.5230	-1.6150
	OB-HFD-4 month vs. OB-HFD-10 month	-2.4550	-6.5480	8.9130	-1.9550	-1.1220	1.5990	2.0250	-2.7710	-3.9920	9.1230	-0.6193	-1.4180

(B)	Adjusted P-value	0U-FA	1U-FA	2U-FA	2U-TG	3U-TG	4U-TG	5U-TG	0U-PC	1U-PC	2U-PC	3U-PC	4U-PC
	Genotype	WT-RCD-4 month vs. WT-RCD-10 month	>0.9999	<0.0001	<0.0001	0.1865	0.8866	0.398	0.3245	0.9988	0.9999	0.9966	0.8796
WT-RCD-4 month vs. WT-HFD-4 month		0.8667	0.0003	0.0017	0.7938	0.1674	0.7893	0.3241	0.7763	0.7887	0.4128	>0.9999	0.0154
WT-RCD-4 month vs. OB-RCD-4 month		0.9862	0.0065	0.0007	>0.9999	0.99	>0.9999	0.9928	0.6143	0.9922	0.0145	>0.9999	0.8929
WT-RCD-10 month vs. WT-HFD-10 month		0.4714	<0.0001	<0.0001	0.9379	0.9321	0.9989	0.8247	0.0146	0.0023	<0.0001	>0.9999	0.9361
Diet	WT-RCD-10 month vs. OB-RCD-10 month	0.0126	0.1996	0.924	0.4893	>0.9999	0.9299	0.7862	0.985	0.001	<0.0001	0.5579	<0.0001
	WT-HFD-4 month vs. WT-HFD-10 month	0.6979	>0.9999	0.7167	0.9065	>0.9999	0.9984	0.9345	<0.0001	<0.0001	<0.0001	0.9964	0.9003
	WT-HFD-4 month vs. OB-HFD-4 month	0.1109	0.9419	0.5418	0.0013	>0.9999	0.0102	0.0626	>0.9999	0.0134	0.0005	>0.9999	0.9983
	WT-HFD-10 month vs. OB-HFD-10 month	0.6726	0.9944	0.2897	0.7251	0.8269	0.7657	0.5311	>0.9999	0.0238	0.0013	0.9728	0.9952
Aging	OB-RCD-4 month vs. OB-RCD-10 month	0.8833	0.5214	>0.9999	0.9972	0.9988	0.995	>0.9999	0.0073	0.0349	>0.9999	0.9987	<0.0001
	OB-RCD-4 month vs. OB-HFD-4 month	>0.9999	>0.9999	>0.9999	>0.9999	>0.9999	>0.9999	>0.9999	0.9901	0.6164	0.4481	>0.9999	0.9997
	OB-RCD-10 month vs. OB-HFD-10 month	0.0126	0.0496	0.9982	0.6779	0.6435	0.8691	>0.9999	0.8609	0.9489	0.0608	0.9992	0.9989
	OB-HFD-4 month vs. OB-HFD-10 month	0.9752	0.1391	0.0078	0.9935	0.9998	0.9982	0.992	0.9584	0.7659	0.0082	>0.9999	0.9993

Table 3.4 The mean differences (A) and adjusted P-values (B) when comparing side chain unsaturation in the adipose tissues from *ob/ob* (OB) mice and wild-type (WT) controls aged between 4 and 10 months fed on a regular chow diet (RCD) or a high-fat diet (HFD) using the Dunnett's multiple comparisons test in two-way ANOVA ($P < 0.05$ were in red). The values are the percentage relative to the sum of all the lipids of the same category (e.g. the sum of all the FAs/DGs/TGs...)

(A)

Genotype	Diet	Age	FA	DG	TG	LysoPC	PC	PE	PS
WT	RCD	2 month	17.33±0.02	17.33±0.02	17.36±0.01				
		4 month	17.38±0.02	17.40±0.08	17.36±0.01	17.80±0.07	17.74±0.10	18.76±0.10	18.25±0.15
		10 month	17.44±0.03	17.46±0.01	17.46±0.01	17.54±0.04	17.27±0.14	18.58±0.11	17.81±0.22
		14 month	17.43±0.04	17.46±0.03	17.44±0.01	17.59±0.03	17.22±0.09	18.47±0.10	17.70±0.17
OB	RCD	2 month	17.22±0.02	17.17±0.02	17.22±0.01	17.68±0.02	17.77±0.02	18.84±0.02	18.35±0.05
		4 month	17.29±0.03	17.27±0.02	17.28±0.01	17.59±0.02	17.53±0.04	18.64±0.07	18.39±0.11
		10 month	17.50±0.02	17.48±0.02	17.46±0.02	17.64±0.03	17.51±0.05	18.57±0.04	18.25±0.06
		14 month	17.45±0.04	17.48±0.02	17.46±0.01	17.55±0.01	17.47±0.04	18.60±0.07	18.42±0.09
WT	HFD	2 month	17.47±0.01	17.63±0.04	17.40±0.00	17.89±0.04	17.52 ±0.1	18.54±0.09	18.01±0.11
		4 month	17.63±0.06	17.65±0.01	17.45±0.01	17.84±0.02	17.73±0.05	18.88±0.06	18.43±0.11
		10 month	17.63±0.04	17.64±0.01	17.49±0.01	17.84±0.04	17.80±0.01	18.89±0.05	18.54±0.11
OB	HFD	2 month	17.41±0.03	17.50±0.01	17.36±0.01	17.76±0.02	17.77±0.01	18.61±0.07	18.38±0.04
		4 month	17.53±0.03	17.62±0.01	17.51±0.01	17.76±0.02	17.60±0.03	18.59±0.05	18.09±0.05
		10 month	17.44±0.03	17.54±0.05	17.48±0.03	17.73±0.05	17.53±0.05	18.63±0.04	18.27±0.12

(B)

Genotype	Diet	Age	FA	DG	TG	LysoPC	PC	PE	PS
WT	RCD	2 month	1.02 ±0.02	1.09 ±0.02	1.11 ±0.01				
		4 month	1.01 ±0.02	1.14 ±0.06	1.10 ±0.01	0.85 ±0.08	1.18 ±0.09	0.80 ±0.05	0.51 ±0.07
		10 month	1.02 ±0.02	1.15 ±0.01	1.11 ±0.01	0.58 ±0.09	0.82 ±0.12	0.62 ±0.07	0.56 ±0.07
		14 month	1.03 ±0.03	1.15 ±0.03	1.10 ±0.01	0.53 ±0.03	0.78 ±0.08	0.58 ±0.04	0.75 ±0.03
OB	RCD	2 month	0.85 ±0.02	0.92 ±0.01	0.96 ±0.01	0.80 ±0.03	1.26 ±0.01	0.82 ±0.01	0.48 ±0.04
		4 month	0.87 ±0.02	0.95 ±0.01	0.95 ±0.00	0.70 ±0.03	1.08 ±0.04	0.74 ±0.03	0.39 ±0.05
		10 month	0.96 ±0.01	1.04 ±0.01	1.01 ±0.01	0.72 ±0.02	1.06 ±0.02	0.72 ±0.02	0.42 ±0.04
		14 month	0.97 ±0.02	1.06 ±0.01	1.02 ±0.01	0.73 ±0.04	1.07 ±0.03	0.74 ±0.04	0.36 ±0.03
WT	HFD	2 month	1.15 ±0.01	1.28 ±0.03	1.15 ±0.01	0.70 ±0.07	0.92 ±0.09	0.66 ±0.05	0.74 ±0.02
		4 month	1.13 ±0.01	1.27 ±0.01	1.16 ±0.00	0.80 ±0.07	1.10 ±0.04	0.82 ±0.04	0.55 ±0.04
		10 month	1.14 ±0.01	1.26 ±0.01	1.16 ±0.00	0.83 ±0.08	1.18 ±0.01	0.86 ±0.02	0.47 ±0.07
OB	HFD	2 month	0.99 ±0.02	1.17 ±0.01	1.09 ±0.00	0.71 ±0.02	1.20 ±0.01	0.86 ±0.02	0.51 ±0.03
		4 month	0.97 ±0.03	1.21 ±0.01	1.11 ±0.00	0.70 ±0.02	1.07 ±0.03	0.75 ±0.02	0.55 ±0.03
		10 month	0.85 ±0.02	1.14 ±0.03	1.08 ±0.01	0.74 ±0.03	1.05 ±0.04	0.73 ±0.03	0.56 ±0.07

Fig 3.10 (A) Average per chain Carbon Number and (B) average per chain Degree of Unsaturation (DU) in adipose tissues from *ob/ob* (OB) mice and wild-type (WT) controls aged between 2 and 14 months fed by regular chow diet (RCD) and high-fat diet (HFD). The color depth indicates the relative content of the FA comparing different animal groups (Red means more; blue means less).

(A)		Adjusted P-value	FA	DG	TG	LysoPC	PC	PE	PS
Genotype	WT-RCD-4 month vs. WT-RCD-10 month		0.9826	0.8252	0.9915	0.2662	0.3054	0.9048	0.7730
	WT-RCD-4 month vs. WT-HFD-4 month		0.9994	>0.9999	>0.9999	0.9659	0.1686	>0.9999	<0.0001
	WT-RCD-4 month vs. OB-RCD-4 month		0.9681	>0.9999	0.9953	0.9864	0.8642	0.0266	0.0045
	WT-RCD-10 month vs. WT-HFD-10 month		0.5053	0.9728	>0.9999	0.9668	0.1044	0.1487	0.1241
Diet	WT-RCD-10 month vs. OB-RCD-10 month		0.1535	0.1995	0.9693	>0.9999	>0.9999	0.8637	0.4392
	WT-HFD-4 month vs. WT-HFD-10 month		0.7945	0.6194	>0.9999	0.0915	<0.0001	0.0565	<0.0001
	WT-HFD-4 month vs. OB-HFD-4 month		0.0949	0.0015	0.1549	0.6473	0.9956	0.9994	0.0322
	WT-HFD-10 month vs. OB-HFD-10 month		0.9934	0.9946	>0.9999	0.9696	>0.9999	0.9963	>0.9999
Aging	OB-RCD-4 month vs. OB-RCD-10 month		0.9993	0.9982	0.9376	0.0814	<0.0001	0.5124	<0.0001
	OB-RCD-4 month vs. OB-HFD-4 month		>0.9999	>0.9999	>0.9999	>0.9999	0.9938	>0.9999	0.9464
	OB-RCD-10 month vs. OB-HFD-10 month		0.2118	0.2509	0.4669	0.9997	>0.9999	0.9933	0.8284
	OB-HFD-4 month vs. OB-HFD-10 month		0.9488	0.9859	>0.9999	>0.9999	0.9901	0.9998	0.4670

(B)		Adjusted P-value	FA	DG	TG	LysoPC	PC	PE	PS
Genotype	WT-RCD-4 month vs. WT-RCD-10 month		0.2794	0.0263	0.1726	0.1566	0.6937	0.9805	0.4952
	WT-RCD-4 month vs. WT-HFD-4 month		0.9952	0.5265	0.6429	0.3403	0.0036	0.7353	0.2448
	WT-RCD-4 month vs. OB-RCD-4 month		0.1412	0.9805	0.9956	0.6744	0.9994	0.8875	>0.9999
	WT-RCD-10 month vs. WT-HFD-10 month		0.0005	0.5051	0.9226	0.8431	0.4182	0.5083	0.8446
Diet	WT-RCD-10 month vs. OB-RCD-10 month		0.6211	0.4949	0.9715	0.9854	0.8894	0.9999	0.9922
	WT-HFD-4 month vs. WT-HFD-10 month		0.8330	0.6211	0.9924	0.0054	<0.0001	0.0123	0.8434
	WT-HFD-4 month vs. OB-HFD-4 month		0.7052	0.0001	0.0885	>0.9999	>0.9999	>0.9999	0.1408
	WT-HFD-10 month vs. OB-HFD-10 month		0.5388	0.6597	0.9048	0.9999	>0.9999	>0.9999	0.2158
Aging	OB-RCD-4 month vs. OB-RCD-10 month		>0.9999	>0.9999	>0.9999	0.0003	<0.0001	0.0677	0.9785
	OB-RCD-4 month vs. OB-HFD-4 month		>0.9999	>0.9999	>0.9999	0.9992	0.9201	0.9990	0.8946
	OB-RCD-10 month vs. OB-HFD-10 month		0.7708	0.7635	0.9838	>0.9999	>0.9999	>0.9999	0.9997
	OB-HFD-4 month vs. OB-HFD-10 month		0.4657	0.8815	0.9984	0.9954	0.9999	>0.9999	>0.9999

Table 3.5 The adjusted P-values when comparing (A) average per chain Carbon Number and (B) average per chain Degree of Unsaturation (DU) in adipose tissues from *ob/ob* (OB) mice and wild-type (WT) controls aged between 4 and 10 months fed by regular chow diet (RCD) and high-fat diet (HFD) using the Dunnett's multiple comparisons test in two-way ANOVA ($P < 0.05$ were in red).

The major changes in intact lipids in adipose tissue are summarized as below:

	Neutral Lipids		Membrane Lipids		Diversity
	Sum FA Carbons	Unsaturation	Sum FA Carbons	Unsaturation	
<i>Ob/ob</i>	↓	↓	↑ (but ↓ in HFD-10M)	↑ (but ↓ in HFD-10M)	-
HFD	↑	↑	↑	↑	↓↓
Aging	↑	-	↓	↓	-

3.5 Discussion

Lipids in adipose tissue are derived from either dietary lipids or DNL and subsequent modifications. When fed with the RCD diet, which only has 11.5% fat and over a half of this is accounted for by C18:2, DNL plays a significant role in determining the adipose FA composition and results in a dominant content of C16:0, C16:1, and C18:1, while there is relatively low proportion of C18:2 in the WT-RCD adipose tissues. DNL is further activated in *ob/ob* mice fed on either RCD or HFD as leptin deficiency leads to mice eating more food and taking in higher carbohydrate from the diet. The activated DNL resulted in shorter and more saturated neutral lipids, dominated by C18:1 rather than other newly synthesized FAs (C16:0, C16:1 and C18:0). This indicates that increased carbohydrate consumption in the leptin-deficient *ob/ob* mice triggers not only DNL through ACC and FAS but also desaturation by SCDs and elongation by ELOVL6. The domination of C18:1 also indicates that further FA modification occurs at a slower pace in *ob/ob* mice, ‘flooding’ the tissue with newly synthesized FAs. The activities of Δ^5 -eicosatrienoyl-CoA desaturase and Δ^6 -oleoyl(linolenoyl)-CoA desaturase are reported to be associated with hyperglycemia and non-alcoholic steatohepatitis, and palmitate can compete with ω -6 linoleic and ω -3 α -linolenic acids for FADS2 mediated Δ^6 -desaturation [448-450].

Numerous studies have shown that the consumption of dietary MUFAs like oleate (C18:1 ω 9), as opposed to saturated fats such as palmitate (C16:0), is protective for insulin resistance and metabolic dysfunctions [451, 452]. However, it is also reported that elevated SCD activity within adipose tissue is closely coupled with the development of insulin resistance [453]. Tan et al. [454] demonstrated that 18-carbon and Δ^9 desaturated TGs, especially oleate, were increased in *ob/ob* mice. They suggested that the protective effects of MUFA-rich diets cannot work by simply increasing the body’s oleate levels and it may be due to a selective partitioning

for the DNL-synthesized oleate toward specific metabolic processes, as opposed to dietary oleate per se. It is also possible that increasing the body's oleate levels benefits metabolic health, and the enhancement of oleate in *ob/ob* mice may be just a compensatory mechanism to maintain normal cellular function through the regulation of the ratio of monounsaturated to saturated fatty acids in conditions of overfeeding induced obesity and increased total fat weight. Actually, many metabolic alterations in obesity which were thought to be pathological mechanisms may be protective in response to nutrient excess [455]. In addition, Tan et al. found that the AdTG-*ob/ob* mice which had increased SCD ratios but decreased Elovl6 ratios in adipose tissue were more obese but relatively metabolic healthy compared with the *ob/ob* mice, while the AKT2 KO mice which are lean but insulin resistant have bigger Elovl6 ratios but not significantly changed SCD ratios compared with wild-type mice. This suggests SCD activity is changed in response to the altered DNL. The more FAs synthesized by the body through DNL, the more SCD activity is activated to alleviate the harmful effects of adiposity. The decreased Elovl6 activity in AdTG-*ob/ob* mice (compared with *ob/ob* mice) indicates that Elovl6 cannot be regulated in response to the DNL activity in the same manner as SCD, and is more likely to be directly influenced by insulin. It has been reported that the Elovl6 activity could be thermogenically regulated in BAT and the Elovl6 KO mice have impaired thermogenic capacity [442] which could be tested in the future. Nevertheless, the strategy of producing more C18:1 cannot fully compensate dysfunction caused by a declining proportion of essential FAs (n-3 and n-6 FAs) such as linoleate (C18:2 ω 6). Another compensatory protective mechanism for over nutrition-induced obesity is to maintain normal membrane phospholipid composition.

Increased C16:0 and C18:1 ω 9, and dropped C18:2 ω 6 led to relatively short and saturated neutral lipids (FAs, DGs, TGs) in *ob/ob* adipose tissue fed on any diet through an increase in 16-carbon FAs, 32-carbon DGs and 50-carbon TGs, and a decrease in 18-carbon FAs, 36-carbon DGs and 54-carbon TGs. However, membrane lipids, especially the PCs, become longer and more unsaturated in *ob/ob* mice. More unsaturated FAs are incorporated into membrane lipids in *ob/ob* mice to maintain the fluidity and normal function of cell membrane against increased DNL. What is more, many HUFA species have been found to increase in PC species (**Fig 3.7C**). HUFAs, in contrast to MUFAs and precursor PUFAs, are usually found in membrane lipids as components of phospholipids where they contribute to the maintenance of membrane fluidity and sensitivity to hormones, and also regulate gene expression through various transcription factors, such as the PPAR receptors, liver-X receptor, HNF4, and SREBP-

1c [40, 175, 456]. Generally, saturated fatty acids make the membrane bilayer less fluid and inactive, which in turn has consequences for protein function and membrane transport [168], whereas unsaturated fatty acids result in a more plastic membrane and improve the function of membrane receptors and sensitivity to hormones [169, 170]. The geometry of the cis-double bond induces a bend in the molecule, thereby precluding rigid lipid bilayers. One process of high relevance to T2DM is glucose transport across the membrane which may be influenced by membrane fluidity [171]. There have been studies reporting the relationship between membrane fluidity of erythrocytes and insulin sensitivity in hypertensive subjects [172], and also changes in the composition of membrane lipids associated with increased insulin sensitivity in skeletal muscles after physical training [173]. However, a study in rat brown adipose tissue [174] showed that the increase of mitochondrial activity in this tissue was related to phospholipid composition changes rather than to membrane fluidity. PUFAs result in an even greater increase in plasticity of membranes [40, 175], and have been associated with improved cardiac function following arrhythmias.

This could be another protective mechanism to maintain normal function and membrane fluidity of adipocytes when there is a large consumption of carbohydrates activates and increased DNL activity in *ob/ob mice*. The FA composition of the cell membrane plays an essential role in metabolic syndrome and a variety of cardiovascular diseases [457, 458]. Generally, saturated fatty acids make the bilayer membrane less fluid and then inactive, while polyunsaturated fatty acids result in a more plastic membrane and improved function of membrane receptors and sensitivity to hormones. The sensitivity of adipocytes to insulin could depend on the composition of their plasma membrane, and greater membrane fluidity improves the incorporation of GLUT4, which results in increased glucose uptake. Interestingly, this protective mechanism seems to be impaired in adipose tissue of mice fed on HFD at the age of 10 months, presumably through oxidative damage from long-term HFD diet [459, 460].

The adipose tissues of WT-HFD mice exhibited similar FA composition to that of the HFD diet, except there was a moderate increase in C16:0 and C18:1 which comes from DNL. Dietary C18:1 and C18:2 led to a significant increase of 18-carbon FAs and DU=1 FAs and DU=2 FAs in WT-HFD adipose tissues compared with WT-RCD mice, making the average composition of all neutral lipids (FAs, DGs, TGs) longer and more unsaturated the following feeding of HFD. Under the HFD diet all the four classes of phospholipids (lysoPCs, PC, PE, and PS) exhibited the same changes in direction as neutral lipids becoming longer and more unsaturated.

However, the diversification of lipids decreased significantly in HFD-fed mice due to the domination of the few dietary FA species consumed in the diet. HFD-fed mice have decreased very long (>18 carbon) and highly-unsaturated (DU>2) FAs incorporated in both neutral and membrane lipids, which could impair the normal functions of adipose tissue. Thus, the HFD-induced adiposity might be more harmful than the *ob/ob*-induced obesity because the regulation effects of transcription factors on DNL, elongation, and desaturation are less effective when most of the FAs incorporated into complex lipids are directly incorporated from diets. Moreover, the high-fat diet produces oxidative stress in cells. Wang [95] demonstrated that myocardial mitochondrial dysfunction was detectable in OB-HFD mice (3 months), much earlier than in OB-RCD mice (14 months), which might also act in adipose tissue as discussed in the next Chapter.

Aged mice seemed to have more C18:1 ω 9 and less C16:0 in their adipose tissue no matter in which genotype or diet group, which led to increases in long-chain TGs as the mice aged. Long-chain TGs seem to be easily stored in adipose tissue and are less consumed compared with short-chain TGs, and thus, they accumulate with age. Interestingly, the *Elovl6* ratios are reported to be related to insulin resistance, but the deletion of *Elovl6* does not prevent the development of insulin resistance or fatty liver disease [461]. Other lipids didn't change as significantly as the TGs did, with the exception of more saturated PCs, which appeared more in older mice. This could impair membrane fluidity and decrease the incorporation of insulin or GLUT4 receptors. Both of these effects might contribute to the increased risk of T2DM which accompanies the normal aging process.

3.6 Conclusions

This chapter demonstrated that FA *de novo* synthesis was activated in *ob/ob* mice by leptin deficiency. In contrast to the shorter and more saturated TGs from DNL, more unsaturated PCs are synthesized in *ob/ob* mice to maintain the fluidity and normal function of cell membrane against increased *de novo* synthesis. However, this protective mechanism can be impaired by the long-term administration of HFD, presumably through oxidative damage. Moreover, most of the lipids stored in the adipose tissue of HFD-fed mice are assembled directly using dietary fatty acids, which dramatically decreased the diversity of lipid composition. Longer TGs and saturated PCs accumulated in adipose tissue of aged mice, which increases susceptibility to metabolic diseases. These characteristic changes nicely complement previous lipidomic studies

only focused on FAs and TGs in adipose tissue, and depict a more comprehensive metabolic network profile in adipose tissue.

Chapter 4 Transcriptomics demonstrates that the peroxisome, AMPK, and PPAR γ pathways are most perturbed in adipose tissue during the progression of obesity and during aging

4.1 Introduction

The previous Chapter focused on lipid profiling of adipose tissue from animal models of genetic and/or diet-induced obesity, and how aging interacts with this process. The predominance of oleate (C18:1 ω 9), the main product from a combination of DNL, elongation by ELOVL6 and desaturation by SCDs, is the key feature of both obesity and aging. However, despite the dominance of oleate in terms of total fatty acid content, neutral lipids (FAs, DGs, TGs) and phospholipids (lysoPCs, PCs, PEs, PSs) exhibited different patterns in chain length and unsaturation. Increased DNL resulted in a decrease in both total chain length and degree of unsaturation of neutral lipids in genetic-induced obesity resulting from a failure to produce leptin in the *ob/ob* mice. In contrast, more elongated and desaturated phospholipids accumulated in adipose tissue of *ob/ob* mice compared with wild-type controls, but then decreased in the older *ob/ob* animals fed on HFD, where previous studies have shown the combination of both an HFD and the *ob/ob* genotype induced metabolic dysfunctions in a range of tissues [94, 95, 462]. The chain length and degree of unsaturation of phospholipids also decreased moderately during aging, while TGs with longer chain lengths accumulated in adipose tissue of aged mice. Moreover, the HFD repressed lipid biosynthesis and decreased the diversity of all the lipids in adipose tissue. Overall, these results suggest a presumably protective mechanism associated with the desaturation of membrane lipids in adipose tissue for maintaining metabolic functions in the initiation of obesity, which becomes impaired when the mice become too obese and as they age. However, the regulatory pathways behind these mechanisms are still unknown. In this Chapter, changes at the transcriptional level resulting from genetic-induced obesity, diet-induced obesity, and aging were compared and contrasted. Gene Ontology (GO, <http://www.geneontology.org>) and Kyoto Encyclopaedia of Genes and Genomes (KEGG, <http://www.kegg.jp>) enrichment analysis were used to depict comprehensive molecular changes across the network, correlating the processes of obesity and aging.

GO is an international standardized gene function classification system. The aim is to establish a language standard that can be applied to various species to define and describe the functions of genes and proteins and to be updated as research proceeds on these genes. GO is divided into three levels of ontology: molecular functions (MF), biological processes (BP), and cell composition (CC). The basic unit of the GO database is the 'term', and each term corresponds to a function or attribute. The software used for GO enrichment analysis is Goseq (<http://www.bioconductor.org/packages/release/bioc/html/goseq.html>). This method is based on the Wallenius non-central hypergeometric distribution. Compared with the ordinary hypergeometric distribution (Hyper-geometric distribution) algorithm, this method considers the probability of individual extraction from one class is different from the probability of selecting it from outside of this class, and this difference of probability is estimated from the different preference to the length of the gene, which can be more accurate to calculate the probability of a differential gene enriched GO term.

The expression of different genes is coordinated with one another *in vivo* in order to result in a function. KEGG is a system for gene function analysis and provides a genome information database. The basic unit of the KEGG database is Pathway. It is helpful to the study of gene expression information to consider it as a whole network with integrated queries of metabolic pathways. By means of Pathway enrichment [463, 464], the major biochemical metabolic pathways and signal transduction pathways behind the differentially expressed genes can be determined.

4.2 Aims and objectives

In this Chapter I aim to:

- i. Profile the transcriptomic changes associated with genetic-induced obesity resulting from a failure to produce leptin in the *ob/ob* mouse.
- ii. Profile the transcriptomic changes associated with diet-induced obesity.
- iii. Profile the transcriptomic changes associated with aging.
- iv. Compare and contrast the influence of obesity and aging on adipose tissue
- v. Correlate the transcriptomic changes with lipid changes described in the previous Chapter.

4.3 Materials and Methods

4.3.1 Animals and diets

We compared changes at both 2 months and 10 months of age as this time point had both genotypes and diets. 40 adipose tissue samples as described in Chapter 2 (section 2.3) were randomly selected (5 in each group of 8 for different genotype (*ob/ob* or wild-type), diet (RCD or HFD) and aging (2 months or 10 months)), as shown below:

Samples	Genotype	Age (months)	Diet	Samples	Genotype	Age (months)	Diet
5	WT	2	RCD	5	<i>ob/ob</i>	2	RCD
5	WT	10	RCD	5	<i>ob/ob</i>	10	RCD
5	WT	2	HFD	5	<i>ob/ob</i>	2	HFD
5	WT	10	HFD	5	<i>ob/ob</i>	10	HFD

4.3.2 Sample preparation and microarray analysis

RNA extraction and microarray analysis of mouse adipose tissue were performed according to Chapter 2 (section 2.9).

4.3.3 Statistical analysis

Statistical analyses were performed using the software R (R software environment for statistical computing; <http://www.R-project.org>). Samples of adipose tissue were matched for genotype (*ob/ob* or wild-type), diet (RCD or HFD) and aging (2 months or 10 months) to calculate the p-value of the difference of gene expression. The genes with the level of significance $P < 0.05$ were used for GO and KEGG enrichment analysis.

The National Center for Biotechnology Information Reference Sequence (NCBI RefSeq) database (Build 36, Release 22) was used for gene annotation. For the GO enrichment analysis, GOseq (version 1.22.0), topGO (version 2.22.0), GO.db (version 3.2.2), and Kyoto Encyclopaedia of Genes and Genomes (KEGG, kobas 2.0, <http://www.kegg.jp>) were used within software tools within packages in R (<https://www.r-project.org/>).

The hypergeometric test / Fisher's exact test was used to find enriched pathways from differentially expressed genes, compared with the whole transcriptome background. The Q-value for multiple testing were calculated using an optimized FDR correction method defined by the Benjamini–Hochberg method.

4.4 Results

4.4.1 Overview and correlation of the transcriptomic changes in adipose tissue *ob/ob* genotype, HFD diet intake, and aging factors

To better understand what molecular changes were associated with the lipidomic patterns detected in the two mouse strains fed on two diets at different ages, a transcriptomic study was conducted to compare the differences in gene expression of adipose tissues using the Illumina MouseRef-8 v2.0 BeadChip which targets approximately 25,600 well-annotated RefSeq transcripts, equating to over 19,100 unique genes. Gene expression was compared using a 95% ($p < 0.05$) confidence interval for each factor (genotype, diet, and age). As a result, a total of 5341 genes were found to be changed in expression significantly (**Table 4.1**). The majority of these genes were associated with the *ob/ob* genotype, while fewer transcriptomic changes were found resulting from an HFD. The severity of obesity (as shown in Chapter 3.4.1) may be a reason for this discrepancy. Aging changed the expression of more genes in *ob/ob* mice compared with wild-type animals. This suggests the aging process might be accelerated in obese mice, which is consistent with the fact that obese people are more likely to be exposed to insulin resistance and metabolic diseases while those with a normal range of BMI tend to have a longer life expectancy. This will be discussed in greater detail below.

Transcriptomic changes associated with each factor (genotype, diet, and aging) were compared across the different groups. Keeping diet and age consistent across comparisons, genotype resulted in significant changes in more than 1000 genes in either of the four group comparisons (comparing different genotypes in the groups of RCD-2, RCD-10, HFD-2, and HFD-10). Interestingly, there were more genes down-regulated (1565) than up-regulated (498) by *ob/ob* genotype in the HFD-10 group, while *ob/ob* genotype resulted in more genes upregulated in the other 3 groups (1219, 819 and 1251 in the RCD-2, HFD-2 and RCD-10 group, respectively). The HFD diet did not exhibit such a significant effect on gene expression patterns of the wild-type mice until they get old (311 genes significantly changed by HFD in the WT-10 group), while expression of 761 genes was altered by HFD in adipose tissue of *ob/ob* mice even in 2-

month-old mice (OB-2). This early-onset of the influence of HFD could be attributed to the rapid accumulation of fat as demonstrated in Chapter 3.4.1. Aging resulted in significantly more changes in gene expression in *ob/ob* mice compared with the wild-type controls, indicating the association between obesity and accelerated the aging process. Interestingly, the expression of more (758) genes was up-regulated by the aging factor in the OB-RCD group compared with the number of genes up-regulated in the OB-HFD group (309). In contrast, many as 1119 genes were down-regulated by aging in the OB-HFD group, while only 321 down-regulated in the OB-RCD group.

Comparison		Gene	GO_MF	GO_CC	GO_BP	
WT vs OB	RCD-2	All	2,077	134	153	1,024
		↓	858	16	36	50
		↑	1,219	119	137	1,173
	HFD-2	All	1,086	112	140	1,112
		↓	267	2	15	2
		↑	819	121	138	1,207
	RCD-10	All	1,895	133	133	1,314
		↓	644	8	22	15
		↑	1,251	165	160	1,591
	HFD-10	All	2,063	80	126	700
		↓	1,565	44	88	431
		↑	498	37	90	431
RCD vs HFD	WT-2	All	2	-	-	-
		↓	-	-	-	-
		↑	2	-	-	-
	OB-2	All	311	19	58	386
		↓	120	-	6	7
		↑	191	12	67	309
	WT-10	All	761	59	85	419
		↓	248	1	22	-
		↑	513	76	99	596
	OB-10	All	1	-	-	-
		↓	1	-	-	-
		↑	-	-	-	-
2-month vs 10 month	WT-RCD	All	5	-	-	-
		↓	2	-	-	-
		↑	3	-	-	-
	WT-HFD	All	80	-	-	-
		↓	14	-	-	-
		↑	66	-	-	-
	OB-RCD	All	1,079	90	104	1,078
		↓	321	5	13	46
		↑	758	91	111	1,055
	OB-HFD	All	1,428	48	105	599

		↓	1,119	24	71	303
		↑	309	22	80	249

Table 4.1 The number of genes of which expression is significantly changed (p -value < 0.05) by genotype/diet/aging in each group and the Gene Ontology (**GO**) terms enriched from the genes. In total 5341 different genes were found to be changed significantly ($p < 0.05$). **MF**: molecular function, **CC**: cellular component, **BP**: biological process. The color means increased (red) or decreased (blue) by OB/HFD/aging.

In order to explore the correlation between transcriptomic changes from different factors, the number of genes simultaneously changed in any two of the 12 groups with 95% ($p < 0.05$) confidence interval were calculated as shown in **Table 4.2**. Expression of many genes was changed in the same direction (increase/decrease) by *ob/ob* genotype in the RCD-2, RCD-10, HFD-2 groups. However, 435 genes were down-regulated in *ob/ob* mice fed on HFD diet in the 10 month age group (HFD-10), but are expressed more in adipose tissue of *ob/ob* mice in the RCD-2 group, compared with the corresponding wild-type mice (**Table 4.2**). This suggests some pathways upregulated by leptin deficiency and overfeeding in the younger mice cannot be activated to a greater extent for older animals fed on an HFD.

Considering the overlap of the alterations induced by genotype and diet-caused obesity on the transcriptomic pattern, a number of genes were found to be changed in the same direction (increased/decreased) in adipose tissues of *ob/ob* and HFD-fed animals. These were the pathways influenced by both the HFD diet and *ob/ob* genotype and will be discussed in the next Chapter. The only exception is that there were very few genes changed by HFD that are influenced also by genotype in the HFD-10 group. The down-regulated genes in adipose tissue of *ob/ob* mice in the HFD-10 group were related to different pathways compared with the genes influenced by an HFD.

There are more genes up or down-regulated both by aging and genotype compared with those influenced by both genotype and diet. 902 genes were down-regulated by aging in the OB-HFD group and also by genotype in the HFD-10 group (the low right rectangle in **Table 4.2**). 209 genes were both up-regulated in the two situations. Interestingly, the influence of age on the OB-HFD mice was also very different compared with the effect of genotype on adipose tissue of mice in the RCD-2 group (431 genes were down-regulated by aging in the OB-HFD group but up-regulated by *ob/ob* genotype in the RCD-2 group). Some pathways inhibited in

the aging process were also down-regulated by *ob/ob* genotype in the HFD-10 group but up-regulated by *ob/ob* genotype in the RCD-2 group.

There is some intriguing similarity observed between aging influence and the HFD effect. Among the 758 genes up-regulated by aging in the OB-RCD group, there were 175 of them up-regulated by HFD in the WT-10 group, and 111 of them were also up-regulated by HFD in the OB-2 group. However, the similarity was not observed in the OB-HFD group.

4.4.2 Gene Ontology (GO) enrichment analysis reveals the different regulation of inflammatory and metabolic pathways in adipose tissue of *ob/ob* mice fed on an HFD

Fig 4.1 illustrates the biological themes annotating genes differentially expressed in adipose tissue of *ob/ob* mice compared with the wild-type controls in four groups in terms of RCD/HFD diet and 2 month/10 month aging, indicated by GO categories using the Molecular Function (MF), Cellular Component (CC) and Biological Process (BP) ontologies.

The genes upregulated in adipose tissue of *ob/ob* mice across the comparisons were mostly annotated by extracellular, vesicle and membrane-bound CC themes, while the majority of the downregulated ones were associated with intracellular CC ontologies, in particular, organelle and cytoplasm themes. Interestingly, a lot of genes downregulated in adipose tissue of *ob/ob* mice at the age of 10 months were annotated by some CC mitochondrial themes, while some genes down-regulated in 2-month *ob/ob* mice were associated with the nucleus and nucleoplasm. This suggests that changes in transcription factors directly affecting the nucleus preceded mitochondrion dysfunction in adipose tissue during both the progression of obesity and aging as reviewed in some other studies [465, 466]. Moreover, 10-month age *ob/ob* mice fed on HFD exhibited fewer changes in genes with catalytic activity annotated, such as oxidoreductase and transferases.

The genes up-regulated in *ob/ob* mice in the RCD-2, HFD-2 and RCD-10 groups are annotated mostly by functional themes associated with the immune system, inflammation, and signaling processes, compared with the wild-type controls. The phosphorus metabolic process was also significantly up-regulated in adipose tissue of *ob/ob* mice in the RCD-3 group. Interestingly, the BP ontologies enriched in *ob/ob* mice of the HFD-10 group exhibited significantly up-regulation of metabolism-associated pathways, while most of the inflammation-related pathways were moderately up-regulated. Most of the down-regulated genes associated with the *ob/ob* genotype in all four comparisons were annotated by different kinds of metabolic GO themes.

Mice fed on RCD at 2 months of age:

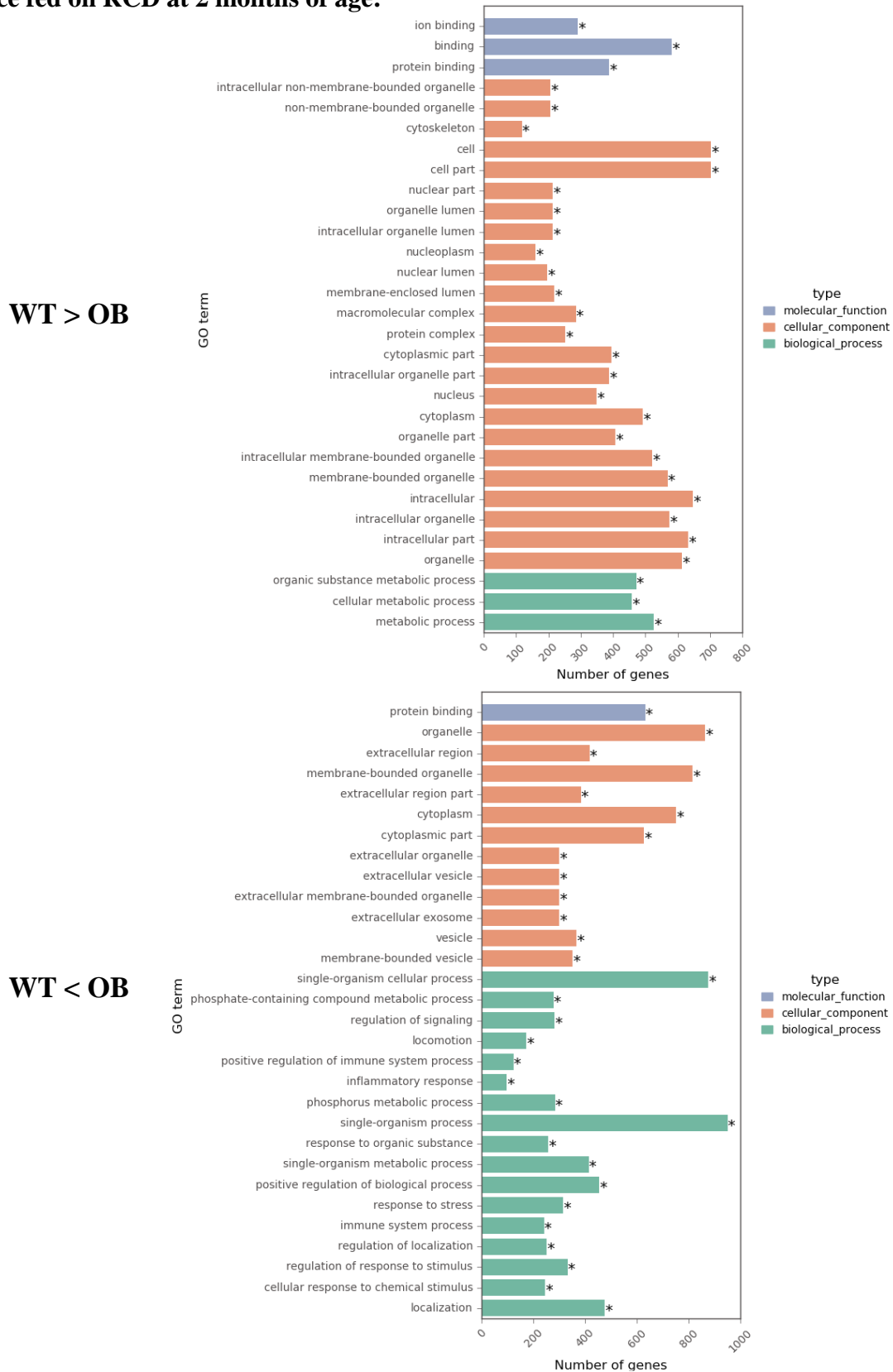
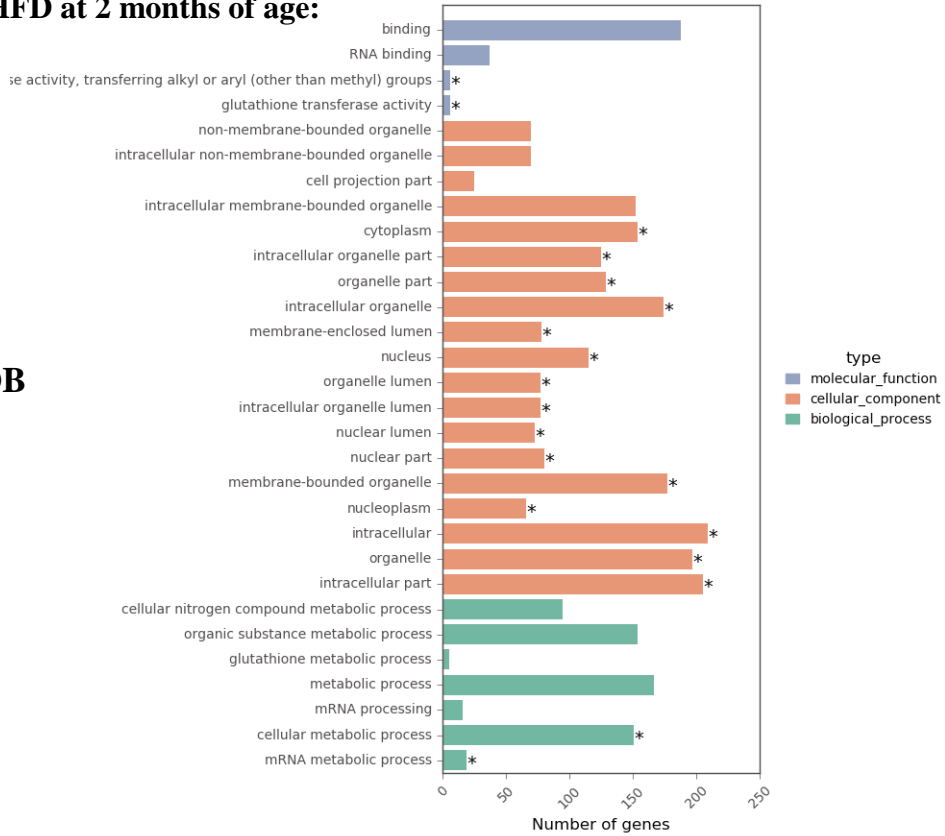


Fig 4.1(A) The TOP 30 GO Molecular Function (MF), Cellular Component (CC) and Biological Process (BP) ontologies annotating genes differentially expressed in the *ob/ob* mice (OB) compared with wild-type controls (WT) in four groups fed on regular chow diet (RCD) at the age of 2 month. *The corrected *p*-value of this GO term calculated by the FDR correction method of Benjamini and Hochberg [467] is less than 0.05.

Mice fed on HFD at 2 months of age:

WT > OB



WT < OB

GO term

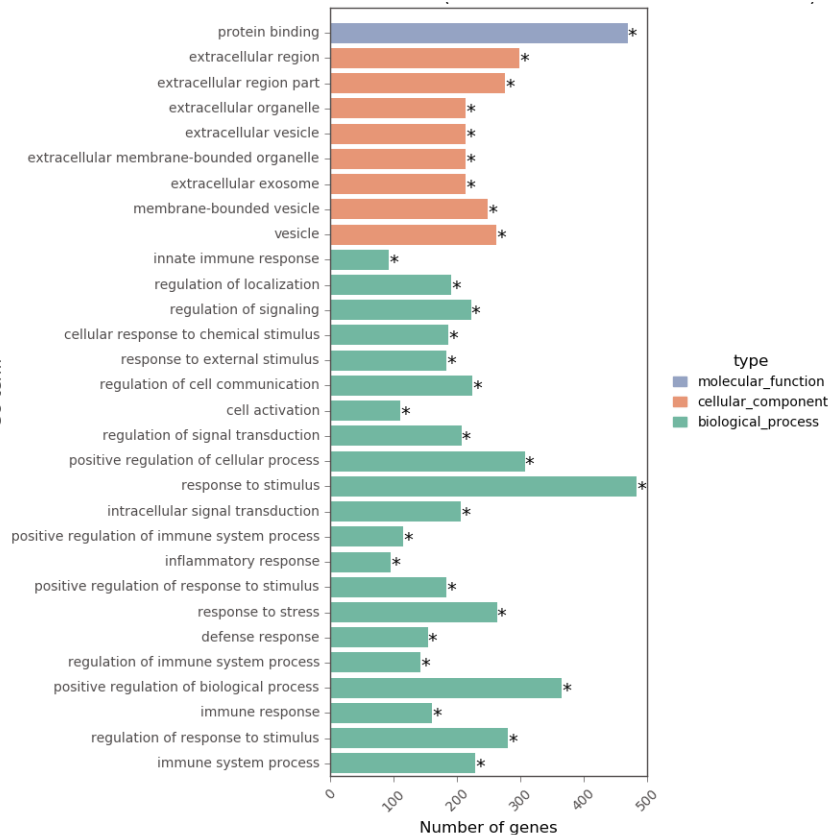


Fig 4.1(B) The TOP 30 GO Molecular Function (MF), Cellular Component (CC) and Biological Process (BP) ontologies annotating genes differentially expressed in the *ob/ob* mice (OB) compared with wild-type controls (WT) in four groups fed on high-fat diet (HFD) at the age of 2 month. *The corrected *p*-value of this GO term calculated by the FDR correction method of Benjamini and Hochberg [467] is less than 0.05.

Mice fed on RCD at 10 month of age:

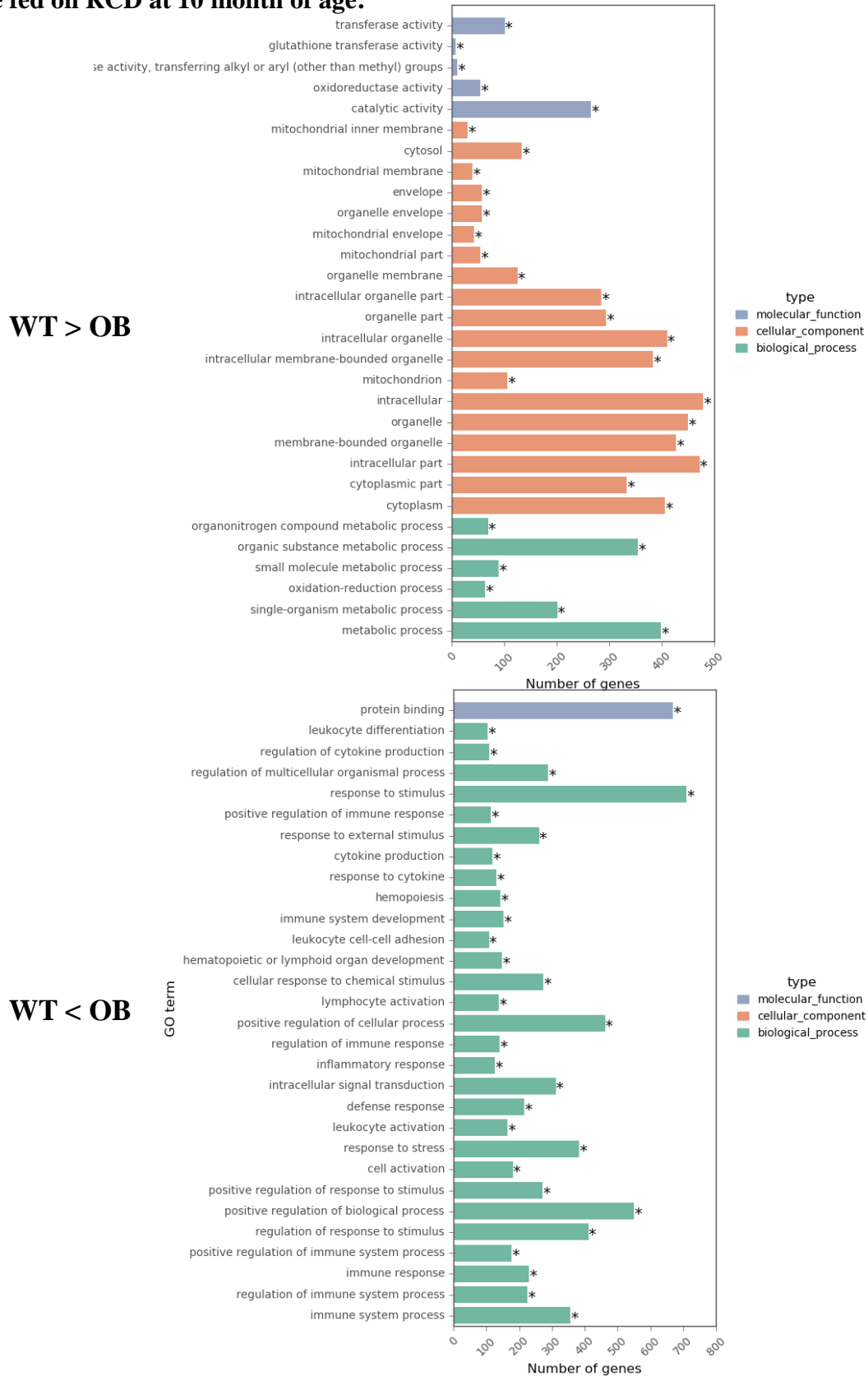


Fig 4.1(C) The TOP 30 GO Molecular Function (MF), Cellular Component (CC) and Biological Process (BP) ontologies annotating genes differentially expressed in the *ob/ob* mice (OB) compared with wild-type controls (WT) in four groups fed on regular chow diet (RCD) at the age of 10 month. *The corrected *p*-value of this GO term calculated by the FDR correction method of Benjamini and Hochberg [467] is less than 0.05.

Mice fed on HFD at 10 months of age:

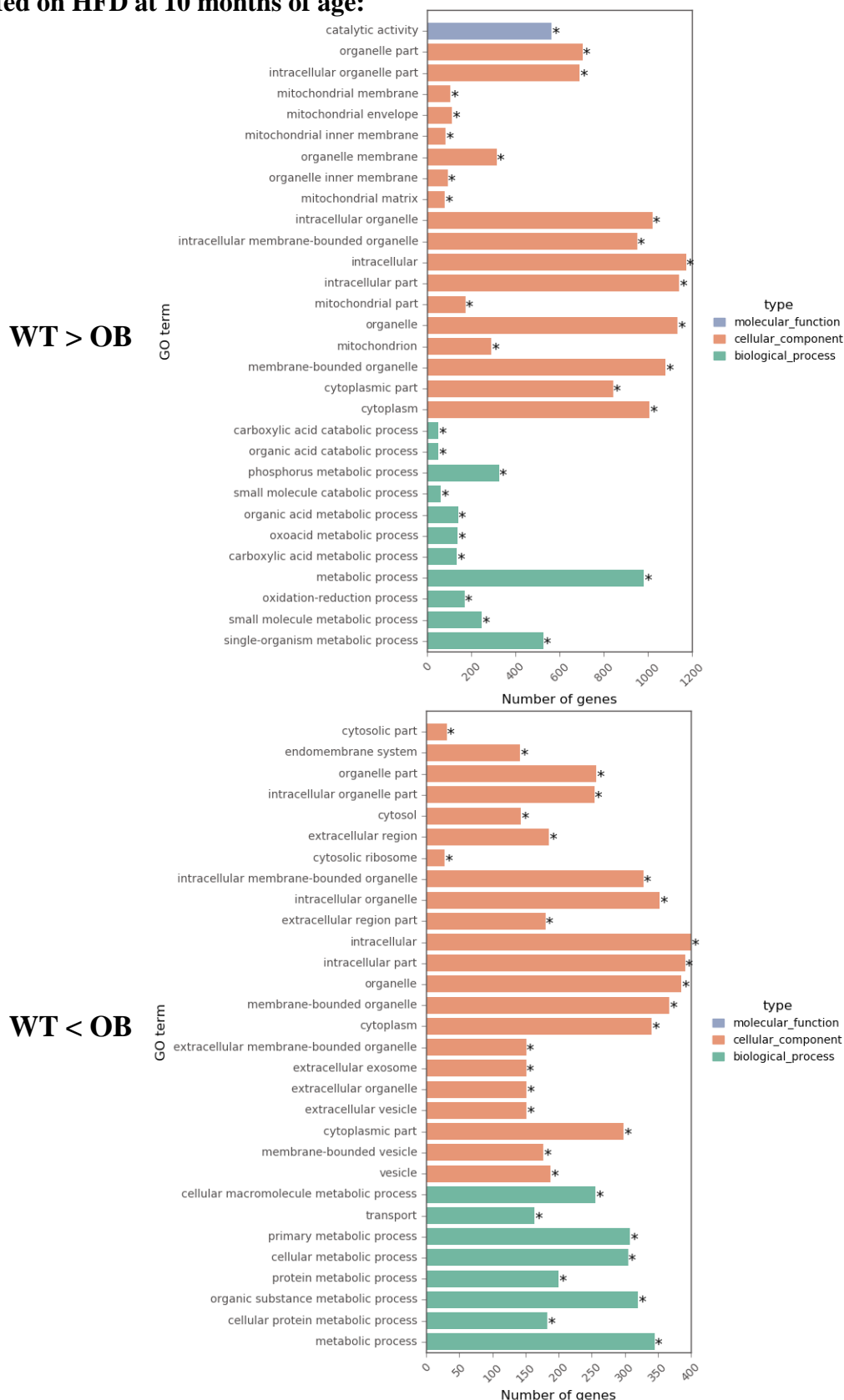


Fig 4.1(D) The TOP 30 GO Molecular Function (MF), Cellular Component (CC) and Biological Process (BP) ontologies annotating genes differentially expressed in the *ob/ob* mice (OB) compared with wild-type controls (WT) in four groups fed on high-fat diet (HFD) at the age of 10 month. *The corrected *p*-value of this GO term calculated by the FDR correction method of Benjamini and Hochberg [467] is less than 0.05.

GO terms enriched by genes significantly up-regulated or down-regulated by HFD diet are shown in **Fig 4.2**. There was no GO terms significantly enriched in the WT-2 and OB-10 groups with the threshold of adjusted p-value > 0.05. In the OB-2 group, adipose tissue from mice fed on the HFD diet was significantly annotated by extracellular and membrane-bounded CC terms. However, intracellular cellular component GO terms were not enriched by the genes down-regulated by the HFD diet in the OB-2 group. The contrast is more obvious in the group of 10-month wild-type mice, in which intracellular CC terms such as nuclear parts were enriched for the genes down-regulated by HFD diet. There were a smaller number of transcription factors influenced by the HFD diet compared with the *ob/ob* genotype, in part because DNL and related metabolic pathways were inhibited when adipose tissue directly stored lipid components of the HFD diet.

The BP terms annotating genes up-regulated by HFD in the OB-2 group were predominantly signaling and cytokine-related biological process, while in the WT-10 group the inflammatory and immune system-related BP terms dominated. Adipose tissue from *ob/ob* mice fed on HFD at the age of 2 months indicated markers of pro-inflammatory status and resembled many of the inflammatory changes in the old wild-type mice fed on HFD. The genes down-regulated in adipose tissue of mice fed on HFD were associated with metabolic processes in both the OB-2 and WT-10 groups, compared with the corresponding animals fed on RCD.

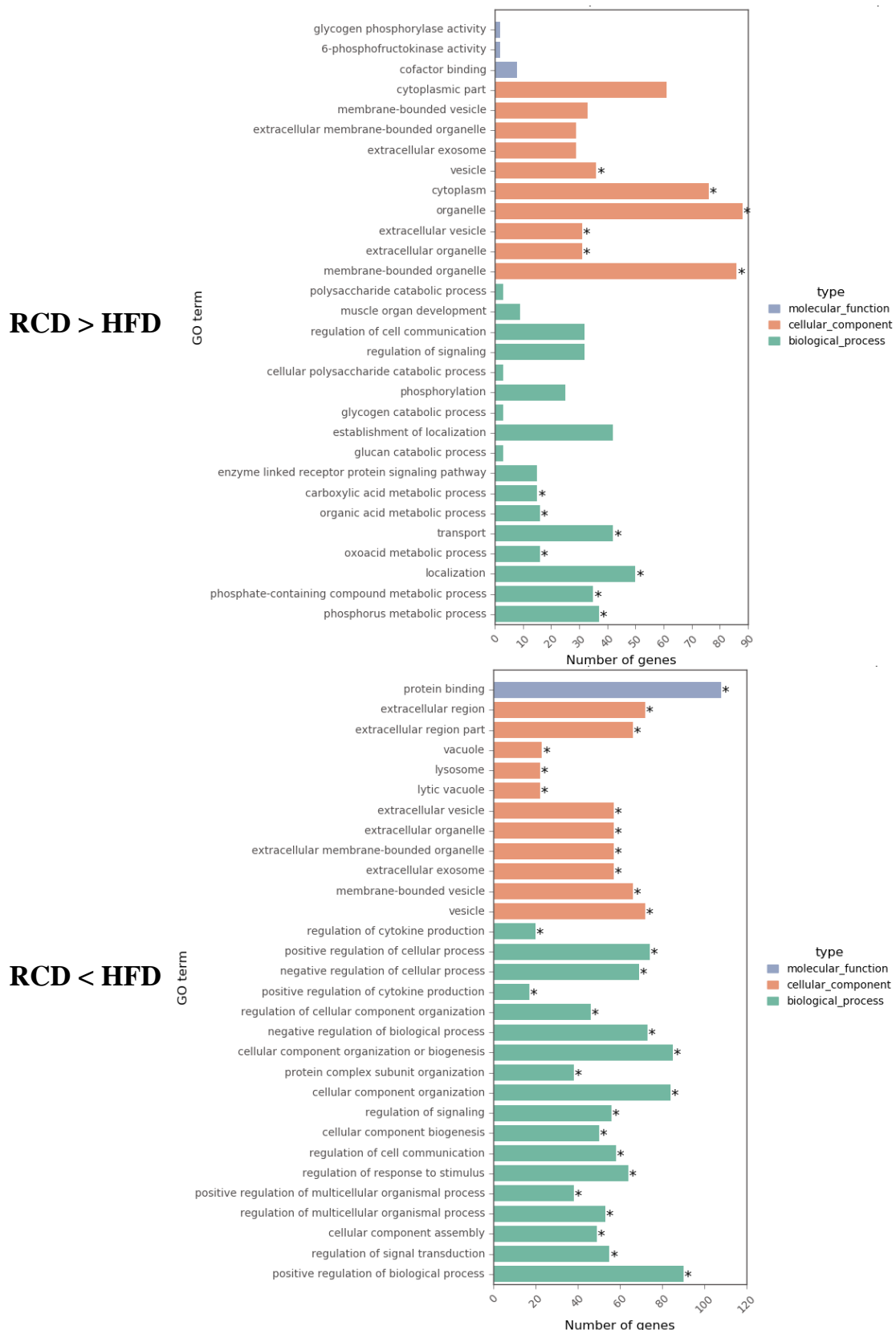
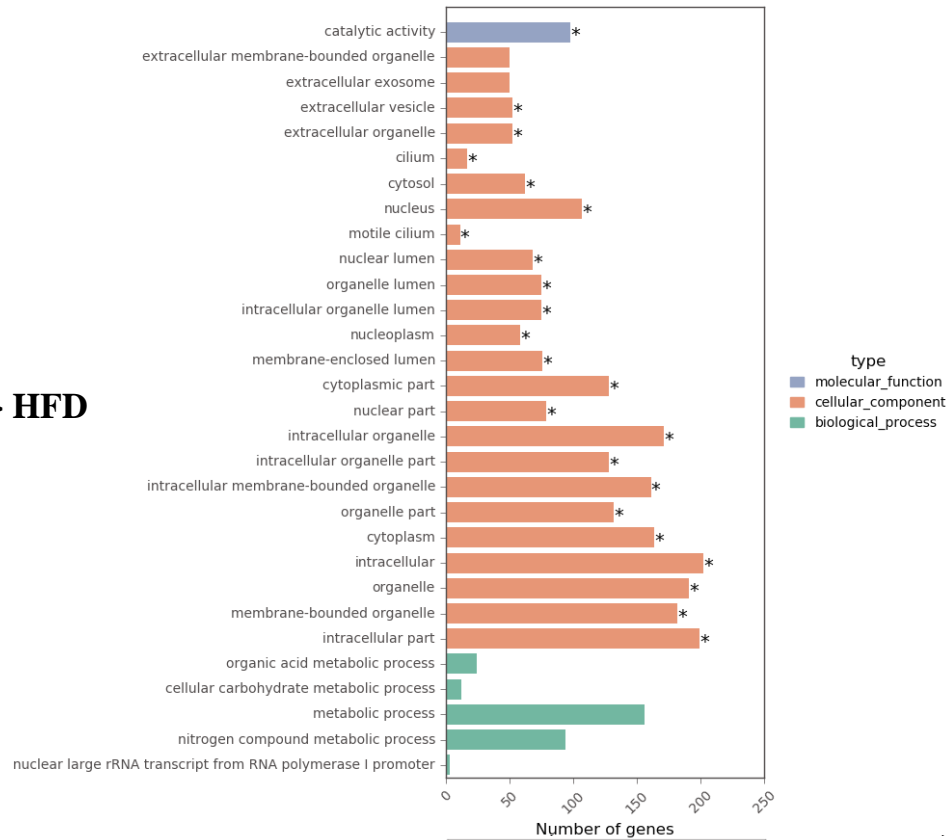


Fig 4.2(A) The TOP 30 GO Molecular Function (MF), Cellular Component (CC) and Biological Process (BP) ontologies annotating genes differentially expressed in the HFD-fed *ob/ob* mice at the age of 2 months compared with RCD-fed controls. *The corrected *p*-value of this GO term calculated by the FDR correction method of Benjamini and Hochberg [467] is less than 0.05.

RCD > HFD



RCD < HFD

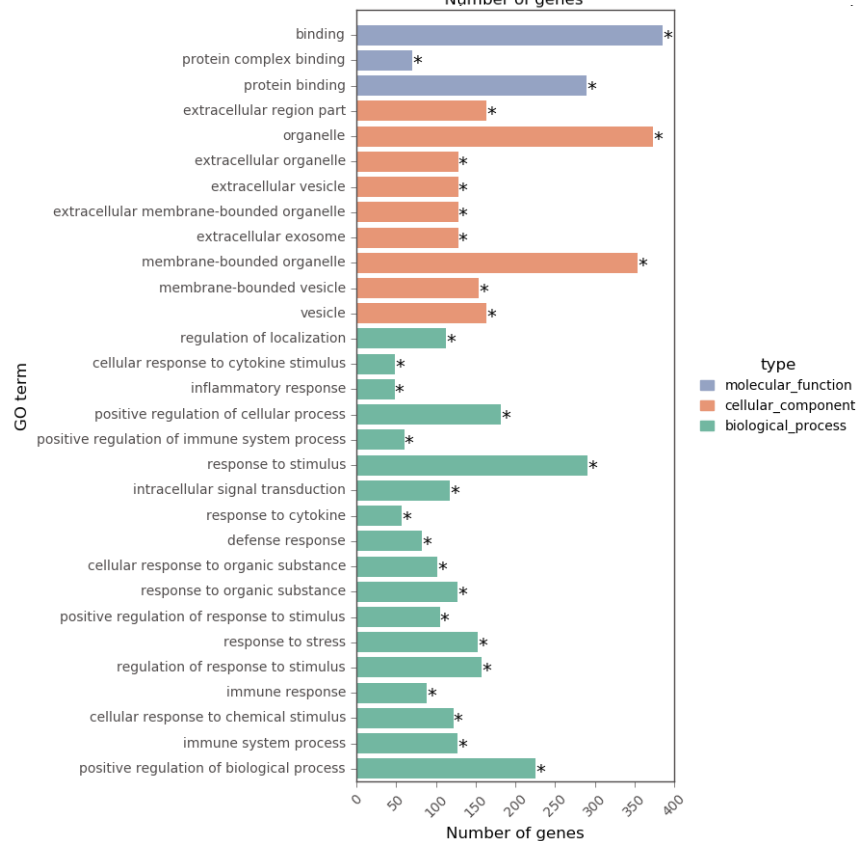


Fig 4.2(B) The TOP 30 GO Molecular Function (MF), Cellular Component (CC) and Biological Process (BP) ontologies annotating genes differentially expressed in the HFD-fed wild-type mice at the age of 10 months compared with RCD-fed controls. *The corrected *p*-value of this GO term calculated by the FDR correction method of Benjamini and Hochberg [467] is less than 0.05.

The influence of aging on gene expression of WAT as determined by annotated GO terms is shown in **Fig 4.3**. Interestingly, the aging factor resulted in significant differences in *ob/ob* mice compared with wild-type mice, as discussed previously. Interestingly, most of the GO terms significantly influenced by aging are also affected by the *ob/ob* genotype as shown in **Fig 4.1**. The genes down-regulated in older animals were annotated by intracellular CC terms, especially organelles such as the mitochondrion, whereas extracellular and membrane-bounded cellular component GO terms were enriched in the 10-month *ob/ob* mice fed on an HFD, compared with corresponding 2-month controls. BP terms associated with different metabolic pathways, in particular, lipid metabolism-related pathways, predominated in adipose tissue of all the younger groups of *ob/ob* mice. The genes up-regulated by aging in adipose tissue of 10-month old *ob/ob* mice fed on RCD were annotated by mostly the immune system and cell-cell adhesion processes GO terms, but this pattern disappeared in the OB-HFD group in which the metabolic processes predominated again.

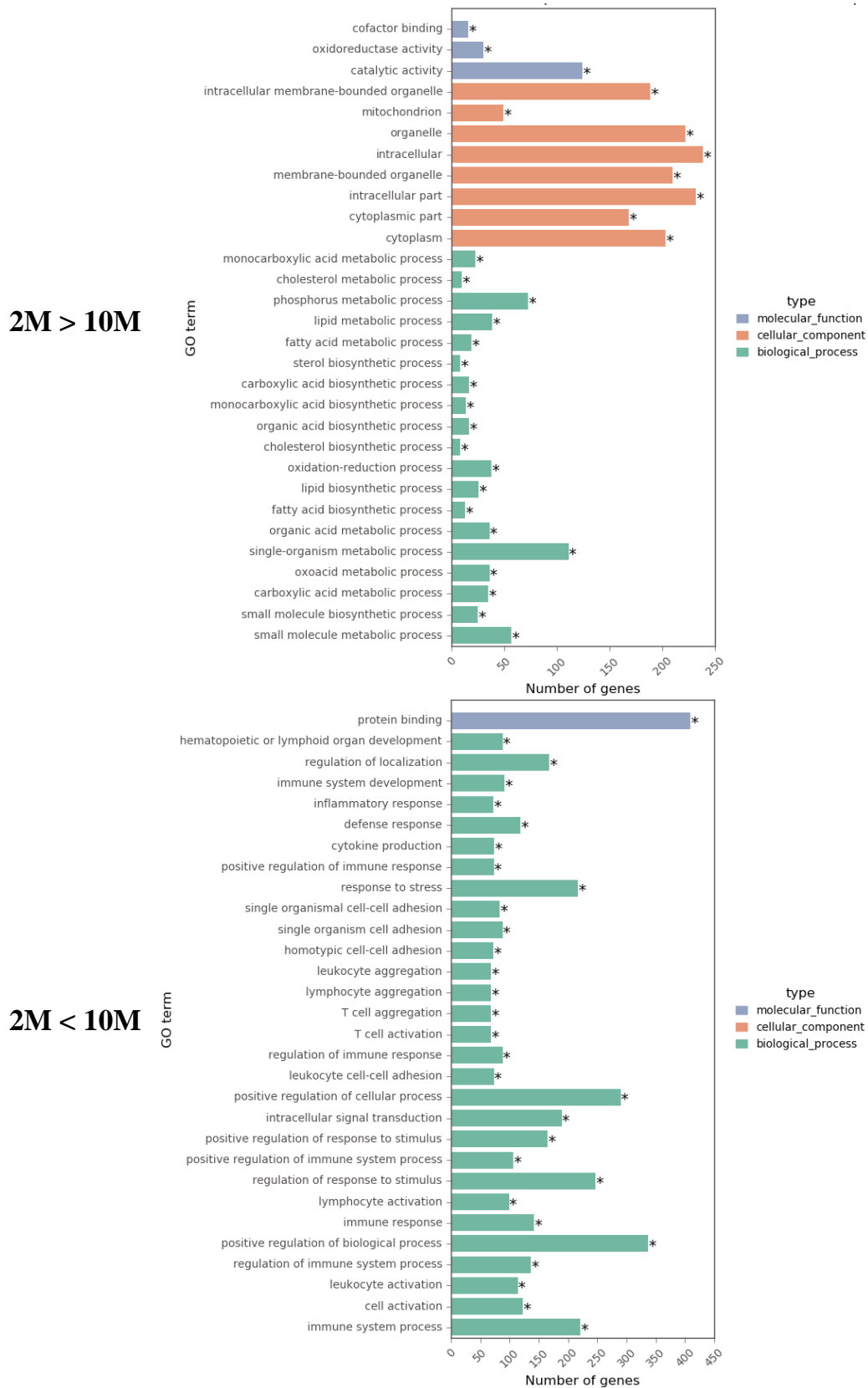


Fig 4.3(A) The TOP 30 GO Molecular Function (MF), Cellular Component (CC) and Biological Process (BP) ontologies annotating genes differentially expressed in the 10-month *ob/ob* mice fed on RCD (10M) compared with the 2-month controls (2M). *The corrected *p*-value of this GO term calculated by the FDR correction method of Benjamini and Hochberg [467] is less than 0.05.

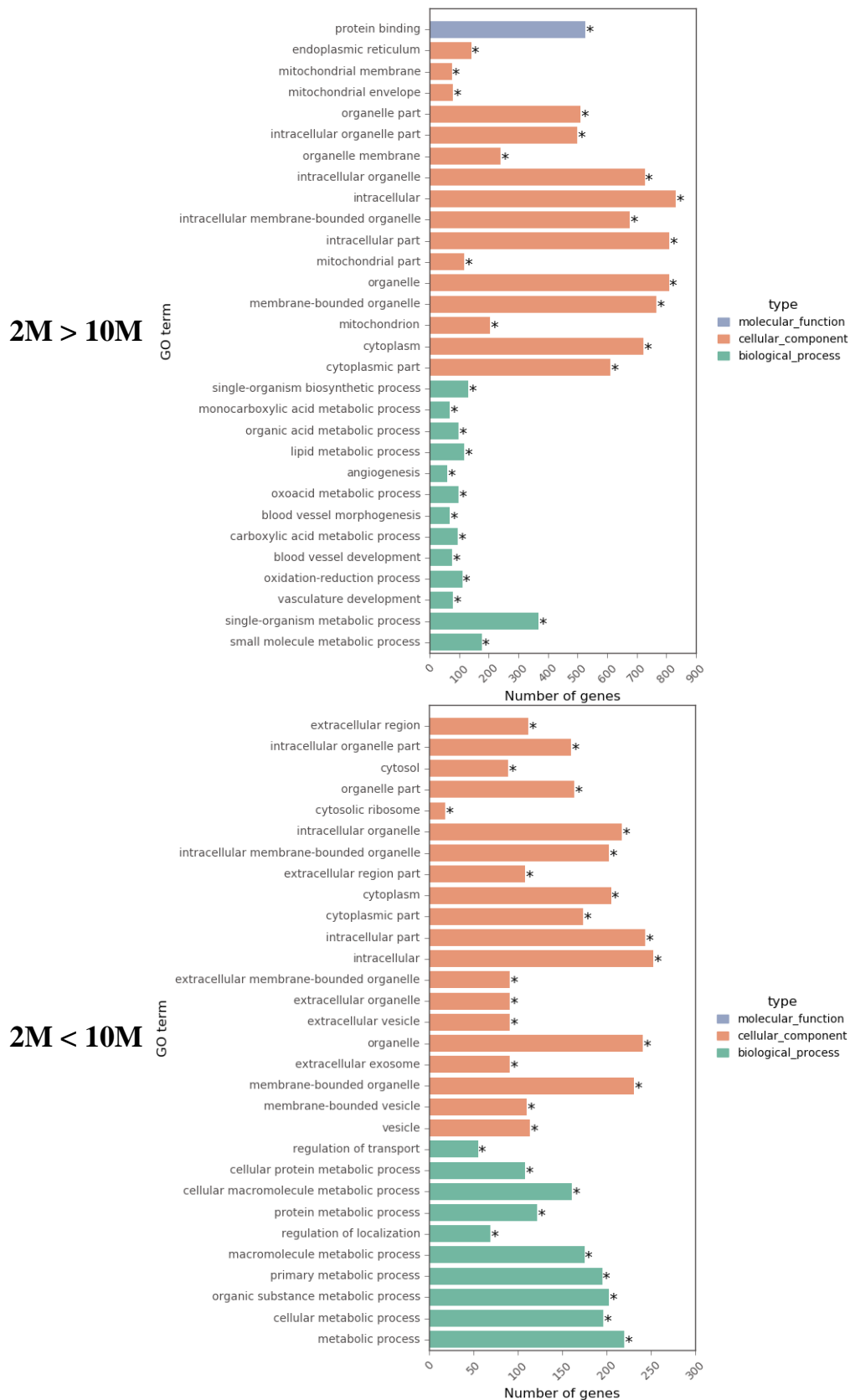


Fig 4.3(B) The TOP 30 GO Molecular Function (MF), Cellular Component (CC) and Biological Process (BP) ontologies annotating genes differentially expressed in the 10-month *ob/ob* mice fed on HFD (10M) compared with the 2-month controls (2M). *The corrected *p*-value of this GO term calculated by the FDR correction method of Benjamini and Hochberg [467] is less than 0.05.

4.4.3 KEGG pathway enrichment analysis reveals the different regulation of inflammatory and metabolic pathways in adipose tissue of *ob/ob* fed on HFD

To further explore the specific pathways regulated by the *ob/ob* genotype, HFD diet, and aging factors, KEGG Pathway Enrichment analysis was conducted among the different groups. The Q-values calculated by Benjamini and Hochberg FDR correction indicated the significance of each enriched pathway. The inflammatory and immune system pathways dominated the up-regulated terms. The Q-values of KEGG pathways annotating the genes significantly changed by genotype/diet/aging factors is summarized in **Table 4.3**. As shown by the shade of every cell, these pathways can be clustered in two typical expression patterns: inflammation-related pathways, and metabolic pathways. All the inflammation-related pathways were significantly up-regulated by the *ob/ob* genotype in all but the HFD-10 group, by the HFD diet in the WT-10 group and by aging in the OB-RCD group. It is interesting that the *ob/ob* genotype, the HFD, and aging didn't increase inflammation in the HFD-10 group, OB-10 group and OB-HFD group, respectively. One possible reason is that inflammation is already upregulated in these adipose tissues and cannot be aggravated anymore.

The KEGG pathways annotated by genes up-regulated by the *ob/ob* genotype in adipose tissue of younger (2 months) mice fed on RCD were associated with the lysosome, phagosome, and diseases associated with inflammation and immune system. In other groups, the *ob/ob* genotype also activated signaling pathways that play a key role in the immune system, such as toll-like receptor, nuclear factor kappa-light-chain-enhancer of activated B cells (NF- κ B) and chemokine signaling pathways. Incorrect regulation of these proteins has been linked to cancer, inflammatory and autoimmune diseases, viral infection, and improper immune development.

The KEGG pathways enriched by genes significantly up- or down-regulated by HFD diet and aging are also similar to those enriched by *ob/ob* genotype. Inflammatory pathways and remodeling associated with organelles like the phagosome and lysosome pathways were up-regulated by the HFD diet in WT-10 and HFD-2 groups, indicating accumulation of fat either by aging or overfeeding could increase the inflammatory response.

The influence of aging on the OB-RCD group is similar to that of *ob/ob* genotype and HFD diet, causing the upregulation of inflammatory and remodeling pathways, for example, the lysosome, B cell and T cell receptor signaling pathway, Osteoclast differentiation,

Hematopoietic cell lineage, NF-kappa B signaling pathway and Rheumatoid arthritis pathways. However, aging no longer demonstrated an obvious effect on the inflammation-related pathways in OB-HFD mice, but demonstrated significantly down-regulated peroxisome and metabolic pathways in general, including carbon metabolism and fatty acid metabolism which are significantly down-regulated in both OB-RCD and OB-HFD groups.

Some of the metabolic pathways (peroxisome, carbon metabolism, fatty acid metabolism, and steroid biosynthesis) were up-regulated in the *ob/ob* genotype for the RCD-2 group and by aging in wild-type animals. However, most of the metabolic pathways were down-regulated by the *ob/ob* genotype in aged mice and by aging in *ob/ob* mice. This is in accordance with the correlation results of gene expression shown in **Table 4.2** that many genes up-regulated by the *ob/ob* genotype in the RCD-2 group were down-regulated by *ob/ob* genotype in HFD-10 group, and also down-regulated by aging in adipose tissue of *ob/ob* mice. In order to elucidate what the underlying mechanisms could be for the reversion of these pathways, all the pathways changed significantly (adjusted p-value < 0.05) by genotype in RCD-2 and HFD-10 groups, and by aging in OB-HFD group were investigated. Most of the key genes of lipid metabolic pathways (**Table 4.4**) were inhibited by combining obesity and aging. To further elucidate the regulating network, changes of genes from Peroxisome, AMPK signaling pathways, insulin pathways, and PPAR signaling pathways are illustrated in **Fig 4.4-4.6**. It is apparent that a lot of important genes of the four key lipid pathways were up-regulated by leptin deficiency in the RCD-2 group, but down-regulated in the HFD-10 group and by aging in the OB-HFD group.



KEGG pathways	Q-value																								
	WT vs OB								RCD vs HFD				2 month vs 10 month												
	RCD-2		HFD-2		RCD-10		HFD-10		WT-2		OB-2		WT-10		OB-10		WT-RCD		WT-HFD		OB-RCD		OB-HFD		
	↓	↑	↓	↑	↓	↑	↓	↑	↓	↑	↓	↑	↓	↑	↓	↑	↓	↑	↓	↑	↓	↑	↓	↑	
Metabolic pathways	0.93	1.00	0.88	1.00	0.50	1.00	0.50	1.00	1.00	1.00	0.63	0.88	0.58	1.00	1.00	1.00	1.00	0.19	0.49	0.94	0.01	1.00	0.51	0.94	
Peroxisome	1.00	0.61	0.83	1.00	0.11	1.00	0.00	1.00	1.00	1.00	0.61	0.87	0.43	1.00	1.00	1.00	1.00	0.05	1.00	1.00	0.17	1.00	0.00	1.00	
Valine, leucine and isoleucine degradation	1.00	1.00	1.00	1.00	0.98	1.00	0.00	1.00	1.00	1.00	0.76	1.00	0.78	1.00	1.00	1.00	1.00	1.00	1.00	1.00	0.87	1.00	0.01	0.94	
Carbon metabolism	0.99	0.49	1.00	1.00	0.98	1.00	0.00	1.00	1.00	1.00	0.61	1.00	0.39	1.00	1.00	1.00	1.00	1.00	1.00	1.00	0.35	1.00	0.01	0.88	
AMPK signaling pathway	0.98	1.00	0.83	1.00	0.98	1.00	0.01	1.00	1.00	1.00	0.61	1.00	0.78	1.00	1.00	1.00	1.00	1.00	1.00	1.00	0.70	0.27	1.00	0.51	0.94
Fatty acid metabolism	1.00	0.42	0.83	1.00	0.24	1.00	0.01	1.00	1.00	1.00	0.63	1.00	0.50	0.84	1.00	1.00	1.00	1.00	1.00	1.00	0.12	1.00	0.61	0.94	
Non-alcoholic fatty liver disease (NAFLD)	0.98	1.00	0.83	1.00	0.98	1.00	0.01	1.00	1.00	1.00	0.76	0.87	0.88	1.00	1.00	1.00	1.00	1.00	1.00	1.00	0.92	1.00	0.78	0.99	
Propanoate metabolism	1.00	0.77	1.00	1.00	0.98	1.00	0.09	1.00	1.00	1.00	0.72	1.00	0.35	1.00	1.00	1.00	1.00	1.00	1.00	1.00	0.19	1.00	0.25	0.94	
Butanoate metabolism	0.73	1.00	0.83	1.00	0.79	1.00	0.13	1.00	1.00	1.00	0.72	1.00	0.39	1.00	1.00	1.00	1.00	1.00	1.00	1.00	0.27	1.00	0.25	0.94	
Glycine, serine and threonine metabolism	0.72	1.00	0.83	1.00	0.34	1.00	0.17	1.00	1.00	1.00	0.76	1.00	0.78	1.00	1.00	1.00	1.00	1.00	1.00	1.00	0.07	1.00	0.63	1.00	
Glutathione metabolism	0.72	1.00	0.83	1.00	0.45	1.00	0.26	1.00	1.00	1.00	1.00	0.87	0.68	1.00	1.00	1.00	1.00	0.04	1.00	0.70	1.00	0.87	1.00	0.99	1.00
Glyoxylate and dicarboxylate metabolism	0.89	1.00	1.00	1.00	0.79	1.00	0.26	1.00	1.00	1.00	0.61	1.00	0.78	1.00	1.00	1.00	1.00	1.00	1.00	1.00	0.27	1.00	0.78	1.00	
Pyruvate metabolism	0.98	1.00	0.83	1.00	0.79	1.00	0.25	0.94	1.00	1.00	0.61	1.00	0.44	1.00	1.00	1.00	1.00	1.00	1.00	1.00	0.21	1.00	0.62	0.91	
Steroid biosynthesis	1.00	0.17	1.00	0.20	0.98	1.00	0.44	1.00	1.00	1.00	1.00	1.00	1.00	0.84	1.00	1.00	1.00	1.00	1.00	1.00	0.64	0.01	1.00	0.15	1.00
Metabolism of xenobiotics by cytochrome	0.98	0.99	0.00	1.00	0.00	1.00	0.47	1.00	1.00	1.00	1.00	1.00	0.05	1.00	1.00	1.00	1.00	0.01	1.00	1.00	0.88	1.00	1.00	0.94	
Drug metabolism - cytochrome P450	0.89	1.00	0.01	1.00	0.95	1.00	0.54	1.00	1.00	1.00	1.00	1.00	0.22	1.00	1.00	1.00	1.00	0.01	1.00	1.00	0.83	1.00	1.00	1.00	
Glycerophospholipid metabolism	0.99	1.00	1.00	1.00	0.20	1.00	0.54	1.00	1.00	1.00	1.00	0.76	0.80	1.00	1.00	1.00	1.00	1.00	1.00	1.00	0.49	1.00	0.25	0.94	
Biosynthesis of unsaturated fatty acids	1.00	0.96	0.68	1.00	0.98	1.00	0.70	1.00	1.00	1.00	0.72	1.00	0.78	1.00	1.00	1.00	1.00	1.00	1.00	1.00	0.27	1.00	0.25	0.94	
Dorso-ventral axis formation	1.00	1.00	1.00	1.00	0.98	1.00	0.90	1.00	1.00	1.00	1.00	1.00	1.00	1.00	1.00	1.00	1.00	1.00	1.00	1.00	0.07	1.00	1.00	1.00	
Ribosome	1.00	1.00	0.88	1.00	0.98	1.00	1.00	0.99	1.00	1.00	1.00	0.87	1.00	1.00	1.00	1.00	1.00	1.00	1.00	1.00	0.96	1.00	1.00	0.99	
Mineral absorption	0.89	1.00	0.83	1.00	1.00	1.00	0.05	1.00	1.00	1.00	1.00	0.87	1.00	1.00	1.00	1.00	1.00	1.00	1.00	1.00	0.92	1.00	0.99	0.31	
FoxO signaling pathway	0.89	0.98	0.88	0.53	0.98	0.84	1.00	1.00	1.00	1.00	0.64	0.82	1.00	1.00	1.00	1.00	1.00	1.00	0.69	0.92	0.03	1.00	0.94	0.94	
Systemic lupus erythematosus	1.00	1.00	1.00	0.42	0.98	0.20	1.00	0.93	1.00	1.00	1.00	0.69	0.88	0.45	1.00	1.00	1.00	1.00	1.00	1.00	0.92	0.34	0.99	0.94	
Regulation of actin cytoskeleton	0.98	0.88	0.83	0.03	0.98	0.18	1.00	1.00	1.00	1.00	0.79	0.72	1.00	0.26	1.00	1.00	1.00	1.00	0.13	0.64	0.92	0.19	1.00	0.94	
Leukocyte transendothelial migration	1.00	0.64	1.00	0.25	0.98	0.11	1.00	1.00	1.00	1.00	0.81	0.71	1.00	0.91	1.00	1.00	1.00	1.00	0.64	0.80	0.05	0.99	0.94	0.94	
Viral myocarditis	1.00	1.00	1.00	0.47	1.00	0.09	1.00	1.00	1.00	1.00	1.00	0.74	0.80	0.03	1.00	1.00	1.00	1.00	0.64	1.00	0.05	1.00	0.94	0.94	
Fc gamma R-mediated phagocytosis	1.00	0.50	1.00	0.04	0.98	0.07	1.00	0.70	1.00	1.00	0.76	0.76	0.80	0.38	1.00	1.00	1.00	1.00	0.64	1.00	0.01	1.00	0.78	0.78	
Allograft rejection	1.00	1.00	1.00	0.24	1.00	0.05	1.00	1.00	1.00	1.00	1.00	0.77	0.78	0.09	1.00	1.00	1.00	1.00	1.00	1.00	0.02	1.00	1.00	1.00	
Antigen processing and presentation	1.00	1.00	1.00	0.24	0.98	0.03	1.00	1.00	1.00	1.00	1.00	0.31	0.80	0.05	1.00	1.00	1.00	1.00	1.00	1.00	0.19	1.00	0.94	0.94	
Natural killer cell mediated cytotoxicity	1.00	0.99	1.00	0.09	0.98	0.03	1.00	1.00	1.00	1.00	0.81	0.87	0.86	0.25	1.00	1.00	1.00	1.00	0.69	1.00	0.76	1.00	0.98	0.98	
Salmonella infection	1.00	0.42	0.83	0.03	0.98	0.03	1.00	0.85	1.00	1.00	1.00	0.69	1.00	0.17	1.00	1.00	1.00	1.00	0.10	0.64	0.92	0.01	1.00	0.94	
Legionellosis	0.82	0.96	1.00	0.01	0.98	0.02	1.00	0.50	1.00	1.00	1.00	0.77	0.78	0.38	1.00	1.00	1.00	1.00	1.00	1.00	0.05	1.00	0.94	0.94	
HTLV-I infection	1.00	1.00	0.88	0.06	0.98	0.02	1.00	1.00	1.00	1.00	0.76	0.76	1.00	0.25	1.00	1.00	1.00	1.00	1.00	0.87	0.92	0.01	1.00	0.94	
Inflammatory bowel disease (IBD)	1.00	0.96	1.00	0.32	1.00	0.01	1.00	1.00	1.00	1.00	0.76	0.77	0.78	0.88	1.00	1.00	1.00	1.00	1.00	1.00	0.92	0.05	1.00	1.00	
Cell adhesion molecules (CAMs)	1.00	1.00	0.88	0.19	1.00	0.01	1.00	1.00	1.00	1.00	1.00	0.74	1.00	0.95	1.00	1.00	1.00	1.00	1.00	1.00	0.15	1.00	0.99	0.99	
Malaria	1.00	0.10	1.00	0.29	1.00	0.00	1.00	1.00	1.00	1.00	1.00	1.00	0.25	1.00	1.00	1.00	1.00	1.00	0.69	1.00	0.19	0.97	0.94	0.94	
Chagas disease (American trypanosomiasis)	1.00	0.31	0.83	0.03	0.98	0.00	1.00	0.94	1.00	1.00	0.76	0.86	1.00	0.84	1.00	1.00	1.00	1.00	0.69	0.92	0.10	1.00	0.94	0.94	
Toxoplasmosis	0.80	0.42	0.86	0.06	0.98	0.00	1.00	1.00	1.00	1.00	0.61	0.74	0.78	0.32	1.00	1.00	1.00	1.00	1.00	0.70	0.95	0.29	1.00	0.98	
B cell receptor signaling pathway	1.00	1.00	1.00	0.02	0.98	0.00	1.00	0.93	1.00	1.00	0.76	0.74	1.00	0.84	1.00	1.00	1.00	1.00	1.00	0.64	1.00	0.00	1.00	0.91	
Asthma	1.00	0.64	1.00	0.02	1.00	0.00	1.00	1.00	1.00	1.00	1.00	0.31	1.00	0.29	1.00	1.00	1.00	1.00	1.00	1.00	0.04	1.00	0.94	0.94	
Pertussis	1.00	0.42	0.84	0.02	0.98	0.00	1.00	0.93	1.00	1.00	1.00	0.80	1.00	0.04	1.00	1.00	1.00	1.00	1.00	1.00	0.92	0.07	1.00	0.94	
Cytokine-cytokine receptor interaction	1.00	0.96	0.83	0.04	1.00	0.00	1.00	1.00	1.00	1.00	0.91	1.00	0.34	1.00	1.00	1.00	1.00	1.00	1.00	0.70	0.92	0.01	1.00	0.94	
Tuberculosis	1.00	0.03	0.90	0.06	0.98	0.00	1.00	0.93	1.00	1.00	1.00	0.31	1.00	0.09	1.00	1.00	1.00	1.00	1.00	0.76	0.94	0.05	1.00	0.89	
Phagosome	1.00	0.01	1.00	0.00	0.98	0.00	1.00	0.93	1.00	1.00	0.88	0.31	1.00	0.00	1.00	1.00	1.00	1.00	1.00	0.64	0.94	0.02	1.00	0.79	
TNF signaling pathway	1.00	0.99	0.86	0.34	0.98	0.00	1.00	1.00	1.00	1.00	0.80	0.74	0.83	0.29	1.00	1.00	1.00	1.00	1.00	0.70	0.88	0.14	1.00	0.94	
Chemokine signaling pathway	1.00	0.17	0.83	0.03	0.98	0.00	1.00	1.00	1.00	1.00	0.89	0.83	1.00	0.17	1.00	1.00	1.00	1.00	1.00	0.64	0.98	0.01	1.00	0.94	
Primary immunodeficiency	1.00	1.00	1.00	0.01	1.00	0.00	1.00	1.00	1.00	1.00	1.00	0.74	1.00	0.49	1.00	1.00	1.00	1.00	1.00	1.00	1.00	0.00	1.00	1.00	
T cell receptor signaling pathway	1.00	1.00	0.86	0.04	0.98	0.00	1.00	1.00	1.00	1.00	0.76	0.77	0.82	1.00	1.00	1.00	1.00	1.00	1.00	0.94	0.06	1.00	1.00	1.00	
Hematopoietic cell lineage	1.00	0.78	1.00	0.01	0.98	0.00	1.00	1.00	1.00	1.00	0.76	0.76	1.00	0.37	1.00	1.00	1.00	1.00	1.00	1.00	0.93	0.00	0.97	0.94	
Toll-like receptor signaling pathway	1.00	0.10	0.86	0.06	0.98	0.00	1.00	0.40	1.00	1.00	0.79	0.77	0.82	0.84	1.00	1.00	1.00	1.00	1.00	0.94	0.01	1.00	0.87	0.87	
Intestinal immune network for IgA production	1.00	1.00	0.83	0.20	0.98	0.00	1.00	1.00	1.00	1.00	1.00	0.74	1.00	0.19	1.00	1.00	1.00	1.00	1.00	1.00	1.00	0.00	1.00	1.00	
St																									

Pathway	Group	RCD-2		HFD-10		OB-HFD	
		WT > OB	WT < OB	WT > OB	WT < OB	2M > 10M	2M < 10M
AMPK signaling pathway		Ulk1, Ccnd1, Tbc1d1, Stk11, Akt1s1, Pdpk1	Gys2, Igf1, Pparg, Pik3cb, Akt2, Pfkp, Lep, Pik3cg, Foxo1, Srebf1, Fasn, Camkk2, Rheb, Ppp2r5b	Cab39l, Prkag3, Stk11, Prkaa2, Pparg, Fasn, Crem, Tsc2, Stradb, Adra1a, Foxo1, Irs2, Irs3, Insr, Adipoq, Ppp2r1b, Adipor2, Slc2a4, Akt2, Gys2, Eif4ebp1, Lipe, Creb5, Akt1s1, Ppp2r5d, Ppp2r5e, Pfkfb3, Ppp2r5b	Ccnd1, Rab8a, Adipor1	Cab39l, Adipor2, Scd2, Foxo1, Irs3, Lep, Pparg, Stradb, Gys2, Fasn, Crem, Pik3r1, Prkaa2, Eif4ebp1, Ppp2r5b	Ccnd1, Rab8a
PPAR signaling pathway		Pdpk1, Fads2, Cyp4a12a	Dbi, Acaa1b, Aqp7, Acsl1, Pparg, Angptl4, Pltp, Fabp5, Acadl, Acadm, Nr1h3	Acaa1b, Acaa1a, Cpt2, Aqp7, Slc27a1, Rxrg, Scp2, Rxra, Pparg, Fabp4, Angptl4, Acadl, Sorbs1, Ehhadh, Acadm, Adipoq, Plin1		Acaa1b, Acaa1a, Cpt2, Aqp7, Scd2, Acsl1, Scp2, Rxrg, Pparg, Fabp4, Angptl4, Sorbs1, Slc27a1, Plin1	
Insulin signaling pathway		Cblc, Pdpk1, Map2k2, Prkacb	Eif4e2, Rheb, Ppp1r3b, Hk3, Pik3cb, Foxo1, Pik3cg, Mapk3, Sh2b2, Gys2, Prkaca, Flot1, Prkx, Fasn, Akt2, Srebf1, Pygl	Prkag3, Prkaa2, Fasn, Tsc2, Ppp1r3c, Mknk2, Insr, Irs2, Irs3, Foxo1, Slc2a4, Phkb, Akt2, Gys2, Eif4ebp1, Sorbs1, Phkg1, Lipe, Hras, Pygb, Rapgef1, Prkaca	Rps6, Hk1, Calm2, Prkacb	Eif4e2, Ppp1r3c, Sh2b2, Mknk2, Prkaa2, Eif4ebp1, Irs3, Foxo1, Gys2, Prkaca, Flot1, Pik3r1, Sorbs1, Fasn, Phkb, Kras	Rps6, Prkacb
Adipocytokine signaling pathway		Stk11, Npy	Lep, Camkk2, Akt2, Acsl1, Tnfrsf1a	Stk11, Adipor2, Ptpn11, Slc2a4, Prkaa2, Irs2, Rxrg, Akt2, Rxra, Irs3, Prkag3, Adipoq	Npy, Slc2a1, Adipor1	Acsl1, Adipor2, Ptpn11, Rxrg, Prkaa2, Irs3, Lep	
Fatty acid metabolism		Fads2	Acaa1b, Hacd2, Echs1, Acsl1, Acaa2, Elovl5, Fasn, Mecn, Acadl, Acadm	Hsd17b12, Acaa1b, Acaa1a, Acads, Echs1, Acadl, Cpt2, Tscr, Acaa2, Acat2, Acadvl, Fasn, Mecn, Hacd2, Ehhadh, Acadm	Ppt1	Hsd17b12, Acaa1b, Acaa1a, Cpt2, Echs1, Scd2, Acsl1, Tscr, Acaa2, Hacd2, Acads, Fasn, Mecn	Fads1
Fatty acid elongation			Hacd2, Acaa2, Echs1, Elovl5, Mecn, Acot7	Hsd17b12, Hacd2, Echs1, Tscr, Acaa2, Mecn	Acot7, Acot1, Ppt1	Hsd17b12, Hacd2, Echs1, Tscr, Acaa2, Mecn	
Fat digestion and absorption		Got2, Plpp2	Lipf, Pla2g12a, Dgat2, Pla2g2e, Agpat2, Mogat2	Plpp3, Dgat1, Pla2g12a, Dgat2, Acat2, Mogat2, Agpat2, Pla2g2e		Plpp1, Plpp3, Dgat1, Pla2g12a, Dgat2, Mogat2, Agpat2, Pla2g2e	
Biosynthesis of unsaturated fatty acids		Fads2	Acot7, Hacd2, Elovl5, Acaa1b	Hsd17b12, Acaa1b, Acaa1a, Hacd2, Tscr	Acot7, Acot1	Hsd17b12, Acaa1b, Acaa1a, Hacd2, Scd2, Tscr	Fads1

Fatty acid degradation	Cyp4a12a	Acaa1b, Echs1, Acs11, Acaa2, Acadl, Acadm	Acaa1b, Acaa1a, Acads, Echs1, Acadl, Cpt2, Acat2, Acaa2, Eci1, Acadvl, Adh4, Ehhadh, Acadm	Aldh2	Acaa1b, Acaa1a, Cpt2, Echs1, Acs11, Acaa2, Eci1, Acads	Aldh2
Fatty acid biosynthesis		Acs11, Fasn	Fasn		Acs11, Fasn	
Sphingolipid metabolism	Sphk1, Plpp2, Kdsr, Sgpp1	Degs1, Smpd1, Asah1, Smpd3	Plpp3, Cers4, Smpd1, Smpd3, Asah2	Acer3, Sphk1, Asah1, Sgpl1, Glb1, Neu1, Sgpp1	Plpp1, Plpp3, Smpd1, Cers4	Sphk1, Asah1, Glb1, Neu1
Ether lipid metabolism	Plpp2	Agps, Pla2g12a, Pla2g6, Pla2g7, Pla2g2e, Pafah1b1	Plpp3, Chpt1, Pla2g2e, Pla2g12a, Ept1	Pafah1b3, Pld3	Plpp1, Plpp3, Pla2g12a, Ept1, Chpt1, Pla2g2e	
Glycerolipid metabolism	Mboat2, Plpp2, Akr1b7	Agpat2, Lipf, Dgat2, Akr1b8, Lpin1	Plpp3, Gpat4, Lpin1, Dgat1, Glyctk, Dgat2, Mgl1, Pnpla2, Agpat2, Agpat9	Akr1a1, Lpin2, Akr1b8, Aldh2	Plpp1, Plpp3, Lpin1, Dgat1, Mgl1, Dgat2, Glyctk, Pnpla2, Agpat2	Akr1b8, Aldh2, Akr1a1
Glycerophospholipid metabolism	Mboat2, Pcyt1b, Taz, Plpp2	Pla2g15, Lpin1, Pla2g12a, Pla2g6, Gpd1, Agpat2, Pgs1, Pla2g2e, Lpgat1	Plpp3, Gpat4, Lpin1, Pla2g12a, Pcyt2, Ept1, Chpt1, Gpd1, Agpat2, Gnpat, Cr1s1, Pla2g2e, Chka, Agpat9	Lpin2, Pld3	Plpp1, Plpp3, Lpin1, Pla2g12a, Pcyt2, Ept1, Chpt1, Gpd1, Agpat2, Gnpat, Pla2g2e, Chka, Lpcat3	Pisd-ps3
Glycosphingolipid biosynthesis - ganglio series	B3galt4, St8sia5	Hexa	St6galnac5	St6galnac4, Hexb, Glb1		Glb1
Glycosphingolipid biosynthesis - lacto and neolacto series	B4galt3, Abo	B3gnt3, Gcnt2	St3gal3, B4gat1, St3gal6, Gcnt2		St3gal3, Gcnt2	
Glycosphingolipid biosynthesis - globo series		Hexa, B3galnt1		Hexb	A4galt	
Oxidative phosphorylation	Ndufa6, Ndufa5, Ndufa3, Ndufa1, Ndufb7, Ndufs6, Cox6b2	Atp6v1c1, Atp6v1a, Atp6v1e1, Atp6v1h, Tcirg1, Atp6v1b2, Atp6v0d1	Atp5c1, Ndufc1, Ndufa8, Ndufa9, Sdhc, Atp5g3, Uqcr10, Uqcr11, Ndufs3, Cox6b1, Uqcrc2, Ndufb8, Ndufb6, Ndufb3, Ppa1, Ndufv3, Ndufv1, Cyc1, BC002163, Cox4i2, Cox7a1, Atp6v0e2, Cox6a1	Atp6v1d, Atp6v1h, Atp6v1g1	Uqcr11, Ndufb3, Ndufa8, BC002163, Cox4i2, Ndufs3, Atp5o, Ppa1, Cox6b1, Cox6a1, Atp5g3, Cox6a2	Atp6v1d, Ndufa5, Atp6v1g1

Table 4.4 The genes associated with lipid metabolic pathways changed significantly ($p < 0.05$) by genotype in the RCD-2 and HFD-10 groups, and by aging in the OB-HFD group.

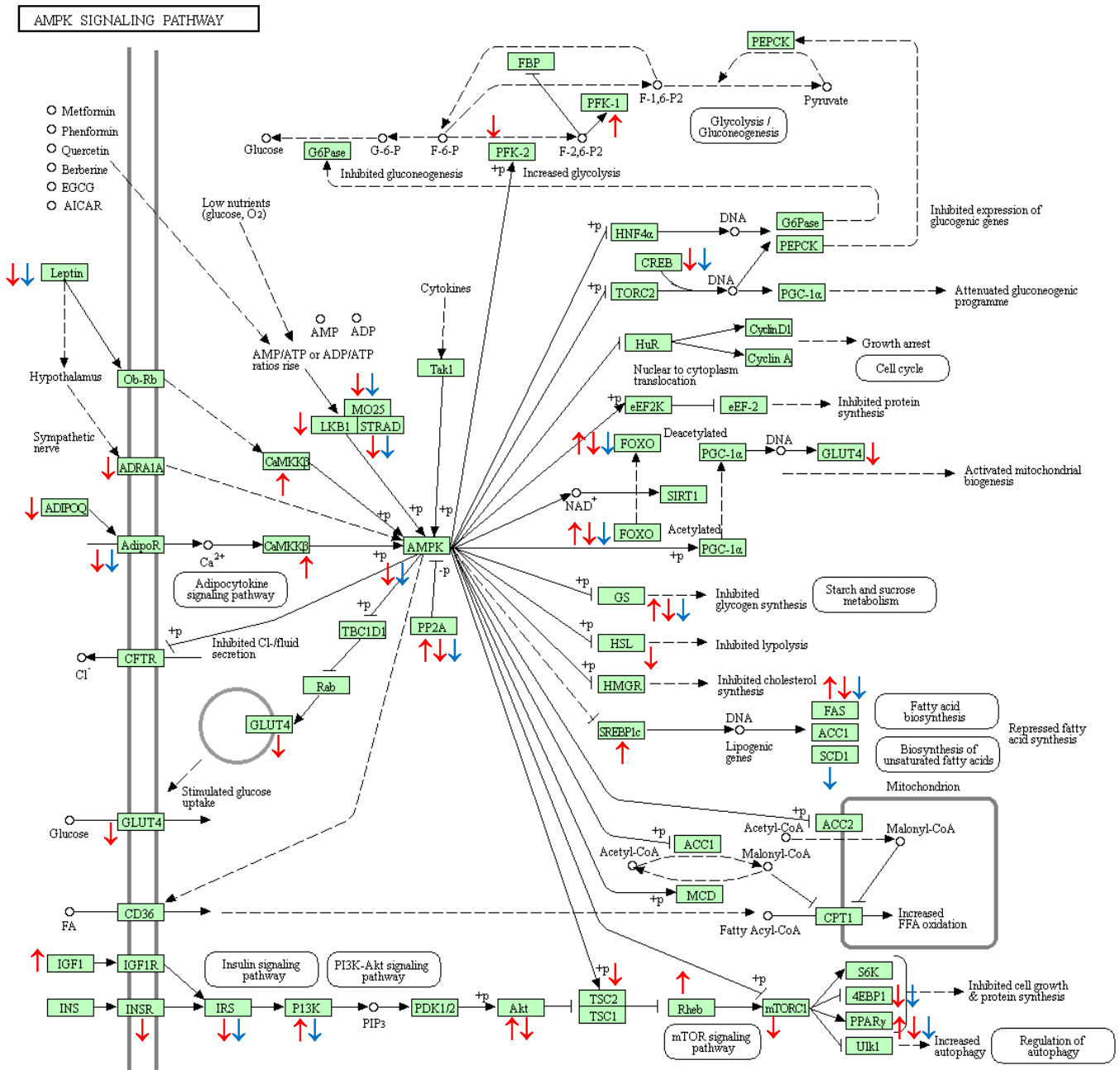
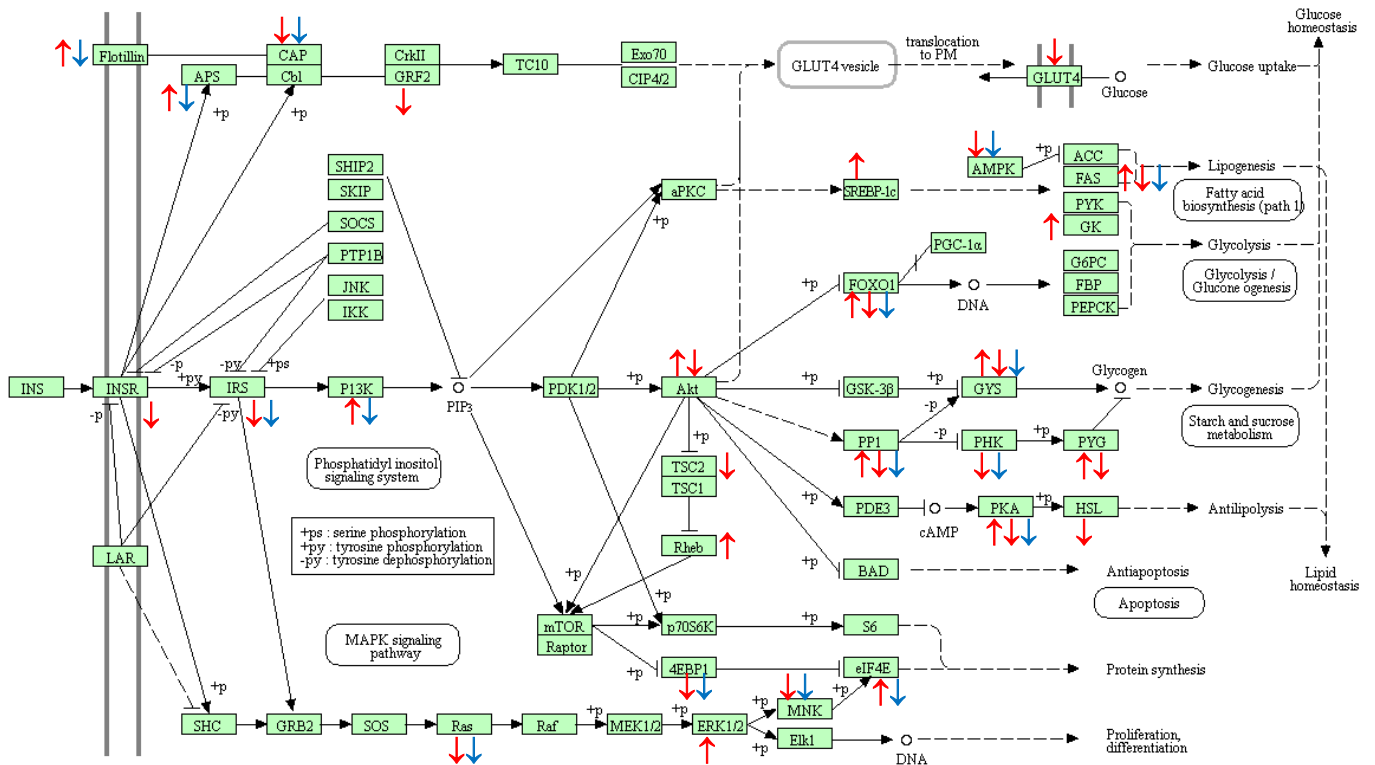


Fig 4.5 The genes associated with AMPK signaling pathways changed significantly ($p < 0.05$) by genotype in RCD-2 and HFD-10 groups, and by aging in the OB-HFD group.
 ↑: up-regulated in the OB-RCD-2 group compared with the WT-RCD-2 group;
 ↓: down-regulated in the OB-HFD-10 group compared with the WT-HFD-10 group;
 ↓: down-regulated in the OB-HFD-10 group compared with the OB-HFD-2 group.
 The figure is modified from the KEGG reference pathway (<http://www.genome.jp/kegg/pathway.html>) by (c) Kanehisa Laboratories 04152 3/6/17.

A INSULIN SIGNALING PATHWAY



B PPAR SIGNALING PATHWAY

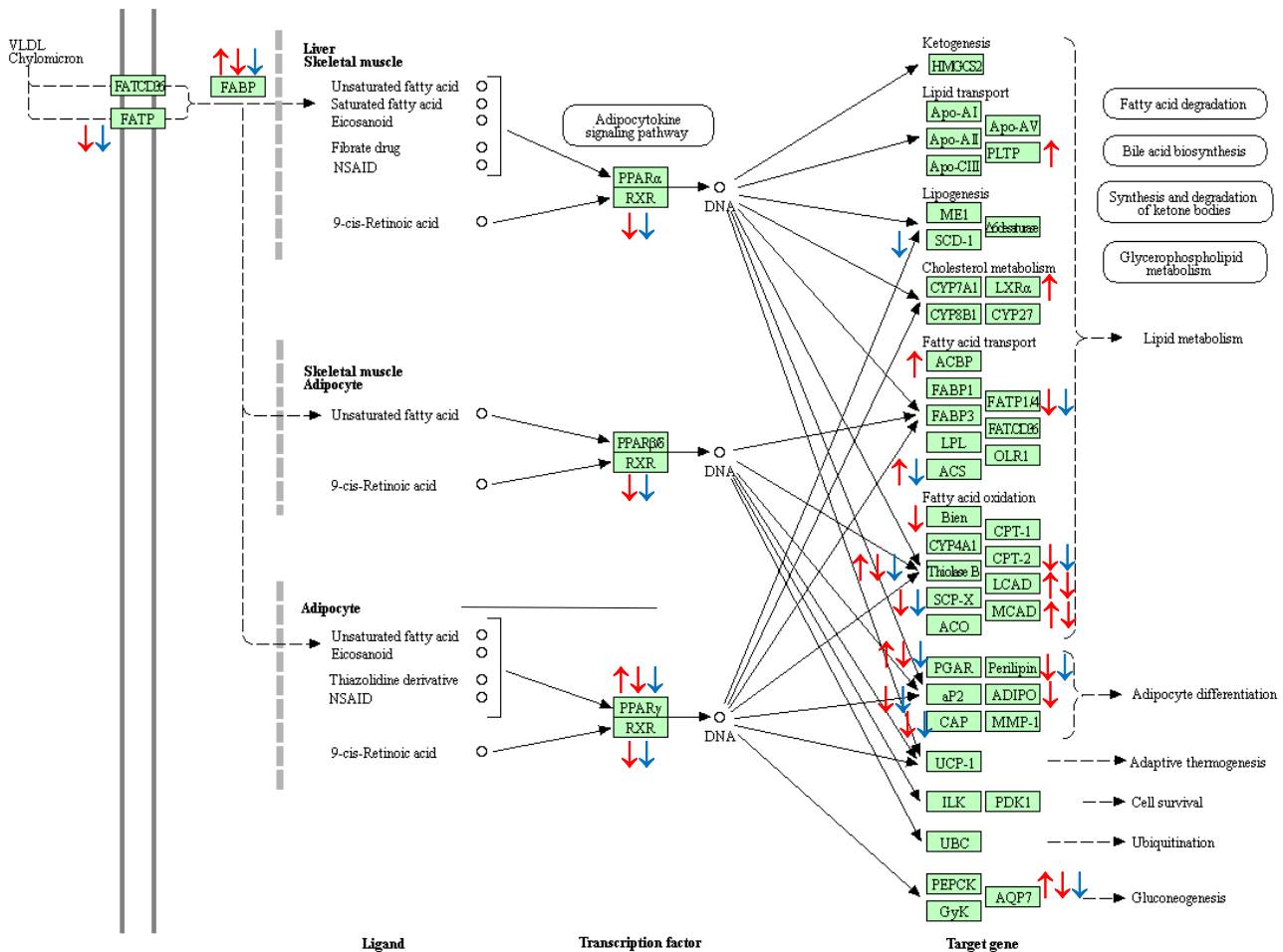


Fig 4.6 (A) The genes associated with insulin signaling pathways changed significantly ($p < 0.05$) by genotype in the RCD-2 and HFD-10 groups, and by aging in the OB-HFD group. ↑: up-regulated in the OB-RCD-2 group compared with the WT-RCD-2 group; ↓: down-regulated in the OB-HFD-10 group compared with the WT-HFD-10 group; ↓: down-regulated in the OB-HFD-10 group compared with the OB-HFD-2 group. The figure is modified from the KEGG reference pathway (<http://www.genome.jp/kegg/pathway.html>) by (c) Kanehisa Laboratories 04910 8/14/15.

(B) The genes associated with the PPAR signaling pathways changed significantly ($p < 0.05$) by genotype in the RCD-2 and HFD-10 groups, and by aging in the OB-HFD group. ↑: up-regulated in the OB-RCD-2 group compared with the WT-RCD-2 group; ↓: down-regulated in the OB-HFD-10 group compared with the WT-HFD-10 group; ↓: down-regulated in the OB-HFD-10 group compared with the OB-HFD-2 group. The figure is modified from the KEGG reference pathway (<http://www.genome.jp/kegg/pathway.html>) by (c) Kanehisa Laboratories 03320 6/3/16.

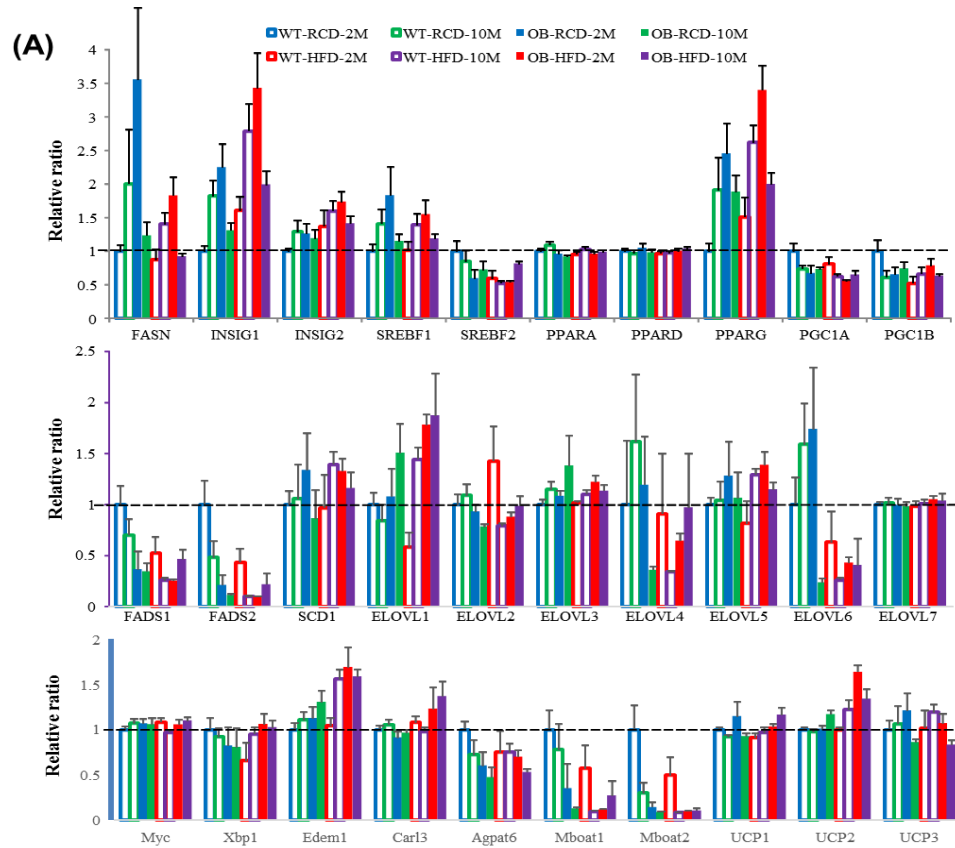
4.4.4 The expression pattern of selected genes in lipid metabolism and adipose tissue demonstrated the similarity between lipidomic and transcriptomic results

To clearly demonstrate the changes in the progression of obesity (induced by *ob/ob* and HFD) and aging, I selected some of the genes described in the literature as regulating pathways of DNL (Fasn [468]), desaturation (Scd1 [469], Fads1 [470], Fads2 [470]), elongation (Elov11-7 [208, 219, 471]), endoplasmic reticulum (ER) stress (Xbp1 [472], Edem1 [473], and Calr3 [474]), TG biosynthesis and lipid remodeling (Agpat6 [475], Mboat1-2 [476, 477]) and some essential transcription factors known to regulate lipid metabolism (Insig1-2 [37, 478-480], Srebf1-2 [481-483], PPAR $\alpha/\delta/\gamma$ [70, 429, 484], Pgc1 α/β [421, 485-487] and Myc [488-490]) to determine variations in expression (**Fig 4.7A**). The transcriptomic patterns of Fasn, Insig1, Insig2, PPAR γ , and Srebf1 were highly similar, and all up-regulated in adipose tissue of *ob/ob* mice at the age of 2 months compared with wild-types but down-regulated at 10 months compared with wild-type controls, up-regulated in adipose tissue of 10 months old wild-type mice during aging but down-regulated in 10 month old *ob/ob* mice compared with the younger animals. It suggests that DNL was activated by leptin deficiency in younger mice and with aging in wild-type animals, but inhibited in adipose tissue of old *ob/ob* mice. Scd1 and Elov16 were regulated in similar directions with Fasn in these groups. Interestingly, average chain length and degree of unsaturation of PCs, as described in **Chapter 3.4.3**, was increased in younger *ob/ob* mice but decreased in 10-month mice fed the HFD, and also decreased with aging, showing similar changes to the genes involved in DNL. Further research is needed to

demonstrate whether the down-regulated elongases and desaturases and related transcription factors resulted in short and saturated PCs accumulated, or the unsaturation status of PCs in the cell membrane is the reason for the changed expression of these genes.

Expression of *Elovl1* was up-regulated by *ob/ob*, the HFD diet and aging in many groups, while *Elovl6* was down-regulated significantly by HFD in the same groups (**Fig 4.7B**), suggesting elongation of C18:0 by ELOVL1 is activated to form more VLCFAs in adipose tissue of either old or obese mice. However, further desaturation of oleate was inhibited as the desaturase genes (*Fads1* and *Fads2*) were down-regulated by *ob/ob*, HFD, and aging. This agrees with the dominance of oleate in adipose tissue of obese and aged mice described in **Chapter 3**. Moreover, the expression of TG biosynthesis and lipid remodeling genes (*Mboat1* and *Mboat2*) were down-regulated by obesity from either *ob/ob* or HFD. Thus, a further modification of FAs and remodeling of WAT were inhibited by obesity and aging while DNL was overly activated.

The ER stress-related genes were not significantly regulated except *Edem1*, which was up-regulated by the HFD diet in the WT-10 group. *UCP2*, which is involved in regulating the generation of mitochondrial-derived ROS [491], was up-regulated not only by leptin deficiency but also by the HFD diet, indicating the increased oxidative stress in adipose tissue of obese mice. Interestingly, *UCP3* which transports FA anions into the mitochondrial intermembrane to form neutral FAs and reduces proton gradients via the PPAR signaling pathways [492-494], was slightly (not significantly) up-regulated by obesity and aging, but significantly down-regulated in 10-month *ob/ob* mice fed on HFD compared with wild-type controls. The increased ER and oxidative stress together may impair fat storage capacity and lead to more dysfunctions of the adipose tissue.



(B)

	WT vs OB				STD vs HFD				2 month vs 10 month			
	STD-2	HFD-2	STD-10	HFD-10	WT-2	OB-2	WT-10	OB-10	WT-STD	OB-STD	WT-HFD	OB-HFD
Fasn	*			*						*		*
Insig1	*	*	*	*						*		*
Insig2	*			*								*
Srebf1	*									*		
Srebf2												*
Ppara α												
Ppara δ												
Ppar γ	*			*								*
Ppargc1a		*										
Ppargc1b												
Fads1		*										*
Fads2	*											
Scd1												
Elovl1		*	*			*	*			*		
Elovl2												
Elovl3												
Elovl4												
Elovl5	*											
Elovl6			*			*	*			*		
Elovl7												
Myc												
Xbp1												
Edem1							*					
Carl3												
Agpat6												
Mboat1												
Mboat2	*											
Ucp1												
Ucp2		*				*						
Ucp3				*								

Fig 4.7 (A) Selected gene expression in adipose tissues from *ob/ob* (OB) mice and wild-type (WT) controls aged between 2 (2M) and 10 (10M) months fed on a regular chow diet (RCD) or high-fat diet (HFD), all data normalized to the WT-RCD-2M group. The genes up-regulated (red) or down-regulated (blue) significantly ($p < 0.05$) are indicated by * in **(B)**.

4.5 Discussion

In this Chapter, transcriptomic patterns of two models of obesity associated with leptin deficiency and/or high-fat diet were studied at two-time points. Alterations in the expression of genes were more pronounced in the adipose tissue of *ob/ob* mice, compared with the HFD model. Interestingly, 1565 genes were significantly down-regulated by leptin deficiency in the HFD-10 group, whereas most of the genes were up-regulated by *ob/ob* genotype in the RCD-2 (1219), HFD-2 (819) and RCD-10 (1251) groups compared with the wild-type controls. As many as 902 genes were down-regulated not only by *ob/ob* genotype in the HFD-10 group but also by aging in the OB-HFD group. This suggests that the initial stages of obesity are associated with an increase in many transcripts but during severe obesity and aging these patterns are reversed. As far as I know, this reversion correlating obesity and aging has never been reported before.

Genes up-regulated by each of the three factors (*ob/ob* genotype, HFD diet, and aging) were mostly annotated by GO functional themes and KEGG pathways associated with the immune system, inflammation, and signaling processes. Both obesity and aging are closely associated with low-grade chronic inflammation [495] characterized by immune system dysfunction. The pro-inflammatory phenotype which alters intercellular communication and accompanies aging in mammals has been termed ‘inflammaging’ [496] and could be caused by different factors such as pro-inflammatory tissue damage, dysfunctional immune system, cytokines secreted by senescent cells, NF- κ B activation and decreased autophagy [497]. Interestingly the enrichment of immune and inflammatory biological process GO terms only appeared in the 10-month old wild-type animals on an HFD, suggesting that obesity caused by leptin-deficiency on any diet is more associated with inflammation than diet-induced obesity. However, cell signaling and cytokine production were upregulated most significantly in the OB-2M group, which might be an initial signal of a pro-inflammatory state.

Extracellular, vesicle and membrane-related cellular components were enriched by the genes up-regulated by the *ob/ob* genotype. Interestingly, the HFD diet also led to an upregulation of genes predominantly annotated by extracellular CC terms, indicating the two models of obesity in our study both resulted in increased extracellular matrix remodeling which has been reported to be a link between obesity and vascular fibrosis and stiffness [498]. Vascular and cardiac fibrosis, amyloid infiltration [499], accumulation of collagen [500] and reduced elastin, lead to

impaired functionality of the cardiovascular system by thickening, stiffening and calcification of the vessel wall and cardiac valves [501]. Moreover, the *ob/ob* genotype and HFD diet activate the expression of genes related to lysosome and phagosome even at early time points (2 months) RCD-fed mice. The autophagy of adipocytes is another common biological process between obesity [372] and aging [502].

A significant number of intracellular components were associated with genes downregulated in *ob/ob* mice, especially mitochondrion-related GO terms in the 10-month aged mice. Reportedly, the progressive expansion of WAT is associated with aging through mitochondria dysfunction [503]. Mitochondrial dynamics are controlled by Sirtuins, AMPK, mTOR, sexual hormones and emerging factors such as prohibitins and sestrins [504]. During obesity, FA oxidation is reduced with inhibition of mitochondrial complex IV by hypoxia-inducible factor-1 α (HIF-1 α) repressing cytochrome c oxidase 5b (Cox5b) [505]. Mitochondrial dysfunction and increased production of ROS can induce insulin resistance, and a local pro-inflammatory status is created by chemokines and cytokines released by immune cells like macrophages and accumulated adipokines together with senescent cells [506]. Fusion, fission and turnover through mito- and autophagy also play important functions in mitochondrial dysfunction. Mitochondrial dysfunction and oxidative stress contribute to both aging and obesity along with chronic inflammation [503, 505]. Increased ROS in adipocytes caused by obesity can cause telomere damage, activation of the tumor suppressor p53, inflammation, and promotion of insulin resistance [507, 508]. The endoplasmic reticulum (ER) is another cellular component enriched by the genes down-regulated in adipose tissue of the obese mice. The ER is where TG droplet formation takes place. ER-dysfunction leads to misfolded or unfolded proteins which may induce inflammation and cell death via apoptosis [509-511].

Aging results in much more significant differences in adipose tissue of *ob/ob* mice than in wild-type animals. Furthermore, the GO enrichment patterns of aging were relatively similar to those of the two obesity models. Extracellular and membrane cellular component-related genes were up-regulated in the 10-month *ob/ob* mice fed on HFD, whereas intracellular component terms, especially for organelles such as the mitochondrion, were down-regulated by aging. The genes up-regulated in 10-month old mice fed on RCD were annotated by mostly the immune system and cell-cell adhesion processes GO terms. This correlates the aging process with obesity, as reported in many previous studies [495, 504, 512-518]. Obesity is associated not only with a lot of age-related disorders but also with the process of aging itself. Obesity shares a lot of

biological similarities with the aging process especially in terms of progressive dysfunction of WAT including metabolic dysfunction (increased adiposity and adipokine production, altered mitochondrial function, accumulated ROS, decreased BAT functional activity), chronic inflammation, impaired function of the immune and endocrine systems, macrophage infiltration, accumulated senescent cells, and disturbed gene expression pattern (DNA damage, telomere shortening, epigenetic alterations) [495, 504, 512-518]. Obese people have been considered by some to be associated with premature aging [517]. Accumulation of lipids and lipophilic compounds with age is considered a heritage of the evolutionary past, resulting in age-related dysfunction of WAT and ectopically stored lipids in non-adipose tissues [519]. As we age, adiposity increases while senescent cells accumulate in the adipose tissue. Adipocyte size, vascularization, and angiogenic capacity are reduced along with increased tissue fibrosis and endothelial dysfunction [502], resulting in excessive FFA release into plasma and subsequent lipotoxicity in the whole body. The risk of obesity increases with age meanwhile the rate of aging is accelerated by obesity [507, 520-522].

The most intriguing biological alterations linking aging and obesity were observed in a number of metabolic pathways as shown in **Table 4.3**. Genes associated with peroxisomes, steroid biosynthesis, carbon metabolism, and FA metabolism were up-regulated by the *ob/ob* genotype in the RCD-2 group, but down-regulated significantly by leptin deficiency in the HFD-10 group. Most of the other metabolism associated genes were down-regulated by the *ob/ob* genotype in all four groups. Interestingly, peroxisome-related genes were also significantly up-regulated by aging in the WT-RCD group, and the AMPK signaling pathway and steroid biosynthesis were enriched moderately by genes up-regulated by aging in WT-RCD, but all of these genes were down-regulated significantly by aging in the OB-HFD group. In addition, almost all of the metabolism-associated genes were down-regulated by the HFD diet, significantly in the WT-10 group and moderately in the OB-2 group, but no significant alterations were caused by HFD diet in the WT-2 and OB-10 groups. In further investigations of the selected genes, some lipid metabolism-related genes (*Fasn*, *Insig1*, *Insig2*, *PPAR γ* , and *Srebf1*) were found up-regulated by leptin deficiency when the mice were young. These genes were also moderately up-regulated when the mice aged. However, expression of these genes was down-regulated dramatically in adipose tissue of aged *ob/ob* mice. This suggests that their regulation is impaired during extreme obesity.

Soukas et al. [523] established that 25% of the expressed transcripts were differentially expressed in *ob/ob* adipose tissue, most of which were inflammatory markers, acute-phase genes, and genes important in lipid biosynthesis. This is similar to our results that most genes related to the immune system were overexpressed in *ob/ob* adipocytes and the enriched GO terms related to the immune system and inflammation, both consistently up-regulated by leptin deficiency. However, they found expression of FA biosynthesis genes such as *Fasn* was decreased 3.1-fold in *ob/ob* WAT. However, some studies have demonstrated increased expression of key lipogenic enzymes in WAT of young *ob/ob* mice [524] and young obese Zucker rats [525-527]. Soukas et al. suggested that the primary source of DNL of FAs may shift from WAT to the liver as *ob/ob* mice age. Our study established not only FA metabolism, but pathways associated with peroxisome, steroid biosynthesis, and carbon metabolism were also activated in WAT of young *ob/ob* mice, but down-regulated in WAT of the older *ob/ob* mice.

The peroxisome, a single-membrane bound ER-derived organelle of the endomembrane system, is involved in catabolism of very long chain FAs, branched chain FAs, D-amino acids and polyamines, biosynthesis of plasmalogens, and detoxification of ROS (especially hydrogen peroxide [528]), but has a highly adaptable enzymatic content [529, 530]. The peroxisome also contains almost 10% of the whole activity of two enzymes in the pentose phosphate pathway [531]. It is still uncertain whether they are involved in cholesterol and isoprenoid synthesis in animals[531]. There have been other metabolic functions of peroxisomes reported in seeds ("glyoxysomes"), leaves, trypanosomes ("glycosomes"), and some yeasts. In our study, a sharp contrast appeared within the peroxisome genes for fatty acid-oxidation (*DBP*, *SCPX*, *ACAA1*, *CRAT*, etc.), lipid biosynthesis (*DHAPAT*, *PMVK*) and ROS metabolism (*MPV17*, *PXMP4*) by genotype in the RCD-2 and HFD-10 groups and by aging in the OB-HFD group. It is clear that these peroxisomal pathways were activated in the early stage of obesity, but reduced in WAT of old *ob/ob* mice. FAs with longer chain lengths (>20 carbons) and dicarboxylic FAs have to be degraded by β -oxidation in peroxisome which directly produces H_2O_2 . The peroxisomal genes that were reduced in expression might be one reason for the accumulation of TGs containing longer fatty acids in the WAT of aged mice (as shown in **Chapter 3.4.4**). The antioxidant systems in peroxisomes were also inhibited in WAT of aged *ob/ob* mice. The increased ROS production by peroxisomes is a key feature for both obesity and aging [532, 533]. Lack of the ROS detoxifying catalase activity results in impaired redox balance [533, 534] and increases the susceptibility to aging-related diseases, e.g. diabetes, atherosclerosis and

cancer [535]. Both mitochondria [536, 537] and peroxisomes [538, 539] are major sources of ROS and are critical for intracellular redox balance. They share structural components for dynamic fission and have molecular tethers, most likely via the endoplasmic reticulum (ER) [540-542]. The peroxisome-mitochondria connection has a great impact on ROS production, redox homeostasis, aging and diseases such as obesity and diabetes [529]. Interestingly, in our KEGG enrichment results, the changes in the peroxisome appeared earlier and to a greater magnitude than those in mitochondria. The study of peroxisomal dysfunction in obesity and aging has lagged mitochondria, but recent studies have demonstrated the damage to mitochondria caused by peroxisomal dysfunction in cultured mammalian cells [543-546], and peroxisomes might be an early target of cellular oxidative damage arising from obesity or aging [547]. Fransen et al. [548] suggested that mitochondria are downstream of peroxisomal generated ROS from lipid peroxidation, rather than a simple diffusion of ROS from peroxisomes to mitochondria. While the mechanisms of the interplay between organelles and ROS are still unknown, some interorganelle contact sites between peroxisomes and mitochondria have been found in yeast model including the ERMES (endoplasmic reticulum-mitochondria encounter structure) and Mdm34-Pex11 interaction [549, 550]. The functional interplay of the two organelles needs to be further studied in terms of the regulation of oxidative stress, dynamic fission, and autophagy. Moreover, the up-regulation of lysosome-related genes by both obesity and aging in almost all groups suggest that autophagy of peroxisomes (pexophagy) and mitochondria (mitophagy) were activated to eliminate dysfunctional peroxisomes or mitochondria, which is an important mechanism to decrease ROS production in damaged peroxisomes and maintain correct redox balance [551]. Starvation also results in pexophagy and mitophagy to eliminate superfluous peroxisomes and mitochondria to decrease in cellular ROS levels [529], which could be studied using obese animal models in the future.

AMPK is a ubiquitous cellular gauge that increases ATP production and reduces energy wastage. The hypothalamic and vascular AMPK signaling pathways have been proven to be important targets for drug development against obesity and its complications [552, 553]. The results of our transcriptomic study suggest that AMPK signaling also plays a key role in the regulation of WAT during obesity and aging. Membrane receptors for leptin (*Adra1a*), adiponectin (*Adipor2*), glucose (GLUT4) and insulin (*Insr*) were all down-regulated in WAT of old *ob/ob* mice, along with inhibited AMPK expression in both obesity and aging. Interestingly, downstream genes such as *Akt*, *FoxO1*, *Srebp1c*, *Fasn*, *PPAR γ* , and *Gys2* were up-regulated by leptin deficiency in the RCD-2 group but then inhibited in the old *ob/ob* mice.

This suggests that in the initiation of obesity caused by leptin deficiency, FA biosynthesis, and mitochondrial biogenesis are activated, but then impaired in the progression of aging. Akt and its downstream FoxO proteins are major targets of insulin and can sense nutrients and mediate gluconeogenesis, glycolysis, lipogenesis, and lipolysis [554-556]. The fluctuation of Akt and FoxO1 represent the major changes resulting from insulin resistance. Wu et al. [557] suggested PGC-1 α is a direct FoxO1 transcriptional target. Reduced expression of FoxO1 and PGC-1 α contribute to mitochondrial dysfunction and increased ROS generation. Interestingly, it is also reported that PGC-1 α binds and co-activates FoxO1 but is inhibited by Akt-mediated phosphorylation [558]. FoxO1 inhibits adipogenesis by binding to the promoter sites of PPAR γ but is excluded from the nucleus after being phosphorylated by Akt stimulated by insulin [559]. Moreover, it is reported FoxO1 can be trapped in the nucleus via sirtuin- and NAD⁺- dependent deacetylation against Akt-phosphorylation-dependent nuclear exclusion. The activity of Sirtuin 1 (SIRT1) has been reported to be inhibited by both a high-fat diet [560] and aging [561]. Expression of the Sirt1 gene in WAT of mice in our study was not found to be significantly down-regulated. However, the reduced expression of AMPK in WAT of old *ob/ob* mice will decrease NAD⁺ production and lead to inhibited SIRT1 activity. This arises because the enzymatic activity of sirtuins is directly linked to the energy status of the cell via NAD⁺, NADH, and nicotinamide, as the sirtuin-mediated deacetylation reaction couples lysine deacetylation to NAD⁺ hydrolysis which yields nicotinamide as an inhibitor of sirtuin activity [562-564]. SIRT1 can improve sensitivity to both leptin and insulin and prevents inflammation and macrophage infiltration [565] by deacetylation of substrates like PGC-1 α and NF- κ B, and is increased by caloric restriction and decreased by aging and overfeeding [566]. The transcriptional activity of PPAR γ and TNF α in adipose tissue could be repressed by SIRT1, increasing fat mobilization and protecting cells from insulin resistance [567, 568]. Moreover, resveratrol, a possible SIRT1 activator, and resveratrol-mimicking drugs such as SRT1720 extended the lifespan of obese mice by 44% [569].

When examining the detailed PPAR signaling pathway, it is found that the expression of PPAR γ is influenced much more than PPAR α and PPAR δ by leptin deficiency, diet-induced obesity, and aging. PPAR α is highly expressed in the liver, heart, muscle, and kidney where it promotes fatty acid β -oxidation and decreases glycolysis [216, 430]. PPAR δ ubiquitously increases total oxidative and the TCA cycle to burn fat and restore insulin sensitivity [373, 570, 571]. PPAR γ is predominantly expressed in adipocytes, promoting adipocyte differentiation,

and sequesters glucose and lipids into WAT [373, 572]. PPAR γ is the only factor without which the adipocyte differentiation cannot occur and no other factor has been identified that can rescue adipogenesis in the absence of PPAR γ . The significant up-regulation but then down-regulation of PPAR γ by combining obesity and aging might be a key node of dysfunctional adipose tissue. Moreover, epigenetic and chromatin-modifying proteins have been found to contribute to adipogenesis and maintenance of mature adipocytes through PPAR γ [273]. There is a complex feedback regulatory system between PPAR γ , insulin, Insig1, and SREBP1. Firstly, PPAR γ agonists can induce Insig1 expression *in vitro* and *in vivo* in WAT [262, 263] to limit the promotion of adipocyte differentiation by PPAR γ itself. Insulin can also activate SREBP1 to promote lipogenesis, while, at the same time inducing the expression of *Insig1* for restricting the production of too much active SREBP1 [262, 264-266]. This autoregulatory feedback loop has not only been suggested as a control mechanism for cholesterol synthesis in the liver [264, 267] but also reported to be involved in the pathophysiological dysregulation of WAT for *in vivo* and *in vitro* obesity models [37]. In the insulin-resistant (IR) state, this negative Insig1/SREBP1 regulatory feedback is suggested to be reset for the downregulation of *Insig1* and maintenance of active SREBP1 levels for maintaining lipid homeostasis. Active SREBP1 ensures an adequate supply of specialized FAs used for the maintenance of membrane lipid homeostasis, effectors of intracellular signaling, and lipid modification of proteins [254]. The concept that SREBP1 needs to be activated to restore the biosynthesis of phosphatidylcholine (PC) and phosphatidylethanolamine (PE) has been suggested both in *Caenorhabditis elegans* and mammalian cells [39] and *Drosophila* heart [41]. This regulatory feedback can compensate lipid perturbations in membranes and specific signaling pathways in obesity and IR, but, simultaneously, increases lipogenesis [37, 41] and may aggravate the associated pathology.

Expression patterns of selected genes involved in the pathways of lipid synthesis and further modification, ER stress, mitochondrial stress, adipose tissue remodeling, and some essential transcription factors have been described in **Chapter 4.4.4**. DNL genes (*Fasn*, *Elovl6*, *Scd1*) and related transcription factors (*Insig1*, *Srebf1*, PPAR γ) were up-regulated by *ob/ob* genotype and aging, respectively, but were down-regulated in adipose tissue of older *ob/ob* mice compared with wild-type or younger animals. Further FA modification by *Elovl1* was up-regulated by *Elovl1* in obese and aged mice, while desaturases (*Fads1* and *Fads2*) were down-regulated in *ob/ob* mice and in older animals. TG synthesis and lipid remodeling were also reduced in adipose tissue when the mice became obese and aged (*Agpat6*, *Mboat1*, and *Mboat2* were down-regulated). It is interesting that lipid remodeling genes correlate well with *Srebp2*

while FA synthetic genes are similarly co-regulated with Srebp1c and PPAR γ . Srebp2 is more related to cholesterol synthesis while Srebp1c regulates fatty acid synthesis [573]. The role of cholesterol in regulating the physiology of bio-membranes implies the important aspects of Srebp2 in obesity and insulin resistance. However, although there are some studies associating FA composition with the mRNA levels of enzymes like SCDs in adipose tissue, it has also been reported that the liver is the major organ where FAs are synthesized through DNL, elongation, and desaturation and adipose tissue lipid composition is just a hybrid of dietary and *de novo* synthesized FAs [454]. Thus, the lipid composition in adipose tissue should be the readout of enzymatic activity of the whole body, especially in the liver, rather than just in adipose tissue. In addition, ER stress (Edem1) and mitochondrial oxidative stress (Ucp2) were induced significantly by an HFD, which impaired coordinated remodeling of the structure and metabolism of adipose tissue developing insulin resistance and cardiovascular diseases [372, 574, 575].

4.6 Conclusion

This Chapter investigated the correlation between transcriptomic patterns of obesity and aging using three factors, i.e. two models of obesity induced by leptin deficiency (*ob/ob* genotype) and high-fat diet (HFD), respectively, and aging. The two obesity models exhibited differently featured expression patterns but both had some changes in common with aging. Inflammation and immune system-related pathways were activated not only in the two models of obesity but also in white adipose tissue of aged mice. On the contrary, metabolic pathways, in particular, those related to lipid metabolism, were activated by leptin deficiency in the initiation of obesity of *ob/ob* mice, but inhibited to a large extent in white adipose tissue of aged *ob/ob* mice, compared to both the wild-type controls and the younger controls. The GO and KEGG enrichment analysis of these genes suggested that peroxisome and AMPK and PPAR γ signaling pathways may act at the forefront in the progression of obesity and aging, as a protective mechanism in the initiation of oxidative damage, but then accumulated damage results in insulin resistance, the metabolic syndrome and T2DM.

Chapter 5 One-Carbon Cycle and DNA Methylation in Adipose Tissue of High-Fat-Diet and *ob/ob* mouse models

5.1 Introduction

Metabolic pathways can be regulated not only transcriptionally but also through epigenetic modifications which refers to the heritable changes in gene expression resulting from modifications to DNA or histones rather than changes in the nucleotide sequence [269, 270]. Epigenetic changes, including methylation and acetylation of DNA and histones, chromatin remodeling, and noncoding RNA expression, have attracted extensive attention in recent years as an alternative mechanism for pathologies associated with metabolic disorders. For example, the epigenetic profile of the genome was suggested to be altered after a carbohydrate-based diet was replaced by a high-fat diet, which resulted in insulin resistance and T2DM in mice [279, 280]. Moreover, although the DNA sequence is comparatively stable, epigenetic patterns can be greatly influenced by external factors, and remain dynamic all the way through the life course [272], providing an important interface between environmental factors and genetics.

Obesity has been associated with accelerated DNA methylation in the human liver [576]. Changed DNA methylation and gene expression have been linked to generation, distribution, and metabolism of subcutaneous adipocytes of obese women [577]. Drogan et al. suggested methylation of the gene (LPL) encoding lipoprotein lipase might be a reason for differential body fat distribution (increased waist circumference), increased methylation in the promoter of LPL was associated with higher BMI, higher visceral adipose tissue mass and weight gain [578]. Accordingly, aging has been reported to be associated with changes in the distribution of 5-methylcytosine and a decrease in genome-wide methylation but more methylation in the promoter regions of specific genes resulting in gene silencing [579]. However, DNA methylation status is in a tissue-specific manner (different in the liver compared within the adipose tissue), especially at intergenic sequences and conserved noncoding elements of some genes that are involved in metabolism and metabolic regulation [580]. Chromatin dysregulation, mRNA metabolism, and RNA slicing have also been reportedly involved in aging from adipose tissue [581].

DNA methylation (e.g. cytosine → 5-methylcytosine) is a major epigenetic modification of the genome that regulates gene expression [271]. S-adenosylmethionine (SAM) is the principal biological methyl donor for DNA and histone methyltransferases in all mammalian cells and plays an important role in a lot of biological processes such as transmethylation, transsulfuration, and polyamine synthesis [285]. The methyl group from SAM can be transferred to nucleic acids, proteins, phospholipids, hormones, neurotransmitters, and certain drugs [281]. SAM is mainly derived from the reaction between methionine and adenosine triphosphate via the enzyme methionine adenosyltransferase (MAT) as part of the choline and one-carbon (1-C) pathway [282-284]. Interestingly, choline is the head group of phosphatidylcholines (PCs) and the normal ratio of PCs to Phosphatidylethanolamines (PEs) are established by SAM methylation [285], which plays a role in lipid metabolism and determines the fluidity or viscosity of the membrane [287]. The greater amount of PC is associated with more fluid or less viscous cell membrane which facilitate the lateral movement of membrane receptors [582]. Thus, this Chapter aims to investigate the interaction of obesity and aging in lipid metabolism, 1-carbon cycle, and DNA methylation in adipose tissues of mice.

5.2 Aims and objectives

In this Chapter I aim to:

- i. Profile the changes in 1-carbon metabolites associated with genetic-induced obesity resulting from a failure to produce leptin in the *ob/ob* mouse.
- ii. Profile the changes in 1-carbon metabolites associated with diet-induced obesity.
- iii. Profile the changes in 1-carbon metabolites associated with aging.
- iv. Correlate the 1-carbon changes with lipid changes in an integrated regulating network.
- v. Profile the global methylation status of the mouse models of obesity and age, and validate this using some genes selected from the literature.

5.3 Materials and Methods

5.3.1 Animals and diets

All animals and samples described in **Chapter 2 (section 2.2)** were used for 1-carbon metabolite determination in this Chapter. For the determination of the methylation status of selected genes, we compared changes at 10 months of age with both genotypes and diets. 20 adipose tissue samples

as described in **Chapter 2 (section 2.2)** were randomly selected (5 in each group for different genotype (*ob/ob* or wild-type), diet (RCD or HFD)), as shown in red below:

No.	Genotype	Age (months)	Diet	No.	Genotype	Age (months)	Diet
wt 01-10	WT	2	RCD	ob 01-10	<i>ob/ob</i>	2	RCD
wt 11-20	WT	4	RCD	ob 11-20	<i>ob/ob</i>	4	RCD
wt 21-30	WT	10	RCD	ob 21-30	<i>ob/ob</i>	10	RCD
wt 31-40	WT	14	RCD	ob 31-40	<i>ob/ob</i>	14	RCD
wt 41-50	WT	2	HFD	ob 41-50	<i>ob/ob</i>	2	HFD
wt 51-60	WT	4	HFD	ob 51-60	<i>ob/ob</i>	4	HFD
wt 61-70	WT	10	HFD	ob 61-70	<i>ob/ob</i>	10	HFD

5.3.2 Determination of 1-carbon metabolites by UHPLC-SRM-MS

The aqueous component of all the extract described in **Chapter 2 (section 2.3.2)** was used and the determination of 1-carbon metabolites by UHPLC-SRM-MS were performed according to **Chapter 2 (section 2.7)**.

5.3.3 Measurement of DNA Percent Methylation

Extraction of DNA and measurement of percent methylation of the genes (*Mus musculus* acyl-CoA synthetase long-chain family member 1 (*Acs11*), *Mus musculus* thymoma viral proto-oncogene 2 (*Akt2*), *Mus musculus* regulator of G-protein signaling 3 (*Rgs3*), *Mus musculus* lipoma HMGIC fusion partner-like 2 (*Lhfp12*)) selected from literature [583-585] were performed according to **Chapter 2 (section 2.8)**.

5.3.4 Multivariate statistical analysis

Correlation of different data was performed using the Orthogonal Partial Least Squares (OPLS) method by SIMCA 14 (Umetrics, Umea, Sweden) according to **Chapter 2 (section 2.10)**.

5.4 Results

5.4.1 1-carbon metabolism in adipose tissue of mice changes significantly with genotypes and correlates well with Phosphatidylcholine data

The 1-carbon metabolites in adipose tissues were semi-quantified from aqueous fraction of adipose tissue through developing a sensitive UHPLC-SRM-MS method. Differences between different genotype/diet-mice became larger in older mice, and the most significant comparison profiles appeared in the 10-month group as shown in **Fig 5.1** (adjusted P-values in **Table 5.1**). It is obvious that there was a great upsurge of almost every 1-carbon metabolite comparing *ob/ob* mice with wild-type controls at the late age states (10 months and 14 months). However, this is not significant in adipose tissue of young (2 months and 4 months) fed on RCD. This suggested the 1-carbon metabolism was activated by leptin deficiency, in particular when the animals became old. Activated lipid metabolism in *ob/ob* mice might be a reason for the increased 1-C intermediates, considering SAM can be used for biosynthesis of PCs, and choline, the head group of PC, is used for production of betaine which is a methyl donor for the transformation from homocysteine to methionine and then SAM (**Fig 5.2**).

The diet exhibits different effects in *ob/ob* and wild-type mice. Most of the 1-C metabolites decreased in adipose tissue from wild-type mice fed on HFD compared with WT-RCD animals, while this pattern disappeared in adipose tissues from *ob/ob* mice. OB-HFD mice had less homocysteine, betaine, cysteine, and glycine but more SAM, SAH, methionine, serine, cytosine, and 5-methylcytosine in adipose tissues compared with OB-RCD mice. The decreased 1-C metabolites in HFD-fed wild-type mice might be due to the decrease of DNL and lipid metabolic pathways as most of the FAs are directly from the diet as discussed in **Chapter 3**.

Interestingly, aging also increased most of the 1-C metabolites in adipose tissue from *ob/ob* mice. This suggests another mechanism correlating the effect of obesity on the aging process. This increase was not significant in the adipose tissue of wild-type mice.

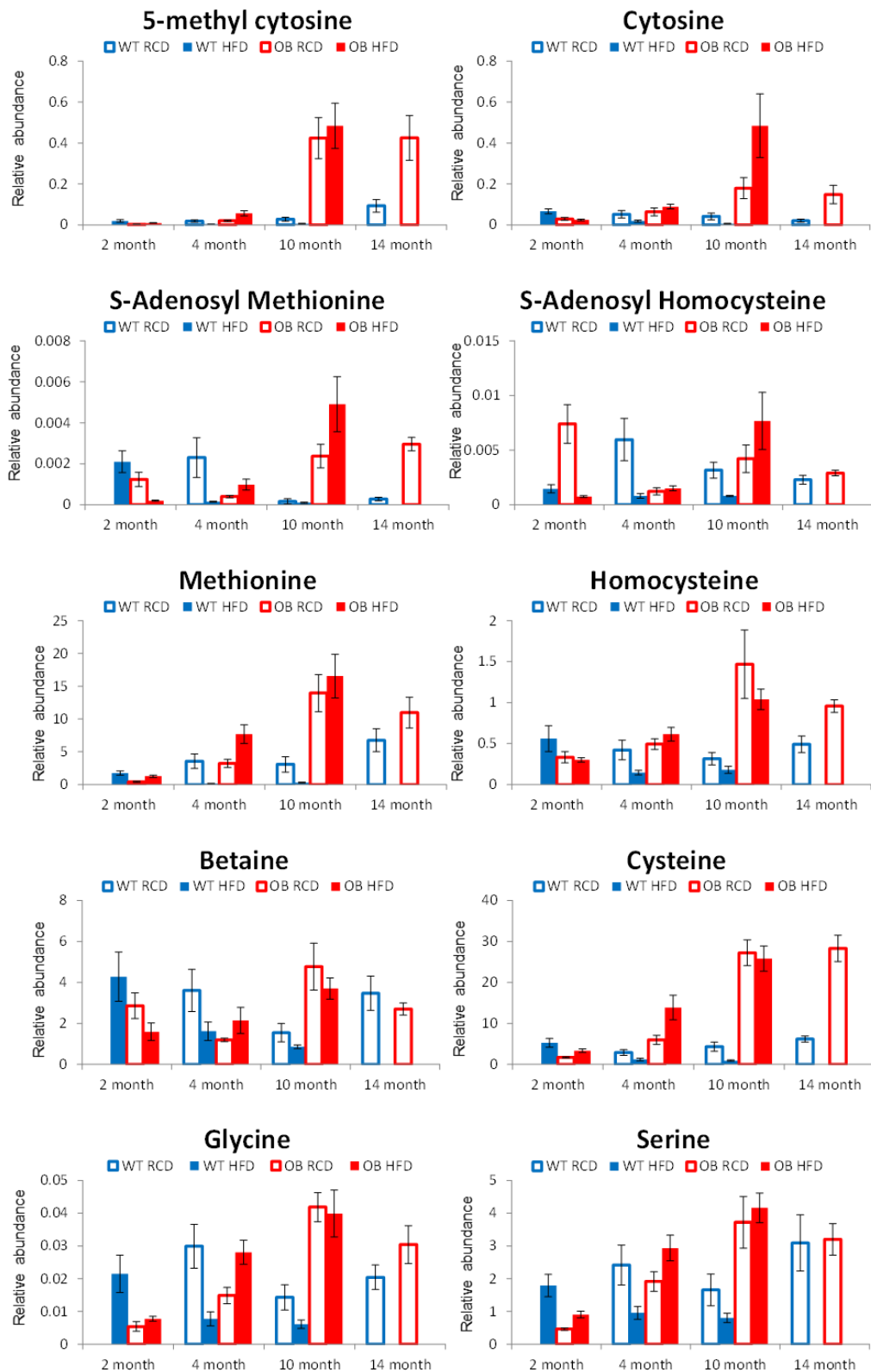


Fig 5.1 1-Carbon metabolites varied in adipose tissues from *ob/ob* (OB) mice and wild-type (WT) controls fed by regular chow diet (RCD) and high-fat diet (HFD) across different age stages (2-14 months). The ion-intensities for peaks of Cysteine and Homocysteine were normalized to the area of the internal standard Homocysteine-d5. Ion-intensities for all the other one-carbon metabolites were normalized to the area of the internal standard Glutamate acid 13C515N1. Note: the adipose tissue of the WT mice fed on RCD at 2 months of age was used in previous experiments outlined in Chapter 3-4, therefore there was insufficient sample remaining for this study. Many 14-month-old mice died after switching to the HFD feeding, therefore they are not shown in the figure.

	Adjusted P-value	Gly.	Ser.	Cys.	Bet.	SAM	Homocys	Mecyt.	Meth.	Cyt	SAH	Mecyt/Cyt
Genotype	WT-RCD-4 month vs. OB-RCD-4 month	0.3922	0.9646	0.2581	0.3394	0.4497	0.9818	0.9818	0.9818	0.9818	0.3489	0.4497
	WT-RCD-10 month vs. OB-RCD-10 month	0.0033	0.1226	<0.0001	0.1226	0.0221	0.1226	0.0187	0.0284	0.1226	0.4952	0.1226
	WT-HFD-4 month vs. OB-HFD-4 month	0.0009	0.0014	0.0014	0.4912	0.0091	0.0003	0.0014	0.0002	0.0002	0.0732	0.0179
	WT-HFD-10 month vs. OB-HFD-10 month	0.0177	0.0006	0.0003	0.0079	0.0646	0.0013	0.0256	0.0156	0.1000	0.1264	0.2610
Diet	WT-RCD-4 month vs. WT-HFD-4 month	0.0592	0.2203	0.2203	0.2504	0.2203	0.2203	0.1386	0.0636	0.2504	0.1386	0.8165
	WT-RCD-10 month vs. WT-HFD-10 month	0.4847	0.5813	0.1992	0.5813	0.8276	0.5813	0.4514	0.4503	0.4514	0.1614	0.8276
	OB-RCD-4 month vs. OB-HFD-4 month	0.0851	0.2823	0.1567	0.5257	0.2282	0.6073	0.1271	0.1126	0.6073	0.6073	0.5257
	OB-RCD-10 month vs. OB-HFD-10 month	0.9934	0.9934	0.9934	0.9687	0.7027	0.9531	0.9934	0.9934	0.6641	0.9400	0.9934
Aging	WT-RCD-4 month vs. WT-RCD-10 month	0.5191	0.8935	0.8481	0.6096	0.5103	0.9039	0.9039	0.9039	0.9039	0.8481	0.0848
	WT-HFD-4 month vs. WT-HFD-10 month	0.9639	0.9639	0.9639	0.8254	0.8456	0.9639	0.6313	0.5811	0.5400	>0.9999	0.0617
	OB-RCD-4 month vs. OB-RCD-10 month	0.0007	0.1706	<0.0001	0.0353	0.0258	0.1706	0.0159	0.0258	0.1706	0.1706	0.0353
	OB-HFD-4 month vs. OB-HFD-10 month	0.2450	0.2450	0.1428	0.2450	0.1565	0.1428	0.0378	0.2450	0.2450	0.2450	0.2450

Table 5.1 The adjusted P-values when comparing 1-Carbon metabolites in adipose tissues from *ob/ob* (OB) mice and wild-type (WT) controls fed by regular chow diet (RCD) and high-fat diet (HFD) across different age stages (4-10 months) using one unpaired t-test. The ion-intensities for peaks of Cysteine and Homocysteine were normalized to the area of the internal standard Homocysteine-d5. Ion-intensities for all the other one-carbon metabolites were normalized to the area of the internal standard Glutamate acid 13C515N1. Gly, Glycine; Ser, Serine; Cys, Cysteine; Bet, Betaine; SAM, S-Adenosyl Methionine; Homocys, Homocysteine; Mecyt., Methylcytosine; Meth, Methionine; Cyt, Cytosine; SAH, S-Adenosyl Homocysteine.

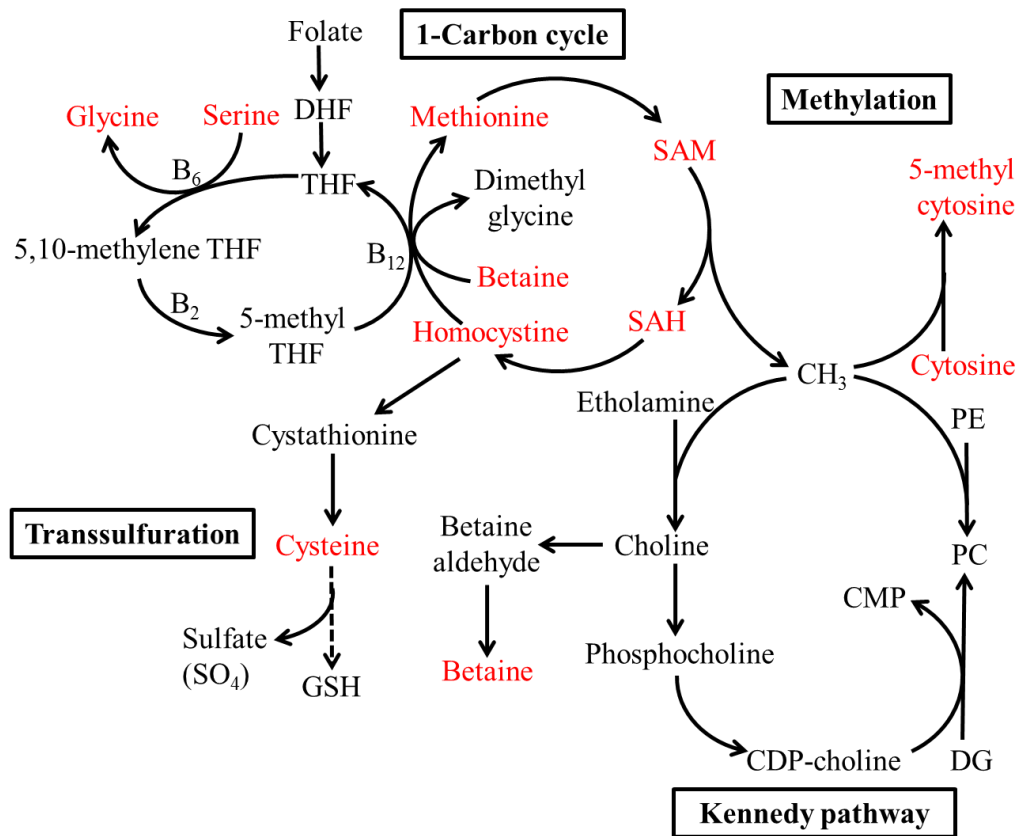


Fig. 5.2 Interconnection between the 1-carbon cycle, Methylation pathway, Transsulfuration pathway and Kennedy pathway (modified from references [286, 287]). DHF, Dihydrofolate; THF, tetrahydrofolate; SAM, S-adenosyl methionine; SAH, S-adenosyl homocysteine; GSH, glutathione. Metabolites increased in adipose tissue of *ob/ob* mice and aged mice are labeled in red.

Cytosine methylation is widespread in both prokaryotes and eukaryotes. Around 60%-80% of CpG is methylated in somatic cells of vertebrates (80-90% for human) [586] while less than 10% of CpG islands (made up of about 65% guanine and cytosine residues) are methylated in intergenic and intragenic regions. There is an inverse relationship between the transcriptional activity of a gene and the CpG methylation in the promoter of the gene. The ratios of 5-methylcytosine to cytosine were calculated in different genotype/diet/age groups to estimate the DNA methylation status in adipose tissue. **Fig 5.3** suggested that free cytosine was more methylated during obesity induced by leptin deficiency and also by aging (adjusted P-values in **Table 5.1**). Cytosine is a part of cytidine triphosphate (CTP) and which can act as an inhibitor of the enzyme aspartate carbamoyltransferase in pyrimidine biosynthesis [587], and deoxy CTPs are building blocks of DNA. More 5-methylcytosine indicates a possibility of higher DNA methylation level by incorporation as 5-methyl deoxycytidine, which means silencing of

some gene expression and loss of pluripotency of adipocytes during obesity and aging. This may be the mechanism of how changes in 1-C metabolism influence gene and protein phenotypes in the process of getting obesity and aging.

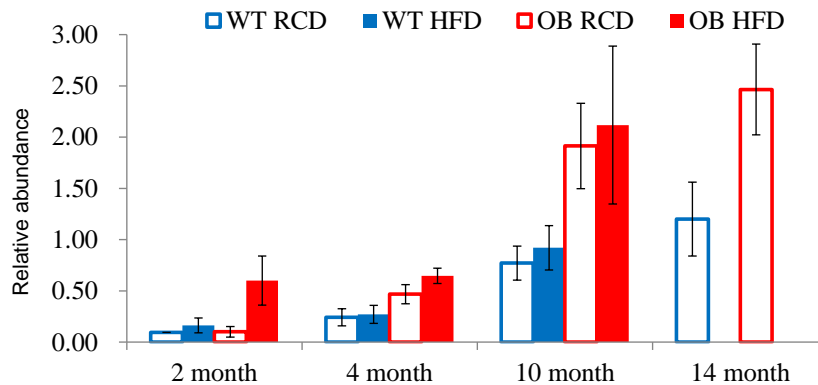


Fig 5.3 The relative abundance of 5-methylcytosine to cytosine varied in adipose tissues from *ob/ob* (OB) mice and wild-type (WT) controls fed by regular chow diet (RCD) and high-fat diet (HFD) across different age stages (2-14 months). Many 14-month-old mice died after switching to the HFD feeding, therefore they are not shown in the figure.

In order to correlate lipidomic results and 1-C metabolic patterns, the Orthogonal Partial Least Squares (OPLS) method, a modification of the PLS algorithm, was used for data integration combining different metabolite data. With this methodology, a systematic variation that overlaps across analytical platforms can be separated from platform-specific systematic variation to validate the correlation between any two sets of data. FAs, TGs, PCs, and 1-C metabolites data were studied using this method in terms of their changes by genotype/diet/age factors. As a result, shown in **Table 5.2**, total FA data and TG data can be correlated well ($Q^2=53.7$), which can be explained as most FAs detected are from TGs stored in adipose tissue as its major energy-storing function. What is more interesting, the 1-C metabolite data correlate with PC data ($Q^2=37.0$) much better than with FA ($Q^2=7.0$) and TG ($Q^2=14.3$). This indicates that the PC metabolism disturbed in obesity and aging may also play a role in regulating 1-C metabolism and changing the supply of SAM for DNA methylation. One of the essential intermediates of 1-C metabolism is choline, which is also the head group of PCs. Moreover, the conversion between PCs and PEs also rely on the methylation function of SAMs (**Fig 5.1**). Another thought-provoking phenomenon is that both the correlations mentioned above are greater in *ob/ob* mice (with greater Q^2 value) than in wild-type mice. One reason may be that the activated DNL and lipid metabolism by leptin deficiency led to more interactions between biological pathways involved in lipid and 1-C metabolism.

	FA vs. TG			1-C vs. PC		
Parameters	All	WT	OB	All	WT	OB
R ₂ X(Cum)%	94.5	85.3	92.7	84.1	87.5	87.0
R ₂ Y(Cum)%	60.0	58.3	63.6	47.5	58.4	50.8
Q ₂ (Cum)%	53.7	48.4	51.9	37.0	27.1	40.0
	TG vs. PC			1-C vs. TG		
Parameters	All	WT	OB	All	WT	OB
R ₂ X(Cum)%	88.3	94.8	85.5	94.9	No model	93.0
R ₂ Y(Cum)%	41.9	40.0	55.8	27.0		32.5
Q ₂ (Cum)%	15.7	0.0	30.6	14.3		16.4
	PC vs. FA			1-C vs. FA		
Parameters	All	WT	OB	All	WT	OB
R ₂ X(Cum)%	83.4	91.9	82.2	56.8	No model	75.8
R ₂ Y(Cum)%	29.3	68.4	50.2	10.2		14.6
Q ₂ (Cum)%	20.4	35.1	34.5	7.0		10.2

Table 5.2 The O2PLS models correlating different metabolic data in adipose tissues from *ob/ob* (OB) mice and wild-type (WT) controls fed by regular chow diet (RCD) and high-fat diet (HFD) across different age stages (2-14 months). The color depth indicates the relative Q-value.

5.4.2 Leptin deficiency results in significant changes in DNA methylation status to influence the gene expression

As the SAM provides methyl groups for the DNA methylation, I also determined the methylation status of four genes screened from literature [583-585] which were highly-correlated with obesity and diabetes. As shown in **Fig 5.4**, ACSL1 and AKT2 are much less methylated in *ob/ob* mice while Rgs3 was more methylated. Thus, in *ob/ob* mice 1-carbon cycle is heavily activated and produces a lot of SAM for DNA methylation which could be used to control the expression of some genes, whereas SAM is used to methylate different genes with high selectivity. This indicates control of methylation of different genes could be another important mechanism in response to obesity and aging. The HFD did not significantly change the methylation status of the four genes, which is consistent with fewer observed 1-C changes by diet compared with changes caused by genotype. But the trend in HFD-fed mice (moderately decreased methylation of ACSL1 and increased Rgs3) was similar to that in *ob/ob* mice compared with lean controls, respectively.

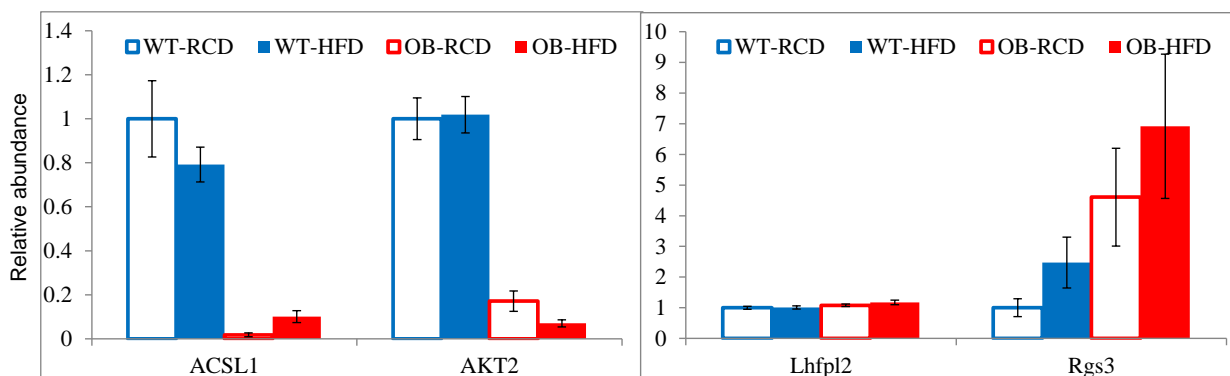


Fig 5.4 DNA methylation of four genes selected from literature in adipose tissues from 10-month *ob/ob* (OB) mice and wild-type (WT) controls fed by regular chow diet (RCD) and high-fat diet (HFD). All data are normalized to the gene methylation in adipose tissue of WT mice fed on RCD. Human Methylated DNA & Non-methylated DNA Standards with an MGMT primer set for validating the OneStep qMethyl™ system.

	ACSL1	AKT2	Lhfpl2	Rgs3
Interaction	0.3488	0.4705	0.4662	0.7956
Genotype	0.0002	<0.0001	0.0445	0.0241
Diet	0.6812	0.6158	0.3633	0.2512

Table 5.3 The P-values when comparing DNA methylation of four genes selected from literature in adipose tissues from 10-month *ob/ob* (OB) mice and wild-type (WT) controls fed by regular chow diet (RCD) and high-fat diet (HFD) using two-way ANOVA. **Red:** P < 0.05.

Methylation can change DNA activity without changing its sequence. DNA methylation typically represses gene transcription when located in the promoter [588, 589]. This is essential in a lot of important processes such as normal development, aging, repression of transposable elements, carcinogenesis, X-chromosome inactivation, and genomic imprinting. There are about 60-70% of genes of human have a CpG island in the promoter region. Around 50% of CpG islands of the human genome (about 25,000) lie in gene promoter regions, while another 25% are located in gene bodies often serving as alternative promoters.

Expression of these four genes was also determined (extracted from the transcriptomic data in **Chapter 4**) as shown in **Fig 5.5**. The genotype resulted in the most significant changes. Expression of *Rgs3* was decreased in adipose tissue of 10-month *ob/ob* mice not only by *ob/ob* genotype but also by HFD diet, in part because of more methylation suppressed its expression. However, expression patterns of *Acsl1*, *Akt2*, and *Lhfpl2* were not consistent with their methylation status. Expression of *Acsl1* and *Akt2* was increased in *ob/ob* mice at the age of 2 months while moderately decreased in *ob/ob* mice fed on HFD at the age of 10 months compared with wild-type controls. *Lhfpl2* was more expressed in *ob/ob* mice but its

methylation was not significantly changed by genotype. HFD also led to increased expression of *Acs11*, *Akt2*, and *Lhfp12* in adipose tissue of 10-month old wild-type mice compared with animals fed on RCD, but their methylation status did not change accordingly. The influence of obesity on these genes might be through some other pathways or by some transcriptional factors rather than being directly affected by their methylation status. It seems that the DNA methylation status is an important factor in the regulation of gene expression but there should also be some other influential factors working together, which need to be studied in further research.

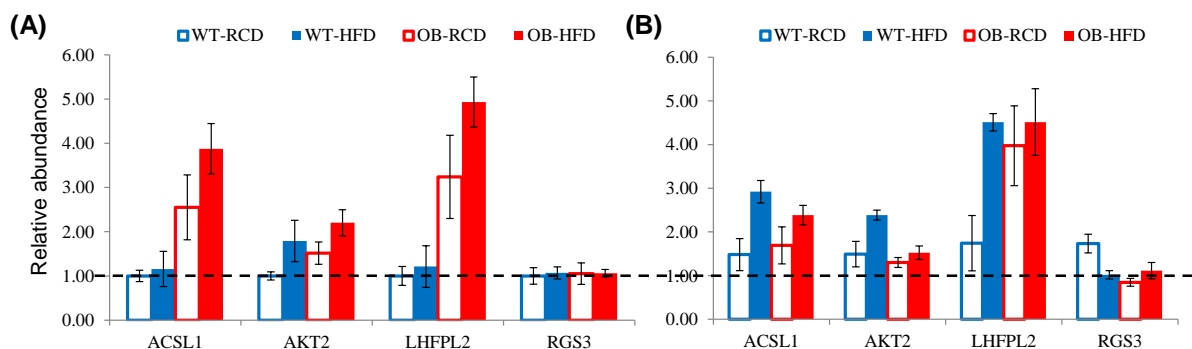


Fig 5.5 Expression of four genes selected from literature in adipose tissues from *ob/ob* (OB) mice and wild-type (WT) controls fed by regular chow diet (RCD) and high-fat diet (HFD) at the age of 2 months (A) and 10 months (B). All data are normalized to expression of the gene of 2-month WT mice fed on RCD.

	ACSL1	AKT2	LHFPL2	RGS3
Age	0.9295	0.7919	0.0230	0.2620
Genotype	0.0027	0.8591	<0.0001	0.1172
Diet	0.0054	0.0010	0.0074	0.4276
Age x Genotype	0.0006	0.0093	0.0494	0.0815
Age x Diet	0.5950	0.6147	0.4477	0.2673
Genotype x Diet	0.7301	0.2865	0.6847	0.0562
Age x Genotype x Diet	0.1235	0.4343	0.0501	0.0320

Fig 5.5 The P-values when comparing expression of four genes selected from literature in adipose tissues from *ob/ob* (OB) mice and wild-type (WT) controls fed by regular chow diet (RCD) and high-fat diet (HFD) at the age of 2 months (A) and 10 month (B) using three-way ANOVA. Red: P < 0.05.

5.5 Discussion

In adipose tissue of *ob/ob* mice, the 1-C cycle was heavily activated and produced an abundance of SAMs for methylation of DNA and/or histones. There was an upsurge in every 1-carbon metabolite comparing *ob/ob* mice with wild-type controls. This indicates that DNL which could be increased by leptin deficiency is also positively correlated with 1-C metabolism. The

influence of HFD on 1-C metabolism was not as significant as leptin deficiency. The influence of aging was much more significant in adipose tissue from *ob/ob* mice compared with wild-type ones and also led to an increased concentration of 1-C metabolites. As shown in **Chapter 3.4.1** showed that leptin deficiency caused a much more increase in body weight and body fat composition than the HFD did. Long-term raised blood glucose and insulin level and cardiac fibrosis were also detected significantly more in *ob/ob* mice. These demonstrated that overdose-induced obesity had more serious and deleterious effects on metabolic health than a high-fat diet.

Zeisel et al. [282] proposed that 1-C metabolism and energy homeostasis can be correlated through choline. Rodents, cattle, swine, and humans with a choline-deficient diet or genetic defect in choline metabolism all become hypermetabolic. Increased betaine has been reported to be associated with insulin sensitivity and increased metabolic rates [590]. Cysteine inhibits lipolysis and stimulates utilization of glucose in DNL as insulin does [591]. This is somewhat intriguing as choline, betaine, and cysteine can be converted into each other in 1-C metabolism. One possible reason could be that increased 1-C metabolites save choline for the production of PCs, which is a type of vital membrane lipid for metabolic homeostasis as discussed in **Chapter 3** and **Chapter 4**. The CDP-choline pathway links choline to PC formation [592]. In 1-C metabolism, SAM can also be used to methylate PE to form PC. The PC composition is under the control of the two pathways (from DG/PE) as shown in **Fig. 5.1**. Reportedly, the SREBP-1 induced by insulin signaling can interact with SAM through 1-C metabolism and lipid metabolism [282, 593, 594]. All of these suggest crosstalk between lipid metabolism and SAM formation. In obese mice, excess fat storage results in greater demand for PCs to be utilized to form and enlarge membrane to support the adipocyte expansion and differentiation, as discussed in **Chapter 3**. It seems that in *ob/ob* mice the whole choline/1-carbon pathway was activated along with the PC formation. We suggest that activated lipid synthesis and metabolism increased the substrate influx into the 1-C cycle which produced increased SAM as a methylation donor for DNA and histones.

A metabolic regulating network connecting choline, 1-carbon cycle and the DNA methylation pathways emerged from the results in this Chapter. The gene methylation profile can be selectively modified using the increased SAM for metabolic regulation of genes to adapt to the excess lipids and metabolic changes. There have been a lot of reports about interactions between lipid metabolism and methylation of DNA and histones. Epigenetic and chromatin-

modifying proteins have been found to contribute to adipogenesis and maintenance of mature adipocytes through PPAR γ [273]. The fat mass and obesity associated gene (FTO) has been found to be associated with a type of demethylase [274]. Furthermore, there is evidence that high-fat diets can affect the methylation of the main anorexigenic neurohormone pro-opiomelanocortin (POMC) and leptin related genes, having an impact on appetite [275, 276]. Methylation of the genes encoding PPAR α and the glucocorticoid receptor (GR) have been shown to be decreased when maternal protein is restricted which have a long-term impact on systemic metabolism [277], and methylation of the melanocortin-r receptor (MC4R) is associated with exposure to long-term exposure to a high-fat diet [278].

In our study, ACSL1, AKT2, Rgs3, and Lhfpl2 were selected from the literature [583-585] which have been reported to undergo epigenetic changes in adipose tissue of both mice and humans. The results showed that SAMs were used to methylate different genes with high selectivity: ACSL1 and AKT2 were significantly less methylated whereas Rgs3 was more methylated in *ob/ob* mice, which are consistent with Multhaup's diabetes-risk experiment [583]. The expression of Rgs3 was decreased in adipose tissues of 10-month old mice, which may be due to its high methylation status, but methylation and expression of the other three genes didn't exhibit a good correlation. Disturbed lipid metabolism, in particular, PC metabolism, may result in insulin resistance through 1-C metabolism and methyl donor supplement for DNA and/or histone methylation as an important part of the energy homeostasis regulatory network. The detailed genes which are directly influenced by PC metabolism through this way need to be further investigated using the sequencing method in the future as discussed in Section 7.3.

Moreover, this study lacks an investigation looking into the methylation status of protein or RNA. Lysine or arginine amino acid residues can be methylated by lysine methyltransferases or arginine methyltransferases, respectively. Methylation in the histones, the chief protein component of chromatin, has been widely studied. Methyl groups are transferred from SAMs to histones which are catalyzed by histone methyltransferases, epigenetically activating or repressing expression of the associated genes [595, 596]. There is a variety of RNA-methyltransferases for RNA methylation which is thought to have existed longer than DNA methylation on the earth. In addition to 5-methylcytosine, N6-methyladenosine is also an abundant and common methylation modification in RNA affecting the regulation of many biological processes such as mRNA translation and RNA stability [597]. The methods to investigate the methylation status of histones and RNA will be discussed in Section 7.3.

5.6 Conclusions

In *ob/ob* mice 1-C cycle was heavily activated and produced an abundance of SAMs for DNA and/or histone methylation. The produced SAM was used to methylate different genes with high selectivity. Lipid metabolism, 1-C metabolism, and epigenetic changes form a good combination for a better understanding of the extremely sophisticated role of adipose tissue in regulating energy homeostasis with the potential to be a barometer for pathophysiological processes of obesity and aging. Whether the activated 1-carbon and methylation pathways are consequences or adaptive protective mechanism along with obesity and aging need to be further validated.

Chapter 6 The PPAR α null mouse is characterized by saturated fatty acids in white and brown adipose tissues

6.1 Introduction

The PPAR family of nuclear receptors is composed of three members: PPAR α , PPAR β/δ (commonly referred to as PPAR δ), and PPAR γ . In Chapter 4, it was found that the expression of PPAR γ was influenced by leptin, diet-induced obesity, and aging, much more than PPAR α and PPAR δ . This may be due to PPAR α and PPAR δ being weakly expressed in adipose tissue compared with PPAR γ . However, Li et al. [428] demonstrated that the expression of PPAR γ increased significantly in PPAR α null mice along with a profound perturbation induced by these changes in terms of metabolism in adipose tissues. Moreover, genes associated with the peroxisomes were changed significantly in obese and old mice, and only PPAR α reportedly activates proliferation of peroxisomes [416], while the activation of PPAR δ and PPAR γ cannot lead to peroxisome proliferation. Furthermore, PPAR α is important for the lipid homeostasis [598-600] through the activation of peroxisomal and mitochondrial β -oxidation, microsomal ω -hydroxylation/oxidation, lipogenesis, ketogenesis, lipid binding, and transport/lipoproteins, and cholesterol metabolism, and has anti-inflammatory and anti-atherogenic effects. PPAR α is highly expressed in tissues that oxidize fatty acids at a rapid rate, such as liver, BAT, heart, intestines, muscle, and kidney [429], where it promotes FA β -oxidation and transport, and decreases glycolysis [216, 429, 430]. Uptake of FAs into the liver can be increased by activation of PPAR α , followed by the activation of peroxisomal β -oxidation and mitochondrial β -oxidation. Thus, PPAR α is thought to have a profound effect on systemic metabolism and in particular the handling of lipids across the organism.

The different functional properties of the PPAR subtypes result from subtle differences in binding site preference, tissue distribution and their ability to bind different co-repressors and coactivators [415]. Roberts et al. [373, 374] contrasted the role of PPAR δ in regulating metabolism in WAT with that of PPAR γ in terms of the TCA cycle, glucose and lipid metabolic pathways. Increased glycolysis and fatty acid desaturation were common pathways for the two nuclear receptors. However, PPAR γ , the master regulator of adipogenesis predominantly expressed in adipocytes, promotes adipocyte differentiation and sequesters glucose and lipids into WAT [373, 572]. The “lipid steal” hypothesis [601, 602] states that activation of PPAR γ

as the target of the thiazolidinedione (TZD) class of insulin-sensitizing drugs facilitates dietary fatty acid storage in WAT rather than in peripheral tissues reducing ectopic lipid deposition which would otherwise bring about lipotoxicity. Treatment with TZDs also results in the normalization of adipocytokine levels [603]. In contrast, PPAR δ is expressed almost ubiquitously and increases total oxidative metabolism and the TCA cycle to burn fat and restore insulin sensitivity [373, 570, 571]. PPAR δ mRNA is expressed at 10 and 50 times the concentrations of PPAR α and PPAR γ mRNA, respectively, in skeletal muscle of adult rat [429]. PPAR δ is activated by several 14 to 18 carbon containing PUFAs, including eicosanoids such as prostaglandin A1, iloprost and carbaprostacyclin, in the micromolar range [604]. Administration of PPAR δ agonists to skeletal muscle of rodents increased the expression of genes involved in fatty acid oxidation, mitochondrial respiration, oxidative metabolism and slow twitch contractile apparatus [605], but are also linked to muscle atrophy, which has been suggested to be the side effect of increased metabolism of branch chain amino acids [373] and reduced synthesis of NAD⁺. In adipose tissue PPAR δ is also related to adipocyte differentiation [606, 607], adipogenesis [608, 609], FFA oxidation and electron transport chain uncoupling protein 1 [610].

The PPAR α null mice are used as a model of spontaneous late-onset obesity with stable caloric intake and a marked sexual dimorphism [426]. Indeed, females have higher serum triglycerides and adiposity than the males, while the males show a delayed occurrence of obesity and original centrilobular-restricted steatosis. Further, hepatic peroxisomal proliferation is inhibited along with decreased expression of some hepatic target genes in these transgenic mice [426]. In **Section 4.4.4**, the expression of genes associated with the peroxisome was perturbed in the obese and aged wild-type mice, which may indicate a possible correlation between PPAR α and aging. Mice lacking the PPAR α gene appear to have normal WAT weight relative to body weight, but are susceptible to adipocyte hypertrophy and spontaneous late onset obesity [426]. It appears that PPAR α plays a limited role in adipogenesis due to the low levels of expression. The endogenous ligands PPAR α include certain metabolites of arachidonic acid such as leukotriene B4 and 15-Hydroxyicosatetraenoic acid family. Activation of PPAR α in 3T3-L1 preadipocytes increases the expression of enzymes of the β -oxidation pathway when co-expressed with PGC-1 [422]. Fibrates reportedly increase FA oxidation [423] and decrease VLDL particles and circulating TAGs [424] through activation of PPAR α . Fibrates also increase HDL cholesterol in a similar way through the activated expression of lipoprotein

lipase and apolipoprotein A-V, and increased macrophage cholesterol efflux helps to alleviate inflammation and atherosclerotic plaque formation in the vasculature, reducing the risk of cardiovascular disease [425]. Other factors that influence the expression and activity of PPAR α include stress, insulin, leptin, growth hormone, hepatocyte nuclear factor 4 (HNF4), and COUP-TFII [611-615]. The metabolomics study conducted by Atherton et al. [431] demonstrated a decrease in the hepatic concentration of glucose and glycogen of PPAR α null mice which increased in an age-dependent manner. This suggested the important role PPAR α plays in gluconeogenesis and its interaction with the aging process. It also demonstrated changes in white adipose tissue despite the low expression of PPAR α in this particular tissue. This was hypothesized to be a consequence of overall changes in systemic metabolism altering the lipids that are stored in white adipose tissue. However, the original lipidomic study only used GC-MS to investigate the composition of total fatty acids and free fatty acids in these tissues. This approach ignores what lipid species these fatty acids are associated with and hence provide a poor picture of overall lipid metabolism. As discussed in Chapter one, to truly understand how the lipidome changes one needs to profile intact lipids directly. Moreover, brown adipose tissue (BAT) which contains a higher number of mitochondria than WAT and plays an important role in non-shivering thermogenesis, might be influenced by PPAR α to a larger extent compared with WAT. This will be investigated in this Chapter.

6.2 Aims and objectives

In this Chapter I aim to:

- i. Profile the lipid changes in BAT and WAT of PPAR α null mice and compared with wild-type controls.
- ii. Compare and contrast the influence of PPAR α on lipid metabolism in BAT and WAT.

6.3 Materials and Methods

6.3.1 Animals and diets

Tissues from 10 male wild-type SVEV/129 mice and 10 male PPAR α -null mice were obtained from Dr. Andrew Murray, Department of Physiology, Development and Neuroscience, University of Cambridge. Mice were fed standard laboratory chow *ad libitum* (Special Diet Services, Essex,

UK) and were sacrificed at the age of 8-10 months. The age range was sort of wide because the focus was not about the age and not many PPAR α -null mice were available in our lab. Animals were killed by CO₂ asphyxiation after overnight fasting. Interscapular brown adipose tissue (BAT), epididymal white adipose tissues (EPI-WAT) and inguinal white adipose tissues (ING-WAT) were rapidly dissected (<60 s post-mortem time prior to freezing), frozen in liquid nitrogen and stored at -80°C. All animal procedures were approved by the UK Home Office and the University of Cambridge and carried out under the supervision of a personal license holder. Only aged male mice were chosen because the PPAR α null mice have been reported to exhibit spontaneous late-onset obesity even with a stable caloric intake and a marked sexual dimorphism [426] as discussed in **Section 6.1**. The females have higher serum triglycerides and gain more fat than the males, while the males show a delayed occurrence of obesity and original centrilobular-restricted steatosis [reference 426?]. The male-specific steatosis in PPAR α null mice indicated discrepancies between the sexes toward lipid metabolism.

6.3.2 Lipid Extraction

Lipid extraction from mouse adipose tissue was performed according to **Chapter 2 (section 2.3)**.

6.3.3 GC-MS analysis for total Fatty Acids

GC-MS analysis for total fatty acids from mouse adipose tissue was performed according to **Chapter 2 (section 2.4)**.

6.3.4 DI-MS/MS analysis for neutral lipids

DI-MS/MS analysis for neutral lipids from mouse adipose tissue was performed according to **Chapter 2 (section 2.5)**.

6.3.5 UPLC-MS analysis for phospholipids

UPLC-MS analysis for phospholipids from mouse adipose tissue was performed according to **Chapter 2 (section 2.6)**.

6.4 Results

6.4.1 Overview of the lipid changes in brown and white adipose tissues from PPAR α null mice

GC-MS and DI-MS/MS were used to profile the total FAs and TGs changes in BAT, EPI-WAT, representing visceral WAT, and inguinal (ING)-WAT, representing subcutaneous WAT, from PPAR α null and wild-type (WT) mice. As the TGs occupied the majority of lipids content in adipose tissue, polar lipids (PLs) were determined by UPLC-MS after an SPE separation method detailed in Chapter 2. In total, 26 fatty acids, 108 TGs, and 175 PLs were detected including ceramides (Cers), lysophosphatidylcholines (lysoPCs), phosphatidylcholines (PCs), phosphatidylethanolamines (PEs), phosphatidylserines (PSs), and sphingomyelins (SMs).

Robust PCA models were built using the three types of lipids (FA, $R^2=0.84$, $Q^2=0.314$, TGs, $R^2=0.919$, $Q^2=0.834$, PLs, $R^2=0.821$, $Q^2=0.696$) as shown in **Fig 6.1**. In all three models by different types of lipids, the ING-WAT was closer to the BAT compared with the EPI-WAT. Interestingly, ING-WAT reportedly expresses significantly higher levels of brite characteristic markers compared to EPI-WAT upon induction by cold [616-618]. The difference between PPAR α null mice and wild-type controls was not clear in the PCA models. Thus, OPLS-DA models (of which parameters are shown in **Table 6.1**) were built for BAT, EPI-WAT and ING-WAT in PPAR α null mice compared with wild-type mice using FAs, TGs, and PLs models, respectively.

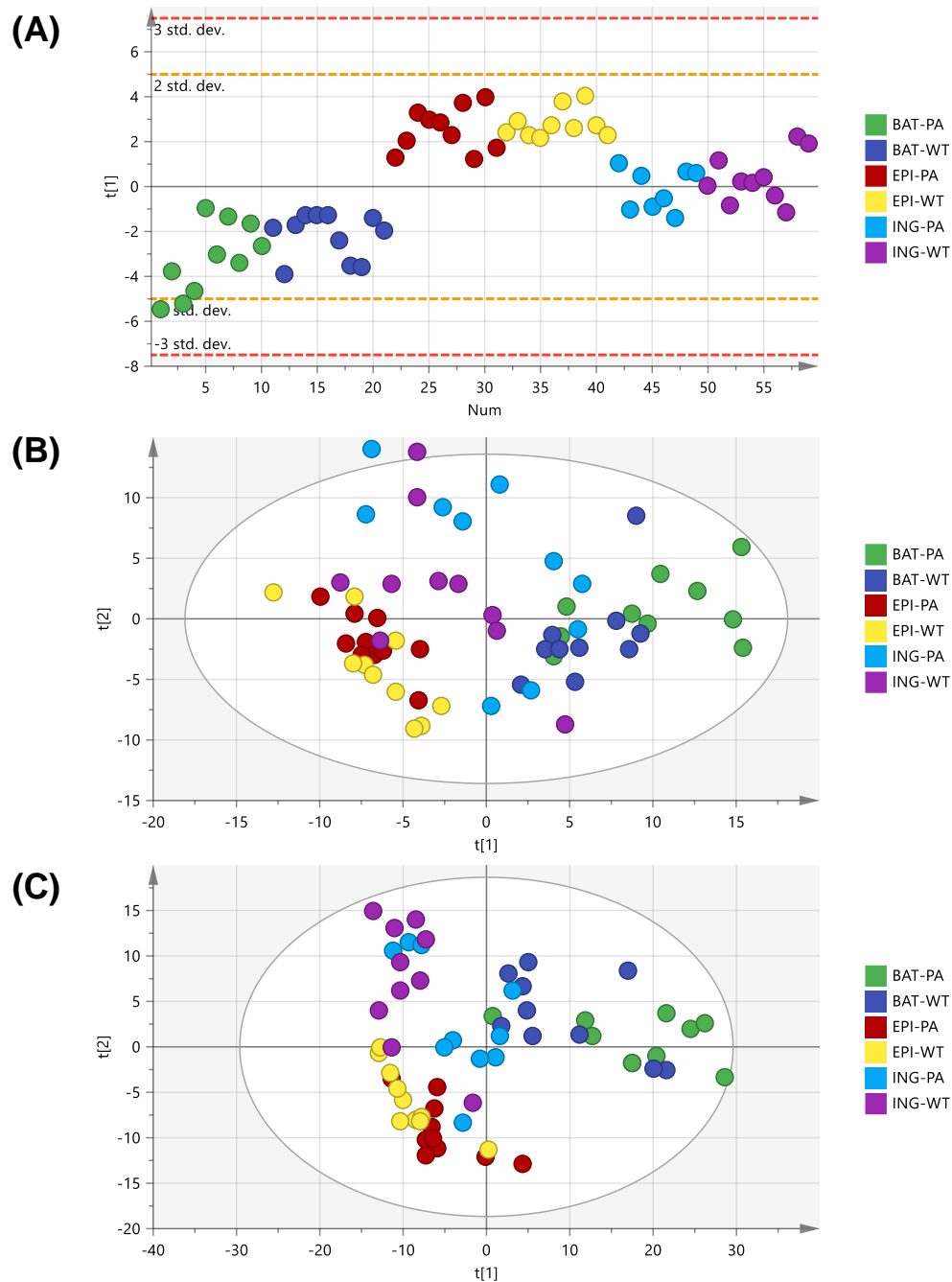


Fig 6.1 PCA models of brown adipose tissues (BAT), epididymal adipose tissues (EPI) and inguinal adipose tissues (ING) from PPAR α null (PA) and wild-type (WT) mice using (A) fatty acids, (B) triacylglycerides and (C) polar lipids including ceramides, lysophosphatidylcholines, phosphatidylcholines, phosphatidylethanolamines, phosphatidylserines, sphingomyelins (10 samples in each group).

The OPLS models built using FAs and TGs separated PPAR α null mice well from wild-type mice only for ING-WAT (FAs, $Q^2=0.712$, TGs, $Q^2=0.397$), while all three PL models were very robust (in BAT, $Q^2=0.683$, in EPI-WAT, $Q^2=0.727$, in ING-WAT, $Q^2=0.713$). These five OPLS-DA models were further investigated (**Fig 6.3-6.5**) to identify individual metabolites responsible for the separation across the two genotypes.

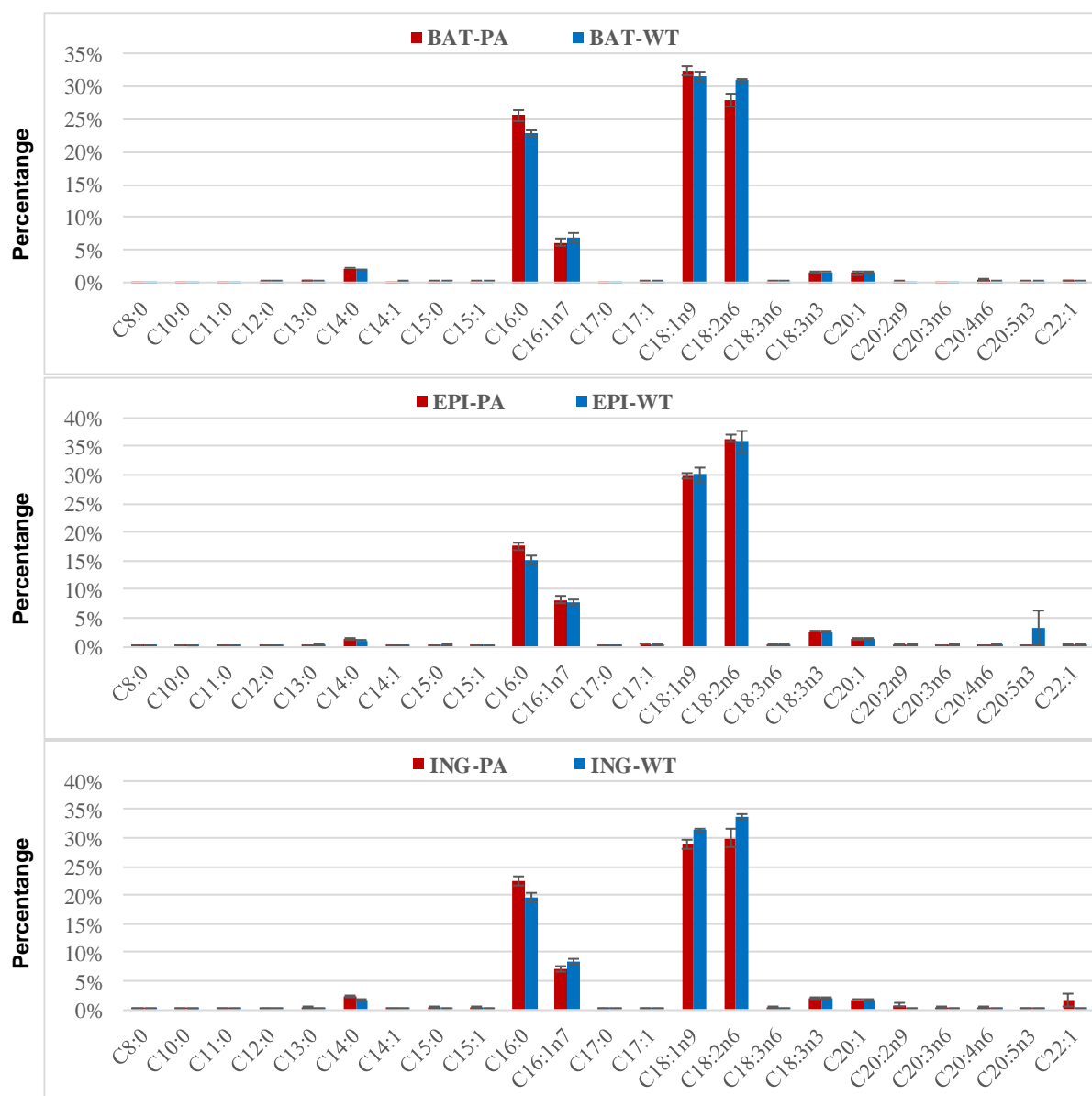
FAs			
Parameters	BAT	EPI	ING
R ₂ X(Cum)%	21.9	31.4	80.0
R ₂ Y(Cum)%	49.1	73.6	78.7
Q ₂ (Cum)%	15.1	31.4	71.2
TGs			
Parameters	BAT	EPI	ING
R ₂ X(Cum)%	39.9	36.0	45.0
R ₂ Y(Cum)%	38.2	29.1	69.8
Q ₂ (Cum)%	23.0	2.9	39.7
PLs			
Parameters	BAT	EPI	ING
R ₂ X(Cum)%	67.9	89.5	68.4
R ₂ Y(Cum)%	97.8	100.0	94.0
Q ₂ (Cum)%	68.3	72.7	71.3

Table 6.1 Parameters of OPLS-DA models of brown adipose tissues (BAT), epididymal adipose tissues (EPI) and inguinal adipose tissues (ING) in PPAR α null mice compared with wild-type mice using fatty acids (FAs), triacylglycerides (TGs) and polar lipids (PLs) including ceramides, lysophosphatidylcholines, phosphatidylcholines, phosphatidylethanolamines, phosphatidylserines, sphingomyelins (10 samples in each group).

6.4.2 Palmitoleic acid, oleic acid, and linoleic acid decreased in inguinal adipose tissues from PPAR α null mice compared with wild-type controls

As shown in **Fig 6.2**, palmitic acid (C16:0), oleic acid (C18:1 ω 9) and ω -6 linoleic acid (C18:2 ω 6) dominated all three adipose tissues in either PPAR α null or wild-type mice. The major products from DNL, C16:0 and C18:1, were increased in BAT compared with WAT, while the essential FAs originated from food, C18:2 ω 6 and C18:2 ω 3, were decreased in BAT compared with the WAT. This suggests that FAs from DNL, rather than those from food, are more stored in BAT compared with WAT, while WAT is better suited for the control of systemic lipid composition through regulating *in vivo* enzymes. As shown in the loading plot of **Fig 6.3B**, most of the FA species were increased in ING-WAT of PPAR α null mice except palmitoleic acid (C16:1n7), oleic acid (C18:1 ω 9) and linoleic acid (C18:2 ω 6) compared with the wild-type controls. This may result from decreased FA oxidation in the liver and muscle of PPAR α null mice. Another reason may be the metabolic perturbations associated with increased expression of PPAR γ in adipose tissues of PPAR α null mice as reported by Li et al. [428] and its influence on SREBP-1c and SCD which will be discussed below.

	C14:0	C16:0	C16:1	C18:1	C18:2n6	C18:3n3	C20:1
BAT-PA	2.17% ± 0.06%	25.62% ± 0.89%	6.17% ± 0.43%	32.52% ± 0.72%	27.94% ± 0.99%	1.55% ± 0.08%	1.41% ± 0.16%
BAT-WT	2.02% ± 0.06%	22.89% ± 0.53%	6.91% ± 0.61%	31.55% ± 0.69%	30.89% ± 0.40%	1.65% ± 0.07%	1.55% ± 0.11%
EPI-PA	1.34% ± 0.07%	17.49% ± 0.57%	8.15% ± 0.56%	29.90% ± 0.49%	36.34% ± 0.69%	2.70% ± 0.11%	1.30% ± 0.17%
EPI-WT	1.06% ± 0.03%	15.19% ± 0.81%	7.67% ± 0.60%	30.00% ± 1.35%	35.76% ± 2.08%	2.48% ± 0.12%	1.29% ± 0.10%
ING-PA	2.16% ± 0.12%	22.40% ± 0.85%	6.99% ± 0.56%	28.93% ± 0.78%	29.97% ± 1.69%	1.97% ± 0.16%	1.76% ± 0.14%
ING-WT	1.58% ± 0.07%	19.43% ± 0.80%	8.39% ± 0.41%	31.27% ± 0.46%	33.71% ± 0.60%	1.93% ± 0.08%	1.54% ± 0.11%



P-value by 2-way ANOVA	C14:0	C16:0	C16:1n7	C18:1n9	C18:2n6	C18:3n3	C20:1n9
Interaction	0.0172	0.7130	0.3760	0.0315	0.4249	0.4446	0.3050
Genotype	<0.0001	<0.0001	0.1221	0.0878	0.0005	0.8772	0.9784
Adipose type	<0.0001	<0.0001	0.0134	0.0110	<0.0001	<0.0001	0.0623

Fig 6.2 Total fatty acid composition in brown adipose tissues (BAT), epididymal adipose tissues (EPI) and inguinal adipose tissues (ING) from PPARα null (PA) and wild-type (WT) mice (10 samples in each group).

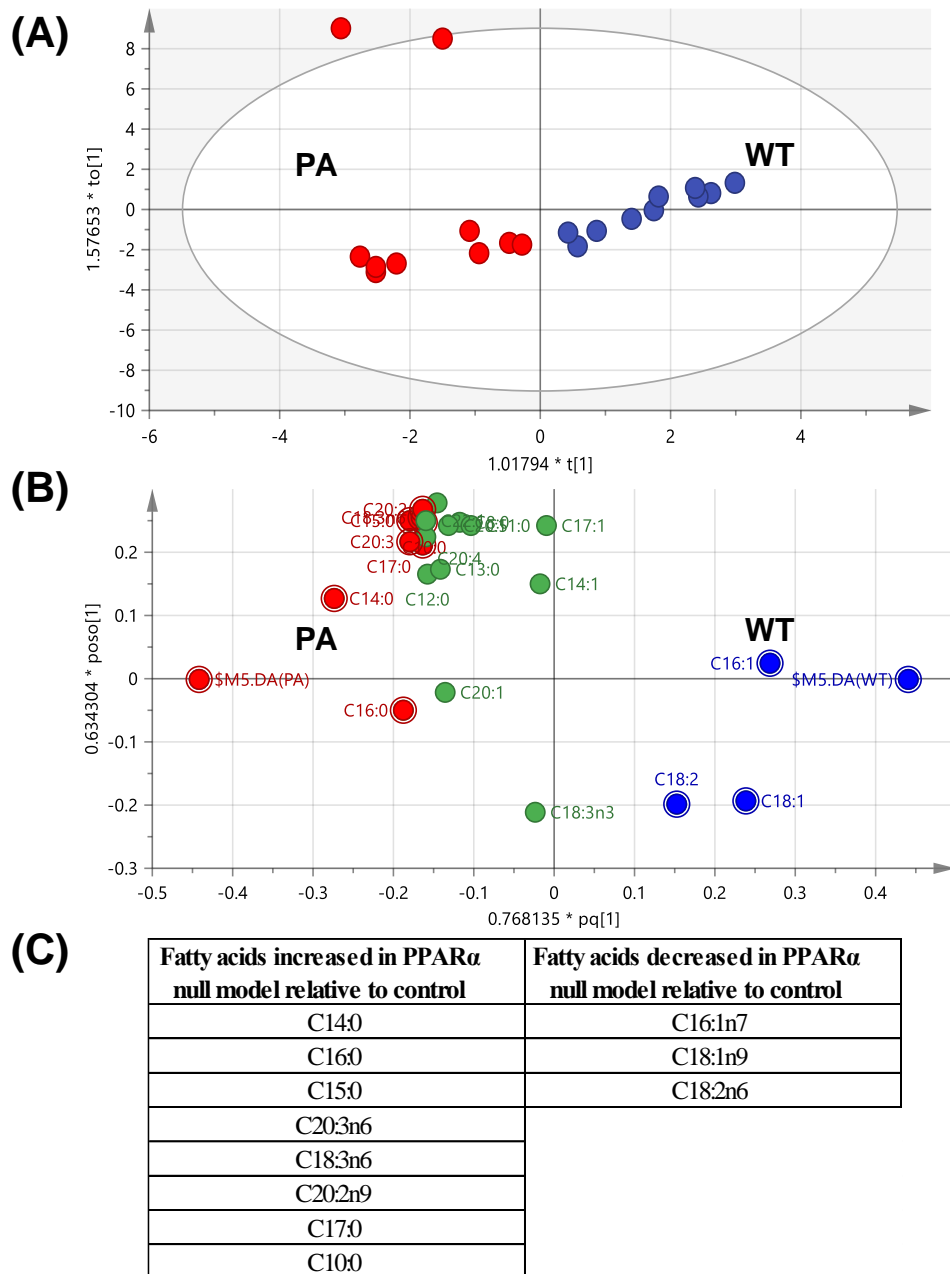


Fig 6.3 OPLS-DA model (A) score plot and (B) loading plot of total fatty acids detected by GC-MS in inguinal adipose tissues (ING) from PPAR α null (PA) and wild-type (WT) mice (10 samples in each group), and (C) identified individual metabolites responsible for the separation across the two genotypes.

6.4.3 Short and unsaturated triacylglycerides are increased in inguinal adipose tissues from PPAR α null mice

As mentioned above, the OPLS-DA model of TGs was only moderately robust for ING-WAT in terms of comparing the two genotypes across the two WAT depots and BAT. Similar to the FA profile, most of the TG species were increased in ING-WAT of PPAR α null mice as shown

in the loading plot of the OPLS-DA model (**Fig 6.4B**). The loading plot identified some saturated and short TGs were particularly increased in ING-WAT of PPAR α null mice, compared with wild-type controls (**Fig 6.4C**). It suggested that most of the TGs decreased in ING-WAT of PPAR α null mice were constituted by the FAs listed in **Fig 6.3C** (C16:1n7, C18:1 ω 9 and C18:2 ω 6).

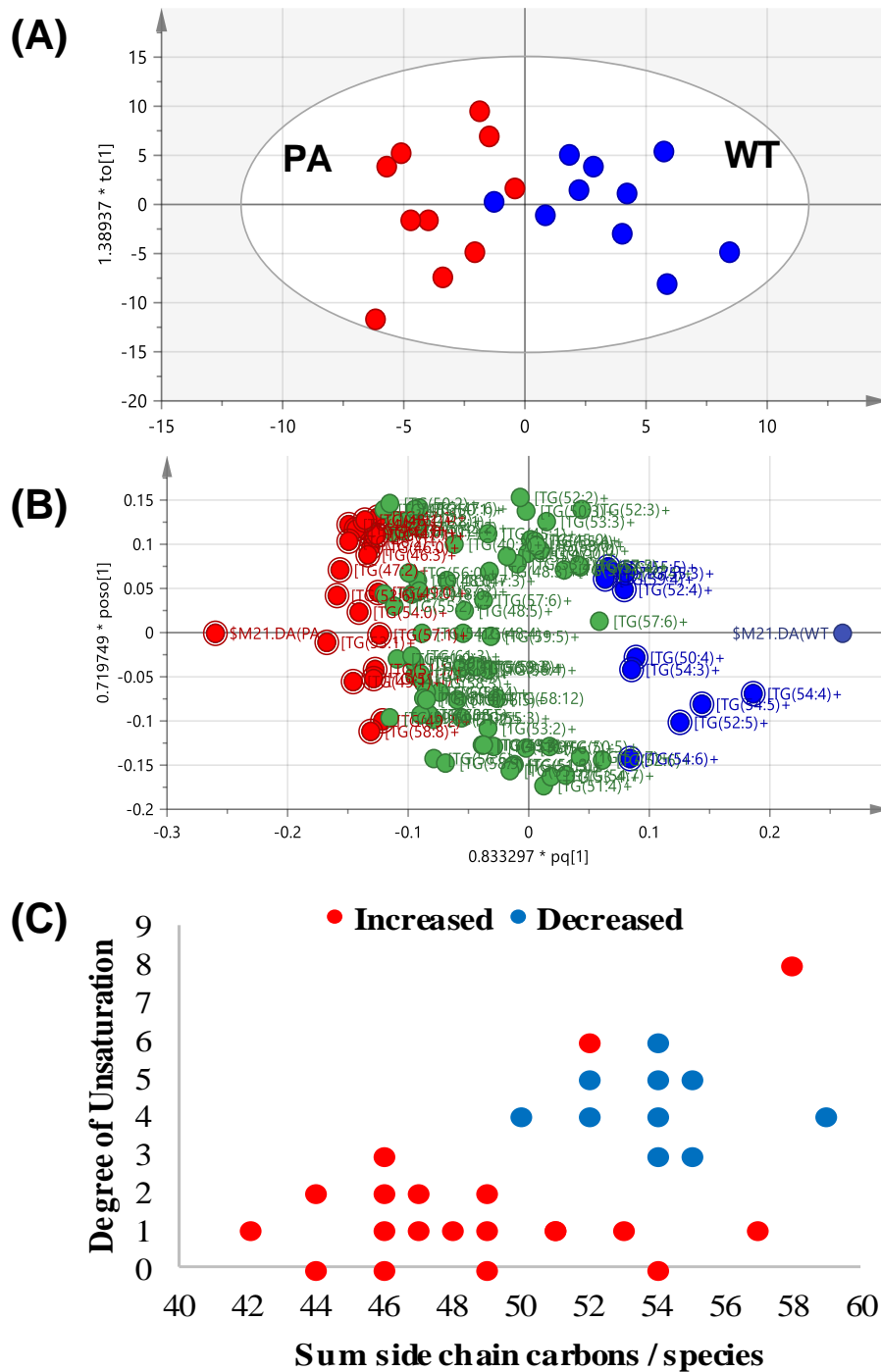


Fig 6.4 OPLS-DA model (A) score plot and (B) loading plot of triacylglycerides in inguinal adipose tissues (ING) from PPAR α null (PA) and wild-type (WT) mice (10 samples)

in each group), and (C) identified individual metabolites responsible for the separation between the two genotypes.

6.4.4 Polar lipids were changed significantly in both brown and white adipose tissues from PPAR α null mice

There had been only a few lipidomic studies focused on adipose tissues from PPAR α null mice [619-624], and none of them have investigated the composition of polar lipids as far as I know, maybe because the spectra of LC-MS data is dominated by TGs in the adipose tissues. This study used an SPE method to selectively remove most of the TGs in the adipose tissue and detected 175 PLs including six lipids classes (Cer, lysoPC, PC, PE, PS, and SM). As shown in **Fig 6.5**, the OPLS-DA models of PLs separated BAT, EPI-WAT, and ING-WAT of PPAR α null mice from those of wild-type mice. Interrogation of the corresponding loadings plots and the variable influence on projection (VIP) plots for these OPLS-DA models identified many polar lipids significantly increased or decreased in BAT, EPI-WAT and ING-WAT of PPAR α null mice (top 20 changed PLs in each group are summarized in **Table 6.2** according to the lipid types). Similar changes to those detected in FAs and TGs were detected in PLs in that more PLs were increased in PPAR α null mice, in particular PCs, the major plasma membrane lipids. The increased PCs may be a response mechanism for decreased FA oxidation and increased glycolysis in PPAR α null mice. Interestingly, most of the decreased PLs are SMs which typically make up 10-20 mol % of plasma membrane lipids. The metabolic perturbations of SMs may influence signal transduction [625]: the synthesis of SMs at the plasma membrane can produce diacylglycerol, an important second messenger, while the degradation of SMs produces ceramides which are involved in the apoptotic signaling pathway. Moreover, most of the PLs (including all the six lipid classes) increased in PPAR α null mice have shorter and more saturated side chains compared with those decreased in PPAR α null mice. This change may lead to decreased fluidity of cell membranes.

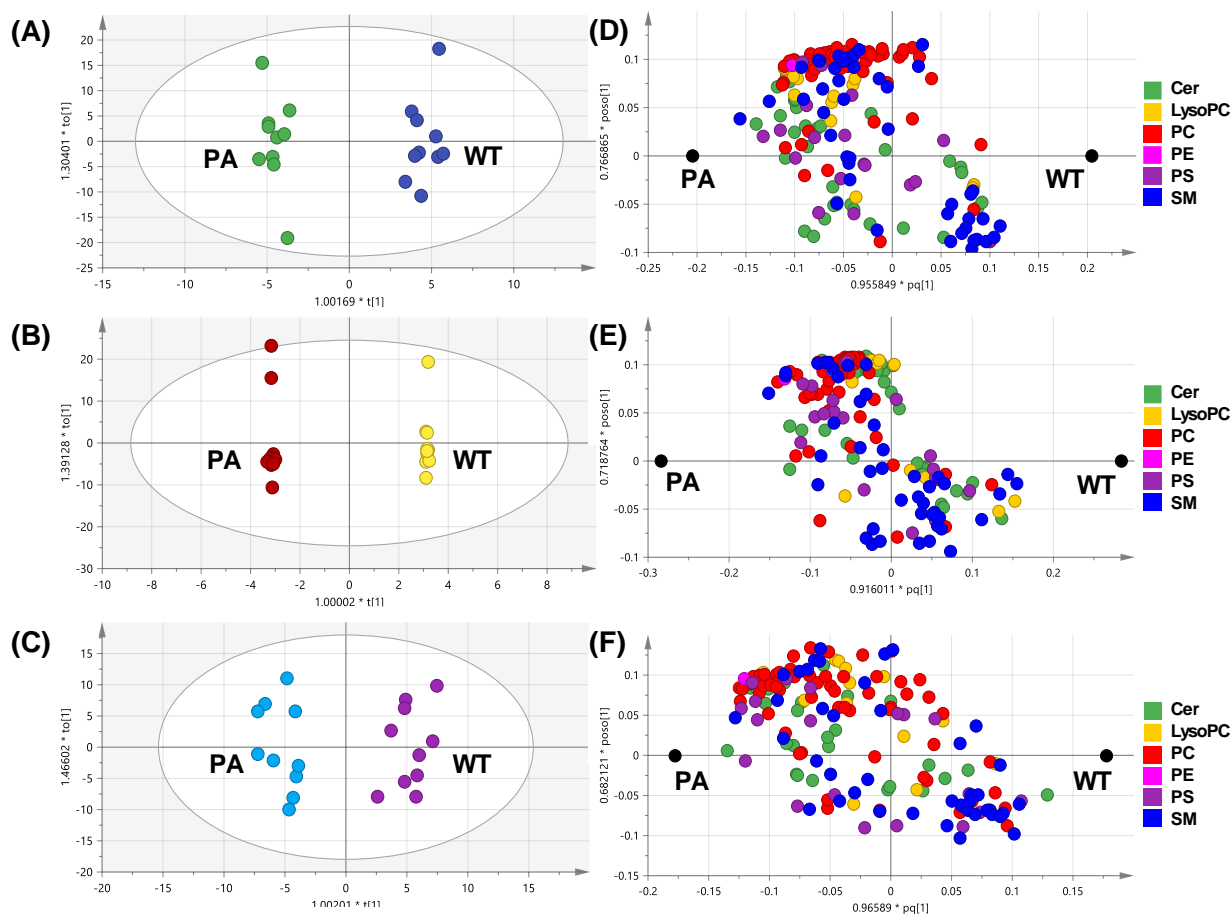


Fig 6.5 OPLS-DA model (A) score plot and (D) loading plot of polar lipids in brown adipose tissues from PPAR α null (PA) and wild-type (WT) mice (10 samples in each group); OPLS-DA model (B) score plot and (E) loading plot of polar lipids in epididymal adipose tissues from PPAR α null (PA) and wild-type (WT) mice (10 samples in each group); OPLS-DA model (C) score plot and (F) loading plot of polar lipids in inguinal adipose tissues from PPAR α null (PA) and wild-type (WT) mice (10 samples in each group). Cer, ceramide, LysoPC, lysophosphatidylcholine, PC, phosphatidylcholine, PE, phosphatidylethanolamine, PS, phosphatidylserines, SM, sphingomyelins.

BAT		EPI		ING	
Increased	Decreased	Increased	Decreased	Increased	Decreased
Cer(38:1)	Cer(32:3)	Cer(29:0)	Cer(32:3)	Cer(36:1)	Cer(42:8)
Cer(40:1)	Cer(39:5)	Cer(30:4)	Cer(32:4)	Cer(38:1)	
Cer(40:2)	Cer(40:2)	Cer(31:0)	Cer(33:1)	Cer(40:1)	
Cer(41:1)	Cer(42:8)		Cer(35:5)	Cer(41:1)	
Cer(41:2)			Cer(39:5)	Cer(41:3)	
Cer(42:1)			Cer(40:2)	Cer(42:1)	
Cer(42:2)			Cer(42:8)	Cer(42:2)	
Cer(42:3)					
LysoPC(18:2)	LysoPC(20:3)		LysoPC(20:3)	LysoPC(20:4)	LysoPC(22:5)
LysoPC(20:4)	LysoPC(22:5)		LysoPC(22:5)		
PC(36:4)	PC(41:1)	PC(33:0)	PC(34:5)	PC(36:0)	PC(36:5)
PC(37:3)	PC(42:8)	PC(35:1)	PC(40:0)	PC(36:1)	PC(40:2)
PC(38:1)		PC(35:2)	PC(41:1)	PC(36:2)	PC(40:7)
PC(38:4)		PC(36:2)		PC(37:3)	PC(41:1)
PC(38:5)		PC(36:5)		PC(38:4)	PC(42:8)
PC(40:3)		PC(37:3)		PC(38:5)	
		PC(38:1)			
		PC(38:4)			
		PC(38:5)			
PE(41:2)		PE(41:2)		PE(41:2)	
PS(30:3)	PS(42:2)	PS(30:3)	PS(25:0)	PS(30:3)	PS(39:3)
PS(41:5)		PS(35:1)		PS(35:1)	PS(42:2)
		PS(37:0)		PS(41:5)	
		PS(43:6)		PS(46:1)	
SM(34:1)	SM(27:0)	SM(34:1)	SM(27:0)	SM(31:1)	SM(27:0)
	SM(30:0)	SM(35:2)	SM(30:0)		SM(34:1)
	SM(34:1)	SM(38:1)	SM(34:2)		SM(40:0)
	SM(34:2)		SM(35:3)		SM(40:1)
	SM(36:0)		SM(37:6)		SM(40:5)
	SM(37:1)		SM(43:5)		SM(40:6)
	SM(40:0)		SM(46:1)		SM(41:1)
	SM(40:5)				SM(42:1)
	SM(43:5)				SM(43:5)
	SM(43:6)				SM(43:6)
	SM(46:1)				SM(46:1)

Table 6.2 Top 20 identified individual metabolites in brown adipose tissues (BAT), epididymal adipose tissues (EPI) and inguinal adipose tissues (ING) of PPAR α null mice compared with wild-type mice by interrogation of the corresponding loadings plots and the variable influence on projection (VIP) for the OPLS-DA models in **Fig 6.4**. Cer, ceramide, LysoPC, lysophosphatidylcholine, PC, phosphatidylcholine, PE, phosphatidylethanolamine, PS, phosphatidylserines, SM, sphingomyelins.

6.5 Discussion

As reviewed by Mandard et al. [626], PPAR α target genes are mostly associated with mitochondrial and peroxisomal FA oxidation, microsomal FA hydroxylation, and are involved in glucose and amino acid metabolism. Studies on the mouse have reported an obvious phenotype when fasted during which decreased FA oxidation led to increased FFA, hypoglycemia, hypoketonaemia, and hypothermia [627-629], or when fed on HFD which caused reduced myocardial FA oxidation and some evidence of cardiomyopathy emerged [630]. Hypoglycemia [627, 628, 631] is thought to result from impaired FA oxidation [627, 632] and failure in producing ketone bodies to spare glucose metabolism in PPAR α null mice. Atherton et al. [431, 633] have conducted a comprehensive metabolomic study of the aqueous tissue extracts of PPAR α null mutant mouse fed *ad libitum* using a combined $^1\text{H-NMR}$ spectroscopy-, magic angle spinning $^1\text{H-NMR}$ spectroscopy- and a gas chromatography-mass spectrometry-based method. Interestingly, increased glycolysis and decreased gluconeogenesis were reported across heart, liver, skeletal muscle and adipose tissues of PPAR α null mice without dietary intervention such as fasting or HFD-feeding. The Cori cycle and some amino acid metabolic pathways such as the alanine-glucose cycle were also decreased in activity. The increase of lactate and amino acids such as alanine which is important hepatic gluconeogenic substrates demonstrated limited gluconeogenesis in PPAR α null mice and a failure by the liver to supply peripheral organs with ketone bodies from fatty acid oxidation. The failure in gluconeogenesis may result from reduced expression of glucose-6-phosphatase (G6pc), phosphoenolpyruvate carboxykinase 1 (Pck1), PGC1 α and/or 6-phosphofructo-2-kinase/fructose-2, 6-biphosphatase (Pfkfb3) which are partly regulated by PPAR α [431]. Moreover, the expression of a gluconeogenic enzyme such as phosphoenolpyruvate carboxykinase (PEPCK) has been reported to be decreased in the liver of PPAR α null mice [631]. Deletion of PPAR α reduces the expression of pyruvate dehydrogenase kinase-4 (PDK4), which in turn inhibits pyruvate dehydrogenase and limits glycolysis across the body, particularly when fatty acids are in excess [626, 634]. The heart, diaphragm, WAT and soleus muscle tissues from the PPAR α null mice also demonstrated decreased glucose and increased lactate too, which suggested limited gluconeogenesis and increased glycolysis, and in addition, the supply of ketone bodies was reduced along with decreased β -hydroxybutyrate in the heart [635, 636].

Considering lipid changes, according to the GC-MS analysis of the total lipid extracts conducted by Atherton et al. [431, 633], oleate (C18:1), linoleate (C18:2) and di-homo- γ -linoleate (C20:3) and arachidonic acid (C20:4) were largely increased in the liver of PPAR α null mice, and it was hypothesized this was because of decreased β -oxidation and ketogenic pathways mediated by PPAR α . Oleate (C18:1) and linoleic acid (C18:2) were increased in the heart tissue from the null mice, while palmitic acid (16:0), docosahexaenoic acid (22:0), tetracosanoic acid (24:0) and arachidonic acid (20:4) decreased. This may be the result of the elongases and desaturase which are in part controlled by PPAR α [637]. WAT from the PPAR α null mice exhibited increased eicosanoic acid (20:0), eicosadienoic acid (20:2), di-homo- γ -linolenic acid (20:3), tridecanoic acid (13:0), docosadienoic acid (22:2) and hexadecadienoic acid (16:2), and decreased concentrations of octadecanoic acid (18:0), heptadecanoic acid (17:0), hexadecenoic acid (16:1) and tetradecanoic acid (14:1).

In the present study, most of the FA species were increased in ING-WAT of PPAR α null mice except palmitoleic acid (C16:1n7), oleic acid (C18:1 ω 9) and ω 6-linoleic acid (C18:2 ω 6). The difference may result from the age of mice (Atherton used 1 month-old mouse but we used animals at the age of 8-10 months in the present study) or the position of adipose tissues (Atherton used abdominal WAT). The increase of long-chain (10-16 carbons, LCFAs) and very-long-chain fatty acids (17-26 carbons, VLCFAs) may be due to lack of peroxisome proliferation because LCFAs and VLCFAs are preferentially oxidized in peroxisomes. Moreover, an eightfold increase in the expression of hepatic SCD activity has been reported by PPAR α activation in wild-type mice [638]. On the other hand, if SCD activity cannot be activated in PPAR α null mice, it seems reasonable that palmitoleic acid and oleic acid were decreased in the WAT of PPAR α null mice. The activity of the desaturase SCD is partly controlled by PPAR α [637], but another reason for changes in lipid composition may be the influence of PPAR γ [639]. PPAR γ is much more abundantly expressed in WAT than PPAR α [429]. Interestingly, Li et al. [428] demonstrated that the expression of PPAR γ increased significantly in PPAR α null mice along with a profound perturbation in metabolism in adipose tissues where PPAR α is weakly expressed. This compensatory upregulation may account for some of the metabolic changes detected. What's more, as PPAR α is important for peroxisome proliferation and β -oxidation [67-70], the dysfunctional peroxisome proliferation may be the reason there are less long and unsaturated FAs in adipose tissues of PPAR α null mice.

Our study not only profiled the FA changes in WAT of PPAR α null mice but also examined intact lipids across a range of lipid classes. In total, 26 fatty acids, 108 TGs and 175 PLs including six lipid classes were detected using a combination of GC-MS, DI-MS/MS and SPE-UPLC-MS methods, and used to build PCA and OPLS-DA models to investigate the influence of PPAR α on BAT, EPI-WAT, and ING-WAT. ING-WAT was similar to the BAT in terms of the types of lipids compared with EPI-WAT, as ING-WAT reportedly expresses significantly higher levels of brite characteristic markers compared to EPI-WAT upon induction by cold [616-618]. Interestingly, neutral lipids (FAs and TGs) in ING-WAT seem to be more influenced by the knock-out of PPAR α compared with those in BAT and EPI-WAT. Moreover, both neutral and polar lipids were more saturated and shorter in adipose tissues of PPAR α null mice, all of which seem to be in accordance with the decrease in palmitoleic acid (C16:1n7), oleic acid (C18:1 ω 9) and ω 6-linoleic acid (C18:2 ω 6) detected. Knight et al. [638] reported that inclusion of the PPAR α activator WY 14,643 in the diet stimulated the hepatic expression of not only genes of the FA oxidation pathway, but also those of the DNL pathways and cholesterol synthesis by increasing the cleavage of the SREBP-1c protein to the active form, accompanied by a rise in SCD mRNA expression. It is possible that a lack of the active form of SREBP-1c and SCD expression may explain the decreased unsaturated lipids in adipose tissues of PPAR α null mice.

Moreover, most of the PLs (including all six lipid classes) increased in PPAR α null mice have shorter and more saturated side chains compared with those decreased in PPAR α null mice. This change may lead to decreased fluidity of the membrane. Generally, saturated fatty acids make the membrane bilayer less fluid and inactive, which in turn has consequences for protein function and membrane transport [168], whereas unsaturated fatty acids result in a more plastic membrane and improve the function of membrane receptors and sensitivity to hormones [169, 170]. The geometry of the cis-double bond induces a bend in the molecule, thereby precluding rigid lipid bilayers. One process of high relevance to T2DM is glucose transport across the membrane which may be influenced by membrane fluidity [171]. There have been studies reporting the relationship between membrane fluidity of erythrocytes and insulin sensitivity in hypertensive subjects [172], and also changes in the composition of membrane lipids associated with increased insulin sensitivity in skeletal muscles after physical training [173].

Interestingly, in Atherton's research, the aging process was also characterized by decreased glucose and glycogen in the liver, heart, diaphragm, WAT, soleus, and gastrocnemius muscle tissues. In the liver, aging was associated with decreases in leucine and isoleucine and increases in lactate and alanine, aspartate and glutamate, suggesting decreased gluconeogenesis. However, the decrease in lactate, alanine, and glutamate suggested that glycolysis was inhibited in an age-dependent manner in heart, diaphragm and muscle tissues [431]. In the liver, FAs, taurine, and choline/phosphocholine were increased and cholesterol synthesis was decreased with age. Palmitic acid (C16:0) arachidonic acid (20:4) increased, while oleate (C18:1) and cholesterol decreased associated with the aging trend in the liver. In muscle and adipose tissues, the aging process was characterized by increases in a number of saturated fatty acids including palmitic acid (16:0), stearic acid (18:0), tetradecanoic acid (14:0) and heptadecanoic acid (17:0), as well as a decrease in docosahexaenoic acid (22:6), the β -oxidation product of tetracosahexaenoic acid (24:6). Thus, there should be an age-dependent study of the BAT and WAT of PPAR α null mice in the future to characterize these changes further and understand better how aging interacts with this process.

6.6 Conclusions

This Chapter profiled total FA composition and different type of intact lipids (TG, Cer, lysoPC, PC, PE, PS, and SM) changes in BAT and WAT of PPAR α null mice compared with wild-type controls. The inguinal WAT was found to be a mixed lipid profile of BAT and EPI-WAT, but it exhibited the most significant FA and TG changes in PPAR α null mice. The differences might result from that the ING-WAT is at superficial depots while the EPI-WAT is one of the largest visceral fat depots with lower volatility. Polar lipids were found to be good in building OPLS-DA models to explain the differences between the two genotypes in both BAT and WAT. Most of the lipids were increased and became more saturated and shorter in PPAR α null mice, which may result from a lack of active form of SREBP-1c and subsequent decreased of SCD expression, or associated with the change in expression of PPAR γ induced in PPAR α null mice.

Chapter 7 Summary and Future Directions

7.1 General discussion and summaries

Obesity is a complex disorder where the genome of an organism interacts with diet and other environmental factors to influence ultimate body mass, composition, and shape, with characteristic excess fat storage in adipose tissue. Numerous studies have investigated how bulk lipid metabolism is influenced by obesity [640-643] but membrane component lipids such as PCs and PEs have been seldom investigated. Cell membrane components contribute to a variety of cellular processes including maintaining organelle functionality, providing an optimized environment for numerous proteins and providing important pools for metabolites, such as choline for one-carbon metabolism (e.g for methylation of DNA). This suggests a possible link between lipid metabolism, one-carbon cycle, DNA/histone methylation, and expression of genes involved in physiological and pathophysiological processes such as obesity and aging.

The first part (Chapter 3) of this thesis is a comprehensive lipidomic study of white adipose tissue in mice that become obese either through genetic modification (*ob/ob* genotype), diet (high-fat diet) or a combination of the two across the life-course. In this chapter, I demonstrated that FA *de novo* synthesis is activated in *ob/ob* mice by leptin deficiency, possibly via an increase in food intake. In contrast to the shorter and more saturated TGs from DNL, more unsaturated PCs are synthesized in *ob/ob* mice to maintain the fluidity and normal function of cell membrane against increased *de novo* synthesis. However, this protective mechanism can be impaired by the long-term administration of an HFD, presumably through oxidative damage. Moreover, most of the lipids stored in the adipose tissue of HFD-fed mice are assembled directly using dietary fatty acids, which dramatically decreased the diversity of lipid composition. Longer TGs and saturated PCs accumulated in adipose tissue of aged mice, which increases susceptibility to metabolic diseases. These characteristic changes nicely complement previous lipidomic studies only focused on FAs and TGs in adipose tissue, and depict a more comprehensive metabolic network profile in adipose tissue.

Secondly, the correlation between transcriptomic patterns of obesity and aging was investigated (Chapter 4). The two obesity models exhibited differently featured expression patterns but both had some changes in common with aging. Inflammation and immune system-

related pathways were activated not only in the two models of obesity but also in white adipose tissue of aged mice. On the contrary, metabolic pathways, in particular, those related to lipid metabolism, were activated by leptin deficiency in the initiation of obesity of *ob/ob* mice, but inhibited to a large extent in white adipose tissue of aged *ob/ob* mice, compared to both the wild-type controls and the younger controls. The GO and KEGG enrichment analysis of these genes suggested that peroxisome and AMPK and PPAR γ signaling pathways may act at the forefront in the progression of obesity and aging, as a protective mechanism in the initiation of oxidative damage, but then accumulated damage results in insulin resistance, the metabolic syndrome and T2DM.

The third part (Chapter 5) linked lipidomic and transcriptomic changes through 1-C cycles and methylation donors. In *ob/ob* mice, the 1-C cycle was heavily activated and produced an abundance of SAMs for DNA and/or histone methylation. The produced SAM was used to methylate different genes with high selectivity. Lipid metabolism, 1-C metabolism, and epigenetic changes form a good combination for a better understanding of the extremely sophisticated role of adipose tissue in regulating energy homeostasis with the potential to be a barometer for pathophysiological processes of obesity and aging. Whether the activated 1-carbon and methylation pathways are consequences or adaptive protective mechanism along with obesity and aging need to be further validated. This could be tested through analysis of genotype/diet-induced obese animal models in which the 1-carbon or methylation pathways were blocked by knock-out of certain genes of key enzymes, such as serine/betaine hydroxymethyltransferase (SHMT/BHMT) or some other kinds of methyltransferases.

As found in Chapter 4, the peroxisome and PPAR γ signaling pathways seem to play a key role in the progression of obesity and aging. It has been reported that the expression of PPAR γ increased significantly in PPAR α null mice [428], and only PPAR α reportedly activates proliferation of peroxisomes [416]. PPAR α is thought to have a profound effect on systemic metabolism and in particular the handling of lipids across the organism. So the last Chapter profiled total FA composition and different type of intact lipids (TG, Cer, lysoPC, PC, PE, PS, and SM) changes in BAT and WAT of PPAR α null mice compared with wild-type controls. The inguinal WAT was found to be a mixed lipid profile of BAT and EPI-WAT, but it exhibited the most significant FA and TG changes in PPAR α null mice. The differences might result from that the ING-WAT is at superficial depots while the EPI-WAT is one of the largest

visceral fat depots with lower volatility. Polar lipids were found to be good in building OPLS-DA models to explain the differences between the two genotypes in both BAT and WAT. Most of the lipids were increased and became more saturated and shorter in PPAR α null mice, which may result from a lack of active form of SREBP-1c and subsequent decreased of SCD expression, or associated with the change in expression of PPAR γ induced in PPAR α null mice.

In summary, my work using different rodent models (*ob/ob*, HFD-fed, and PPAR α -null) and multi-omics techniques (lipidomics, metabolomics, and transcriptomics) demonstrated a protective metabolic mechanism activated in the initiation but impaired at the end of the processes of obesity and aging. This may explain the similarity of obesity and aging in terms of the high incidence of metabolic syndrome and related diseases. First, although there were more short and saturated neutral lipids in the adipose tissue of *ob/ob* mice due to increased *de novo* synthesis, phospholipids became more unsaturated to maintain the fluidity and normal function of the membrane. Interestingly, this protective mechanism was found to be impaired by long-term administration of an HFD, presumably through oxidative damage. Similarly, saturated PCs were found to be accumulated in adipose tissue of aged mice, increasing the susceptibility to metabolic diseases. Secondly, the transcriptomic study also demonstrated the correlation between obesity and aging in the firstly activated but then inhibited lipid metabolic pathways regulated by peroxisome, AMPK, insulin, and PPAR γ signaling in the progress of obesity and aging, along with the up-regulation of inflammation in the whole process. Thirdly, phospholipids correlate better with transcriptional changes and one-carbon/choline/S-adenosylmethionine metabolism within the adipose cells, suggesting that while triglycerides within the adipose tissue may be a relatively inert store of lipids, the compositional changes occur in cell membranes with more far-reaching functional consequences (epigenetics). Finally, another rodent model, knock-out of the PPAR α which has a profound effect on both peroxisome and PPAR γ signaling, demonstrated more saturated and short polar lipids, which is in good accordance with the former aspects of this thesis that advance our understanding of metabolic alternations implicated in the obesity and aging process.

7.2 Limitations of the study

Animal models have the advantage of ease of selective genetic manipulation and drug interventions and better tissue and organ availability over human tissue studies. This study

utilized genetically modified mice and diet manipulation to expand our understanding of the underlying mechanism of both obesity and the aging process. However, there are a vast number of differences between the animal models and humans, and when some variables are not controlled for, such as food intake, wrong conclusions may be drawn.

Firstly, it has been reported that *ob/ob* mice tend to eat more food compared with the wild-type controls [387, 394, 398]. On the contrary, rodents fed an HFD diet may regulate their food intake to compensate for the increased calorie content of the diets [644]. The differences observed in either lipidomics, transcriptomics or DNA methylation might be owing to the modified food consumption and thereby differential uptake of other nutrients such as protein, vitamin, minerals, rather than the lipids *per se*. In particular, the methyl groups of SAMs are derived from one-carbon metabolites (folate, choline, betaine, methionine, etc., as illustrated in **Figure 1.1**) which can be obtained from the diet. Food intake can affect the results to some extent. For example, low folate diets have been reported to lower methylation of some genes such as *p53* in rat liver [645], and folate supplementation increased methylation in the promoter regions of glucocorticoid receptor and insulin receptor, PPAR α , during the juvenile-pubertal period of the rat [646]. The methylation status of these genes can have an effect on the transcription and expression of other genes and can alter energy metabolism as a result. Deficiency or redundancy of choline [647-649] and betaine [650, 651], which are crucial for the one-carbon metabolism, can also influence gene methylation and expression in many tissues. While food intake was not measured in the current study, this could be addressed in future studies so that the intake of different nutrients can be calculated, and the effects of them on lipid and one-carbon metabolism and DNA methylation can be taken into account.

Another limitation of the animal experiment design is that only male mice were studied. Pubertal parameters, such as cycling, estrus and vaginal opening, have all been reported [432] to be influenced by leptin signaling, which may add uncertainty to my metabolism study. In the second animal study in **Chapter 6**, only old male mice were chosen because the PPAR α null mice have been reported to exhibit spontaneous late-onset obesity even with a stable caloric intake and a marked sexual dimorphism [426]. Female PPAR α mice may be shown to have higher serum triglycerides and gain more fat than males, while males show a delayed occurrence of obesity and original centrilobular-restricted steatosis [reference 426?]. The male-specific steatosis in PPAR α null mice indicated discrepancies between the sexes toward lipid

metabolism. There have been many variables (PPAR α null or wild-type, BAT/EPI/ING adipose tissue) contributing to the statistical complexity, so only male animals, which have more steatosis compared with the female mice, were studied to reduce the complexity of multivariate statistics. In the future, the influence of sex on the lipid/one-carbon/methylation mechanism could be addressed.

In the present study, white adipose tissue (WAT) from paired gonadal depots within the abdominal cavity in male mice was primarily examined, due to the abundance and availability of this tissue and previous reports demonstrating the signaling functions of the WAT (e.g. through producing leptin and adipokines) while the BAT seems to mainly respond to signals and generates body heat [174, 235, 442]. Further, the visceral adipose tissue is linked to insulin resistance [443], type 2 diabetes [444], inflammatory diseases [445], and other obesity-related diseases [446]. In future studies, different fat depots as those examined in **Chapter 6** could be examined.

7.3 Future directions

First, polyunsaturated fatty acids (PUFA) have been reported to prevent insulin resistance [10, 11], and improve cardiovascular and metabolic health when combined with regular exercise [12]. These fatty acids are also able to increase adipose tissue fatty acid oxidation and reduce lipogenesis [13], modulate adipose tissue inflammation [14] and regulate adipokine secretion [15]. One proposal is to design an animal experiment to examine the epigenetic and metabolic effects of PUFA supplementation to further understand the mechanism by which improvements in insulin sensitivity and other metabolic conditions occur. A custom-produced diet with or without these micronutrients would be used to feed mice (n=10 /genotype/age group) for similar lengths of time and be sacrificed at similar ages as the high-fat diet group in **Chapter 2.2** to study the interaction between diet and epigenetic and metabolic modifications in WAT. To further understand the influence of diet on adipose tissue metabolism and epigenetics, I proposed to examine a combination of two or more diets including the following groups: (1) regular chow diet (no supplementation); (2) regular chow diet + methionine/choline/folate/other micronutrients; (3) high-fat diet (no supplementation); (4) high-fat diet + methionine/choline/folate/other micronutrients; (5) high-fat diet + polyunsaturated fatty acid (~50%); (6) high-fat diet switched to regular chow diet again (to

examine the dynamic processes of epigenetic marking and metabolism); (7) other nutritional models, such as mice fed a high fructose or cholesterol diet.

Other interventions not related to the diet could also be utilized to investigate the role of adipose tissues in obesity and aging. For example, the beneficial role of exercise in remodeling adipose tissues has been reported in animal models including inducing adaptive changes of lipolysis in the WAT [652, 653], activation of the BAT and beiging of the WAT [652, 653], regulating inflammation [654, 655] and metabolic dysfunction and adipokines [656-658].

Although *ob/ob* mice and obese human share a lot of similar metabolic phenotypes, leptin deficiency may result in differences in the severity of metabolic syndrome and diabetes. For example, unlike the *ob/ob* mice, there have been only a few diabetic humans reported without enough leptin [659-663]. Combination models could be utilized in future studies including but not limited to: *db/db* mice, PPAR α knockout mice, SREBP-1c transgenic mice, and acyl-coenzyme A oxidase (AOX) null mice. In humans, obesity is commonly caused by excessive food intake along with a lack of physical activity and genetic susceptibility. Therefore, a combination of genetic and diet interventions will offer a better model for metabolic diseases. Moreover, tissue-dependent metabolic effects are more complicated due to systemic changes. Some tissue-specific genetic models have been developed in which activation, overexpression, and ablation of genes can be limited in only one type of tissue such as the rodent models of overexpression of PPAR δ in the adipose tissue [610] which have been developed under the control of the enhancer-promoter region of the adipocyte fatty acid binding protein (aP2) gene. In addition, RNAi techniques [664] can be used to inhibit expression of selected genes and test the control points of the pathways discussed in **Chapter 4** with high selectivity and versatility as opposed to knock-out and metabolic inhibitors.

Ideally, it would be best to obtain human adipose tissue to see if the same metabolic and epigenetic changes occur as those observed in the animal models utilized in this thesis. However, to make the analysis more statistically robust, large sample size is required, which is technically very difficult to achieve. Therefore, breeding studies in other animals to examine the interaction of diet with epigenetic modifications could be a consideration for further analysis. Small animals such as using *Caenorhabditis elegans* (*C.elegans*) or fruit flies (*Drosophila*) are easier to manipulate and take a much shorter time to observe the interactions of diet, obesity, and aging. However, these small animals are more difficult to mimic human's

pathophysiological responses and to test the tissue-specific changes. Large animal models recapitulate the anatomy, physiology, and function of human's organs and tissues, making them a better link in the translation of basic research to clinical practice [665]. The research can also be expanded by the development of cell lines derived from the adipose tissue. The cell lines would be good tissue-specific models and are easy to manipulate and determine. But it should be cautious because all immortalized cell lines do not behave identically to their *in vivo* counterparts. Primary cells would be better to surmount the disadvantages even though they can suffer from a lack of homogeneity, a rarity of supply, mortality, and intransigence to growth in culture [666].

I have examined the methylation status of four genes known to be implicated in metabolic diseases as mentioned above. It was assumed that the global DNA methylation status and the methyl donors involved in epigenetic modifications will help us to develop a further understanding of the mechanism of obesity, metabolic syndromes, and the aging process. However, only four genes cannot fully explain the regulating network involving metabolic and epigenetic pathways. Future studies could use bisulfite sequencing to monitor the methylation status of the whole genome of adipose tissue samples in the processes of obesity and aging. Not only markers of obesity, but also those of senescence such as telomeres [667, 668], plasminogen activator inhibitor-1 [669], and senescence marker protein-30 (SMP30) [670]. Moreover, the polar, aqueous soluble metabolites other than one-carbon metabolites, such as the intermediates in the TCA cycle, protein, and glucose metabolism, could be determined by LC-MS to further define the role of adipose tissue in obesity and aging. The turnover of the metabolites could be determined by using ¹³C labeled substrate studies to provide more than a "snapshot" of the metabolic status in the adipose tissue. Through the use of a selection of the cell lines/primary cells/animal models discussed above and the application of different intervention methods, metabolomic techniques (DI-MS/GC-MS/LC-MS with SPE separation and ¹³C labelled substrate), transcriptomics and bisulphite sequencing methods, it would be possible to improve our understanding and further characterise the complex interactions between metabolites and genes involving in the systematic biological networks and their perturbation in the adipose tissue during the processes of obesity and aging.

References

1. World Health Organization., *Global status report on noncommunicable diseases*. 2014, World Health Organization: Geneva, Switzerland.
2. Bevilacqua, S., et al., *Operation of Randle's cycle in patients with NIDDM*. *Diabetes*, 1990. **39**(3): p. 383-9.
3. Bell, G.I. and K.S. Polonsky, *Diabetes mellitus and genetically programmed defects in beta-cell function*. *Nature*, 2001. **414**(6865): p. 788-91.
4. Poole, R. and C.D. Byrne, *The metabolic syndrome and type 2 diabetes*. *Minerva endocrinologica*, 2005. **30**(3): p. 139-159.
5. Stenvinkel, P., *Obesity--a disease with many aetiologies disguised in the same oversized phenotype: has the overeating theory failed?* *Nephrol Dial Transplant*, 2015. **30**(10): p. 1656-64.
6. Prieto-Hontoria, P.L., et al., *Role of obesity-associated dysfunctional adipose tissue in cancer: a molecular nutrition approach*. *Biochim Biophys Acta*, 2011. **1807**(6): p. 664-78.
7. Manning, A.K., et al., *A genome-wide approach accounting for body mass index identifies genetic variants influencing fasting glycemc traits and insulin resistance*. *Nat Genet*, 2012. **44**(6): p. 659-69.
8. Heinonen, S., et al., *Adipocyte morphology and implications for metabolic derangements in acquired obesity*. *Int J Obes (Lond)*, 2014. **38**(11): p. 1423-31.
9. Suzuki, K., et al., *The role of gut hormones and the hypothalamus in appetite regulation*. *Endocr J*, 2010. **57**(5): p. 359-72.
10. Lopaschuk, G.D., J.R. Ussher, and J.S. Jaswal, *Targeting intermediary metabolism in the hypothalamus as a mechanism to regulate appetite*. *Pharmacol Rev*, 2010. **62**(2): p. 237-64.
11. Neary, N.M., A.P. Goldstone, and S.R. Bloom, *Appetite regulation: from the gut to the hypothalamus*. *Clin Endocrinol (Oxf)*, 2004. **60**(2): p. 153-60.
12. Henry, B.A., *Links between the appetite regulating systems and the neuroendocrine hypothalamus: lessons from the sheep*. *J Neuroendocrinol*, 2003. **15**(7): p. 697-709.
13. Lira, L.A., et al., *Perinatal undernutrition increases meal size and neuronal activation of the nucleus of the solitary tract in response to feeding stimulation in adult rats*. *Int J Dev Neurosci*, 2014. **38**: p. 23-9.
14. Uchoa, E.T., et al., *Oxytocin projections to the nucleus of the solitary tract contribute to the increased meal-related satiety responses in primary adrenal insufficiency*. *Exp Physiol*, 2013. **98**(10): p. 1495-504.
15. Emond, M., G.J. Schwartz, and T.H. Moran, *Meal-related stimuli differentially induce c-Fos activation in the nucleus of the solitary tract*. *Am J Physiol Regul Integr Comp Physiol*, 2001. **280**(5): p. R1315-21.
16. Mansbach, C.M., 2nd and F. Gorelick, *Development and physiological regulation of intestinal lipid absorption. II. Dietary lipid absorption, complex lipid synthesis, and the intracellular packaging and secretion of chylomicrons*. *Am J Physiol Gastrointest Liver Physiol*, 2007. **293**(4): p. G645-50.
17. Gofman, J.W., et al., *Blood lipids and human atherosclerosis*. *Circulation*, 1950. **2**(2): p. 161-78.
18. Garcia-Rios, A., et al., *LDL and HDL subfractions, dysfunctional HDL: treatment options*. *Curr Pharm Des*, 2014. **20**(40): p. 6249-55.
19. Cho, H.P., M.T. Nakamura, and S.D. Clarke, *Cloning, expression, and nutritional regulation of the mammalian Delta-6 desaturase*. *Journal of Biological Chemistry*, 1999. **274**(1): p. 471-477.
20. Ntambi, J.M., *The Regulation of Stearoyl-Coa Desaturase (Scd)*. *Progress in Lipid Research*, 1995. **34**(2): p. 139-150.
21. Tang, C.R., et al., *Regulation of human Delta-6 desaturase gene transcription: identification of a functional direct repeat-1 element*. *Journal of Lipid Research*, 2003. **44**(4): p. 686-695.

22. Bessesen, D.H., S.H. Vensor, and M.R. Jackman, *Trafficking of dietary oleic, linolenic, and stearic acids in fasted or fed lean rats*. American Journal of Physiology-Endocrinology and Metabolism, 2000. **278**(6): p. E1124-E1132.
23. Brownsey, R.W., et al., *Regulation of acetyl-CoA carboxylase*. Biochem Soc Trans, 2006. **34**(Pt 2): p. 223-7.
24. Harwood, H.J., Jr., *Acetyl-CoA carboxylase inhibition for the treatment of metabolic syndrome*. Curr Opin Investig Drugs, 2004. **5**(3): p. 283-9.
25. Kim, K.H. and H.J. Tae, *Pattern and regulation of acetyl-CoA carboxylase gene expression*. J Nutr, 1994. **124**(8 Suppl): p. 1273S-1283S.
26. *Rates of synthesis and degradation of hepatic acetyl CoA carboxylase in fed, fasted, fasted-refed, and diabetic rats*. Nutr Rev, 1971. **29**(7): p. 167-70.
27. Sanders, F.W. and J.L. Griffin, *De novo lipogenesis in the liver in health and disease: more than just a shunting yard for glucose*. Biol Rev Camb Philos Soc, 2016. **91**(2): p. 452-68.
28. Hardie, D.G., *Regulation of fatty acid synthesis via phosphorylation of acetyl-CoA carboxylase*. Prog Lipid Res, 1989. **28**(2): p. 117-46.
29. Kim, K.H., et al., *Role of reversible phosphorylation of acetyl-CoA carboxylase in long-chain fatty acid synthesis*. FASEB J, 1989. **3**(11): p. 2250-6.
30. Griffin, M.J. and H.S. Sul, *Insulin regulation of fatty acid synthase gene transcription: roles of USF and SREBP-1c*. IUBMB Life, 2004. **56**(10): p. 595-600.
31. Smith, S., *The animal fatty acid synthase: one gene, one polypeptide, seven enzymes*. FASEB J, 1994. **8**(15): p. 1248-59.
32. Goodridge, A.G., *Regulation of the gene for fatty acid synthase*. Fed Proc, 1986. **45**(9): p. 2399-405.
33. Sul, H.S., et al., *Regulation of the fatty acid synthase promoter by insulin*. J Nutr, 2000. **130**(2S Suppl): p. 315S-320S.
34. Shpilka, T., et al., *Fatty acid synthase is preferentially degraded by autophagy upon nitrogen starvation in yeast*. Proc Natl Acad Sci U S A, 2015. **112**(5): p. 1434-9.
35. Borer, K.T., *Counterregulation of insulin by leptin as key component of autonomic regulation of body weight*. World J Diabetes, 2014. **5**(5): p. 606-29.
36. Shimano, H., *[SREBP-1c and Elovl6 as Targets for Obesity-related Disorders]*. Yakugaku Zasshi, 2015. **135**(9): p. 1003-9.
37. Carobbio, S., et al., *Adaptive changes of the Insig1/SREBP1/SCD1 set point help adipose tissue to cope with increased storage demands of obesity*. Diabetes, 2013. **62**(11): p. 3697-708.
38. Hagen, R.M., S. Rodriguez-Cuenca, and A. Vidal-Puig, *An allostatic control of membrane lipid composition by SREBP1*. FEBS Lett, 2010. **584**(12): p. 2689-98.
39. Walker, A.K., et al., *A conserved SREBP-1/phosphatidylcholine feedback circuit regulates lipogenesis in metazoans*. Cell, 2011. **147**(4): p. 840-52.
40. Pietilainen, K.H., et al., *Association of lipidome remodeling in the adipocyte membrane with acquired obesity in humans*. PLoS Biol, 2011. **9**(6): p. e1000623.
41. Lim, H.Y., et al., *Phospholipid homeostasis regulates lipid metabolism and cardiac function through SREBP signaling in Drosophila*. Genes Dev, 2011. **25**(2): p. 189-200.
42. Garg, M.L., A.M. Snoswell, and J.R. Sabine, *Influence of dietary cholesterol on desaturase enzymes of rat liver microsomes*. Progress in Lipid Research, 1986. **25**(0): p. 639-644.
43. Garg, M.L., et al., *Dietary cholesterol and/or n - 3 fatty acid modulate Δ9-desaturase activity in rat liver microsomes*. Biochimica et Biophysica Acta (BBA) - Lipids and Lipid Metabolism, 1988. **962**(3): p. 330-336.
44. Landau, J.M., A. Sekowski, and M.W. Hamm, *Dietary cholesterol and the activity of stearyl CoA desaturase in rats: Evidence for an indirect regulatory effect*. Biochimica Et Biophysica Acta-Lipids and Lipid Metabolism, 1997. **1345**(3): p. 349-357.

45. Peluffo, R.O., A.M. Nervi, and R.R. Brenner, *Linoleic-Acid Desaturation Activity of Liver-Microsomes of Essential Fatty-Acid Deficient and Sufficient Rats*. *Biochimica Et Biophysica Acta*, 1976. **441**(1): p. 25-31.
46. Holloway, C.T. and P.W. Holloway, *Stearyl coenzyme A desaturase activity in mouse liver microsomes of varying lipid composition*. *Archives of Biochemistry and Biophysics*, 1975. **167**(2): p. 496-504.
47. Ntambi, J.M., A.M. Sessler, and T. Takova, *A model cell line to study regulation of stearyl-CoA desaturase gene 1 expression by insulin and polyunsaturated fatty acids*. *Biochemical and Biophysical Research Communications*, 1996. **220**(3): p. 990-995.
48. Nakamura, M.T. and T.Y. Nara, *Structure, function, and dietary regulation of Delta 6, Delta 5, and Delta 9 desaturases*. *Annual Review of Nutrition*, 2004. **24**: p. 345-376.
49. Sun, H., et al., *The effect of LXRA, ChREBP and Elovl6 in liver and white adipose tissue on medium- and long-chain fatty acid diet-induced insulin resistance*. *Diabetes Res Clin Pract*, 2013. **102**(3): p. 183-92.
50. Ament, Z., et al., *PPAR-pan activation induces hepatic oxidative stress and lipidomic remodelling*. *Free Radic Biol Med*, 2015.
51. Sanders, F.W. and J.L. Griffin, *De novo lipogenesis in the liver in health and disease: more than just a shunting yard for glucose*. *Biol Rev Camb Philos Soc*, 2015.
52. Coleman, R.A. and D.P. Lee, *Enzymes of triacylglycerol synthesis and their regulation*. *Prog Lipid Res*, 2004. **43**(2): p. 134-76.
53. Coleman, R.A., T.M. Lewin, and D.M. Muoio, *Physiological and nutritional regulation of enzymes of triacylglycerol synthesis*. *Annu Rev Nutr*, 2000. **20**: p. 77-103.
54. Hama, S., C. Ogino, and A. Kondo, *Enzymatic synthesis and modification of structured phospholipids: recent advances in enzyme preparation and biocatalytic processes*. *Appl Microbiol Biotechnol*, 2015. **99**(19): p. 7879-91.
55. Tata, J.R., *Co-ordinated synthesis of membrane phospholipids with the formation of ribosomes and accelerated protein synthesis during growth and development*. *Biochem Soc Symp*, 1972(35): p. 333-46.
56. Baer, E., *From the Trioses To the Synthesis of Natural Phospholipids: A Research Trial of Forty Years*. *J Am Oil Chem Soc*, 1965. **42**: p. 257-66.
57. Ahmadian, M., Y. Wang, and H.S. Sul, *Lipolysis in adipocytes*. *Int J Biochem Cell Biol*, 2010. **42**(5): p. 555-9.
58. Chilliard, Y., et al., *A review of nutritional and physiological factors affecting goat milk lipid synthesis and lipolysis*. *J Dairy Sci*, 2003. **86**(5): p. 1751-70.
59. Coppack, S.W., M.D. Jensen, and J.M. Miles, *In vivo regulation of lipolysis in humans*. *J Lipid Res*, 1994. **35**(2): p. 177-93.
60. Meisner, H. and J.R. Carter, Jr., *Regulation of lipolysis in adipose tissue*. *Horiz Biochem Biophys*, 1977. **4**: p. 91-129.
61. Morigny, P., et al., *Adipocyte lipolysis and insulin resistance*. *Biochimie*, 2016. **125**: p. 259-66.
62. Ogasawara, J., et al., *The Molecular Mechanism Underlying Continuous Exercise Training-Induced Adaptive Changes of Lipolysis in White Adipose Cells*. *J Obes*, 2015. **2015**: p. 473430.
63. Bolsoni-Lopes, A. and M.I. Alonso-Vale, *Lipolysis and lipases in white adipose tissue - An update*. *Arch Endocrinol Metab*, 2015. **59**(4): p. 335-42.
64. Fruhbeck, G., et al., *Regulation of adipocyte lipolysis*. *Nutr Res Rev*, 2014. **27**(1): p. 63-93.
65. Stryer, L., J.M. Berg, and J.L. Tymoczko, *Biochemistry (6th ed.)*. 2007, W.H. Freeman: San Francisco. p. 625-626.
66. Salway, J.G., *Medical Biochemistry at a Glance*. 2006, Wiley. p. 50.
67. Baes, M. and P.P. Van Veldhoven, *Mouse models for peroxisome biogenesis defects and beta-oxidation enzyme deficiencies*. *Biochim Biophys Acta*, 2012. **1822**(9): p. 1489-500.
68. Reddy, J.K. and T. Hashimoto, *Peroxisomal beta-oxidation and peroxisome proliferator-activated receptor alpha: an adaptive metabolic system*. *Annu Rev Nutr*, 2001. **21**: p. 193-230.

69. Latruffe, N., et al., *Regulation of the peroxisomal beta-oxidation-dependent pathway by peroxisome proliferator-activated receptor alpha and kinases*. *Biochem Pharmacol*, 2000. **60**(8): p. 1027-32.
70. Dreyer, C., et al., *Positive regulation of the peroxisomal beta-oxidation pathway by fatty acids through activation of peroxisome proliferator-activated receptors (PPAR)*. *Biol Cell*, 1993. **77**(1): p. 67-76.
71. Aoyama, T. and R. Sato, *High pressure liquid chromatography methods for separation of omega- and (omega-1)-hydroxy fatty acids: their applications to microsomal fatty acid omega-oxidation*. *Anal Biochem*, 1988. **170**(1): p. 73-82.
72. Nilsson, A., et al., *Studies on the interrelated stimulation of microsomal omega-oxidation and peroxisomal beta-oxidation in rat liver with a partially hydrogenated fish oil diet*. *Biochim Biophys Acta*, 1987. **920**(2): p. 114-9.
73. Hare, W.R. and K.W. Wahle, *The effects of physiological state and plane of nutrition on the concentrations of microsomal cytochromes and the omega-oxidation of fatty acids in various tissues of the sheep (Ovis aries)*. *Int J Biochem*, 1985. **17**(4): p. 455-62.
74. Wada, F., et al., *Participation of the microsomal electron transport system involving cytochrome P-450 in omega-oxidation of fatty acids*. *Biochim Biophys Acta*, 1968. **162**(4): p. 518-24.
75. Bartelt, A., M. Merkel, and J. Heeren, *A new, powerful player in lipoprotein metabolism: brown adipose tissue*. *J Mol Med (Berl)*, 2012. **90**(8): p. 887-93.
76. Zechner, R., et al., *The role of lipoprotein lipase in adipose tissue development and metabolism*. *Int J Obes Relat Metab Disord*, 2000. **24 Suppl 4**: p. S53-6.
77. Cryer, A., *Lipoprotein lipase and the uptake of lipids by adipose cells during development*. *Reprod Nutr Dev*, 1985. **25**(1B): p. 255-70.
78. Choudhury, R.P., J.M. Lee, and D.R. Greaves, *Mechanisms of disease: macrophage-derived foam cells emerging as therapeutic targets in atherosclerosis*. *Nat Clin Pract Cardiovasc Med*, 2005. **2**(6): p. 309-15.
79. Wang, J., et al., *Daintain/AIF-1 plays roles in coronary heart disease via affecting the blood composition and promoting macrophage uptake and foam cell formation*. *Cell Physiol Biochem*, 2013. **32**(1): p. 121-6.
80. Ivan, E., et al., *Expansive arterial remodeling is associated with increased neointimal macrophage foam cell content: the murine model of macrophage-rich carotid artery lesions*. *Circulation*, 2002. **105**(22): p. 2686-91.
81. Yano, T., et al., *Atherosclerotic plaques composed of a large core of foam cells covered with thin fibrous caps in twice-injured carotid arterial specimens obtained from high cholesterol diet-fed rabbits*. *J Atheroscler Thromb*, 2000. **7**(2): p. 83-90.
82. Eom, M., K.L. Hudkins, and C.E. Alpers, *Foam cells and the pathogenesis of kidney disease*. *Curr Opin Nephrol Hypertens*, 2015. **24**(3): p. 245-51.
83. Angelovich, T.A., A.C. Hearps, and A. Jaworowski, *Inflammation-induced foam cell formation in chronic inflammatory disease*. *Immunol Cell Biol*, 2015. **93**(8): p. 683-93.
84. Bhupathiraju, S.N. and F.B. Hu, *Epidemiology of Obesity and Diabetes and Their Cardiovascular Complications*. *Circ Res*, 2016. **118**(11): p. 1723-35.
85. Masuo, K., et al., *Cardiovascular and renal complications of type 2 diabetes in obesity: role of sympathetic nerve activity and insulin resistance*. *Curr Diabetes Rev*, 2010. **6**(2): p. 58-67.
86. Ohvo-Rekila, H., et al., *Cholesterol interactions with phospholipids in membranes*. *Prog Lipid Res*, 2002. **41**(1): p. 66-97.
87. Incardona, J.P. and S. Eaton, *Cholesterol in signal transduction*. *Curr Opin Cell Biol*, 2000. **12**(2): p. 193-203.
88. Payne, A.H. and D.B. Hales, *Overview of steroidogenic enzymes in the pathway from cholesterol to active steroid hormones*. *Endocr Rev*, 2004. **25**(6): p. 947-70.

89. Marinier, E., et al., *Contribution of the shunt pathway of mevalonate metabolism to the regulation of cholesterol synthesis in rat liver*. J Biol Chem, 1987. **262**(35): p. 16936-40.
90. Pool, F., et al., *A mathematical model of the mevalonate cholesterol biosynthesis pathway*. J Theor Biol, 2018. **443**: p. 157-176.
91. Proulx, P., et al., *Studies on the mechanism of cholesterol uptake and on the effects of bile salts on this uptake by brush-border membranes isolated from rabbit small intestine*. Biochim Biophys Acta, 1984. **778**(3): p. 586-93.
92. Gallo-Torres, H.E., O.N. Miller, and J.G. Hamilton, *A comparison of the effects of bile salts on the absorption of cholesterol from the intestine of the rat*. Biochim Biophys Acta, 1969. **176**(3): p. 605-15.
93. Suzuki, R., *Specific requirements of bile salts for absorption of cholesterol from the intestine*. Keio J Med, 1968. **17**(3): p. 169-87.
94. Wang, X., (PhD thesis) *Defining the metabolic abnormalities underlying diabetic cardiomyopathy*, in Department of Biochemistry. 2013, University of Cambridge: Cambridge.
95. Wang, X., et al., *Comprehensive Metabolic Profiling of Age-Related Mitochondrial Dysfunction in the High-Fat-Fed ob/ob Mouse Heart*. J Proteome Res, 2015. **14**(7): p. 2849-62.
96. Doenst, T., et al., *Decreased rates of substrate oxidation ex vivo predict the onset of heart failure and contractile dysfunction in rats with pressure overload*. Cardiovasc Res, 2010. **86**(3): p. 461-70.
97. Young, M.E., et al., *Impaired long-chain fatty acid oxidation and contractile dysfunction in the obese Zucker rat heart*. Diabetes, 2002. **51**(8): p. 2587-95.
98. Goodwin, G.W. and H. Taegtmeyer, *Regulation of fatty acid oxidation of the heart by MCD and ACC during contractile stimulation*. Am J Physiol, 1999. **277**(4): p. E772-7.
99. Chu, Y., *A Metabolomics Investigation of Non-alcoholic Fatty Liver Disease to Define Mechanisms of Induction and Pathology*. PhD dissertation, in Department of Biochemistry. 2014, University of Cambridge: Cambridge, U.K.
100. Starley, B.Q., C.J. Calcagno, and S.A. Harrison, *Nonalcoholic fatty liver disease and hepatocellular carcinoma: a weighty connection*. Hepatology, 2010. **51**(5): p. 1820-32.
101. Koppen, A. and E. Kalkhoven, *Brown vs white adipocytes: The PPAR gamma coregulator story*. Febs Letters, 2010. **584**(15): p. 3250-3259.
102. Rothwell, N.J. and M.J. Stock, *Effects of Age on Diet-Induced Thermogenesis and Brown Adipose-Tissue Metabolism in the Rat*. International Journal of Obesity, 1983. **7**(6): p. 583-589.
103. Commins, S.P., et al., *Induction of uncoupling protein expression in brown and white adipose tissue by leptin*. Endocrinology, 1999. **140**(1): p. 292-300.
104. Cinti, S., et al., *Immunohistochemical localization of leptin and uncoupling protein in white and brown adipose tissue*. Endocrinology, 1997. **138**(2): p. 797-804.
105. Goossens, G.H., *The role of adipose tissue dysfunction in the pathogenesis of obesity-related insulin resistance*. Physiology & Behavior, 2008. **94**(2): p. 206-218.
106. Lettner, A. and M. Roden, *Ectopic fat and insulin resistance*. Curr Diab Rep, 2008. **8**(3): p. 185-91.
107. Goossens, G.H., *The role of adipose tissue dysfunction in the pathogenesis of obesity-related insulin resistance*. Physiol Behav, 2008. **94**(2): p. 206-18.
108. Koyama, K., et al., *Tissue triglycerides, insulin resistance, and insulin production: implications for hyperinsulinemia of obesity*. American Journal of Physiology-Endocrinology and Metabolism, 1997. **273**(4): p. E708-E713.
109. Qatanani, M. and M.A. Lazar, *Mechanisms of obesity-associated insulin resistance: many choices on the menu*. Genes & Development, 2007. **21**(12): p. 1443-1455.
110. Klimcakova, E., et al., *Adipokines and dietary interventions in human obesity*. Obes Rev, 2010. **11**(6): p. 446-56.
111. Gnacinska, M., et al., *Role of adipokines in complications related to obesity: a review*. Adv Med Sci, 2009. **54**(2): p. 150-7.

112. Ahima, R.S. and S.Y. Osei, *Adipokines in obesity*. Front Horm Res, 2008. **36**: p. 182-97.
113. Antuna-Puente, B., et al., *Adipokines: the missing link between insulin resistance and obesity*. Diabetes Metab, 2008. **34**(1): p. 2-11.
114. Frayn, K.N., P. Arner, and H. Yki-Jarvinen, *Fatty acid metabolism in adipose tissue, muscle and liver in health and disease*. Essays in Biochemistry, Vol 42, 2006. **42**: p. 89-103.
115. Shrago, E., J.A. Glennon, and E.S. Gordon, *Comparative Aspects of Lipogenesis in Mammalian Tissues*. Metabolism-Clinical and Experimental, 1971. **20**(1): p. 54-&.
116. Kim, S. and N. Moustaid-Moussa, *Secretory, endocrine and autocrine/paracrine function of the adipocyte*. Journal of Nutrition, 2000. **130**(12): p. 3110s-3115s.
117. Ronti, T., G. Lupattelli, and E. Mannarino, *The endocrine function of adipose tissue: an update*. Clinical Endocrinology, 2006. **64**(4): p. 355-365.
118. Farooqi, I.S. and S. O'Rahilly, *Leptin: a pivotal regulator of human energy homeostasis*. American Journal of Clinical Nutrition, 2009. **89**(3): p. 980s-984s.
119. Makki, K., P. Froguel, and I. Wolowczuk, *Adipose tissue in obesity-related inflammation and insulin resistance: cells, cytokines, and chemokines*. ISRN Inflamm, 2013. **2013**: p. 139239.
120. Sun, S., et al., *Mechanisms of inflammatory responses in obese adipose tissue*. Annu Rev Nutr, 2012. **32**: p. 261-86.
121. Berg, A.H. and P.E. Scherer, *Adipose tissue, inflammation, and cardiovascular disease*. Circ Res, 2005. **96**(9): p. 939-49.
122. Sarantopoulos, C.N., et al., *Elucidating the Preadipocyte and Its Role in Adipocyte Formation: a Comprehensive Review*. Stem Cell Rev, 2018. **14**(1): p. 27-42.
123. Nam, S.Y. and P.E. Lobie, *The mechanism of effect of growth hormone on preadipocyte and adipocyte function*. Obes Rev, 2000. **1**(2): p. 73-86.
124. Sorisky, A., *From preadipocyte to adipocyte: differentiation-directed signals of insulin from the cell surface to the nucleus*. Crit Rev Clin Lab Sci, 1999. **36**(1): p. 1-34.
125. Lafontan, M., *Advances in adipose tissue metabolism*. International Journal of Obesity, 2008. **32**: p. S39-S51.
126. Poirier, Y., et al., *Peroxisomal beta-oxidation--a metabolic pathway with multiple functions*. Biochim Biophys Acta, 2006. **1763**(12): p. 1413-26.
127. Gilham, D. and R. Lehner, *The physiological role of triacylglycerol hydrolase in lipid metabolism*. Rev Endocr Metab Disord, 2004. **5**(4): p. 303-9.
128. Dolinsky, V.W., et al., *Triacylglycerol hydrolase: role in intracellular lipid metabolism*. Cell Mol Life Sci, 2004. **61**(13): p. 1633-51.
129. Grabner, G.F., et al., *Monoglyceride lipase as a drug target: At the crossroads of arachidonic acid metabolism and endocannabinoid signaling*. Pharmacol Ther, 2017. **175**: p. 35-46.
130. Scalvini, L., D. Piomelli, and M. Mor, *Monoglyceride lipase: Structure and inhibitors*. Chem Phys Lipids, 2016. **197**: p. 13-24.
131. Large, V., et al., *Metabolism of lipids in human white adipocyte*. Diabetes Metab, 2004. **30**(4): p. 294-309.
132. Frayn, K.N., *Adipose tissue and the insulin resistance syndrome*. Proceedings of the Nutrition Society, 2001. **60**(3): p. 375-380.
133. Savage, D.B., K.F. Petersen, and G.I. Shulman, *Disordered lipid metabolism and the pathogenesis of insulin resistance*. Physiological Reviews, 2007. **87**(2): p. 507-520.
134. Shoelson, S.E., J. Lee, and A.B. Goldfine, *Inflammation and insulin resistance*. Journal of Clinical Investigation, 2006. **116**(7): p. 1793-1801.
135. Yonezawa, T., et al., *Regulation of hormone-sensitive lipase expression by saturated fatty acids and hormones in bovine mammary epithelial cells*. Biochem Biophys Res Commun, 2008. **376**(1): p. 36-9.
136. Bartelt, A. and J. Heeren, *Adipose tissue browning and metabolic health*. Nat Rev Endocrinol, 2014. **10**(1): p. 24-36.

137. Nedergaard, J., et al., *Norepinephrine as a morphogen?: its unique interaction with brown adipose tissue*. *Int J Dev Biol*, 1995. **39**(5): p. 827-37.
138. Giralt, M., M. Cairo, and F. Villarroya, *Hormonal and nutritional signalling in the control of brown and beige adipose tissue activation and recruitment*. *Best Pract Res Clin Endocrinol Metab*, 2016. **30**(4): p. 515-525.
139. Algire, C., D. Medrikova, and S. Herzig, *White and brown adipose stem cells: from signaling to clinical implications*. *Biochim Biophys Acta*, 2013. **1831**(5): p. 896-904.
140. Cannon, B., et al., *Signal transduction in brown adipose tissue recruitment: noradrenaline and beyond*. *Int J Obes Relat Metab Disord*, 1996. **20 Suppl 3**: p. S36-42.
141. Unamuno, X., et al., *Adipokine dysregulation and adipose tissue inflammation in human obesity*. *Eur J Clin Invest*, 2018. **48**(9): p. e12997.
142. Shah, D., et al., *Obesity-induced adipokine imbalance impairs mouse pulmonary vascular endothelial function and primes the lung for injury*. *Sci Rep*, 2015. **5**: p. 11362.
143. Wei, Z., et al., *C1q/TNF-related protein-12 (CTRP12), a novel adipokine that improves insulin sensitivity and glycemic control in mouse models of obesity and diabetes*. *J Biol Chem*, 2012. **287**(13): p. 10301-15.
144. Boucher, J., et al., *Adipokine expression profile in adipocytes of different mouse models of obesity*. *Horm Metab Res*, 2005. **37**(12): p. 761-7.
145. Iwasa, A., et al., *Aromatase controls Sjogren syndrome-like lesions through monocyte chemotactic protein-1 in target organ and adipose tissue-associated macrophages*. *Am J Pathol*, 2015. **185**(1): p. 151-61.
146. Gao, Z., et al., *Sirtuin 1 (SIRT1) protein degradation in response to persistent c-Jun N-terminal kinase 1 (JNK1) activation contributes to hepatic steatosis in obesity*. *J Biol Chem*, 2011. **286**(25): p. 22227-34.
147. Pal, M., M.A. Febbraio, and G.I. Lancaster, *The roles of c-Jun NH2-terminal kinases (JNKs) in obesity and insulin resistance*. *J Physiol*, 2016. **594**(2): p. 267-79.
148. Olszanecka-Glinianowicz, M., et al., *Serum concentrations of nitric oxide, tumor necrosis factor (TNF)-alpha and TNF soluble receptors in women with overweight and obesity*. *Metabolism*, 2004. **53**(10): p. 1268-73.
149. Francisco, V., et al., *Obesity, Fat Mass and Immune System: Role for Leptin*. *Front Physiol*, 2018. **9**: p. 640.
150. Perez-Perez, A., et al., *Role of leptin as a link between metabolism and the immune system*. *Cytokine Growth Factor Rev*, 2017. **35**: p. 71-84.
151. Gong, J., et al., *Adipose tissue palmitoleic acid and obesity in humans: does it behave as a lipokine?* *Am J Clin Nutr*, 2011. **93**(1): p. 186-91.
152. Dennis, E.A. and P.C. Norris, *Eicosanoid storm in infection and inflammation*. *Nat Rev Immunol*, 2015. **15**(8): p. 511-23.
153. Valenzuela, R. and L.A. Videla, *The importance of the long-chain polyunsaturated fatty acid n-6/n-3 ratio in development of non-alcoholic fatty liver associated with obesity*. *Food Funct*, 2011. **2**(11): p. 644-8.
154. Roberts, L.D., A. Koulman, and J.L. Griffin, *Towards metabolic biomarkers of insulin resistance and type 2 diabetes: progress from the metabolome*. *Lancet Diabetes Endocrinol*, 2014. **2**(1): p. 65-75.
155. Chow, L.S., et al., *Estimated plasma stearoyl co-A desaturase-1 activity and risk of incident diabetes: the Atherosclerosis Risk in Communities (ARIC) study*. *Metabolism*, 2013. **62**(1): p. 100-8.
156. Rhee, E.P., et al., *Lipid profiling identifies a triacylglycerol signature of insulin resistance and improves diabetes prediction in humans*. *J Clin Invest*, 2011. **121**(4): p. 1402-11.
157. Morcillo, S., et al., *ELOVL6 genetic variation is related to insulin sensitivity: a new candidate gene in energy metabolism*. *PLoS One*, 2011. **6**(6): p. e21198.

158. Mozaffarian, D., et al., *Circulating palmitoleic acid and risk of metabolic abnormalities and new-onset diabetes*. Am J Clin Nutr, 2010. **92**(6): p. 1350-8.
159. Kotronen, A., et al., *Serum saturated fatty acids containing triacylglycerols are better markers of insulin resistance than total serum triacylglycerol concentrations*. Diabetologia, 2009. **52**(4): p. 684-90.
160. Hodge, A.M., et al., *Plasma phospholipid and dietary fatty acids as predictors of type 2 diabetes: interpreting the role of linoleic acid*. Am J Clin Nutr, 2007. **86**(1): p. 189-97.
161. Pamplona, R., *Membrane phospholipids, lipoxidative damage and molecular integrity: a causal role in aging and longevity*. Biochim Biophys Acta, 2008. **1777**(10): p. 1249-62.
162. Calhoun, E.A., J. Ro, and J.B. Williams, *Perspectives on the membrane fatty acid unsaturation/pacemaker hypotheses of metabolism and aging*. Chem Phys Lipids, 2015. **191**: p. 48-60.
163. Huang, H.Y., et al., *Effects of vitamin C and vitamin E on in vivo lipid peroxidation: results of a randomized controlled trial*. Am J Clin Nutr, 2002. **76**(3): p. 549-55.
164. Hulbert, A.J., *On the importance of fatty acid composition of membranes for aging*. J Theor Biol, 2005. **234**(2): p. 277-88.
165. Hulbert, A.J., *Explaining longevity of different animals: is membrane fatty acid composition the missing link?* Age (Dordr), 2008. **30**(2-3): p. 89-97.
166. Pamplona, R., G. Barja, and M. Portero-Otin, *Membrane fatty acid unsaturation, protection against oxidative stress, and maximum life span: a homeoviscous-longevity adaptation?* Ann N Y Acad Sci, 2002. **959**: p. 475-90.
167. Naudi, A., et al., *Membrane lipid unsaturation as physiological adaptation to animal longevity*. Front Physiol, 2013. **4**: p. 372.
168. Tsuda, K. and I. Nishio, *Membrane fluidity and hypertension*. American Journal of Hypertension, 2003. **16**(3): p. 259-261.
169. McElhaneey, R.N., *The effect of alterations in the physical state of the membrane lipids on the ability of Acholeplasma laidlawii B to grow at various temperatures*. Journal of Molecular Biology, 1974. **84**(1): p. 145-157.
170. Oldfield, E. and D. Chapman, *Dynamics of lipids in membranes: Heterogeneity and the role of cholesterol*. FEBS Letters, 1972. **23**(3): p. 285-297.
171. Vazquez, C.M., et al., *Developmental changes in glucose transport, lipid composition, and fluidity of jejunal BBM*. Am J Physiol, 1997. **273**(3 Pt 2): p. R1086-93.
172. Tsuda, K., et al., *Hyperinsulinemia is a determinant of membrane fluidity of erythrocytes in essential hypertension*. Am J Hypertens, 2001. **14**(5 Pt 1): p. 419-23.
173. Helge, J.W. and F. Dela, *Effect of training on muscle triacylglycerol and structural lipids: a relation to insulin sensitivity?* Diabetes, 2003. **52**(8): p. 1881-7.
174. Senault, C., et al., *Relation between membrane phospholipid composition, fluidity and function in mitochondria of rat brown adipose tissue. Effect of thermal adaptation and essential fatty acid deficiency*. Biochim Biophys Acta, 1990. **1023**(2): p. 283-9.
175. Lopategi, A., et al., *Role of bioactive lipid mediators in obese adipose tissue inflammation and endocrine dysfunction*. Mol Cell Endocrinol, 2015.
176. Brenner, R.R., *Effect of unsaturated acids on membrane structure and enzyme kinetics*. Prog Lipid Res, 1984. **23**(2): p. 69-96.
177. Hulbert, A.J., L.A. Beard, and G.C. Grigg, *The exceptional longevity of an egg-laying mammal, the short-beaked echidna (Tachyglossus aculeatus) is associated with peroxidation-resistant membrane composition*. Exp Gerontol, 2008. **43**(8): p. 729-33.
178. Else, P.L., et al., *Molecular activity of Na⁺,K⁺-ATPase relates to the packing of membrane lipids*. Ann N Y Acad Sci, 2003. **986**: p. 525-6.
179. Else, P.L. and A.J. Hulbert, *Membranes as metabolic pacemakers*. Clin Exp Pharmacol Physiol, 2003. **30**(8): p. 559-64.

180. Wu, B.J., et al., *Molecular activity of Na(+)/K(+)-ATPase from different sources is related to the packing of membrane lipids*. J Exp Biol, 2001. **204**(Pt 24): p. 4271-80.
181. Hulbert, A.J. and P.L. Else, *Membranes as possible pacemakers of metabolism*. J Theor Biol, 1999. **199**(3): p. 257-74.
182. Quinn, P.J., *A lipid matrix model of membrane raft structure*. Prog Lipid Res, 2010. **49**(4): p. 390-406.
183. Wassall, S.R. and W. Stillwell, *Polyunsaturated fatty acid-cholesterol interactions: domain formation in membranes*. Biochim Biophys Acta, 2009. **1788**(1): p. 24-32.
184. Lucero, H.A. and P.W. Robbins, *Lipid rafts-protein association and the regulation of protein activity*. Arch Biochem Biophys, 2004. **426**(2): p. 208-24.
185. Shaikh, S.R., et al., *How polyunsaturated fatty acids modify molecular organization in membranes: insight from NMR studies of model systems*. Biochim Biophys Acta, 2015. **1848**(1 Pt B): p. 211-9.
186. Wassall, S.R., et al., *Order from disorder, corralling cholesterol with chaotic lipids. The role of polyunsaturated lipids in membrane raft formation*. Chem Phys Lipids, 2004. **132**(1): p. 79-88.
187. Fujii, T., et al., *K+-Cl- Cotransporter-3a Up-regulates Na+,K+-ATPase in Lipid Rafts of Gastric Luminal Parietal Cells*. J Biol Chem, 2008. **283**(11): p. 6869-77.
188. Welker, P., et al., *Role of lipid rafts in membrane delivery of renal epithelial Na+-K+-ATPase, thick ascending limb*. Am J Physiol Regul Integr Comp Physiol, 2007. **292**(3): p. R1328-37.
189. Lingwood, D., G. Harauz, and J.S. Ballantyne, *Regulation of fish gill Na(+)-K(+)-ATPase by selective sulfatide-enriched raft partitioning during seawater adaptation*. J Biol Chem, 2005. **280**(44): p. 36545-50.
190. Furse, S., et al., *Synthesis of unsaturated phosphatidylinositol 4-phosphates and the effects of substrate unsaturation on SopB phosphatase activity*. Org Biomol Chem, 2015. **13**(7): p. 2001-11.
191. Yang, Q., et al., *Influence of the membrane lipid structure on signal processing via G protein-coupled receptors*. Mol Pharmacol, 2005. **68**(1): p. 210-7.
192. Epanand, R.M., et al., *Promotion of hexagonal phase formation and lipid mixing by fatty acids with varying degrees of unsaturation*. Chem Phys Lipids, 1991. **57**(1): p. 75-80.
193. Escriba, P.V., M. Sastre, and J.A. Garcia-Sevilla, *Disruption of cellular signaling pathways by daunomycin through destabilization of nonlamellar membrane structures*. Proc Natl Acad Sci U S A, 1995. **92**(16): p. 7595-9.
194. Vogler, O., et al., *The Gbetagamma dimer drives the interaction of heterotrimeric Gi proteins with nonlamellar membrane structures*. J Biol Chem, 2004. **279**(35): p. 36540-5.
195. Martinez, J., et al., *Membrane structure modulation, protein kinase C alpha activation, and anticancer activity of minerval*. Mol Pharmacol, 2005. **67**(2): p. 531-40.
196. Seddon, J.M., *Structure of the inverted hexagonal (HII) phase, and non-lamellar phase transitions of lipids*. Biochim Biophys Acta, 1990. **1031**(1): p. 1-69.
197. Hulbert, A.J., *Metabolism and longevity: is there a role for membrane fatty acids?* Integr Comp Biol, 2010. **50**(5): p. 808-17.
198. Kelly, M.A., et al., *Diet fatty acid profile, membrane composition and lifespan: an experimental study using the blowfly (Calliphora stygia)*. Mech Ageing Dev, 2014. **138**: p. 15-25.
199. Konarzewski, M. and A. Ksiazek, *Determinants of intra-specific variation in basal metabolic rate*. J Comp Physiol B, 2013. **183**(1): p. 27-41.
200. Valencak, T.G. and T. Ruf, *N-3 polyunsaturated fatty acids impair lifespan but have no role for metabolism*. Aging Cell, 2007. **6**(1): p. 15-25.
201. Battam, H., et al., *Chemical composition and tissue energy density of the cuttlefish (Sepia apama) and its assimilation efficiency by Diomedea albatrosses*. J Comp Physiol B, 2010. **180**(8): p. 1247-55.
202. Paula, S., et al., *Permeation of protons, potassium ions, and small polar molecules through phospholipid bilayers as a function of membrane thickness*. Biophys J, 1996. **70**(1): p. 339-48.

203. van Meer, G., D.R. Voelker, and G.W. Feigenson, *Membrane lipids: where they are and how they behave*. Nat Rev Mol Cell Biol, 2008. **9**(2): p. 112-24.
204. Guillou, H., et al., *The key roles of elongases and desaturases in mammalian fatty acid metabolism: Insights from transgenic mice*. Prog Lipid Res, 2010. **49**(2): p. 186-99.
205. Yamashita, A., et al., *Acyltransferases and transacylases that determine the fatty acid composition of glycerolipids and the metabolism of bioactive lipid mediators in mammalian cells and model organisms*. Prog Lipid Res, 2014. **53**: p. 18-81.
206. Tamura, K., et al., *Novel lipogenic enzyme ELOVL7 is involved in prostate cancer growth through saturated long-chain fatty acid metabolism*. Cancer Res, 2009. **69**(20): p. 8133-40.
207. Kitazawa, H., et al., *Development of a high-density assay for long-chain fatty acyl-CoA elongases*. Lipids, 2009. **44**(8): p. 765-73.
208. Agbaga, M.P., et al., *Role of Stargardt-3 macular dystrophy protein (ELOVL4) in the biosynthesis of very long chain fatty acids*. Proc Natl Acad Sci U S A, 2008. **105**(35): p. 12843-8.
209. Wang, Y., et al., *Tissue-specific, nutritional, and developmental regulation of rat fatty acid elongases*. J Lipid Res, 2005. **46**(4): p. 706-15.
210. Moon, Y.A., et al., *Identification of a mammalian long chain fatty acyl elongase regulated by sterol regulatory element-binding proteins*. J Biol Chem, 2001. **276**(48): p. 45358-66.
211. Tvrdik, P., et al., *Role of a new mammalian gene family in the biosynthesis of very long chain fatty acids and sphingolipids*. J Cell Biol, 2000. **149**(3): p. 707-18.
212. Leonard, A.E., et al., *Cloning of a human cDNA encoding a novel enzyme involved in the elongation of long-chain polyunsaturated fatty acids*. Biochem J, 2000. **350 Pt 3**: p. 765-70.
213. Oh, C.S., et al., *ELO2 and ELO3, homologues of the Saccharomyces cerevisiae ELO1 gene, function in fatty acid elongation and are required for sphingolipid formation*. J Biol Chem, 1997. **272**(28): p. 17376-84.
214. Goldberg, I., I. Shechter, and K. Bloch, *Fatty acyl-coenzyme A elongation in brain of normal and quaking mice*. Science, 1973. **182**(4111): p. 497-9.
215. Luthria, D.L. and H. Sprecher, *Studies to determine if rat liver contains multiple chain elongating enzymes*. Biochim Biophys Acta, 1997. **1346**(3): p. 221-30.
216. Chakravarthy, M.V., et al., *Identification of a physiologically relevant endogenous ligand for PPARalpha in liver*. Cell, 2009. **138**(3): p. 476-88.
217. Brown, D.A., *Lipid rafts, detergent-resistant membranes, and raft targeting signals*. Physiology (Bethesda), 2006. **21**: p. 430-9.
218. Matsuzaka, T., et al., *Cloning and characterization of a mammalian fatty acyl-CoA elongase as a lipogenic enzyme regulated by SREBPs*. J Lipid Res, 2002. **43**(6): p. 911-20.
219. Matsuzaka, T., et al., *Crucial role of a long-chain fatty acid elongase, Elovl6, in obesity-induced insulin resistance*. Nat Med, 2007. **13**(10): p. 1193-202.
220. Jakobsson, A., R. Westerberg, and A. Jacobsson, *Fatty acid elongases in mammals: their regulation and roles in metabolism*. Prog Lipid Res, 2006. **45**(3): p. 237-49.
221. Kaestner, K.H., et al., *Differentiation-induced gene expression in 3T3-L1 preadipocytes. A second differentially expressed gene encoding stearoyl-CoA desaturase*. J Biol Chem, 1989. **264**(25): p. 14755-61.
222. Ntambi, J.M., et al., *Differentiation-induced gene expression in 3T3-L1 preadipocytes. Characterization of a differentially expressed gene encoding stearoyl-CoA desaturase*. J Biol Chem, 1988. **263**(33): p. 17291-300.
223. Miyazaki, M., et al., *Identification and characterization of murine SCD4, a novel heart-specific stearoyl-CoA desaturase isoform regulated by leptin and dietary factors*. J Biol Chem, 2003. **278**(36): p. 33904-11.
224. Strittmatter, P., et al., *Purification and properties of rat liver microsomal stearyl coenzyme A desaturase*. Proc Natl Acad Sci U S A, 1974. **71**(11): p. 4565-9.

225. Zheng, Y., et al., *Scd3--a novel gene of the stearoyl-CoA desaturase family with restricted expression in skin*. Genomics, 2001. **71**(2): p. 182-91.
226. Zhang, L., et al., *Human stearoyl-CoA desaturase: alternative transcripts generated from a single gene by usage of tandem polyadenylation sites*. Biochem J, 1999. **340** (Pt 1): p. 255-64.
227. Wang, J., et al., *Characterization of HSCD5, a novel human stearoyl-CoA desaturase unique to primates*. Biochem Biophys Res Commun, 2005. **332**(3): p. 735-42.
228. Marquardt, A., et al., *cDNA cloning, genomic structure, and chromosomal localization of three members of the human fatty acid desaturase family*. Genomics, 2000. **66**(2): p. 175-83.
229. Blanchard, H., P. Legrand, and F. Pedrono, *Fatty Acid Desaturase 3 (Fads3) is a singular member of the Fads cluster*. Biochimie, 2011. **93**(1): p. 87-90.
230. Cho, H.P., M. Nakamura, and S.D. Clarke, *Cloning, expression, and fatty acid regulation of the human delta-5 desaturase*. J Biol Chem, 1999. **274**(52): p. 37335-9.
231. Cho, H.P., M.T. Nakamura, and S.D. Clarke, *Cloning, expression, and nutritional regulation of the mammalian Delta-6 desaturase*. J Biol Chem, 1999. **274**(1): p. 471-7.
232. Chu, K., et al., *Stearoyl-coenzyme A desaturase 1 deficiency protects against hypertriglyceridemia and increases plasma high-density lipoprotein cholesterol induced by liver X receptor activation*. Mol Cell Biol, 2006. **26**(18): p. 6786-98.
233. Dobrzyn, P., et al., *Stearoyl-CoA desaturase 1 deficiency increases fatty acid oxidation by activating AMP-activated protein kinase in liver*. Proc Natl Acad Sci U S A, 2004. **101**(17): p. 6409-14.
234. Lee, S.H., et al., *Lack of stearoyl-CoA desaturase 1 upregulates basal thermogenesis but causes hypothermia in a cold environment*. J Lipid Res, 2004. **45**(9): p. 1674-82.
235. Rahman, S.M., et al., *Stearoyl-CoA desaturase 1 deficiency increases insulin signaling and glycogen accumulation in brown adipose tissue*. Am J Physiol Endocrinol Metab, 2005. **288**(2): p. E381-7.
236. Rahman, S.M., et al., *Stearoyl-CoA desaturase 1 deficiency elevates insulin-signaling components and down-regulates protein-tyrosine phosphatase 1B in muscle*. Proc Natl Acad Sci U S A, 2003. **100**(19): p. 11110-5.
237. Sampath, H., et al., *Skin-specific deletion of stearoyl-CoA desaturase-1 alters skin lipid composition and protects mice from high fat diet-induced obesity*. J Biol Chem, 2009. **284**(30): p. 19961-73.
238. Miyazaki, M., F.E. Gomez, and J.M. Ntambi, *Lack of stearoyl-CoA desaturase-1 function induces a palmitoyl-CoA Delta6 desaturase and represses the stearoyl-CoA desaturase-3 gene in the preputial glands of the mouse*. J Lipid Res, 2002. **43**(12): p. 2146-54.
239. Aki, T., et al., *Molecular cloning and functional characterization of rat delta-6 fatty acid desaturase*. Biochem Biophys Res Commun, 1999. **255**(3): p. 575-9.
240. Park, W.J., et al., *An alternate pathway to long-chain polyunsaturates: the FADS2 gene product Delta8-desaturates 20:2n-6 and 20:3n-3*. J Lipid Res, 2009. **50**(6): p. 1195-202.
241. Stroud, C.K., et al., *Disruption of FADS2 gene in mice impairs male reproduction and causes dermal and intestinal ulceration*. J Lipid Res, 2009. **50**(9): p. 1870-80.
242. DeBose-Boyd, R.A. and J. Ye, *SREBPs in Lipid Metabolism, Insulin Signaling, and Beyond*. Trends Biochem Sci, 2018. **43**(5): p. 358-368.
243. Shimano, H. and R. Sato, *SREBP-regulated lipid metabolism: convergent physiology - divergent pathophysiology*. Nat Rev Endocrinol, 2017. **13**(12): p. 710-730.
244. Horton, J.D., J.L. Goldstein, and M.S. Brown, *SREBPs: transcriptional mediators of lipid homeostasis*. Cold Spring Harb Symp Quant Biol, 2002. **67**: p. 491-8.
245. Repa, J.J., et al., *Regulation of mouse sterol regulatory element-binding protein-1c gene (SREBP-1c) by oxysterol receptors, LXRalpha and LXRBeta*. Genes Dev, 2000. **14**(22): p. 2819-30.

246. Shimomura, I., Y. Bashmakov, and J.D. Horton, *Increased levels of nuclear SREBP-1c associated with fatty livers in two mouse models of diabetes mellitus*. J Biol Chem, 1999. **274**(42): p. 30028-32.
247. Goldstein, J.L. and M.S. Brown, *The clinical investigator: bewitched, bothered, and bewildered-but still beloved*. J Clin Invest, 1997. **99**(12): p. 2803-12.
248. Mastrocola, R., et al., *Accumulation of advanced glycation end-products and activation of the SCAP/SREBP Lipogenic pathway occur in diet-induced obese mouse skeletal muscle*. PLoS One, 2015. **10**(3): p. e0119587.
249. McPherson, R. and A. Gauthier, *Molecular regulation of SREBP function: the Insig-SCAP connection and isoform-specific modulation of lipid synthesis*. Biochem Cell Biol, 2004. **82**(1): p. 201-11.
250. Bi, Y., et al., *Role for sterol regulatory element binding protein-1c activation in mediating skeletal muscle insulin resistance via repression of rat insulin receptor substrate-1 transcription*. Diabetologia, 2014. **57**(3): p. 592-602.
251. Wang, H., et al., *The transcription factor SREBP-1c is instrumental in the development of beta-cell dysfunction*. J Biol Chem, 2003. **278**(19): p. 16622-9.
252. Verges, B., *New insight into the pathophysiology of lipid abnormalities in type 2 diabetes*. Diabetes Metab, 2005. **31**(5): p. 429-39.
253. Salek, L., et al., *Effects of SREBF-1a and SCAP polymorphisms on plasma levels of lipids, severity, progression and regression of coronary atherosclerosis and response to therapy with fluvastatin*. J Mol Med (Berl), 2002. **80**(11): p. 737-44.
254. Reed, B.D., et al., *Genome-wide occupancy of SREBP1 and its partners NFY and SP1 reveals novel functional roles and combinatorial regulation of distinct classes of genes*. PLoS Genet, 2008. **4**(7): p. e1000133.
255. Horton, J.D., J.L. Goldstein, and M.S. Brown, *SREBPs: activators of the complete program of cholesterol and fatty acid synthesis in the liver*. J Clin Invest, 2002. **109**(9): p. 1125-31.
256. Le Lay, S., et al., *Insulin and sterol-regulatory element-binding protein-1c (SREBP-1C) regulation of gene expression in 3T3-L1 adipocytes. Identification of CCAAT/enhancer-binding protein beta as an SREBP-1C target*. J Biol Chem, 2002. **277**(38): p. 35625-34.
257. Shimano, H., et al., *Isoform 1c of sterol regulatory element binding protein is less active than isoform 1a in livers of transgenic mice and in cultured cells*. J Clin Invest, 1997. **99**(5): p. 846-54.
258. Shimomura, I., et al., *Nuclear sterol regulatory element-binding proteins activate genes responsible for the entire program of unsaturated fatty acid biosynthesis in transgenic mouse liver*. J Biol Chem, 1998. **273**(52): p. 35299-306.
259. Ericsson, J., et al., *Identification of glycerol-3-phosphate acyltransferase as an adipocyte determination and differentiation factor 1- and sterol regulatory element-binding protein-responsive gene*. J Biol Chem, 1997. **272**(11): p. 7298-305.
260. Kast, H.R., et al., *CTP:phosphocholine cytidyltransferase, a new sterol- and SREBP-responsive gene*. J Lipid Res, 2001. **42**(8): p. 1266-72.
261. Ridgway, N.D. and T.A. Lagace, *Regulation of the CDP-choline pathway by sterol regulatory element binding proteins involves transcriptional and post-transcriptional mechanisms*. Biochem J, 2003. **372**(Pt 3): p. 811-9.
262. Kast-Woelbern, H.R., et al., *Rosiglitazone induction of Insig-1 in white adipose tissue reveals a novel interplay of peroxisome proliferator-activated receptor gamma and sterol regulatory element-binding protein in the regulation of adipogenesis*. J Biol Chem, 2004. **279**(23): p. 23908-15.
263. Way, J.M., et al., *Comprehensive messenger ribonucleic acid profiling reveals that peroxisome proliferator-activated receptor gamma activation has coordinate effects on gene expression in multiple insulin-sensitive tissues*. Endocrinology, 2001. **142**(3): p. 1269-77.

264. Goldstein, J.L., R.A. DeBose-Boyd, and M.S. Brown, *Protein sensors for membrane sterols*. Cell, 2006. **124**(1): p. 35-46.
265. Yabe, D., M.S. Brown, and J.L. Goldstein, *Insig-2, a second endoplasmic reticulum protein that binds SCAP and blocks export of sterol regulatory element-binding proteins*. Proc Natl Acad Sci U S A, 2002. **99**(20): p. 12753-8.
266. Yabe, D., et al., *Liver-specific mRNA for Insig-2 down-regulated by insulin: implications for fatty acid synthesis*. Proc Natl Acad Sci U S A, 2003. **100**(6): p. 3155-60.
267. Gong, Y., et al., *Sterol-regulated ubiquitination and degradation of Insig-1 creates a convergent mechanism for feedback control of cholesterol synthesis and uptake*. Cell Metab, 2006. **3**(1): p. 15-24.
268. Matthews, H.R., (MPhil Thesis) *The interaction of diet and age to influence the metabolic phenotype of adipose tissue*, in Department of Biochemistry. 2013, University of Cambridge.
269. Li, E., *Chromatin modification and epigenetic reprogramming in mammalian development*. Nature Reviews Genetics, 2002. **3**(9): p. 662-673.
270. Li, E., T.H. Bestor, and R. Jaenisch, *Targeted mutation of the DNA methyltransferase gene results in embryonic lethality*. Cell, 1992. **69**(6): p. 915-26.
271. Reik, W., W. Dean, and J. Walter, *Epigenetic reprogramming in mammalian development*. Science, 2001. **293**(5532): p. 1089-93.
272. Park, J.H., et al., *Development of type 2 diabetes following intrauterine growth retardation in rats is associated with progressive epigenetic silencing of Pdx1*. Journal of Clinical Investigation, 2008. **118**(6): p. 2316-2324.
273. Musri, M.M. and M. Parrizas, *Epigenetic regulation of adipogenesis*. Curr Opin Clin Nutr Metab Care, 2012. **15**(4): p. 342-9.
274. Gerken, T., et al., *The obesity-associated FTO gene encodes a 2-oxoglutarate-dependent nucleic acid demethylase*. Science, 2007. **318**(5855): p. 1469-72.
275. Milagro, F.I., et al., *High fat diet-induced obesity modifies the methylation pattern of leptin promoter in rats*. J Physiol Biochem, 2009. **65**(1): p. 1-9.
276. Plagemann, A., et al., *Hypothalamic proopiomelanocortin promoter methylation becomes altered by early overfeeding: an epigenetic model of obesity and the metabolic syndrome*. J Physiol, 2009. **587**(Pt 20): p. 4963-76.
277. Lillycrop, K.A., et al., *Dietary protein restriction of pregnant rats induces and folic acid supplementation prevents epigenetic modification of hepatic gene expression in the offspring*. J Nutr, 2005. **135**(6): p. 1382-6.
278. Widiker, S., et al., *High-fat diet leads to a decreased methylation of the Mc4r gene in the obese BFMI and the lean B6 mouse lines*. J Appl Genet, 2010. **51**(2): p. 193-7.
279. Chen, J.H., E.C. Cottrell, and S.E. Ozanne, *Early Growth and Ageing*. Importance of Growth for Health and Development, 2010. **65**: p. 41-54.
280. Selhub, J., *Homocysteine metabolism*. Annual Review of Nutrition, 1999. **19**: p. 217-246.
281. Mato, J.M., M.L. Martinez-Chantar, and S.C. Lu, *S-adenosylmethionine metabolism and liver disease*. Ann Hepatol, 2013. **12**(2): p. 183-9.
282. Zeisel, S.H., *Metabolic crosstalk between choline/1-carbon metabolism and energy homeostasis*. Clin Chem Lab Med, 2013. **51**(3): p. 467-75.
283. Corbin, K.D. and S.H. Zeisel, *Choline metabolism provides novel insights into nonalcoholic fatty liver disease and its progression*. Curr Opin Gastroenterol, 2012. **28**(2): p. 159-65.
284. Anderson, O.S., K.E. Sant, and D.C. Dolinoy, *Nutrition and epigenetics: an interplay of dietary methyl donors, one-carbon metabolism and DNA methylation*. Journal of Nutritional Biochemistry, 2012. **23**(8): p. 853-859.
285. Nouredin, M., J.M. Mato, and S.C. Lu, *Nonalcoholic fatty liver disease: update on pathogenesis, diagnosis, treatment and the role of S-adenosylmethionine*. Exp Biol Med (Maywood), 2015. **240**(6): p. 809-20.

286. Anderson, O.S., K.E. Sant, and D.C. Dolinoy, *Nutrition and epigenetics: an interplay of dietary methyl donors, one-carbon metabolism and DNA methylation*. *J Nutr Biochem*, 2012. **23**(8): p. 853-9.
287. Bottiglieri, T., *S-Adenosyl-L-methionine (SAME): from the bench to the bedside--molecular basis of a pleiotrophic molecule*. *Am J Clin Nutr*, 2002. **76**(5): p. 1151S-7S.
288. Hsu, F.F., *Mass spectrometry-based shotgun lipidomics - a critical review from the technical point of view*. *Anal Bioanal Chem*, 2018. **410**(25): p. 6387-6409.
289. Blanksby, S.J. and T.W. Mitchell, *Advances in mass spectrometry for lipidomics*. *Annu Rev Anal Chem (Palo Alto Calif)*, 2010. **3**: p. 433-65.
290. Han, X. and R.W. Gross, *Global analyses of cellular lipidomes directly from crude extracts of biological samples by ESI mass spectrometry: a bridge to lipidomics*. *J Lipid Res*, 2003. **44**(6): p. 1071-9.
291. Cooks, R.G., K.L. Busch, and G.L. Glish, *Mass spectrometry: analytical capabilities and potentials*. *Science*, 1983. **222**(4621): p. 273-91.
292. Fenn, J.B., et al., *Electrospray ionization for mass spectrometry of large biomolecules*. *Science*, 1989. **246**(4926): p. 64-71.
293. Michopoulos, F., et al., *UPLC-MS-based analysis of human plasma for metabonomics using solvent precipitation or solid phase extraction*. *J Proteome Res*, 2009. **8**(4): p. 2114-21.
294. Prakash, C., C.L. Shaffer, and A. Nedderman, *Analytical strategies for identifying drug metabolites*. *Mass Spectrom Rev*, 2007. **26**(3): p. 340-69.
295. Hodson, M.P., et al., *A gender-specific discriminator in Sprague-Dawley rat urine: the deployment of a metabolic profiling strategy for biomarker discovery and identification*. *Anal Biochem*, 2007. **362**(2): p. 182-92.
296. Griffin, J.L. and A. Vidal-Puig, *Current challenges in metabolomics for diabetes research: a vital functional genomic tool or just a ploy for gaining funding?* *Physiol Genomics*, 2008. **34**(1): p. 1-5.
297. Jemal, M. and Y.Q. Xia, *LC-MS Development strategies for quantitative bioanalysis*. *Curr Drug Metab*, 2006. **7**(5): p. 491-502.
298. Cech, N.B. and C.G. Enke, *Practical implications of some recent studies in electrospray ionization fundamentals*. *Mass Spectrom Rev*, 2001. **20**(6): p. 362-87.
299. Ikonomidou, M.G., A.T. Blades, and P. Kebarle, *Electrospray mass spectrometry of methanol and water solutions suppression of electric discharge with SF6 gas*. *J Am Soc Mass Spectrom*, 1991. **2**(6): p. 497-505.
300. Higuera, F.J., *Ion evaporation from the surface of a Taylor cone*. *Phys Rev E Stat Nonlin Soft Matter Phys*, 2003. **68**(1 Pt 2): p. 016304.
301. Talukder, S., et al., *A parallel tempering based study of Coulombic explosion and identification of dissociating fragments in charged noble gas clusters*. *J Chem Phys*, 2013. **139**(16): p. 164312.
302. Wu, C., et al., *Coulomb explosion of nitrogen and oxygen molecules through non-Coulombic states*. *Phys Chem Chem Phys*, 2011. **13**(41): p. 18398-408.
303. Kebarle, P., *A brief overview of the present status of the mechanisms involved in electrospray mass spectrometry*. *J Mass Spectrom*, 2000. **35**(7): p. 804-17.
304. Herrmann, S.S., L. Duedahl-Olesen, and K. Granby, *Simultaneous determination of volatile and non-volatile nitrosamines in processed meat products by liquid chromatography tandem mass spectrometry using atmospheric pressure chemical ionisation and electrospray ionisation*. *J Chromatogr A*, 2014. **1330**: p. 20-9.
305. Zhu, L., et al., *Simultaneous sampling of volatile and non-volatile analytes in beer for fast fingerprinting by extractive electrospray ionization mass spectrometry*. *Anal Bioanal Chem*, 2010. **398**(1): p. 405-13.
306. Chung, W.C., S.C. Tso, and S.T. Sze, *Separation of polar mushroom toxins by mixed-mode hydrophilic and ionic interaction liquid chromatography-electrospray ionization-mass spectrometry*. *J Chromatogr Sci*, 2007. **45**(2): p. 104-11.

307. Roussis, S.G. and J.W. Fedora, *Quantitative determination of polar and ionic compounds in petroleum fractions by atmospheric pressure chemical ionization and electrospray ionization mass spectrometry*. Rapid Commun Mass Spectrom, 2002. **16**(13): p. 1295-303.
308. Wang, Z., H. Zhu, and G. Huang, *Ion suppression effect in desorption electrospray ionization and electrospray ionization mass spectrometry*. Rapid Commun Mass Spectrom, 2017. **31**(23): p. 1957-1962.
309. Muller, C., et al., *Ion suppression effects in liquid chromatography-electrospray-ionisation transport-region collision induced dissociation mass spectrometry with different serum extraction methods for systematic toxicological analysis with mass spectra libraries*. J Chromatogr B Analyt Technol Biomed Life Sci, 2002. **773**(1): p. 47-52.
310. Han, X. and R.W. Gross, *Shotgun lipidomics: multidimensional MS analysis of cellular lipidomes*. Expert Rev Proteomics, 2005. **2**(2): p. 253-64.
311. Han, X., K. Yang, and R.W. Gross, *Multi-dimensional mass spectrometry-based shotgun lipidomics and novel strategies for lipidomic analyses*. Mass Spectrom Rev, 2012. **31**(1): p. 134-78.
312. Cajka, T. and O. Fiehn, *Comprehensive analysis of lipids in biological systems by liquid chromatography-mass spectrometry*. Trends Analyt Chem, 2014. **61**: p. 192-206.
313. Haag, A.M., *Mass Analyzers and Mass Spectrometers*. Adv Exp Med Biol, 2016. **919**: p. 157-169.
314. Forcisi, S., et al., *Liquid chromatography-mass spectrometry in metabolomics research: mass analyzers in ultra high pressure liquid chromatography coupling*. J Chromatogr A, 2013. **1292**: p. 51-65.
315. Degn, H., R.P. Cox, and D. Lloyd, *Continuous measurement of dissolved gases in biochemical systems with the quadrupole mass spectrometer*. Methods Biochem Anal, 1985. **31**: p. 165-94.
316. Yost, R.A. and R.K. Boyd, *Tandem mass spectrometry: quadrupole and hybrid instruments*. Methods Enzymol, 1990. **193**: p. 154-200.
317. Jonscher, K.R. and J.R. Yates, 3rd, *The quadrupole ion trap mass spectrometer--a small solution to a big challenge*. Anal Biochem, 1997. **244**(1): p. 1-15.
318. Hopfgartner, G., et al., *Triple quadrupole linear ion trap mass spectrometer for the analysis of small molecules and macromolecules*. J Mass Spectrom, 2004. **39**(8): p. 845-55.
319. Chernushevich, I.V., A.V. Loboda, and B.A. Thomson, *An introduction to quadrupole-time-of-flight mass spectrometry*. J Mass Spectrom, 2001. **36**(8): p. 849-65.
320. Rashed, M.S., *Clinical applications of tandem mass spectrometry: ten years of diagnosis and screening for inherited metabolic diseases*. J Chromatogr B Biomed Sci Appl, 2001. **758**(1): p. 27-48.
321. Bartlett, K. and M. Pourfarzam, *Tandem mass spectrometry--the potential*. J Inherit Metab Dis, 1999. **22**(4): p. 568-71.
322. van Deventer, H.E. and S.J. Soldin, *The expanding role of tandem mass spectrometry in optimizing diagnosis and treatment of thyroid disease*. Adv Clin Chem, 2013. **61**: p. 127-52.
323. Martin-Venegas, R., O. Jauregui, and J.J. Moreno, *Liquid chromatography-tandem mass spectrometry analysis of eicosanoids and related compounds in cell models*. J Chromatogr B Analyt Technol Biomed Life Sci, 2014. **964**: p. 41-9.
324. Kuchar, L., et al., *Tandem Mass Spectrometry of Sphingolipids: Applications for Diagnosis of Sphingolipidoses*. Adv Clin Chem, 2016. **77**: p. 177-219.
325. Wells, J.M. and S.A. McLuckey, *Collision-induced dissociation (CID) of peptides and proteins*. Methods Enzymol, 2005. **402**: p. 148-85.
326. Murphy, R.C. and P.H. Axelsen, *Mass spectrometric analysis of long-chain lipids*. Mass Spectrom Rev, 2011. **30**(4): p. 579-99.
327. Kostianen, R., et al., *Liquid chromatography/atmospheric pressure ionization-mass spectrometry in drug metabolism studies*. J Mass Spectrom, 2003. **38**(4): p. 357-72.

328. Liu, K., et al., *Simultaneous determination of 6R-leucovorin, 6S-leucovorin and 5-methyltetrahydrofolate in human plasma using solid phase extraction and chiral liquid chromatography-tandem mass spectrometry*. Journal of Chromatography B-Analytical Technologies in the Biomedical and Life Sciences, 2009. **877**(10): p. 902-910.
329. Douglas, D.J., A.J. Frank, and D. Mao, *Linear ion traps in mass spectrometry*. Mass Spectrom Rev, 2005. **24**(1): p. 1-29.
330. Milne, S., et al., *Lipidomics: an analysis of cellular lipids by ESI-MS*. Methods, 2006. **39**(2): p. 92-103.
331. Koulman, A., et al., *High-throughput direct-infusion ion trap mass spectrometry: a new method for metabolomics*. Rapid Commun Mass Spectrom, 2007. **21**(3): p. 421-8.
332. Petkovic, M., et al., *Detection of individual phospholipids in lipid mixtures by matrix-assisted laser desorption/ionization time-of-flight mass spectrometry: phosphatidylcholine prevents the detection of further species*. Anal Biochem, 2001. **289**(2): p. 202-16.
333. Knochenmuss, R., *A quantitative model of ultraviolet matrix-assisted laser desorption/ionization including analyte ion generation*. Anal Chem, 2003. **75**(10): p. 2199-207.
334. Peterson, B.L. and B.S. Cummings, *A review of chromatographic methods for the assessment of phospholipids in biological samples*. Biomed Chromatogr, 2006. **20**(3): p. 227-43.
335. Villas-Boas, S.G., et al., *Mass spectrometry in metabolome analysis*. Mass Spectrom Rev, 2005. **24**(5): p. 613-46.
336. Barth, H.G., et al., *Column liquid chromatography*. Anal Chem, 1986. **58**(5): p. 211R-250R.
337. Bruckner, C.A., et al., *Column liquid chromatography: equipment and instrumentation*. Anal Chem, 1994. **66**(12): p. 1R-16R.
338. Arakawa, T., et al., *Solvent modulation of column chromatography*. Protein Pept Lett, 2008. **15**(6): p. 544-55.
339. Martin, A.J. and R.L. Synge, *A new form of chromatogram employing two liquid phases: A theory of chromatography. 2. Application to the micro-determination of the higher monoamino-acids in proteins*. Biochem J, 1941. **35**(12): p. 1358-68.
340. Gohlke, R.S. and F.W. McLafferty, *Early gas chromatography/mass spectrometry*. J Am Soc Mass Spectrom, 1993. **4**(5): p. 367-71.
341. Zaikin, V.G. and J.M. Halket, *Review: Derivatization in mass spectrometry--2. Acylation*. Eur J Mass Spectrom (Chichester), 2003. **9**(5): p. 421-34.
342. Halket, J.M. and V.G. Zaikin, *Derivatization in mass spectrometry--1. Silylation*. Eur J Mass Spectrom (Chichester), 2003. **9**(1): p. 1-21.
343. Morrison, W.R. and L.M. Smith, *Preparation of Fatty Acid Methyl Esters and Dimethylacetals from Lipids with Boron Fluoride--Methanol*. J Lipid Res, 1964. **5**: p. 600-8.
344. Kuksis, A., *Newer developments in determination of bile acids and steroids by gas chromatography*. Methods Biochem Anal, 1966. **14**: p. 325-454.
345. Scott, R.P., *Gas-liquid chromatography: recent developments in apparatus and technique*. Br Med Bull, 1966. **22**(2): p. 131-6.
346. Perry, S.G., *Peak identification in gas chromatography*. Chromatogr Rev, 1967. **9**(1): p. 1-22.
347. Chattoraj, S.C. and N.W. Tietz, *Gas chromatography: fundamentals and application*. Hosp Top, 1969. **47**(10): p. 81-100.
348. Marriott, P.J., *Addressing the Challenges to Identification in Gas Chromatography by Increased Resolution and Enhanced Detection Modalities*. Chem Asian J, 2018.
349. Palma, P., et al., *Electron ionization in LC-MS: recent developments and applications of the direct-EI LC-MS interface*. Anal Bioanal Chem, 2011. **399**(8): p. 2683-93.
350. Cappiello, A., et al., *New trends in the application of electron ionization to liquid chromatography-mass spectrometry interfacing*. Mass Spectrom Rev, 2001. **20**(2): p. 88-104.
351. Barker, P.E., *Cancer biomarker validation: standards and process: roles for the National Institute of Standards and Technology (NIST)*. Ann N Y Acad Sci, 2003. **983**: p. 142-50.

352. Marcos, J. and O.J. Pozo, *Derivatization of steroids in biological samples for GC-MS and LC-MS analyses*. *Bioanalysis*, 2015. **7**(19): p. 2515-36.
353. Halket, J.M., et al., *Chemical derivatization and mass spectral libraries in metabolic profiling by GC/MS and LC/MS/MS*. *J Exp Bot*, 2005. **56**(410): p. 219-43.
354. Whitehouse, C.M., et al., *Electrospray interface for liquid chromatographs and mass spectrometers*. *Anal Chem*, 1985. **57**(3): p. 675-9.
355. Morris, H.R., et al., *High sensitivity collisionally-activated decomposition tandem mass spectrometry on a novel quadrupole/orthogonal-acceleration time-of-flight mass spectrometer*. *Rapid Commun Mass Spectrom*, 1996. **10**(8): p. 889-96.
356. Wenk, M.R., et al., *Phosphoinositide profiling in complex lipid mixtures using electrospray ionization mass spectrometry*. *Nat Biotechnol*, 2003. **21**(7): p. 813-7.
357. Malavolta, M., et al., *Normal phase liquid chromatography-electrospray ionization tandem mass spectrometry analysis of phospholipid molecular species in blood mononuclear cells: application to cystic fibrosis*. *J Chromatogr B Analyt Technol Biomed Life Sci*, 2004. **810**(2): p. 173-86.
358. Saldanha, T., et al., *HPLC separation and determination of 12 cholesterol oxidation products in fish: comparative study of RI, UV, and APCI-MS detectors*. *J Agric Food Chem*, 2006. **54**(12): p. 4107-13.
359. Hvattum, E., et al., *Quantification of phosphatidylserine, phosphatidic acid and free fatty acids in an ultrasound contrast agent by normal-phase high-performance liquid chromatography with evaporative light scattering detection*. *J Pharm Biomed Anal*, 2006. **42**(4): p. 506-12.
360. McNabb, T.J., et al., *The separation and direct detection of ceramides and sphingoid bases by normal-phase high-performance liquid chromatography and evaporative light-scattering detection*. *Anal Biochem*, 1999. **276**(2): p. 242-50.
361. Johnson, D., B. Boyes, and R. Orlando, *The use of ammonium formate as a mobile-phase modifier for LC-MS/MS analysis of tryptic digests*. *J Biomol Tech*, 2013. **24**(4): p. 187-97.
362. Claessens, H.A. and M.A. van Straten, *Review on the chemical and thermal stability of stationary phases for reversed-phase liquid chromatography*. *J Chromatogr A*, 2004. **1060**(1-2): p. 23-41.
363. Vailaya, A. and C. Horvath, *Retention in reversed-phase chromatography: partition or adsorption?* *J Chromatogr A*, 1998. **829**(1-2): p. 1-27.
364. Wheeler, J.F., et al., *Phase transitions of reversed-phase stationary phases. Cause and effects in the mechanism of retention*. *J Chromatogr*, 1993. **656**(1-2): p. 317-33.
365. Olsson, N.U. and N. Salem, Jr., *Molecular species analysis of phospholipids*. *J Chromatogr B Biomed Sci Appl*, 1997. **692**(2): p. 245-56.
366. Rainville, P.D., et al., *Novel application of reversed-phase UPLC-oeTOF-MS for lipid analysis in complex biological mixtures: a new tool for lipidomics*. *J Proteome Res*, 2007. **6**(2): p. 552-8.
367. Schmelzer, K., et al., *The lipid maps initiative in lipidomics*. *Methods Enzymol*, 2007. **432**: p. 171-83.
368. Garcia, Y. and J. Diaz-Castro, *Advantages and disadvantages of the animal models v. in vitro studies in iron metabolism: a review*. *Animal*, 2013. **7**(10): p. 1651-8.
369. Gardner, D.S. and P. Rhodes, *Developmental origins of obesity: programming of food intake or physical activity?* *Adv Exp Med Biol*, 2009. **646**: p. 83-93.
370. Maxfield, E. and F. Konishi, *Patterns of food intake and physical activity in obesity*. *J Am Diet Assoc*, 1966. **49**(5): p. 406-8.
371. Dalle Molle, R., et al., *Gene and environment interaction: Is the differential susceptibility hypothesis relevant for obesity?* *Neurosci Biobehav Rev*, 2017. **73**: p. 326-339.
372. Cummins, T.D., et al., *Metabolic remodeling of white adipose tissue in obesity*. *Am J Physiol Endocrinol Metab*, 2014. **307**(3): p. E262-77.

373. Roberts, L.D., et al., *The contrasting roles of PPARdelta and PPARgamma in regulating the metabolic switch between oxidation and storage of fats in white adipose tissue*. *Genome Biol*, 2011. **12**(8): p. R75.
374. Roberts, L.D., et al., *Increased hepatic oxidative metabolism distinguishes the action of Peroxisome proliferator-activated receptor delta from Peroxisome proliferator-activated receptor gamma in the ob/ob mouse*. *Genome Med*, 2009. **1**(12): p. 115.
375. Nagai, M., et al., *Estimating visceral fat area by multifrequency bioelectrical impedance*. *Diabetes Care*, 2010. **33**(5): p. 1077-9.
376. Porter, S.A., et al., *Abdominal subcutaneous adipose tissue: a protective fat depot?* *Diabetes Care*, 2009. **32**(6): p. 1068-75.
377. Hill, J.H., C. Solt, and M.T. Foster, *Obesity associated disease risk: the role of inherent differences and location of adipose depots*. *Horm Mol Biol Clin Investig*, 2018. **33**(2).
378. Thalmann, S. and C.A. Meier, *Local adipose tissue depots as cardiovascular risk factors*. *Cardiovasc Res*, 2007. **75**(4): p. 690-701.
379. Montague, C.T., *Adipose depot-specific effects of PPAR gamma agonists: a consequence of differential expression of PPAR gamma in adipose tissue depots?* *Diabetes Obes Metab*, 2002. **4**(6): p. 356-61.
380. Birbrair, A., et al., *Role of pericytes in skeletal muscle regeneration and fat accumulation*. *Stem Cells Dev*, 2013. **22**(16): p. 2298-314.
381. Bachmanov, A.A., et al., *Nutrient preference and diet-induced adiposity in C57BL/6ByJ and 129P3/J mice*. *Physiol Behav*, 2001. **72**(4): p. 603-13.
382. Yang, Y.K., et al., *Human mesenteric adipose tissue plays unique role versus subcutaneous and omental fat in obesity related diabetes*. *Cell Physiol Biochem*, 2008. **22**(5-6): p. 531-8.
383. Mardian, E.B., et al., *Agpat4/Lpaatdelta deficiency highlights the molecular heterogeneity of epididymal and perirenal white adipose depots*. *J Lipid Res*, 2017. **58**(10): p. 2037-2050.
384. Mattacks, C.A., D. Sadler, and C.M. Pond, *Site-specific differences in fatty acid composition of dendritic cells and associated adipose tissue in popliteal depot, mesentery, and omentum and their modulation by chronic inflammation and dietary lipids*. *Lymphat Res Biol*, 2004. **2**(3): p. 107-29.
385. Bernasochi, G.B., et al., *Pericardial adipose and aromatase: A new translational target for aging, obesity and arrhythmogenesis?* *J Mol Cell Cardiol*, 2017. **111**: p. 96-101.
386. Marchington, J.M. and C.M. Pond, *Site-specific properties of pericardial and epicardial adipose tissue: the effects of insulin and high-fat feeding on lipogenesis and the incorporation of fatty acids in vitro*. *Int J Obes*, 1990. **14**(12): p. 1013-22.
387. Lindstrom, P., *The physiology of obese-hyperglycemic mice [ob/ob mice]*. *ScientificWorldJournal*, 2007. **7**: p. 666-85.
388. Kline, A.D., et al., *Leptin is a four-helix bundle: Secondary structure by NMR*. *Febs Letters*, 1997. **407**(2): p. 239-242.
389. Lord, G.M., et al., *Leptin modulates the T-cell immune response and reverses starvation-induced immunosuppression*. *Nature*, 1998. **394**(6696): p. 897-901.
390. Morton, N.M., et al., *Leptin action in intestinal cells*. *Journal of Biological Chemistry*, 1998. **273**(40): p. 26194-26201.
391. Sierra-Honigmann, M.R.o., et al., *Biological Action of Leptin as an Angiogenic Factor*. *Science*, 1998. **281**(5383): p. 1683-1686.
392. Ingalls, A.M., M.M. Dickie, and G.D. Snell, *Obese, a new mutation in the house mouse*. *Obesity Research*, 1996. **4**(1): p. 101-101.
393. Toye, A.A., et al., *A new mouse model of type 2 diabetes, produced by N-ethyl-nitrosourea mutagenesis, is the result of a missense mutation in the glucokinase gene*. *Diabetes*, 2004. **53**(6): p. 1577-1583.
394. Dubuc, P.U., *The development of obesity, hyperinsulinemia, and hyperglycemia in ob/ob mice*. *Metabolism*, 1976. **25**(12): p. 1567-1574.

395. Bergh, A.V.d., et al., *Dyslipidaemia in type II diabetic mice does not aggravate contractile impairment but increases ventricular stiffness*. Cardiovascular Research, 2007.
396. Bigorgne, A.E., et al., *Obesity-induced lymphocyte hyperresponsiveness to chemokines: A new mechanism of fatty liver inflammation in obese mice*. Gastroenterology, 2008. **134**(5): p. 1459-1469.
397. Halaas, J.L., et al., *Weight-Reducing Effects of the Plasma-Protein Encoded by the Obese Gene*. Science, 1995. **269**(5223): p. 543-546.
398. Pellemounter, M.A., et al., *Effects of the Obese Gene-Product on Body-Weight Regulation in Ob/Ob Mice*. Science, 1995. **269**(5223): p. 540-543.
399. Rentsch, J., N. Levens, and M. Chiesi, *Recombinant Ob-Gene Product Reduces Food-Intake in Fasted Mice*. Biochemical and Biophysical Research Communications, 1995. **214**(1): p. 131-136.
400. Soukas, A., et al., *Leptin-specific patterns of gene expression in white adipose tissue*. Genes & Development, 2000. **14**(8): p. 963-980.
401. Lee, G.H., et al., *Abnormal splicing of the leptin receptor in diabetic mice*. Nature, 1996. **379**(6566): p. 632-635.
402. Shimomura, I., et al., *Decreased IRS-2 and increased SREBP-1c lead to mixed insulin resistance and sensitivity in livers of lipodystrophic and ob/ob mice*. Mol Cell, 2000. **6**(1): p. 77-86.
403. Tabor, D.E., et al., *Identification of conserved cis-elements and transcription factors required for sterol-regulated transcription of stearoyl-CoA desaturase 1 and 2*. Journal of Biological Chemistry, 1999. **274**(29): p. 20603-20610.
404. Magana, M.M., et al., *Sterol regulation of acetyl coenzyme A carboxylase promoter requires two interdependent binding sites for sterol regulatory element binding proteins*. Journal of Lipid Research, 1997. **38**(8): p. 1630-1638.
405. Magana, M.M. and T.F. Osborne, *Two tandem binding sites for sterol regulatory element binding proteins are required for sterol regulation of fatty-acid synthase promoter*. Journal of Biological Chemistry, 1996. **271**(51): p. 32689-32694.
406. Moon, Y.A., et al., *Identification of a mammalian long chain fatty acyl elongase regulated by sterol regulatory element-binding proteins*. Journal of Biological Chemistry, 2001. **276**(48): p. 45358-45366.
407. Nara, T.Y., et al., *The E-box like sterol regulatory element mediates the suppression of human Delta-6 desaturase gene by highly unsaturated fatty acids*. Biochemical and Biophysical Research Communications, 2002. **296**(1): p. 111-117.
408. Foretz, M., et al., *ADD1/SREBP-1c is required in the activation of hepatic lipogenic gene expression by glucose*. Molecular and Cellular Biology, 1999. **19**(5): p. 3760-3768.
409. Kim, J.B., et al., *Nutritional and insulin regulation of fatty acid synthetase and leptin gene expression through ADD1/SREBP1*. Journal of Clinical Investigation, 1998. **101**(1): p. 1-9.
410. Kakuma, T., et al., *Leptin, troglitazone, and the expression of sterol regulatory element binding proteins in liver and pancreatic islets*. Proceedings of the National Academy of Sciences of the United States of America, 2000. **97**(15): p. 8536-8541.
411. Shimomura, L., et al., *Insulin selectively increases SREBP-1c mRNA in the livers of rats with streptozotocin-induced diabetes*. Proceedings of the National Academy of Sciences of the United States of America, 1999. **96**(24): p. 13656-13661.
412. Cao, H.M., et al., *Identification of a lipokine, a lipid hormone linking adipose tissue to systemic metabolism*. Cell, 2008. **134**(6): p. 933-944.
413. Ament, Z., M. Masoodi, and J.L. Griffin, *Applications of metabolomics for understanding the action of peroxisome proliferator-activated receptors (PPARs) in diabetes, obesity and cancer*. Genome Med, 2012. **4**(4): p. 32.
414. McCombie, G., et al., *Metabolomic and Lipidomic Analysis of the Heart of Peroxisome Proliferator-Activated Receptor-gamma Coactivator 1-beta Knock Out Mice on a High Fat Diet*. Metabolites, 2012. **2**(2): p. 366-81.

415. Kliewer, S.A., et al., *Peroxisome proliferator-activated receptors: from genes to physiology*. Recent Prog Horm Res, 2001. **56**: p. 239-63.
416. Issemann, I. and S. Green, *Activation of a member of the steroid hormone receptor superfamily by peroxisome proliferators*. Nature, 1990. **347**(6294): p. 645-50.
417. Temple, K.A., et al., *An intact DNA-binding domain is not required for peroxisome proliferator-activated receptor gamma (PPARgamma) binding and activation on some PPAR response elements*. J Biol Chem, 2005. **280**(5): p. 3529-40.
418. Cronet, P., et al., *Structure of the PPARalpha and -gamma ligand binding domain in complex with AZ 242; ligand selectivity and agonist activation in the PPAR family*. Structure, 2001. **9**(8): p. 699-706.
419. Hardwick, J.P., et al., *PPAR/RXR Regulation of Fatty Acid Metabolism and Fatty Acid omega-Hydroxylase (CYP4) Isozymes: Implications for Prevention of Lipotoxicity in Fatty Liver Disease*. PPAR Res, 2009. **2009**: p. 952734.
420. Brodie, A.E., V.A. Manning, and C.Y. Hu, *Inhibitors of preadipocyte differentiation induce COUP-TF binding to a PPAR/RXR binding sequence*. Biochem Biophys Res Commun, 1996. **228**(3): p. 655-61.
421. Meirhaeghe, A., et al., *Characterization of the human, mouse and rat PGC1 beta (peroxisome-proliferator-activated receptor-gamma co-activator 1 beta) gene in vitro and in vivo*. Biochem J, 2003. **373**(Pt 1): p. 155-65.
422. Vega, R.B., J.M. Huss, and D.P. Kelly, *The coactivator PGC-1 cooperates with peroxisome proliferator-activated receptor alpha in transcriptional control of nuclear genes encoding mitochondrial fatty acid oxidation enzymes*. Mol Cell Biol, 2000. **20**(5): p. 1868-76.
423. Cabrero, A., et al., *Bezafibrate reduces mRNA levels of adipocyte markers and increases fatty acid oxidation in primary culture of adipocytes*. Diabetes, 2001. **50**(8): p. 1883-90.
424. Staels, B. and J.C. Fruchart, *Therapeutic roles of peroxisome proliferator-activated receptor agonists*. Diabetes, 2005. **54**(8): p. 2460-70.
425. Hennuyer, N., et al., *PPARalpha, but not PPARgamma, activators decrease macrophage-laden atherosclerotic lesions in a nondiabetic mouse model of mixed dyslipidemia*. Arterioscler Thromb Vasc Biol, 2005. **25**(9): p. 1897-902.
426. Costet, P., et al., *Peroxisome proliferator-activated receptor alpha-isoform deficiency leads to progressive dyslipidemia with sexually dimorphic obesity and steatosis*. J Biol Chem, 1998. **273**(45): p. 29577-85.
427. Zamaninour, N., et al., *Peroxisome proliferator-activated receptor gamma coactivator 1alpha variation: a closer look at obesity onset age and its related metabolic status and body composition*. Appl Physiol Nutr Metab, 2018. **43**(12): p. 1321-1325.
428. Li, Y., T.Y. Nara, and M.T. Nakamura, *Peroxisome proliferator-activated receptor alpha is required for feedback regulation of highly unsaturated fatty acid synthesis*. J Lipid Res, 2005. **46**(11): p. 2432-40.
429. Braissant, O., et al., *Differential expression of peroxisome proliferator-activated receptors (PPARs): tissue distribution of PPAR-alpha, -beta, and -gamma in the adult rat*. Endocrinology, 1996. **137**(1): p. 354-66.
430. Barbier, O., et al., *Pleiotropic actions of peroxisome proliferator-activated receptors in lipid metabolism and atherosclerosis*. Arterioscler Thromb Vasc Biol, 2002. **22**(5): p. 717-26.
431. Atherton, H.J., et al., *Metabolomics of the interaction between PPAR-alpha and age in the PPAR-alpha-null mouse*. Mol Syst Biol, 2009. **5**: p. 259.
432. Ahima, R.S., et al., *Leptin accelerates the onset of puberty in normal female mice*. J Clin Invest, 1997. **99**(3): p. 391-5.
433. Murray, A.J., et al., *Deterioration of physical performance and cognitive function in rats with short-term high-fat feeding*. The FASEB Journal, 2009. **23**(12): p. 4353-4360.
434. Folch, J., M. Lees, and G. Sloane-Stanley, *A simple method for the isolation and purification of total lipids from animal tissues*. J Biol Chem, 1957. **226**(1): p. 497-509.

435. Bligh, E.G. and W.J. Dyer, *A RAPID METHOD OF TOTAL LIPID EXTRACTION AND PURIFICATION*. Canadian Journal of Biochemistry and Physiology, 1959. **37**(8): p. 911-917.
436. Gromski, P.S., et al., *A tutorial review: Metabolomics and partial least squares-discriminant analysis--a marriage of convenience or a shotgun wedding*. Anal Chim Acta, 2015. **879**: p. 10-23.
437. Boulesteix, A.L. and K. Strimmer, *Partial least squares: a versatile tool for the analysis of high-dimensional genomic data*. Brief Bioinform, 2007. **8**(1): p. 32-44.
438. Bylesjo, M., et al., *Data integration in plant biology: the O2PLS method for combined modeling of transcript and metabolite data*. Plant J, 2007. **52**(6): p. 1181-91.
439. Ingalls, A.M., M.M. Dickie, and G.D. Snell, *Obese, a new mutation in the house mouse*. Obes Res, 1996. **4**(1): p. 101.
440. Campfield, L.A., F.J. Smith, and P. Burn, *The OB protein (leptin) pathway--a link between adipose tissue mass and central neural networks*. Horm Metab Res, 1996. **28**(12): p. 619-32.
441. Trayhurn, P. and D.V. Rayner, *Hormones and the ob gene product (leptin) in the control of energy balance*. Biochem Soc Trans, 1996. **24**(2): p. 565-70.
442. Tan, C.Y., et al., *Brown Adipose Tissue Thermogenic Capacity Is Regulated by Elovl6*. Cell Rep, 2015. **13**(10): p. 2039-47.
443. Kern, P.A., et al., *Adipose tissue tumor necrosis factor and interleukin-6 expression in human obesity and insulin resistance*. Am J Physiol Endocrinol Metab, 2001. **280**(5): p. E745-51.
444. Montague, C.T. and S. O'Rahilly, *The perils of portliness: causes and consequences of visceral adiposity*. Diabetes, 2000. **49**(6): p. 883-8.
445. Marette, A., *Molecular mechanisms of inflammation in obesity-linked insulin resistance*. Int J Obes Relat Metab Disord, 2003. **27 Suppl 3**: p. S46-8.
446. Mokdad, A.H., et al., *Prevalence of obesity, diabetes, and obesity-related health risk factors, 2001*. JAMA, 2003. **289**(1): p. 76-9.
447. Belle, J.E.L., et al., *A comparison of cell and tissue extraction techniques using high-resolution 1H-NMR spectroscopy*. NMR in Biomedicine, 2002. **15**(1): p. 37-44.
448. Ramanadham, S., et al., *Delta6-, Stearoyl CoA-, and Delta5-desaturase enzymes are expressed in beta-cells and are altered by increases in exogenous PUFA concentrations*. Biochim Biophys Acta, 2002. **1580**(1): p. 40-56.
449. Park, H.G., et al., *Palmitic acid (16:0) competes with omega-6 linoleic and omega-3 a-linolenic acids for FADS2 mediated Delta6-desaturation*. Biochim Biophys Acta, 2016. **1861**(2): p. 91-7.
450. Lopez-Vicario, C., et al., *Molecular interplay between Delta5/Delta6 desaturases and long-chain fatty acids in the pathogenesis of non-alcoholic steatohepatitis*. Gut, 2014. **63**(2): p. 344-55.
451. Kien, C.L., et al., *A lipidomics analysis of the relationship between dietary fatty acid composition and insulin sensitivity in young adults*. Diabetes, 2013. **62**(4): p. 1054-63.
452. Perez-Jimenez, F., et al., *A Mediterranean and a high-carbohydrate diet improve glucose metabolism in healthy young persons*. Diabetologia, 2001. **44**(11): p. 2038-43.
453. Sjogren, P., et al., *Fatty acid desaturases in human adipose tissue: relationships between gene expression, desaturation indexes and insulin resistance*. Diabetologia, 2008. **51**(2): p. 328-35.
454. Yew Tan, C., et al., *Adipose tissue fatty acid chain length and mono-unsaturation increases with obesity and insulin resistance*. Sci Rep, 2015. **5**: p. 18366.
455. Connor, T., et al., *Metabolic remodelling in obesity and type 2 diabetes: pathological or protective mechanisms in response to nutrient excess?* Clin Exp Pharmacol Physiol, 2015. **42**(1): p. 109-15.
456. Jump, D.B., *Dietary polyunsaturated fatty acids and regulation of gene transcription*. Curr Opin Lipidol, 2002. **13**(2): p. 155-64.
457. Perona, J.S., *Membrane lipid alterations in the metabolic syndrome and the role of dietary oils*. Biochim Biophys Acta Biomembr, 2017. **1859**(9 Pt B): p. 1690-1703.

458. Hayden, M.R., J.R. Sowers, and S.C. Tyagi, *The central role of vascular extracellular matrix and basement membrane remodeling in metabolic syndrome and type 2 diabetes: the matrix preloaded*. *Cardiovasc Diabetol*, 2005. **4**: p. 9.
459. Charradi, K., et al., *High-fat diet induced an oxidative stress in white adipose tissue and disturbed plasma transition metals in rat: prevention by grape seed and skin extract*. *J Physiol Sci*, 2013. **63**(6): p. 445-55.
460. Pereira, S.S., et al., *Differences in adipose tissue inflammation and oxidative status in C57BL/6 and ApoE^{-/-} mice fed high fat diet*. *Anim Sci J*, 2012. **83**(7): p. 549-55.
461. Moon, Y.A., et al., *Deletion of ELOVL6 blocks the synthesis of oleic acid but does not prevent the development of fatty liver or insulin resistance*. *J Lipid Res*, 2014. **55**(12): p. 2597-605.
462. Chu, Y., *A Metabolomics Investigation of Non-alcoholic Fatty Liver Disease to Define Mechanisms of Induction and Pathology*, in *Department of Biochemistry*. 2014, University of Cambridge: Cambridge.
463. Curtis, R.K., M. Oresic, and A. Vidal-Puig, *Pathways to the analysis of microarray data*. *Trends Biotechnol*, 2005. **23**(8): p. 429-35.
464. Werner, T., *Bioinformatics applications for pathway analysis of microarray data*. *Curr Opin Biotechnol*, 2008. **19**(1): p. 50-4.
465. Altshuler-Keylin, S. and S. Kajimura, *Mitochondrial homeostasis in adipose tissue remodeling*. *Sci Signal*, 2017. **10**(468).
466. Boudina, S. and T.E. Graham, *Mitochondrial function/dysfunction in white adipose tissue*. *Exp Physiol*, 2014. **99**(9): p. 1168-78.
467. Benjamini, Y. and Y.J.J.o.t.r.s.s.S.B. Hochberg, *Controlling the false discovery rate: a practical and powerful approach to multiple testing*. 1995: p. 289-300.
468. Impheng, H., et al., *The selective target of capsaicin on FASN expression and de novo fatty acid synthesis mediated through ROS generation triggers apoptosis in HepG2 cells*. *PLoS One*, 2014. **9**(9): p. e107842.
469. Zhang, X., et al., *Liver X receptor activation increases hepatic fatty acid desaturation by the induction of SCD1 expression through an LXRA α -SREBP1c-dependent mechanism*. *J Diabetes*, 2014. **6**(3): p. 212-20.
470. Schaeffer, L., et al., *Common genetic variants of the FADS1 FADS2 gene cluster and their reconstructed haplotypes are associated with the fatty acid composition in phospholipids*. *Hum Mol Genet*, 2006. **15**(11): p. 1745-56.
471. Xue, X., et al., *Characterization of the fatty acyl elongase (elovl) gene family, and hepatic elovl and delta-6 fatty acyl desaturase transcript expression and fatty acid responses to diets containing camelina oil in Atlantic cod (Gadus morhua)*. *Comp Biochem Physiol B Biochem Mol Biol*, 2014. **175**: p. 9-22.
472. Cao, X.F., et al., *High-fat diet induces aberrant hepatic lipid secretion in blunt snout bream by activating endoplasmic reticulum stress-associated IRE1/XBP1 pathway*. *Biochim Biophys Acta Mol Cell Biol Lipids*, 2018. **1864**(3): p. 213-223.
473. Olivari, S., et al., *EDEM1 regulates ER-associated degradation by accelerating de-mannosylation of folding-defective polypeptides and by inhibiting their covalent aggregation*. *Biochem Biophys Res Commun*, 2006. **349**(4): p. 1278-84.
474. Biber, L.A., et al., *Non-Endoplasmic Reticulum-Based Calr (Calreticulin) Can Coordinate Heterocellular Calcium Signaling and Vascular Function*. *Arterioscler Thromb Vasc Biol*, 2018. **38**(1): p. 120-130.
475. Takeuchi, K. and K. Reue, *Biochemistry, physiology, and genetics of GPAT, AGPAT, and lipin enzymes in triglyceride synthesis*. *Am J Physiol Endocrinol Metab*, 2009. **296**(6): p. E1195-209.
476. Arroyo-Caro, J.M., et al., *Molecular characterization of a lysophosphatidylcholine acyltransferase gene belonging to the MBOAT family in Ricinus communis L*. *Lipids*, 2013. **48**(7): p. 663-74.

477. Matsuda, S., et al., *Member of the membrane-bound O-acyltransferase (MBOAT) family encodes a lysophospholipid acyltransferase with broad substrate specificity*. *Genes Cells*, 2008. **13**(8): p. 879-88.
478. Liu, X., et al., *The INSIG1 gene, not the INSIG2 gene, associated with coronary heart disease: tagSNPs and haplotype-based association study. The Beijing Atherosclerosis Study*. *Thromb Haemost*, 2008. **100**(5): p. 886-92.
479. Smith, A.J., et al., *INSIG2 gene polymorphism is not associated with obesity in Caucasian, Afro-Caribbean and Indian subjects*. *Int J Obes (Lond)*, 2007. **31**(11): p. 1753-5.
480. Cervino, A.C., et al., *Integrating QTL and high-density SNP analyses in mice to identify Insig2 as a susceptibility gene for plasma cholesterol levels*. *Genomics*, 2005. **86**(5): p. 505-17.
481. Chen, Z., et al., *Sterol regulatory element-binding transcription factor (SREBF)-2, SREBF cleavage-activating protein (SCAP), and premature coronary artery disease in a Chinese population*. *Mol Biol Rep*, 2011. **38**(5): p. 2895-901.
482. Eberle, D., et al., *SREBF-1 gene polymorphisms are associated with obesity and type 2 diabetes in French obese and diabetic cohorts*. *Diabetes*, 2004. **53**(8): p. 2153-7.
483. Salek, L., et al., *Effects of SREBF-1a and SCAP polymorphisms on plasma levels of lipids, severity, progression and regression of coronary atherosclerosis and response to therapy with fluvastatin*. *J Mol Med (Berl)*, 2002. **80**(11): p. 737-44.
484. Corrales, P., A. Vidal-Puig, and G. Medina-Gomez, *PPARs and Metabolic Disorders Associated with Challenged Adipose Tissue Plasticity*. *Int J Mol Sci*, 2018. **19**(7).
485. Puigserver, P., *Tissue-specific regulation of metabolic pathways through the transcriptional coactivator PGC1-alpha*. *Int J Obes (Lond)*, 2005. **29 Suppl 1**: p. S5-9.
486. Patti, M.E., et al., *Coordinated reduction of genes of oxidative metabolism in humans with insulin resistance and diabetes: Potential role of PGC1 and NRF1*. *Proc Natl Acad Sci U S A*, 2003. **100**(14): p. 8466-71.
487. Cornelis, G., P.M. Bennett, and J. Grinsted, *Properties of pGC1, a lac plasmid originating in Yersinia enterocolitica 842*. *J Bacteriol*, 1976. **127**(3): p. 1058-62.
488. Goetzman, E.S. and E.V. Prochownik, *The Role for Myc in Coordinating Glycolysis, Oxidative Phosphorylation, Glutaminolysis, and Fatty Acid Metabolism in Normal and Neoplastic Tissues*. *Front Endocrinol (Lausanne)*, 2018. **9**: p. 129.
489. Dang, C.V., *A Time for MYC: Metabolism and Therapy*. *Cold Spring Harb Symp Quant Biol*, 2016. **81**: p. 79-83.
490. Dang, C.V., *c-Myc target genes involved in cell growth, apoptosis, and metabolism*. *Mol Cell Biol*, 1999. **19**(1): p. 1-11.
491. Casteilla, L., M. Rigoulet, and L. Penicaud, *Mitochondrial ROS metabolism: modulation by uncoupling proteins*. *IUBMB Life*, 2001. **52**(3-5): p. 181-8.
492. Garlid, K.D., M. Jaburek, and P. Jezek, *The mechanism of proton transport mediated by mitochondrial uncoupling proteins*. *FEBS Lett*, 1998. **438**(1-2): p. 10-4.
493. Murray, A.J., et al., *Plasma free fatty acids and peroxisome proliferator-activated receptor alpha in the control of myocardial uncoupling protein levels*. *Diabetes*, 2005. **54**(12): p. 3496-502.
494. Murray, A.J., et al., *Uncoupling proteins in human heart*. *Lancet*, 2004. **364**(9447): p. 1786-8.
495. Frasca, D., et al., *Ageing and obesity similarly impair antibody responses*. *Clin Exp Immunol*, 2017. **187**(1): p. 64-70.
496. Salminen, A., K. Kaarniranta, and A. Kauppinen, *Inflammaging: disturbed interplay between autophagy and inflammasomes*. *Aging (Albany NY)*, 2012. **4**(3): p. 166-75.
497. Lopez-Otin, C., et al., *The hallmarks of aging*. *Cell*, 2013. **153**(6): p. 1194-217.
498. Jia, G., et al., *Vascular stiffness in insulin resistance and obesity*. *Front Physiol*, 2015. **6**: p. 231.
499. Maurer, M.S., *Noninvasive Identification of ATTRwt Cardiac Amyloid: The Re-emergence of Nuclear Cardiology*. *Am J Med*, 2015. **128**(12): p. 1275-80.

500. Olivetti, G., et al., *Cardiomyopathy of the aging human heart. Myocyte loss and reactive cellular hypertrophy*. *Circ Res*, 1991. **68**(6): p. 1560-8.
501. Hinton, R.B. and K.E. Yutzey, *Heart valve structure and function in development and disease*. *Annu Rev Physiol*, 2011. **73**: p. 29-46.
502. Donato, A.J., et al., *The impact of ageing on adipose structure, function and vasculature in the B6D2F1 mouse: evidence of significant multisystem dysfunction*. *J Physiol*, 2014. **592**(18): p. 4083-96.
503. Li, Q.O.Y., I. Soro-Arnaiz, and J. Aragonés, *Age-dependent obesity and mitochondrial dysfunction*. *Adipocyte*, 2017. **6**(2): p. 161-166.
504. Lopez-Lluch, G., *Mitochondrial activity and dynamics changes regarding metabolism in ageing and obesity*. *Mech Ageing Dev*, 2017. **162**: p. 108-121.
505. Soro-Arnaiz, I., et al., *Role of Mitochondrial Complex IV in Age-Dependent Obesity*. *Cell Rep*, 2016. **16**(11): p. 2991-3002.
506. Kalinkovich, A. and G. Livshits, *Sarcopenic obesity or obese sarcopenia: A cross talk between age-associated adipose tissue and skeletal muscle inflammation as a main mechanism of the pathogenesis*. *Ageing Res Rev*, 2017. **35**: p. 200-221.
507. Ahima, R.S., *Connecting obesity, aging and diabetes*. *Nat Med*, 2009. **15**(9): p. 996-7.
508. Minamino, T., et al., *A crucial role for adipose tissue p53 in the regulation of insulin resistance*. *Nat Med*, 2009. **15**(9): p. 1082-7.
509. Zhao, L. and S.L. Ackerman, *Endoplasmic reticulum stress in health and disease*. *Curr Opin Cell Biol*, 2006. **18**(4): p. 444-52.
510. Mori, K., *Tripartite management of unfolded proteins in the endoplasmic reticulum*. *Cell*, 2000. **101**(5): p. 451-4.
511. Monteiro, R. and I. Azevedo, *Chronic inflammation in obesity and the metabolic syndrome*. *Mediators Inflamm*, 2010. **2010**.
512. Burton, D.G.A. and R.G.A. Faragher, *Obesity and type-2 diabetes as inducers of premature cellular senescence and ageing*. *Biogerontology*, 2018. **19**(6): p. 447-459.
513. Franceschi, C., *Healthy ageing in 2016: Obesity in geroscience - is cellular senescence the culprit?* *Nat Rev Endocrinol*, 2017. **13**(2): p. 76-78.
514. Iozzo, P., et al., *Developmental ORIGins of Healthy and Unhealthy AgeiNg: the role of maternal obesity--introduction to DORIAN*. *Obes Facts*, 2014. **7**(2): p. 130-51.
515. Jura, M. and L.P. Kozak, *Obesity and related consequences to ageing*. *Age (Dordr)*, 2016. **38**(1): p. 23.
516. Michalakis, K., et al., *Obesity in the ageing man*. *Metabolism*, 2013. **62**(10): p. 1341-9.
517. Perez, L.M., et al., *'Adipaging': ageing and obesity share biological hallmarks related to a dysfunctional adipose tissue*. *J Physiol*, 2016. **594**(12): p. 3187-207.
518. Trim, W., J.E. Turner, and D. Thompson, *Parallels in Immunometabolic Adipose Tissue Dysfunction with Ageing and Obesity*. *Front Immunol*, 2018. **9**: p. 169.
519. Tereshina, E.V. and S.I. Ivanenko, *Age-related obesity is a heritage of the evolutionary past*. *Biochemistry (Mosc)*, 2014. **79**(7): p. 581-92.
520. Canning, K.L., et al., *Relationship between obesity and obesity-related morbidities weakens with aging*. *J Gerontol A Biol Sci Med Sci*, 2014. **69**(1): p. 87-92.
521. Tzanetakou, I.P., et al., *"Is obesity linked to aging?": adipose tissue and the role of telomeres*. *Ageing Res Rev*, 2012. **11**(2): p. 220-9.
522. Villareal, D.T., et al., *Obesity in older adults: technical review and position statement of the American Society for Nutrition and NAASO, The Obesity Society*. *Obes Res*, 2005. **13**(11): p. 1849-63.
523. Soukas, A., et al., *Leptin-specific patterns of gene expression in white adipose tissue*. *Genes Dev*, 2000. **14**(8): p. 963-80.
524. Coleman, D.L., *Obese and diabetes: two mutant genes causing diabetes-obesity syndromes in mice*. *Diabetologia*, 1978. **14**(3): p. 141-8.

525. Guichard, C., et al., *Genetic regulation of fatty acid synthetase expression in adipose tissue: overtranscription of the gene in genetically obese rats*. J Lipid Res, 1992. **33**(5): p. 679-87.
526. Rolland, V., et al., *Evidence of increased glyceraldehyde-3-phosphate dehydrogenase and fatty acid synthetase promoter activities in transiently transfected adipocytes from genetically obese rats*. J Biol Chem, 1995. **270**(3): p. 1102-6.
527. Boizard, M., et al., *Obesity-related overexpression of fatty-acid synthase gene in adipose tissue involves sterol regulatory element-binding protein transcription factors*. J Biol Chem, 1998. **273**(44): p. 29164-71.
528. Bonekamp, N.A., et al., *Reactive oxygen species and peroxisomes: struggling for balance*. Biofactors, 2009. **35**(4): p. 346-55.
529. Pascual-Ahuir, A., S. Manzanares-Estreded, and M. Proft, *Pro- and Antioxidant Functions of the Peroxisome-Mitochondria Connection and Its Impact on Aging and Disease*. Oxid Med Cell Longev, 2017. **2017**: p. 9860841.
530. Gabaldon, T., *Peroxisome diversity and evolution*. Philos Trans R Soc Lond B Biol Sci, 2010. **365**(1541): p. 765-73.
531. Wanders, R.J. and H.R. Waterham, *Biochemistry of mammalian peroxisomes revisited*. Annu Rev Biochem, 2006. **75**: p. 295-332.
532. Del Rio, L.A. and E. Lopez-Huertas, *ROS Generation in Peroxisomes and its Role in Cell Signaling*. Plant Cell Physiol, 2016. **57**(7): p. 1364-1376.
533. Fransen, M., et al., *Role of peroxisomes in ROS/RNS-metabolism: implications for human disease*. Biochim Biophys Acta, 2012. **1822**(9): p. 1363-73.
534. Kirkman, H.N. and G.F. Gaetani, *Mammalian catalase: a venerable enzyme with new mysteries*. Trends Biochem Sci, 2007. **32**(1): p. 44-50.
535. Goth, L. and J.W. Eaton, *Hereditary catalase deficiencies and increased risk of diabetes*. Lancet, 2000. **356**(9244): p. 1820-1.
536. Eisner, V., G. Csordas, and G. Hajnoczky, *Interactions between sarco-endoplasmic reticulum and mitochondria in cardiac and skeletal muscle - pivotal roles in Ca(2)(+) and reactive oxygen species signaling*. J Cell Sci, 2013. **126**(Pt 14): p. 2965-78.
537. Papa, S. and V.P. Skulachev, *Reactive oxygen species, mitochondria, apoptosis and aging*. Mol Cell Biochem, 1997. **174**(1-2): p. 305-19.
538. Sandalio, L.M., et al., *Role of peroxisomes as a source of reactive oxygen species (ROS) signaling molecules*. Subcell Biochem, 2013. **69**: p. 231-55.
539. Singh, I., *Mammalian peroxisomes: metabolism of oxygen and reactive oxygen species*. Ann N Y Acad Sci, 1996. **804**: p. 612-27.
540. Dakik, P. and V.I. Titorenko, *Communications between Mitochondria, the Nucleus, Vacuoles, Peroxisomes, the Endoplasmic Reticulum, the Plasma Membrane, Lipid Droplets, and the Cytosol during Yeast Chronological Aging*. Front Genet, 2016. **7**: p. 177.
541. Wanders, R.J., H.R. Waterham, and S. Ferdinandusse, *Metabolic Interplay between Peroxisomes and Other Subcellular Organelles Including Mitochondria and the Endoplasmic Reticulum*. Front Cell Dev Biol, 2015. **3**: p. 83.
542. Gabaldon, T., *Evolutionary considerations on the origin of peroxisomes from the endoplasmic reticulum, and their relationships with mitochondria*. Cell Mol Life Sci, 2014. **71**(13): p. 2379-82.
543. Hwang, I., et al., *Catalase deficiency accelerates diabetic renal injury through peroxisomal dysfunction*. Diabetes, 2012. **61**(3): p. 728-38.
544. Walton, P.A. and M. Pizzitelli, *Effects of peroxisomal catalase inhibition on mitochondrial function*. Front Physiol, 2012. **3**: p. 108.
545. Wang, B., et al., *Mitochondria are targets for peroxisome-derived oxidative stress in cultured mammalian cells*. Free Radic Biol Med, 2013. **65**: p. 882-94.
546. Ivashchenko, O., et al., *Intraperoxisomal redox balance in mammalian cells: oxidative stress and interorganellar cross-talk*. Mol Biol Cell, 2011. **22**(9): p. 1440-51.

547. Cipolla, C.M. and I.J. Lodhi, *Peroxisomal Dysfunction in Age-Related Diseases*. Trends Endocrinol Metab, 2017. **28**(4): p. 297-308.
548. Fransen, M., et al., *Aging, age-related diseases and peroxisomes*. Subcell Biochem, 2013. **69**: p. 45-65.
549. Mattiazzi Usaj, M., et al., *Genome-Wide Localization Study of Yeast Pex11 Identifies Peroxisome-Mitochondria Interactions through the ERMES Complex*. J Mol Biol, 2015. **427**(11): p. 2072-87.
550. Kornmann, B., et al., *An ER-mitochondria tethering complex revealed by a synthetic biology screen*. Science, 2009. **325**(5939): p. 477-81.
551. Oku, M. and Y. Sakai, *Pexophagy in yeasts*. Biochim Biophys Acta, 2016. **1863**(5): p. 992-8.
552. Lopez, M., *EJE PRIZE 2017: Hypothalamic AMPK: a golden target against obesity?* Eur J Endocrinol, 2017. **176**(5): p. R235-R246.
553. Garcia-Prieto, C.F., et al., *Vascular AMPK as an attractive target in the treatment of vascular complications of obesity*. Vascul Pharmacol, 2015. **67-69**: p. 10-20.
554. Zhang, W., et al., *Integrated Regulation of Hepatic Lipid and Glucose Metabolism by Adipose Triacylglycerol Lipase and FoxO Proteins*. Cell Rep, 2016. **15**(2): p. 349-59.
555. Wu, Y., et al., *Effect of high-fat diet-induced obesity on the Akt/FoxO/Smad signaling pathway and the follicular development of the mouse ovary*. Mol Med Rep, 2016. **14**(4): p. 3894-900.
556. Moll, L. and M. Schubert, *The Role of Insulin and Insulin-Like Growth Factor-1/FoxO-Mediated Transcription for the Pathogenesis of Obesity-Associated Dementia*. Curr Gerontol Geriatr Res, 2012. **2012**: p. 384094.
557. Wu, L., et al., *Activation of FoxO1/ PGC-1alpha prevents mitochondrial dysfunction and ameliorates mesangial cell injury in diabetic rats*. Mol Cell Endocrinol, 2015. **413**: p. 1-12.
558. Puigserver, P., et al., *Insulin-regulated hepatic gluconeogenesis through FOXO1-PGC-1alpha interaction*. Nature, 2003. **423**(6939): p. 550-5.
559. Armoni, M., et al., *FOXO1 represses peroxisome proliferator-activated receptor-gamma1 and -gamma2 gene promoters in primary adipocytes. A novel paradigm to increase insulin sensitivity*. J Biol Chem, 2006. **281**(29): p. 19881-91.
560. Chalkiadaki, A. and L. Guarente, *High-fat diet triggers inflammation-induced cleavage of SIRT1 in adipose tissue to promote metabolic dysfunction*. Cell Metab, 2012. **16**(2): p. 180-8.
561. Poulou, N. and R. Raju, *Sirtuin regulation in aging and injury*. Biochim Biophys Acta, 2015. **1852**(11): p. 2442-55.
562. You, Z., Y. Liu, and X. Liu, *Nicotinamide N-methyltransferase enhances the progression of prostate cancer by stabilizing sirtuin 1*. Oncol Lett, 2018. **15**(6): p. 9195-9201.
563. Yang, S.J., et al., *Nicotinamide improves glucose metabolism and affects the hepatic NAD-sirtuin pathway in a rodent model of obesity and type 2 diabetes*. J Nutr Biochem, 2014. **25**(1): p. 66-72.
564. Avalos, J.L., K.M. Bever, and C. Wolberger, *Mechanism of sirtuin inhibition by nicotinamide: altering the NAD(+) cosubstrate specificity of a Sir2 enzyme*. Mol Cell, 2005. **17**(6): p. 855-68.
565. Gillum, M.P., et al., *Sirt1 regulates adipose tissue inflammation*. Diabetes, 2011. **60**(12): p. 3235-45.
566. Sasaki, T., *Age-Associated Weight Gain, Leptin, and SIRT1: A Possible Role for Hypothalamic SIRT1 in the Prevention of Weight Gain and Aging through Modulation of Leptin Sensitivity*. Front Endocrinol (Lausanne), 2015. **6**: p. 109.
567. Picard, F., et al., *Sirt1 promotes fat mobilization in white adipocytes by repressing PPAR-gamma*. Nature, 2004. **429**(6993): p. 771-6.
568. Yoshizaki, T., et al., *SIRT1 exerts anti-inflammatory effects and improves insulin sensitivity in adipocytes*. Mol Cell Biol, 2009. **29**(5): p. 1363-74.
569. Mitchell, S.J., et al., *The SIRT1 activator SRT1720 extends lifespan and improves health of mice fed a standard diet*. Cell Rep, 2014. **6**(5): p. 836-43.

570. Muoio, D.M., et al., *Fatty acid homeostasis and induction of lipid regulatory genes in skeletal muscles of peroxisome proliferator-activated receptor (PPAR) alpha knock-out mice. Evidence for compensatory regulation by PPAR delta.* J Biol Chem, 2002. **277**(29): p. 26089-97.
571. Peters, J.M., et al., *Growth, adipose, brain, and skin alterations resulting from targeted disruption of the mouse peroxisome proliferator-activated receptor beta(delta).* Mol Cell Biol, 2000. **20**(14): p. 5119-28.
572. Lee, C.H., P. Olson, and R.M. Evans, *Minireview: lipid metabolism, metabolic diseases, and peroxisome proliferator-activated receptors.* Endocrinology, 2003. **144**(6): p. 2201-7.
573. Shimano, H., *SREBPs: physiology and pathophysiology of the SREBP family.* FEBS J, 2009. **276**(3): p. 616-21.
574. Sun, K., C.M. Kusminski, and P.E. Scherer, *Adipose tissue remodeling and obesity.* J Clin Invest, 2011. **121**(6): p. 2094-101.
575. Lee, M.J., Y. Wu, and S.K. Fried, *Adipose tissue remodeling in pathophysiology of obesity.* Curr Opin Clin Nutr Metab Care, 2010. **13**(4): p. 371-6.
576. Horvath, S., et al., *Obesity accelerates epigenetic aging of human liver.* Proc Natl Acad Sci U S A, 2014. **111**(43): p. 15538-43.
577. Arner, P., et al., *The epigenetic signature of subcutaneous fat cells is linked to altered expression of genes implicated in lipid metabolism in obese women.* Clin Epigenetics, 2015. **7**: p. 93.
578. Drogan, D., et al., *Regional distribution of body fat in relation to DNA methylation within the LPL, ADIPOQ and PPARgamma promoters in subcutaneous adipose tissue.* Nutr Diabetes, 2015. **5**: p. e168.
579. Li, Y., M. Daniel, and T.O. Tollefsbol, *Epigenetic regulation of caloric restriction in aging.* BMC Med, 2011. **9**: p. 98.
580. Thompson, R.F., et al., *Tissue-specific dysregulation of DNA methylation in aging.* Aging Cell, 2010. **9**(4): p. 506-18.
581. Stransky, C.A., et al., *Beyond fat grafting: what adipose tissue can teach us about the molecular mechanisms of human aging.* Ann Plast Surg, 2012. **69**(4): p. 489-92.
582. Crews, F.T., *Effects of membrane fluidity on secretion and receptor stimulation.* Psychopharmacol Bull, 1982. **18**(4): p. 135-43.
583. Multhaup, M.L., et al., *Mouse-human experimental epigenetic analysis unmasks dietary targets and genetic liability for diabetic phenotypes.* Cell Metab, 2015. **21**(1): p. 138-49.
584. Benton, M.C., et al., *An analysis of DNA methylation in human adipose tissue reveals differential modification of obesity genes before and after gastric bypass and weight loss.* Genome Biol, 2015. **16**: p. 8.
585. Dick, K.J., et al., *DNA methylation and body-mass index: a genome-wide analysis.* Lancet, 2014. **383**(9933): p. 1990-8.
586. Ehrlich, M., et al., *Amount and distribution of 5-methylcytosine in human DNA from different types of tissues of cells.* Nucleic Acids Res, 1982. **10**(8): p. 2709-21.
587. Blackburn, G.M., *Nucleic Acids in Chemistry and Biology.* 2006: The Royal Society of Chemistry. p.119-120.
588. Zemach, A., et al., *Genome-wide evolutionary analysis of eukaryotic DNA methylation.* Science, 2010. **328**(5980): p. 916-9.
589. Feng, S., et al., *Conservation and divergence of methylation patterning in plants and animals.* Proc Natl Acad Sci U S A, 2010. **107**(19): p. 8689-94.
590. Cholewa, J.M., L. Guimaraes-Ferreira, and N.E. Zanchi, *Effects of betaine on performance and body composition: a review of recent findings and potential mechanisms.* Amino Acids, 2014. **46**(8): p. 1785-93.
591. Elshorbagy, A.K., et al., *Cysteine and obesity: consistency of the evidence across epidemiologic, animal and cellular studies.* Curr Opin Clin Nutr Metab Care, 2012. **15**(1): p. 49-57.

592. Fagone, P. and S. Jackowski, *Phosphatidylcholine and the CDP-choline cycle*. *Biochim Biophys Acta*, 2013. **1831**(3): p. 523-32.
593. Esfandiari, F., et al., *S-adenosylmethionine attenuates hepatic lipid synthesis in micropigs fed ethanol with a folate-deficient diet*. *Alcohol Clin Exp Res*, 2007. **31**(7): p. 1231-9.
594. Christensen, K.E., et al., *High folic acid consumption leads to pseudo-MTHFR deficiency, altered lipid metabolism, and liver injury in mice*. *Am J Clin Nutr*, 2015. **101**(3): p. 646-58.
595. Grewal, S.I. and J.C. Rice, *Regulation of heterochromatin by histone methylation and small RNAs*. *Curr Opin Cell Biol*, 2004. **16**(3): p. 230-8.
596. Nakayama, J., et al., *Role of histone H3 lysine 9 methylation in epigenetic control of heterochromatin assembly*. *Science*, 2001. **292**(5514): p. 110-3.
597. Choi, J., et al., *N(6)-methyladenosine in mRNA disrupts tRNA selection and translation-elongation dynamics*. *Nat Struct Mol Biol*, 2016. **23**(2): p. 110-5.
598. Hrebicek, J., *[PPARs: the role in glucose and lipid homeostasis, insulin resistance and atherosclerosis]*. *Cesk Fysiol*, 2004. **53**(1): p. 4-16.
599. Ricote, M., A.F. Villedor, and C.K. Glass, *Decoding transcriptional programs regulated by PPARs and LXRs in the macrophage: effects on lipid homeostasis, inflammation, and atherosclerosis*. *Arterioscler Thromb Vasc Biol*, 2004. **24**(2): p. 230-9.
600. Yang, Q. and Y. Li, *Roles of PPARs on regulating myocardial energy and lipid homeostasis*. *J Mol Med (Berl)*, 2007. **85**(7): p. 697-706.
601. Rangwala, S.M. and M.A. Lazar, *Peroxisome proliferator-activated receptor gamma in diabetes and metabolism*. *Trends Pharmacol Sci*, 2004. **25**(6): p. 331-6.
602. Ye, J.M., et al., *Direct demonstration of lipid sequestration as a mechanism by which rosiglitazone prevents fatty-acid-induced insulin resistance in the rat: comparison with metformin*. *Diabetologia*, 2004. **47**(7): p. 1306-1313.
603. Larsen, T.M., S. Toubro, and A. Astrup, *PPARgamma agonists in the treatment of type II diabetes: is increased fatness commensurate with long-term efficacy?* *Int J Obes Relat Metab Disord*, 2003. **27**(2): p. 147-61.
604. Forman, B.M., J. Chen, and R.M. Evans, *Hypolipidemic drugs, polyunsaturated fatty acids, and eicosanoids are ligands for peroxisome proliferator-activated receptors alpha and delta*. *Proc Natl Acad Sci U S A*, 1997. **94**(9): p. 4312-7.
605. Wang, Y.X., et al., *Regulation of muscle fiber type and running endurance by PPARdelta*. *PLoS Biol*, 2004. **2**(10): p. e294.
606. Grimaldi, P.A., *The roles of PPARs in adipocyte differentiation*. *Prog Lipid Res*, 2001. **40**(4): p. 269-81.
607. Valmaseda, A., et al., *Opposite regulation of PPAR-alpha and -gamma gene expression by both their ligands and retinoic acid in brown adipocytes*. *Mol Cell Endocrinol*, 1999. **154**(1-2): p. 101-9.
608. Bastie, C., et al., *Alterations of peroxisome proliferator-activated receptor delta activity affect fatty acid-controlled adipose differentiation*. *J Biol Chem*, 2000. **275**(49): p. 38768-73.
609. Hansen, J.B., et al., *Peroxisome proliferator-activated receptor delta (PPARdelta)-mediated regulation of preadipocyte proliferation and gene expression is dependent on cAMP signaling*. *J Biol Chem*, 2001. **276**(5): p. 3175-82.
610. Wang, Y.X., et al., *Peroxisome-proliferator-activated receptor delta activates fat metabolism to prevent obesity*. *Cell*, 2003. **113**(2): p. 159-70.
611. Marcus, S.L., J.P. Capone, and R.A. Rachubinski, *Identification of COUP-TFII as a peroxisome proliferator response element binding factor using genetic selection in yeast: COUP-TFII activates transcription in yeast but antagonizes PPAR signaling in mammalian cells*. *Mol Cell Endocrinol*, 1996. **120**(1): p. 31-9.
612. Inoue, J., et al., *PPARalpha gene expression is up-regulated by LXR and PXR activators in the small intestine*. *Biochem Biophys Res Commun*, 2008. **371**(4): p. 675-8.

613. Poynter, M.E. and R.A. Daynes, *Peroxisome proliferator-activated receptor alpha activation modulates cellular redox status, represses nuclear factor-kappaB signaling, and reduces inflammatory cytokine production in aging*. J Biol Chem, 1998. **273**(49): p. 32833-41.
614. Chung, S. and C.W. Park, *Role of Peroxisome Proliferator-Activated Receptor alpha in Diabetic Nephropathy*. Diabetes Metab J, 2011. **35**(4): p. 327-36.
615. Pineda Torra, I., et al., *Characterization of the human PPARalpha promoter: identification of a functional nuclear receptor response element*. Mol Endocrinol, 2002. **16**(5): p. 1013-28.
616. Schulz, T.J., et al., *Identification of inducible brown adipocyte progenitors residing in skeletal muscle and white fat*. Proc Natl Acad Sci U S A, 2011. **108**(1): p. 143-8.
617. Walden, T.B., et al., *Recruited vs. nonrecruited molecular signatures of brown, "brite," and white adipose tissues*. Am J Physiol Endocrinol Metab, 2012. **302**(1): p. E19-31.
618. Siersbaek, M.S., et al., *Genome-wide profiling of peroxisome proliferator-activated receptor gamma in primary epididymal, inguinal, and brown adipocytes reveals depot-selective binding correlated with gene expression*. Mol Cell Biol, 2012. **32**(17): p. 3452-63.
619. Regnier, M., et al., *Insights into the role of hepatocyte PPARalpha activity in response to fasting*. Mol Cell Endocrinol, 2018. **471**: p. 75-88.
620. Acharjee, A., et al., *Integration of metabolomics, lipidomics and clinical data using a machine learning method*. BMC Bioinformatics, 2016. **17**(Suppl 15): p. 440.
621. Ament, Z., et al., *PPAR-pan activation induces hepatic oxidative stress and lipidomic remodelling*. Free Radic Biol Med, 2016. **95**: p. 357-68.
622. Kopf, T., et al., *Influence of fenofibrate treatment on triacylglycerides, diacylglycerides and fatty acids in fructose fed rats*. PLoS One, 2014. **9**(9): p. e106849.
623. Adamovich, Y., et al., *Circadian clocks and feeding time regulate the oscillations and levels of hepatic triglycerides*. Cell Metab, 2014. **19**(2): p. 319-30.
624. Shi, X., et al., *Lipidomic profiling reveals protective function of fatty acid oxidation in cocaine-induced hepatotoxicity*. J Lipid Res, 2012. **53**(11): p. 2318-30.
625. Kolesnick, R., *Signal transduction through the sphingomyelin pathway*. Mol Chem Neuropathol, 1994. **21**(2-3): p. 287-97.
626. Mandard, S., M. Muller, and S. Kersten, *Peroxisome proliferator-activated receptor alpha target genes*. Cell Mol Life Sci, 2004. **61**(4): p. 393-416.
627. Leone, T.C., C.J. Weinheimer, and D.P. Kelly, *A critical role for the peroxisome proliferator-activated receptor alpha (PPARalpha) in the cellular fasting response: the PPARalpha-null mouse as a model of fatty acid oxidation disorders*. Proc Natl Acad Sci U S A, 1999. **96**(13): p. 7473-8.
628. Kersten, S., et al., *Peroxisome proliferator-activated receptor alpha mediates the adaptive response to fasting*. J Clin Invest, 1999. **103**(11): p. 1489-98.
629. Djouadi, F., et al., *A gender-related defect in lipid metabolism and glucose homeostasis in peroxisome proliferator-activated receptor alpha-deficient mice*. J Clin Invest, 1998. **102**(6): p. 1083-91.
630. Watanabe, K., et al., *Constitutive regulation of cardiac fatty acid metabolism through peroxisome proliferator-activated receptor alpha associated with age-dependent cardiac toxicity*. J Biol Chem, 2000. **275**(29): p. 22293-9.
631. Xu, J., et al., *Peroxisome proliferator-activated receptor alpha (PPARalpha) influences substrate utilization for hepatic glucose production*. J Biol Chem, 2002. **277**(52): p. 50237-44.
632. Djouadi, F., et al., *The role of the peroxisome proliferator-activated receptor alpha (PPAR alpha) in the control of cardiac lipid metabolism*. Prostaglandins Leukot Essent Fatty Acids, 1999. **60**(5-6): p. 339-43.
633. Atherton, H.J., et al., *A combined 1H-NMR spectroscopy- and mass spectrometry-based metabolomic study of the PPAR-alpha null mutant mouse defines profound systemic changes in metabolism linked to the metabolic syndrome*. Physiol Genomics, 2006. **27**(2): p. 178-86.

634. Wu, P., J.M. Peters, and R.A. Harris, *Adaptive increase in pyruvate dehydrogenase kinase 4 during starvation is mediated by peroxisome proliferator-activated receptor alpha*. *Biochem Biophys Res Commun*, 2001. **287**(2): p. 391-6.
635. Kersten, S., B. Desvergne, and W. Wahli, *Roles of PPARs in health and disease*. *Nature*, 2000. **405**(6785): p. 421-4.
636. Barak, Y. and S. Kim, *Genetic manipulations of PPARs: effects on obesity and metabolic disease*. *PPAR Res*, 2007. **2007**: p. 12781.
637. Wang, Y., et al., *Regulation of hepatic fatty acid elongase and desaturase expression in diabetes and obesity*. *J Lipid Res*, 2006. **47**(9): p. 2028-41.
638. Knight, B.L., et al., *A role for PPARalpha in the control of SREBP activity and lipid synthesis in the liver*. *Biochem J*, 2005. **389**(Pt 2): p. 413-21.
639. Ye, P., et al., *Effect of aging on the expression of peroxisome proliferator-activated receptor gamma and the possible relation to insulin resistance*. *Gerontology*, 2006. **52**(2): p. 69-75.
640. Ferro, M., et al., *The emerging role of obesity, diet and lipid metabolism in prostate cancer*. *Future Oncol*, 2017. **13**(3): p. 285-293.
641. Mount, P., et al., *Obesity-Related Chronic Kidney Disease-The Role of Lipid Metabolism*. *Metabolites*, 2015. **5**(4): p. 720-32.
642. Schug, T.T. and X. Li, *Sirtuin 1 in lipid metabolism and obesity*. *Ann Med*, 2011. **43**(3): p. 198-211.
643. Nestel, P. and B. Goldrick, *Obesity: changes in lipid metabolism and the role of insulin*. *Clin Endocrinol Metab*, 1976. **5**(2): p. 313-35.
644. Bake, T., et al., *Large, binge-type meals of high fat diet change feeding behaviour and entrain food anticipatory activity in mice*. *Appetite*, 2014. **77**: p. 60-71.
645. Kim, Y.I., et al., *Folate deficiency in rats induces DNA strand breaks and hypomethylation within the p53 tumor suppressor gene*. *Am J Clin Nutr*, 1997. **65**(1): p. 46-52.
646. Burdge, G.C., et al., *Folic acid supplementation during the juvenile-pubertal period in rats modifies the phenotype and epigenotype induced by prenatal nutrition*. *J Nutr*, 2009. **139**(6): p. 1054-60.
647. Niculescu, M.D., C.N. Craciunescu, and S.H. Zeisel, *Dietary choline deficiency alters global and gene-specific DNA methylation in the developing hippocampus of mouse fetal brains*. *FASEB J*, 2006. **20**(1): p. 43-9.
648. Mehedint, M.G., et al., *Choline deficiency alters global histone methylation and epigenetic marking at the Re1 site of the calbindin 1 gene*. *FASEB J*, 2010. **24**(1): p. 184-95.
649. Kovacheva, V.P., et al., *Gestational choline deficiency causes global and Igf2 gene DNA hypermethylation by up-regulation of Dnmt1 expression*. *J Biol Chem*, 2007. **282**(43): p. 31777-88.
650. Du, Y.P., et al., *Assessment of the effect of betaine on p16 and c-myc DNA methylation and mRNA expression in a chemical induced rat liver cancer model*. *BMC Cancer*, 2009. **9**: p. 261.
651. Xing, J., L. Kang, and Y. Jiang, *Effect of dietary betaine supplementation on lipogenesis gene expression and CpG methylation of lipoprotein lipase gene in broilers*. *Mol Biol Rep*, 2011. **38**(3): p. 1975-81.
652. Sanchez-Delgado, G., et al., *Role of Exercise in the Activation of Brown Adipose Tissue*. *Ann Nutr Metab*, 2015. **67**(1): p. 21-32.
653. Stanford, K.I., R.J. Middelbeek, and L.J. Goodyear, *Exercise Effects on White Adipose Tissue: Beiging and Metabolic Adaptations*. *Diabetes*, 2015. **64**(7): p. 2361-8.
654. Park, Y.M., M. Myers, and V.J. Vieira-Potter, *Adipose tissue inflammation and metabolic dysfunction: role of exercise*. *Mo Med*, 2014. **111**(1): p. 65-72.
655. Pond, C.M., *Adipose tissue, the immune system and exercise fatigue: how activated lymphocytes compete for lipids*. *Biochem Soc Trans*, 2002. **30**(2): p. 270-5.
656. Sepa-Kishi, D.M. and R.B. Ceddia, *Exercise-Mediated Effects on White and Brown Adipose Tissue Plasticity and Metabolism*. *Exerc Sport Sci Rev*, 2016. **44**(1): p. 37-44.

657. Sakurai, T., et al., *The effects of exercise training on obesity-induced dysregulated expression of adipokines in white adipose tissue*. *Int J Endocrinol*, 2013. **2013**: p. 801743.
658. McMurray, R.G. and A.C. Hackney, *Interactions of metabolic hormones, adipose tissue and exercise*. *Sports Med*, 2005. **35**(5): p. 393-412.
659. Coppari, R. and C. Bjorbaek, *Leptin revisited: its mechanism of action and potential for treating diabetes*. *Nat Rev Drug Discov*, 2012. **11**(9): p. 692-708.
660. Oral, E.A., *Leptin for type 1 diabetes: coming onto stage to be (or not?)*. *Pediatr Diabetes*, 2012. **13**(1): p. 68-73.
661. Wang, Y., et al., *Leptin gene therapy in the fight against diabetes*. *Expert Opin Biol Ther*, 2010. **10**(10): p. 1405-14.
662. Al-Daghri, N., et al., *Role of leptin in glucose metabolism in type 2 diabetes*. *Diabetes Obes Metab*, 2002. **4**(3): p. 147-55.
663. Wolf, G., *Insulin resistance associated with leptin deficiency in mice: a possible model for noninsulin-dependent diabetes mellitus*. *Nutr Rev*, 2001. **59**(6): p. 177-9.
664. Saurabh, S., A.S. Vidyarthi, and D. Prasad, *RNA interference: concept to reality in crop improvement*. *Planta*, 2014. **239**(3): p. 543-64.
665. Dixon, J.A. and F.G. Spinale, *Large animal models of heart failure: a critical link in the translation of basic science to clinical practice*. *Circ Heart Fail*, 2009. **2**(3): p. 262-71.
666. Runge, D., et al., *Serum-free, long-term cultures of human hepatocytes: maintenance of cell morphology, transcription factors, and liver-specific functions*. *Biochem Biophys Res Commun*, 2000. **269**(1): p. 46-53.
667. Bernadotte, A., V.M. Mikhelson, and I.M. Spivak, *Markers of cellular senescence. Telomere shortening as a marker of cellular senescence*. *Aging (Albany NY)*, 2016. **8**(1): p. 3-11.
668. Tempaku, P.F., D.R. Mazzotti, and S. Tufik, *Telomere length as a marker of sleep loss and sleep disturbances: a potential link between sleep and cellular senescence*. *Sleep Med*, 2015. **16**(5): p. 559-63.
669. Vaughan, D.E., et al., *Plasminogen Activator Inhibitor-1 Is a Marker and a Mediator of Senescence*. *Arterioscler Thromb Vasc Biol*, 2017. **37**(8): p. 1446-1452.
670. Kondo, Y. and A. Ishigami, *Involvement of senescence marker protein-30 in glucose metabolism disorder and non-alcoholic fatty liver disease*. *Geriatr Gerontol Int*, 2016. **16 Suppl 1**: p. 4-16.